2809658505

REFERENCE ONLY

UNIVERSITY OF LONDON THESIS

Degree PhD Year 2007 Name of Author COPPERWHEAT, Christopher Michael

COPYRIGHT
This is a thesis accepted for a Higher Degree of the University of London. It is an unpublished typescript and the copyright is held by the author. All persons consulting this thesis must read and abide by the Copyright Declaration below.

COPYRIGHT DECLARATION
I recognise that the copyright of the above-described thesis rests with the author and that no quotation from it or information derived from it may be published without the prior written consent of the author.

LOANS
Theses may not be lent to individuals, but the Senate House Library may lend a copy to approved libraries within the United Kingdom, for consultation solely on the premises of those libraries. Application should be made to: Inter-Library Loans, Senate House Library, Senate House, Malet Street, London WC1E 7HU.

REPRODUCTION
University of London theses may not be reproduced without explicit written permission from the Senate House Library. Enquiries should be addressed to the Theses Section of the Library. Regulations concerning reproduction vary according to the date of acceptance of the thesis and are listed below as guidelines.

A. Before 1962. Permission granted only upon the prior written consent of the author. (The Senate House Library will provide addresses where possible).

B. 1962-1974. In many cases the author has agreed to permit copying upon completion of a Copyright Declaration.

C. 1975-1988. Most theses may be copied upon completion of a Copyright Declaration.

D. 1989 onwards. Most theses may be copied.

This thesis comes within category D.

☐ This copy has been deposited in the Library of ____________________

☐ This copy has been deposited in the Senate House Library, Senate House, Malet Street, London WC1E 7HU.

The Optical Emission from Ultraluminous X-ray Sources

Christopher Michael Copperwheat

Mullard Space Science Laboratory
Department of Space and Climate Physics
University College London

A thesis submitted to the University of London
for the degree of Doctor of Philosophy

ProQuest LLC
789 East Eisenhower Parkway
P.O. Box 1346
Ann Arbor, MI 48106-1346

I, Christopher Copperwheat, confirm that the work presented in this thesis is my own. Where information has been derived from other sources, I confirm that this has been indicated in the thesis.

Abstract

Ultraluminous X-ray sources (ULXs) are point-like, non-nuclear sources which exceed the Eddington luminosity for a stellar mass black hole (BH). The emission from these sources might be beamed or super-Eddington, but it has also been proposed that the compact object in these sources are intermediate mass BHs (IMBHs), which fit in the mass range between the two known populations of BH in the galaxy. The existence of IMBHs is under intense debate, and study of the X-ray data has been unable to resolve this issue. This thesis describes a model I have constructed in order to examine the optical/IR emission from these sources; an alternative channel by which their nature may be understood.

I assume a binary model with a black hole accreting matter from a Roche lobe filling companion star. I consider the effects of radiative transport and radiative equilibrium in the irradiated surfaces of both the star and a thin accretion disc. I use current stellar evolutionary models as an input component in this model, and hence determine the mass, radius and age of the donor stars in a range of ULX systems, and in some cases provide limits on the BH mass. In addition I determine the mass transfer rate in these systems from the X-ray luminosity and compare this to transfer rate calculations based on the stellar evolutionary models. Since this method is independent of the optical data it is a powerful additional constraint on the parameter space. For systems where optical observations are available at multiple epochs, I make further determinations of the binary parameters based on the optical variability.

Where it is possible to constrain the masses of the BHs, I find them to be consistent with BHs of up to $\sim 100M_\odot$. I find that in general the donor stars are older and less massive than previously thought, and are consistent with being of spectral type B. I discuss how these results affect our understanding of the evolution and history of ULXs. I discuss how future studies of ULX optical counterparts will be even more revealing, and I make predictions for these optical campaigns, estimating binary periods, variability and the results of IR observational campaigns, which my results suggest will be a important tool in future studies of the nature of this class of sources.

Contents

List of Figures

List of Tables

Chapter 1

Introduction

1.1 Overview

Ultraluminous X-ray sources (ULXs) are a class of luminous, point-like, non-nuclear sources in external galaxies. They are thought to be binary systems consisting of a black hole (BH) accreting matter from a companion star, but their exact nature still eludes us.

ULXs are interesting because their high luminosities imply an exotic nature either for the BH or the way it accretes. This chapter therefore begins with a brief overview of the known populations of BH in the universe and the electromagnetic radiation we observe from them, so as to provide a context for ULXs. I then examine the observational properties of ULXs, discuss the theoretical models proposed to explain their physical nature, and review the current observational evidence. In this thesis, an understanding of the nature of ULXs is sought through the examination of their optical counterparts. I discuss why this is an effective avenue of investigation. Finally, I outline the structure of the thesis.

The model detailed in Chapter 2 was published in Copperwheat et al. (2005). The results presented in Chapters 3 and 4 were, for the most part, published in Copperwheat et al. (2007).

1.2 Black Holes

1.2.1 Stellar-mass black holes

The idea of an object so massive that it has an escape velocity in excess of the speed of light was first proposed in the eighteenth century (Michell, 1784). In the twentieth century the existence of BHs was proposed as a consequence of the equations of general relativity, and in the modern era the existence of BHs in the universe is well supported by observation (see Casares 2006; Mueller 2007 for recent reviews). Because BHs cannot be observed directly their presence is inferred from the influence of their gravitational potential on luminous matter. For example, stellar motions in the Galactic centre require the presence of a massive BH (Genzel et al., 1997).

The discovery of an extra-solar X-ray source in the 1960s (Scorpius X-1: Giacconi et al. 1962) led to the advent of X-ray astronomy. Sco X-1 was the first of many luminous, non-nuclear, and pointlike X-ray sources discovered within the Galaxy, and later other local galaxies. The high X-ray luminosities and short timescale variability led to a model where the X-ray emission has its origin in material accreting onto compact objects. The compact object in these cases exists in a binary system with a companion ('donor') star. Material from this companion star falls into the gravitational well of the compact object, forming an accretion disc around the object. The disc is extremely hot in its inner regions and emits X-ray and ultraviolet radiation. A system of this nature is termed an X-ray binary (XRB).

The compact object in this case is the end product of an evolved star. The nature of the compact object will depend on the mass of the star. Lower mass stars will end their lives as white dwarfs (WD). More massive stars end their lives more violently in a supernova explosion, leaving behind a neutron star (NS) or a BH (Carroll & Ostlie, 2007).

The mass of the compact object can be determined from radial velocity measurements of the binary system. A neutron star has an upper limit (the Tolman-Oppenheimer-Volkoff limit) on its mass, of $\sim 3M_{\odot}$ (Bombaci, 1996). If the compact object is found to exceed this mass then it is thought to be a BH, simply because there is no other convincing theoretical explanation for an object of this mass and compactness to withstand gravitational forces. The first identification of a BH XRB was Cygnus X-1 (Bolton, 1972), and many more BHs in accreting binaries have been identifed since.

BHs of this type are known as 'stellar-mass' BHs, since they are the end product of the evolution of massive stars. The lower limit on the mass range of stellar mass BHs is $\sim 3M_{\odot}$, as noted above. Theoretical studies of 'normal' stellar evolution of massive stars suggest the upper limit is $\sim 20M_{\odot}$ (Fryer & Kalogera, 2001). This is consistent with the mass determinations made of BH candidates in our galaxy, none of which exceed this (Casares, 2006). However, more recent theoretical work has suggested the actual upper limit may actually be up to $\sim 50M_{\odot}$ (Heger et al., 2003). Calculations are complex, but one important factor is the metallicity of the progenitor: stars of low metallicity lose less mass in stellar winds thus ending their lives with bigger cores, which can more easily collapse directly into more massive BHs.

1.2.2 Supermassive black holes

In the early part of the last century, observations of the central regions of the galaxy NGC 1068 showed the presence of line emission (Fath, 1909). A later study by Carl Seyfert showed that a small percentage of otherwise-normal galaxies have bright nuclei with broad emission lines (Seyfert, 1943). These so-called 'Active Galactic Nuclei' (AGN) are compact sources, and different sources are highly luminous over some or all of the radio, infrared, optical, ultra-violet, X-ray and gamma-ray wavebands. The menagerie of AGN in the universe is large and varied (see Ferrarese & Ford 2004 for a recent review), but the current consensus is that the central engine for all AGN is accretion onto a supermassive BH (SMBH, Rees 1984), with masses in the range of 10^5 - $10^{10}M_{\odot}$. SMBHs are now generally believed to be ubiquitous in the centres of galaxies, whether they are evident from accretion or dormant.

Further discussion of SMBHs is not relevant to this work. It should however be noted that there are many similarities between SMBHs and stellar-mass BHs. The mechanism of the accretion process is essentially the same: the difference is one of scale (Mirabel, 2006). However, while the formation mechanism of a stellar-mass BH has a sound theoretical basis, the process of forming a SMBH is unclear (Rees, 1984). The centres of galaxies are dense environments, and so a massive BH could have formed from the collapse of dense gas clouds or stellar clusters. On the other hand, a SMBH may have formed from the slow accretion of matter onto a stellar mass BH, which later migrated to the centre of its host galaxy. However, if there is an evolutionary link between the two BH populations, one would expect to observe an intermediate population.

1.3 Electromagnetic radiation from accreting BHs

1.3.1 The luminosity of an accreting BH

The total energy of a mass m of material orbiting a BH of mass M at a radius r is

$$E = \frac{GMm}{r}. \tag{1.1}$$

As this material falls deeper into the potential well of the BH, its gravitational potential energy is converted into electromagnetic radiation (Frank et al., 2002). The virial theorem states that the potential energy is half of the total energy. The energy liberated from the system as electromagnetic radiation is therefore

$$E_{rad} = \frac{1}{2}\frac{GMm}{R}, \tag{1.2}$$

where R is the last stable orbit. Any remaining energy is advected into the BH. By taking the time derivative of this equation an accretion luminosity in terms of the mass accretion rate $\dot{m}$ is found:

$$L_{acc} = \frac{1}{2}\frac{GM\dot{m}}{R}. \tag{1.3}$$

The last stable orbit for a non-rotating BH is approximately 3 times the Schwarzschild radius $R_s = 2GM/c^2$. When this is substituted in we find

$$L_{acc} = \eta \dot{m} c^2, \tag{1.4}$$

where η is an efficiency term of order 0.1.

1.3.2 The Eddington limit

It can be seen from Equation 1.4 that the luminosity of an accreting BH varies with the accretion rate. At high luminosities the accreting material experiences radiation pressure from the high photon flux, which acts against it (Frank et al., 2002).

Eddington assumed that the accretion is spherically symmetric, the accreting material is fully ionized hydrogen and the radiation exerts a force on the particles through Thomson scattering. This is the minimum opacity source: any other sources will add to the radiation pressure.

Following Frank et al. (2002), the outward radial force on the particles is equal to the rate at which they absorb momentum.

$$F = \frac{\sigma_T S}{c} \tag{1.5}$$

where S is the radiant energy flux and σ_T is the Thomson cross-section. This is given by

$$\sigma_T = \frac{8\pi}{3}\left(\frac{q^2}{mc^2}\right)^2 \tag{1.6}$$

where q and m are the charge and the mass of the particle respectively. It can be seen that that σ_T is significantly less for a proton than for an electron, so the radiation pressure force on the electrons is much greater and protons are neglected.

The gravitational force is larger for the protons than the electrons. However, the attractive electrostatic Coulomb force means electron-proton pairs act together. The net force on an electro-proton pair will therefore be

$$\left(GMm_p - \frac{L\sigma_T}{4\pi c}\right)\frac{1}{r^2} \tag{1.7}$$

where m_p is the mass of a proton, L is the luminosity of the accreting compact object and $S = L/4\pi r^2$.

There is a luminosity at which this net force vanishes. This is the Eddington luminosity, determined from rearranging equation 1.7:

$$\begin{aligned} L_{Edd} &= \frac{4\pi G M m_p c}{\sigma_T} && (1.8) \\ &\simeq 1.3 \times 10^{38} (M/M_\odot) \mathrm{erg\ s^{-1}} && (1.9) \end{aligned}$$

This is an upper bound on the accretion luminosity within the conditions assumed for the accretion: if the luminosity exceeds this then the mass transfer will cease. Given the upper limit on the mass of a stellar mass BH of $\sim 20 M_\odot$ (Section 1.2.1), this implies a maximum luminosity for XRB of $\sim 10^{39}$erg s^{-1}. This agrees well with observation, as recent determinations of the luminosity function for XRB in local galaxies have shown (Grimm et al., 2006). Accreting SMBH are much more massive, and are correspondingly much more luminous.

1.4 Ultraluminous X-ray Sources

Observations of nearby galaxies with the *Einstein* observatory led to the discovery of a class of sources termed Ultraluminous X-ray Sources (ULXs) (Fabbiano, 1989), or less commonly, Intermediate X-ray Objects (IXOs). They are point-like, non-nuclear sources, with very high inferred X-ray luminosities, ranging from 10^{39} – 10^{41}ergs s^{-1}, asuming isotropic X-ray emission. Further studies with *ROSAT*, and latterly *Chandra* and XMM-*Newton*, led to the discovery of many more of these sources in local galaxies, implying they are populous (see, *e.g.*, Fabbiano & White 2003; Swartz et al. 2004; Liu et al. 2005). Some of these sources have since been identified as supernova remnants (SNR) or background quasars, but the majority of sources display X-ray spectra and time variability that is indicative of compact, accreting sources in local galaxies (Colbert & Mushotzky, 1999).

There is much debate as to how to reconcile the apparent XRB nature for ULXs with X-ray luminosities which are in excess of the Eddington limit for stellar mass BHs. Various models have been proposed, which I will discuss in the next section. In Section 1.6, I will discuss the available observational evidence in the context of these theoretical models.

1.5 Theoretical models for ULXs

Equation 1.9 shows that in an accreting binary, the Eddington limit is proportional to the mass of the BH. The high X-ray luminosities of ULXs can therefore be explained by supposing the compact object in these systems is a very massive BH.

1.5.1 Intermediate mass black holes

It has been proposed that a population of BHs with a mass of $20 - 10000M_{\odot}$ exist and are the accretors in these systems. This mass range fits between those of the two well-known BH populations: the stellar mass BHs described in Section 1.2.1 and the supermassive BHs in AGN, described in section 1.2.2, and so subsequently these BHs have been termed intermediate mass black holes (IMBHs) (Colbert & Mushotzky, 1999; Makishima et al., 2000). This is perhaps the simplest explanation for the properties of ULXs, and a clear advantage of this model is that it requires no new physics: ULXs are simply XRBs with very massive accretors. There is as yet no consensus on how a BH of this mass could form. As I discussed in section 1.2.1, one possibility is that they are formed in very low metallicity environments. Alternatively, the primordial collapse of Population III stars could be the progenitor of a population of IMBHs in the present epoch (Madau & Rees, 2001). Other authors have proposed binary evolution as a route to massive BH formation (Fryer & Kalogera, 2001). Further models involve mergers in dense environments (Miller & Colbert, 2004), be it either mergers of massive stars in superstar clusters (Portegies Zwart & McMillan, 2002), or mergers of lower mass BHs (Miller & Hamilton, 2002).

1.5.2 Beamed emission from stellar mass black holes

As an alternative to the IMBH hypothesis, some authors suggest that the compact objects in these sources are stellar-mass BHs. The theoretical difficulty is then to reconcile a low BH mass with the apparent ultraluminous X-ray emission. One way of doing this is to presume that the sources are not truly 'ultraluminous'.

It is possible that the high inferred X-ray luminosities of these sources are overestimations. These determinations are dependent on the assumption that the emission from ULXs is isotropic. If the emission is beamed towards the observer, then these sources are not 'ultraluminous' since the Eddington limit need not be violated. The theoretical difficulty with these models is understanding the accretion physics that would lead to heavily collimated emission. King et al. (2001) proposed that the geometry of the accretion disc might lead to beamed emission. If the disc were to have a lower scattering optical depth over a small range of solid angle, the X-ray emission would preferentially emerge in those directions. Alternatively, the observed emission could be Doppler-boosted in relativistic jets (Körding et al., 2002; Fabrika, 2004), so that ULXs are analagous to the microquasars observed in our own Galaxy.

1.5.3 Super-Eddington accretion onto stellar mass black holes

The beaming argument cannot account for all ULXs, since I will show in Section 1.6 that there is observational evidence for some being truly ultraluminous (Fabbiano, 2004). As an alternative to the beaming scenario, one can presume that the BHs are somehow accreting at super-Eddington rates. It has therefore been proposed that some sources are stellar mass BHs at super-Eddington rates. Again, the theoretical difficulty is understanding the accretion physics which would lead to this state. Super-Eddington accretion is by no means impossible: the determination of the Eddington luminosity contains a number of approximations which may not be valid for all sources. For example, it assumes both the infalling matter and the outgoing radiation is isotropic. One proposed model in which the Eddington limit is defeated involves collimation by an inhomogeneous accretion disc. A disc dominated by radiation pressure may exhibit strong density clumping. If the density inhomogeneities are on length scales much smaller than the disc scale height, such clumpy accretion discs could permit the radiation luminosity to exceed L_{Edd} by factors of $\sim 10 - 100$ (Begelman, 2002). Other authors have suggested that super-Eddington accretion can occur in BH systems through a thin disc covered by a hot, Comptonizing corona (Socrates & Davis, 2005; Done & Kubota, 2006).

1.6 Observational evidence for ULX models

1.6.1 X-ray observations of ULXs

X-ray spectra

The X-ray emission from both of the established classes of BH in the universe is thought to originate within the accretion disc. The spectrum can often be fit, to first order, to a power law, or a power law with a disc blackbody component (Colbert & Mushotzky, 1999). The power law component is hard and is a result of Comptonization in the optically thick disc. The blackbody component is soft and is a result of thermal emission processes. Sources which feature a blackbody-like spectrum are unlikely to be relativistically beamed. Emission from relativistically beamed electrons would be expected to be non-thermal direct synchrotron emission or optically thin Componized emission, both of which would produce a power law spectrum.

There is a relationship between the maximum colour temperature $T_{col}^{(max)}$ of the accretion disc and the BH mass, given by

$$T_{col}^{(max)} \simeq 1.3\mathrm{keV} \left(\frac{T_{col}/T_{eff}}{1.7}\right) \left(\frac{\dot{M}}{\dot{M}_{Edd}}\right)^{1/4} \left(\frac{M}{7M_{\odot}}\right)^{-1/4} \tag{1.10}$$

(Ebisawa et al., 2001), where T_{eff} is the effective disc temperature and $\dot{M}_{Edd}$ is the Eddington mass accretion rate, so that $\dot{M}/\dot{M}_{Edd} = 1$ gives the Eddington luminosity as defined in Equation 1.8. By fitting models to X-ray spectra, this $T \propto M^{-1/4}$ relationship between disc temperature and BH mass has been observed to be valid for both stellar mass and supermassive BHs (Makishima et al., 2000; Porquet et al., 2004; Gierliński & Done, 2004). If the X-ray spectra of ULXs are also described well by this model, then the disc temperature can be used to determine the mass of the BH in these systems.

From Equation 1.10, one would expect an IMBH to have a colour temperature of $<$ 1keV. Analysis of *ASCA* data showed many ULXs have $T_{color} >$ 2keV, which is inconsistent with a high BH mass (see *e.g.* Colbert & Mushotzky 1999; Makishima et al. 2000). This may be evidence for stellar mass BHs in these systems, although alternative models were proposed to account for this discrepancy, such as the advection-dominated optically thick 'slim' disc (Ebisawa et al., 2003). It has also been noted that Equation 1.10 assumes a Schwarzschild BH. If the accretors in ULX systems were Kerr BHs, then for the same mass they would have a lower inner radius and hence a higher disc temperature.

XMM-*Newton* and *Chandra* offered significant advances over *ASCA* in terms of spatial resolution and sensitivity at soft wavelengths. Observations with these observatories resulted in the detection of low temperature components which can be fit well with blackbody spectra with $0.1 < kT <$ 0.3keV (Miller et al., 2004a,b; Roberts et al., 2005). These low temperatures are indicative of a massive BH. One example is ULX X-7 in NGC 4559. The spectrum of this source is fit well by a power law and a blackbody-like component with $kT \sim$ 0.14keV (Cropper et al., 2004). If this temperature is used to derive an inner disc radius, and if this radius is assumed to be the last stable orbit around a Schwartzschild BH, the implied BH mass is $\sim 1.6 \times 10^3 M_\odot$, which in turn implies a bolometric luminosity of $L_{bol} \sim 6 \times 10^{40}$ergs s^{-1}. However, the validity of the spectral fits from which these low temperature components have been determined has been called into question (Goncalves & Soria, 2006). Some authors have proposed that alternative spectral models fit well with the data (Stobbart et al., 2006; Goad et al., 2006). These fits support high-temperature, super-Eddington discs around a lower mass BH. Goad et al. (2006) examined ULX X-1 in Holmberg II and suggested its BH mass to be no more than $100 M_\odot$. Stobbart et al. (2006) examined thirteen ULXs and from these conclude that the majority of the ULX population have masses of $< 80 M_\odot$, although they note they cannot rule out the presence of more massive BHs in individual cases. In general, it is apparent that the determination of BH masses from ULX X-ray spectra is highly model dependent.

Time variability

Many ULXs display random or periodic variability in X-rays on timescales of months to years: a study by Colbert & Ptak (2002) estimated random variability of > 50% in over half of the ULX population. This is strong evidence that ULXs are indeed single, compact sources, rather than SNR or a cluster of lower luminosity XRB. While SNR can have luminosities of $\sim 10^{39}$ergs s^{-1}, they remain constant or fade in luminosity over that timescale. Similarly, a cluster of X-ray sources would not show this degree of variability.

Some ULXs have shown variability on timescales of the order of hours. Some examples include the source CGX-1 in the Circinus galaxy, in which a periodic variation of 7.5hr was claimed by Bauer et al. (2001), the ULX in IC 342 where there is evidence for a 31 or 41hr period (Sugiho et al., 2001), and the ULX in M51 which was observed to vary by more than 50% in $\sim$ 2hrs (Terashima & Wilson, 2003). While variability on this timescale could have a number of causes, it is comparable to what would be expected to be the orbital period in these systems. Currently, these claims of periodicity are based on observations of only a few cycles. Further study will reveal whether these periods are orbital, in which case they would be highly coherent.

Some ULXs show variability on much shorter timescales, and analysis of this variation provides clues to the mass of the accreting object. There is evidence through examination of the power density spectra (PDS) of AGN and Galactic BHs that, for similar accretion states, various characteristic timescales scale with BH mass (Markowitz et al., 2003; McHardy et al., 2006). The PDS can be fit with a power law which breaks at a certain frequency. This frequency, along with the accretion rate, gives an indication of the BH mass. The break frequency for some ULXs is low, indicative of an accretor that is more massive than Galactic BHs (NGC 4559 X:7: Cropper et al. 2004; NGC 5408 X-1: Soria et al. 2004). In addition to low frequency breaks, the PDS of some ULXs reveal quasi-periodic oscillations (QPOs). Unlikely the sharply defined features which represent variation at one particular frequency, QPOs show up in PDS as features spread over a range of frequencies. QPOs have been observed in numerous ULXs (M82 X-1: Strohmayer & Mushotzky 2003; Holmberg IX X-1: Dewangan et al. 2006; NGC 5408 X-1: Strohmayer et al. 2007) with mean frequencies lower than those observed in Galactic BHs. The fact that QPOs are observed in these sources is evidence against beaming. The QPO is thought to originate in the disc. If the observed emission contained a large beamed component, then the amplitude of the disc variation would need to be extremely high in order to be observable. In addition, the lower mean frequency could suggest a larger X-ray emitting region, and hence a more massive BH.

1.6.2 Population studies of ULXs

Some authors have performed population studies of ULXs, in order to determine their environments and their luminosity function. ULXs can occur in any type of galaxy, but they tend to be more prevelant in star forming galaxies (Humphrey et al., 2003). They tend to be associated with young stellar populations (Swartz et al., 2004), and are commonly found in interacting galaxies such as the Antennae (Zezas et al., 2006).

Population studies based on the luminosity function of ULXs suggest that, if the compact object in these sources are IMBHs, then the upper limit on the mass is more modest than previously thought. A break in the luminosity function at

$\sim 2.5 \times 10^{40}$ergs s^{-1} (Swartz et al. 2004; Gilfanov et al. 2004) suggests the bulk of the IMBH population lies below $\sim 150 M_{\odot}$, assuming accretion at the Eddington limit. Swartz et al. (2004) conclude that the ULXs are a heterogenous class of objects. They claim ULXs found in star forming galaxies mainly originate in a young, short-lived population, and can be classified as part of the known population of HMXB. Conversely, the number of ULXs found in early type galaxies scale with BH mass and Swartz et al. (2004) suggest these sources can be attributed to the high-luminosity end of the LMXB population.

1.6.3 Multiwavelength observations

Optical associations

Optical studies of ULXs have been useful in understanding these sources. It has been observed that a number of ULXs are associated with extended, diffuse Hα nebulae (Pakull & Mirioni, 2002; Miller et al., 2003). A natural explanation for these nebulae is that they result from illumination of the interstellar medium by the X-ray source. The implication is that the emission from the X-ray source is not significantly beamed. The extent of these nebulae ($\sim$ 100pc in some cases) can be used to derive an the age of the ULX as an active X-ray source (Pakull et al., 2006), which provides clues as to the formation and history of the compact object.

As well as the photoionised nebulae observed around many ULXs, observations with *HST* and 8m-class ground based telescopes have, in a number of cases, identifed one or more candidates for the optical counterparts of various ULXs. Many observations showed that ULXs are associated with young stellar clusters (*e.g.* in the Antennae, Zezas et al. 2002; in M81, Matsushita 2000). Further observations revealed optical counterparts with luminosities and colours consistent with being blue, single stars (*e.g.* Liu et al. 2002, 2004; Kaaret et al. 2004; Kuntz et al. 2005). If all of this light comes from a donor star that is indistinguishable from a single star, then the blue colour of the counterparts suggest massive, early type donors.

The high mass transfer rates implied by the observed X-ray luminosities also suggest massive donor stars. However, other authors have claimed that the optical emission in these sources will be dominated by light from the accretion disc (Pakull et al., 2006).

Radio associations

As in the optical case, the association of radio emission with any ULX provides a useful tool with which to probe its nature. The $L_X = 10^{40}$ergs s^{-1} ULX in NGC 5408 is a case in point. (Kaaret et al., 2003) reported unresolved radio emission from this source, consistent with a beamed microquasar explanation for the ULX. However, more recent studies (Soria et al., 2006) have suggested that the radio emission is from a lobe powered by a jet from the BH, due to the radio flux and spectral index. Soria et al. (2006) also report speculative evidence that the radio emission is in fact resolved, which is inconsistent with the microquasar hypothesis.

Another unambigous radio source association is with the $L_X = 10^{40}$ergs s^{-1} ULX in Holmberg II (Miller et al., 2005). In this case the radio source is resolved and has a size of $\simeq$ 50pc, and is apparently associated with an HeII nebula surrounding the radio source. The optical nebula and the properties of the radio emission suggest isotropic X-ray emission from the ULX and a truly ultraluminous nature for this object.

1.7 Which model is correct?

Of the three classes of model, the IMBH hypothesis is conceptually the simplest explanation and involves no new physics. The argument that it is unknown how an IMBH would form is not particularly compelling since the existence of SMBHs in the universe shows that very massive BHs can form, given the right environments. ULXs are preferentially found in young, star forming environments; it is unclear as to whether the ULX or the environment is the progenitor in these cases. It may well be that these environments are ideal for the formation of massive BH.

On the other hand, some would argue that it is unnecessary to introduce an entirely new class of object when the observational data does not conclusively support such an introduction. Many ULXs can be adequately explained as normal XRB in unusual accretion states. There are additional difficulties with the IMBH scenario beyond those which have already been mentioned: for example if ULXs are indeed emitting isotropically the accretion rate in these systems must be very high. The-lifetime of the donor star will be correspondingly short. This implies there must be very many 'quiescent' ULXs for every one that is observable as an X-ray source in the current epoch (King et al., 2001). Any formation scenario for IMBH must account for this large 'quiescent' population.

It seems increasingly likely that the ULX population is heterogeneous, with evidence to support stellar mass BHs in some cases and IMBHs in others (Fabbiano, 2004). The sources with X-ray luminosities $\sim 10^{39}$ergs s^{-1} may be more easily explained as stellar mass BHs, but objects with luminosities of $> 10^{40}$ergs s^{-1} are good candidates for IMBHs. It may be that many sources are both more massive than Galactic stellar-mass BHs, perhaps in the $\sim 20 - 100M_{\odot}$ range, and additionally are in a high state of accretion, and exhibiting mildly super-Eddington behaviour. However, the observational data, as it stands, has been unable to definitively resolve the nature of even one of these objects.

1.8 Open Questions

The focus of most of the investigation into ULXs has been to determine the mass of the BH. If ULXs contain stellar mass BHs, then an advance in our understanding of accretion processes in binary systems is necessary in order to resolve their natures. There are many possibilities. It may be that these sources are not that peculiar, and a short-duration ULX phase is common in XRB. Conversely, an IMBH interpretation for ULXs throws up very different questions, mainly related to how these objects are formed, and how populous they are. The confirmation of the existence of IMBH could lead to a deeper understanding of BH as a whole. As I noted in Section 1.2.2, it is still a mystery how SMBHs were formed. A continuous BH mass spectrum would suggest an evolutionary link between the three classes, thus allowing us to better understand BH formation in the younger universe.

It is also important to resolve the nature of the donor star in these systems. A super-Eddington state of accretion or an IMBH may require a donor with specific characteristics. The mass of the donor star is an indication of the lifetime of the ULX as an X-ray source, since the mass accretion rate necessary to support X-ray emission at ULX rates will result in low mass stars being completely consumed on a timescale that is much shorter than their normal evolution. An understanding of the lifetime of ULXs is an indication of the number of 'quiescent' ULXs in the universe, which is particularly important if the accretor in these systems is an IMBH.

The environments of ULXs prompt a number of questions. ULXs are observed in all types of galaxies, but we see more in interacting galaxies, such as the Antennae. ULXs tend to be found in metal-poor regions, and are commonly associated with regions of active star formation. The question of why ULXs 'prefer' these environments is open. In the case of the association with star forming regions, one can ask whether these regions are conducive to the formation of ULXs, or whether the region itself formed due to an existing ULX. The extent of the photoionised nebulae around some ULXs is also of interest, since this is another indication of the lifetime of the ULX as an X-ray source.

Finally, the evolution and history of ULXs are of interest. Understanding the nature of the donor star may lead to an understanding of how these systems form. If the BH and the donor are coeval, then determination of the parameters of the donor leads to information about the BH (age, local conditions at time of formation). If the donor was captured by the BH some time after their formation, then the statistics of the spectral type and mass distribution of the donor stars can be used to set constraints on the capture rate and hence provide estimates to the IMBH populations.

1.9 Motivation for investigating the optical counterparts of ULXs

In Section 1.6.1 I pointed out that the X-ray data can be interpreted in a variety of different ways. The X-ray emission from the disc in the immediate environment of the ULX is highly model dependent, and the physics at these high accretion rates near the event horizon is poorly understood. In this thesis an alternative channel is sought by which the nature of ULXs can be elucidated.

Assuming the X-ray emission is isotropic, the optical/infrared (optical/IR) properties of the donor star and accretion disc will be strongly influenced by the proximity of such an intense X-ray radiation field. In particular, the heating effect of the X-ray radiation incident on the surfaces of the a star and disc will induce intensity and colour shifts compared to normal stars, and these will vary at orbital periods. X-ray irradiation has been shown to drive evolution in XRB (Podsiadlowski, 1991; Ruderman et al., 1989), and cause significant colour and magnitude changes of the optical counterpart. This has been observed in the sub-Eddington regime. One example is the Her X-1 system, an X-ray binary consisting of a neutron star accreting matter from a non-degenerate stellar companion. The X-ray luminosity is a third of the Eddington luminosity (Howarth & Wilson, 1983), and the binary period is 1.7 days. The neutron star accretes matter via Roche lobe overflow through an accretion disc (Vrtilek et al., 2001), and so is a good analogy to ULX systems. The star has been observed to change spectral type from A to B over the binary period. Bahcall & Bahcall (1972) observed a B magnitude amplitude of 1.5 mag and interpreted this variation as a result of X-ray heating of a late A-type star. Other authors interpret the variation in terms of heating of the star and a tilted, precessing accretion disc (Gerend & Boynton, 1976; Howarth & Wilson, 1983).

If X-ray irradiation can affect the optical emission from the binary in the sub-Eddington regime, then one would expect it to have a strong effect in ULXs and be a useful diagnostic of their nature. The optical emission originates in the accretion disc and the star, so any model would have to account for both of these components, since it is unclear as to which component (if any) will dominate the emission. It may be that the star is the dominant optical component, as in the case of high mass X-ray binaries, and has been assumed in most studies of ULX optical counterparts to date. Alternatively, theoretical modelling has shown that the heated accretion disc might dominate (Rappaport et al., 2005), analogous to low mass X-ray binaries. A model of the optical emission from ULXs could answer this question, and may shed light on all of the questions raised in Section 1.8.

1.10 Structure of this thesis

In Chapter 2 the model used to investigate the Optical/IR emission from ULXs is discussed. I introduce each component of the model individually, and then show how these are combined in order to provide an accurate model of opt/IR emission in ULXs. The basic results of the model is then be outlined by inputting sample parameters and examining the effects.

In Chapters 3 and 4 I apply the model of Chapter 2 to all of the available photometric data of ULX counterparts. I begin in Chapter 3 by discussing and justifying the input parameters which I use, and I go on to presented results for each source in turn. The results in that chapter are for sources where only a single set of observational data exists. In Chapter 4 I present results for sources for which there are observations at multiple epochs. For these sources, I make additional comments on any variability observed in the optical data.

In Chapter 5 I collect and analyse the results of Chapters 3 and 4. I discuss the nature of the donor stars, and I examined the effect of these results on our understanding of evolution and history of ULXs. I detail the constraints I have determined on the BH masses in these systems, and I re-examine the various explanations as to the nature of ULXs in light of these results. Finally, I discuss potential systematic effects.

In Chapter 6 I summarise this work. I discuss how future observations of ULX counterparts can further reveal the nature of these sources, and make predictions for the sources I have examined.

Chapter 2

A description of the model

2.1 Introduction

In this chapter I detail the model constructed to study the optical emission from ULXs. The basic assumptions that underpin the model are listed, and I go on to describe the individual components that have gone into it. Finally, I demonstrate the basic results of the model when using example parameters.

2.2 Initial model assumptions

In constructing any model it is necessary to make a number of assumptions as to the nature of the system that is being modelled. I therefore begin by first explicitly identifying the fundamental assumptions that underly this work. As I detail the various components of the model further, I will discuss and justify any more detailed assumptions I have made about the nature of ULXs.

2.2.1 ULX composition

Firstly, it is assumed that ULXs are binary systems, consisting of a compact object and a companion star that are gravitationally bound to each other.

Secondly, the compact object is a black hole. Note that no assumptions are made about the BH mass. Neither are any assumptions made as to the properties of the companion star, save that is not a compact star: it is an active MS or evolved object.

Thirdly, it is assumed that matter is being transferred from the companion (or 'donor') star onto the BH. It is this material that is the source of the observed X-ray emission.

It is fair to say that these assumptions are generally accepted to the point that they form part of the definition of ULXs as a class of objects. I will therefore not justify these assumptions further.

2.2.2 Electromagnetic emission

It is assumed that the matter from the donor is being transferred to the compact object via an accretion disc, in order to conserve the angular momentum of the transferred matter. I assume in this work that the observed light which makes up the optical/IR counterpart of ULXs originates only from this disc and the companion star – there is no other source of opt/IR emission in the system.

The X-rays originate from the inner region of the accretion disc. The premise behind this work is that the intense X-ray radiation field has a modifying effect on the optical/IR properties of the star and the outer regions of the disc. However, as was detailed in Section 1.6 there is evidence for non-beamed emission in many ULXs. I therefore assume that the X-ray emission is isotropic.

There may indeed be some degree of beaming in these sources – if there is beaming then the X-ray illumination must be reduced by the beaming factor. Hence the suggestions of King et al. (2001), Körding et al. (2002) and Fabrika (2004) can be accomodated if necessary. I have chosen here to use the simplest case where the emission is completely isotropic, and hence mention this as a potential systematic effect.

2.3 Introduction to the model components

There are three separate components to the model detailed in this chapter.

The first component is the donor star itself. For the stellar parameters, I use publically available sets of stellar evolutionary tracks. I model it geometrically to account for its binary nature. I then determine the optical/IR luminosity of the star, accounting for darkening effects and the influence of the X-ray radiation field.

The second component is the accretion disc. I assume a geometric disc model and calculate its optical/IR luminosity, which results from a combination of viscous forces in the disc and the X-ray irradiation.

The third component is the BH which makes its presence felt through its gravitational field.

Through the combination of these components I calculate a combined optical/IR luminosity for a binary system, for any given set of input parameters. Some of these parameters I set, such as the inclination, orientation, BH mass, X-ray luminosity etc.

Finally, I model the mass transfer rate in these systems. The mass transfer can be inferred from the X-ray luminosity and is most likely driven by the nuclear evolution of the donor. This can be determined from the assumed stellar evolutionary tracks, so this allows the application of more constraints to the system parameters beyond those available from the opt/IR data.

2.4 Modelling the donor star

The temperature of the donor star is not constant over its entire surface. Various physical effects cause the temperature and hence the emergent optical radiation to vary from point to point. In this section I will describe these effects and how I have accounted for them in constructing the model. This section is divided into three subsections. I first discuss effects which affect the geometry of the star itself, then the darkening effects on the star which occur irrespective of the external X-ray radiation field, and finally the effect of the X-ray irradiation on the star.

2.4.1 Stellar geometry (1) - Semi-detached binaries

I begin by examining the constraints we can apply to the system geometry. At the simplest level the binary period P can be related to the binary separation a and the masses of the primary and secondary (M_1 and M_2 respectively) through Kepler's laws. In this section I will show how the geometry of the star can be described completely, given these three parameters and some assumptions about the mass transfer.

Mechanics of the mass transfer

In Section 2.2 it was noted that there is an interaction between the two binary components, in that mass is being transferred from the secondary (the donor star) to the primary (the BH). There are two possible causes for this mass transfer. Firstly, material is ejected from the donor in the form of a stellar wind. Some of this will be captured gravitationally by the primary. Secondly, evolution of the binary may cause part of the envelope of the donor to fall under the gravitational influence of the BH, and be lost from the donor.

The X-ray emission of the ULX is a consequence of the mass accretion from the donor onto the BH. The mass transfer rate can therefore be estimated from the X-ray luminosity. The relationship between accretion luminosity and mass transfer rate was given in Equation 1.4. If an accretion efficiency of $\eta = 0.1$ is assumed, this equation implies an accretion rate of $\sim 1.8 \times 10^{-6} M_{\odot}\mathrm{yr}^{-1}$ for an X-ray luminosity of $10^{40}\mathrm{ergs\ s}^{-1}$ (as found in the brightest ULXs). If the accretion is taken to be driven via a stellar wind, the donor star must therefore be losing mass at a rate of $\sim 10^{-4} M_{\odot}\mathrm{yr}^{-1}$, since only a few percent of the mass expelled by the star will be gravitationally captured by the BH. This is too high to be generally available, based on our current knowledge of stellar evolution.

The faintest ULXs have X-ray luminosities of $L_x \sim 10^{39}$ergs s^{-1}, which requires a wind loss rate of $\sim 10^{-5} M_{\odot}\mathrm{yr}^{-1}$. A massive supergiant can have wind losses at this rate over a small part of its lifetime, so stellar wind accretion cannot be ruled out for every object in the ULX class. However, this is unlikely to be the mass transfer mechanism for most sources, so in this model it is assumed that active removal of material by the gravitational influence of the BH is the driver of the mass transfer.

Roche lobe overflow

The gravitational potential for a two-body system is given by the Roche potential (Frank et al., 2002),

$$\begin{aligned}\Phi(x,y,z) = & \frac{-GM_1}{\sqrt{(x+a)^2+y^2+z^2}} - \frac{GM_2}{\sqrt{x^2+y^2+z^2}} \\ & -\frac{\Omega_{orb}^2}{2}[(x+a(1-\mu))^2+y^2] \end{aligned} \tag{2.1}$$

Where

$$\Omega_{orb} = \frac{2\pi}{P} \quad P^2 = \frac{4\pi a^3}{G(M_1+M_2)} \quad \mu = \frac{M_2}{(M_1+M_2)}$$

and M_1, M_2 are the masses of the primary (BH) and the secondary (donor star) respectively, and a is the binary separation; the distance between the centres-of-mass of the two objects.

The coordinate system here rotates with the binary and is defined with the origin at the centre of the secondary, with the x-axis aligned along the line of centres of the secondary and the primary, with the primary in the negative x direction. The z-axis is perpendicular to the orbital plane and the y-axis is in the direction of orbital motion of the primary. The Roche solution assumes circular orbits of the two components in a plane, and they are regarded as point masses for dynamical purposes. This is usually a good approximation for binary systems.

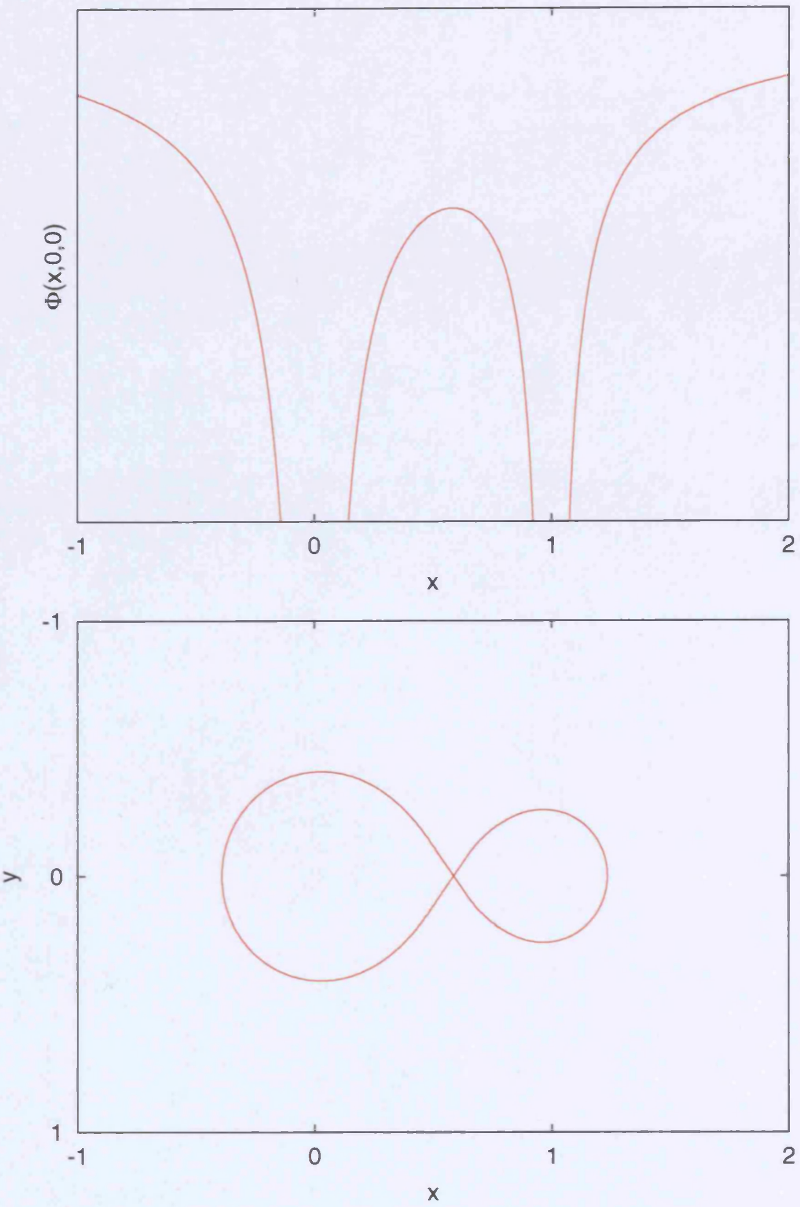

Figure 2.1: An illustration of Roche lobe geometry in one and two dimensions. In the top plot, the Roche potential along the $(x, 0, 0)$ axis is hown. The x-axis scale is given in units of a, where a is the binary separation. The mass ratio M_2/M_1 is set to 0.5, with the centre of mass of the primary at $x = 0$ and the centre of mass of the secondary at $x = 1$. The L1 point is the point between $x = 0$ and 1 where $\frac{\partial\Phi(x,0,0)}{\partial x} = 0$. In the bottom plot the equipotential surface in the (x, y) plane of the potential at the L1 point is shown. These equipotentials are the Roche lobes of the primary and secondary.

I show in the first plot of Figure 2.1 the one-dimensional Roche potential along the $\Phi(x, 0, 0)$ axis. The 1st Lagrangian Point (L1), at which the gravitational influences of the primary and secondary component are equal and opposite, is labelled. In the second plot the equipotentials through the L1 point are shown. These equipotentials define critical surfaces around the primary and secondary, known as the Roche lobes.

When the Roche potential is examined in three dimensions it can be seen that the L1 point is a saddle point, so material inside one Roche lobe in the vicinity of L1 will pass more easily into the other Roche lobe than into the space outside of this critical surface. The mechanism for the mass transfer from the donor to the BH is therefore apparent; if the donor is in hydrostatic equilibrium in this two-body system, the surface of the star must lie on the equipotential which passes through the L1 point. Any further perturbation of the star will cause material to be pushed over the L1 point, and hence captured and accreted by the BH.

When the donor star fills its Roche lobe, the binary is described as a semi-detached system. Mass-transfer will occur as long as the star remains in contact with its Roche lobe.

By taking Kepler's third law into account (the relationship for orbital period, P, defined above as part of Equation 2.1) it can be seen that

$$\Phi(x, y, z) = \frac{GM_1}{a} F\left(\frac{x}{a}, \frac{y}{a}, \frac{z}{a}, q\right) \tag{2.2}$$

demonstrating explicitly the fact that the shapes of the Roche equipotentials $\Phi =$ const are functions only of the mass ratio $q = M_2/M_1$, and their scale is determined by a (*e.g.* Warner 1995).

An important consequence is that the system can be scaled based on the fact that the donor is filling its Roche lobe. The volume of this lobe will be equal to the volume of the spherical, undistorted star. R_L is defined to be the 'volume radius': the radius of a sphere with the same volume as the secondary Roche lobe. There are various approximate analytic formulae for R_L. The formula of Eggleton (1983)

$$\frac{R_L}{a} = \frac{0.49q^{2/3}}{0.6q^{2/3} + \ln(1 + q^{1/3})} \tag{2.3}$$

is used in this work, which is accurate to within 1% for any mass ratio. Consequently the geometry of this binary system can be described by three parameters: the masses of the two components and the radius of the undistorted secondary star.

2.4.2 Stellar geometry (2) - Radiation pressure effects

The X-ray irradiation will have an effect on the optical/IR colours of the donor star: this is discussed later. I first consider the effect it will have on the geometry of the donor star, through irradiation pressure effects. For this the formulation of Phillips & Podsiadlowski (2002) is used. This is a simple formulation for irradiation pressure in binary systems which uses a modified Roche potential, in which the radiation pressure force is parameterised using the ratio of the radiation to the gravitational force. The limitation of this formulation is that it does not allow for any surface motion. In reality the external irradiation will drive circulatory currents in the stellar surface, and a full treatment will require all hydrodynamical motions to be considered (see, *e.g.*, Beer & Podsiadlowski 2002). Such a model is beyond the scope of this work. The Phillips & Podsiadlowski (2002) formulation is therefore something of an extreme case. Moreover there is some doubt that the surface will be modified at all – see for example Howarth (1997). Until a concensus is reached we allow for such effects using the Phillips & Podsiadlowski (2002) formulation as an option. Through application of this formulation it is possible to investigate the regions of the parameter space where this effect may be important.

Phillips & Podsiadlowski (2002) begin with the equation of hydrostatic equilibrium and modify it to account for the external radiation pressure. They go on to express the forces resulting from gravity and radiation pressure from the primary as a 'reduced' gravitational force

$$\mathbf{F}^{eff}_{grav} = \mathbf{F}_{grav} - \mathbf{F}_{rad} = (1 - \delta)\mathbf{F}_{grav}, \tag{2.4}$$

where δ is the dimensionless ratio $|\mathbf{F}_{rad}|/|\mathbf{F}_{grav}|$.

This reduced force from the primary can be extended to define a reduced potential. The Roche equation as expressed in Equation 2.1 is therefore modified to

$$\Phi(x,y,z) = \frac{-GM_1[1-\delta(x,y,z)]}{\sqrt{(x+a)^2+y^2+z^2}} - \frac{GM_2}{\sqrt{x^2+y^2+z^2}} \\ -\frac{\Omega_{orb}^2}{2}[(x+a(1-\mu))^2+y^2] \tag{2.5}$$

The form of δ is a constant term multiplied by $\cos\gamma$, where γ is the angle between the flux vector and the normal vector of the irradiated surface. The constant is the maximum value of δ, which is obtained when these two vectors are parallel, so this constant is termed δ_{max}. Phillips & Podsiadlowski (2002) go on to show that

$$\delta_{max} = q\frac{L}{L_{Edd}}, \tag{2.6}$$

where q is the mass ratio M_2/M_1.

As the value of δ_{max} increases, the radiation pressure force increases over the entire stellar surface. If δ_{max} is greater than 1, then the radiation pressure force at the L1 point (where $\cos\gamma = 1$) will be greater than the gravitational force from the primary. This will cause detachment from the L1 point. It is apparent from Equation 2.6 that the radiation pressure force will be larger if the primary is a stellar mass BH than if it is an IMBH; in the stellar mass BH case the mass ratio q will be ~ 1, and the ratio L/L_{Edd} will exceed 1 by a factor which depends on the X-ray luminosity. In the IMBH case, the mass ratio q will most likely be ~ 0.1 and the ratio L/L_{Edd} will be less than 1, and so the value of δ_{max} will therefore be substantially lower.

As I have noted, this radiation pressure formulation does not account for circulation currents. The assumption that the surface is an equipotential effectively assumes that these currents are minimal, and hence this model represents an extreme case, with the other extreme being the unperturbed Roche potential. It should be noted that the modified potential described here introduces a fictitious and unphysical force. However, Phillips & Podsiadlowski (2002) note that the formulation provides a good representation of the actual forces if enough boundary conditions to the surface are provided. This can be done since many points on the surface will be shadowed by the star or accretion disc and their positions will therefore be unmodified by radiation pressure.

The simplest condition is as follows

$$\delta(x,y,z) = \begin{cases} \delta_{max}\cos\gamma(x,y,z) & \text{if } \cos\gamma > 0 \\ 0 & \text{otherwise} \end{cases} \tag{2.7}$$

which results in points which are not in the line of sight of the X-ray source being unperturbed by radiation pressure. However, this can be modified to account for an accretion disc in the system. The disc will be opaque, and will shield part of the star from the radiation. Phillips & Podsiadlowski (2002) use

$$\delta(x,y,z) = \begin{cases} \delta_{max}T\cos\gamma(x,y,z) & \text{if } \cos\gamma > 0 \\ 0 & \text{otherwise} \end{cases} \tag{2.8}$$

where T is a transmission function given by

$$T = \begin{cases} 0 & \text{if } \theta \leq \beta_1 \\ \frac{1}{2}\left\{1 - \cos[(\frac{\theta-\beta}{\alpha-\beta})\pi]\right\} & \text{if } \beta_1 \leq \theta \leq \alpha \\ 1 & \text{if } \theta \geq \alpha \end{cases} . \tag{2.9}$$

Here, θ is the angle between the x-axis and the point on the stellar surface. The disc is defined by α and β, where α is the opening (half) angle of the disc and β is the opening angle of the completely opaque part of the disc. Between β and α the disc transforms smoothly from opaque to transparent. Phillips & Podsiadlowski (2002) find the smooth sinusoidal dependence given by this form of T improves the rate of convergence in the numerical iteration process necessary to determine the modified equipotential surface.

All of the radiation pressure calculations made in this work will assume a thin accretion disc, with a geometry that will be defined in Section 2.5.1. When the L1 point is shadowed by an opaque disc, the possibility of radiation-pressure induced detachment of the star from this point is of course negated. Moreover, in the stellar mass / super-Eddington part of the parameter space where I noted the effect of radiation pressure is most significant, the disc may become extended and thick, which would increase the area of the star which is shielded. These issues will be discussed further in Section 2.9 and Chapter 5.

2.4.3 Darkening effects

Limb darkening

The intensity of optical radiation emergent from a star towards the observer is not constant over the entire stellar surface. The intensity of the stellar disc decreases as the observer moves his line of sight from the centre to the limb. This is due to the fact that visible surface of the star is at a constant optical depth over the surface of the entire disc. As the line of sight is moved towards the limb, this surface of constant optical depth is at an increasing distance from the stellar center. The material that is observed is therefore cooler and less dense towards the limb.

There are various analytical approximations for this effect. The simplest is the linear limb-darkening law

$$I(\mu)/I(1) = 1 - x(1 - \mu) \tag{2.10}$$

where I is the intensity at a point on the stellar surface and is a function of μ, where $\mu = \cos\theta$ and θ is the angle between the line of sight and the normal to the stellar surface. x is the linear limb-darkening coefficient, and is approximately 1/3, although it varies from star to star (see van Hamme 1993 for tables of limb-darkening coefficients, given as a function of effective temperature and surface gravity). Many authors have proposed non-linear limb-darkening laws (see, *e.g.*, Manduca et al. 1977; Wade & Rucinski 1985; Claret & Giménez 1990; Klinglesmith & Sobieski 1970), but the simple law is used in this work.

In the first plot of Figure 2.2 I illustrate the effect of limb darkening by plotting

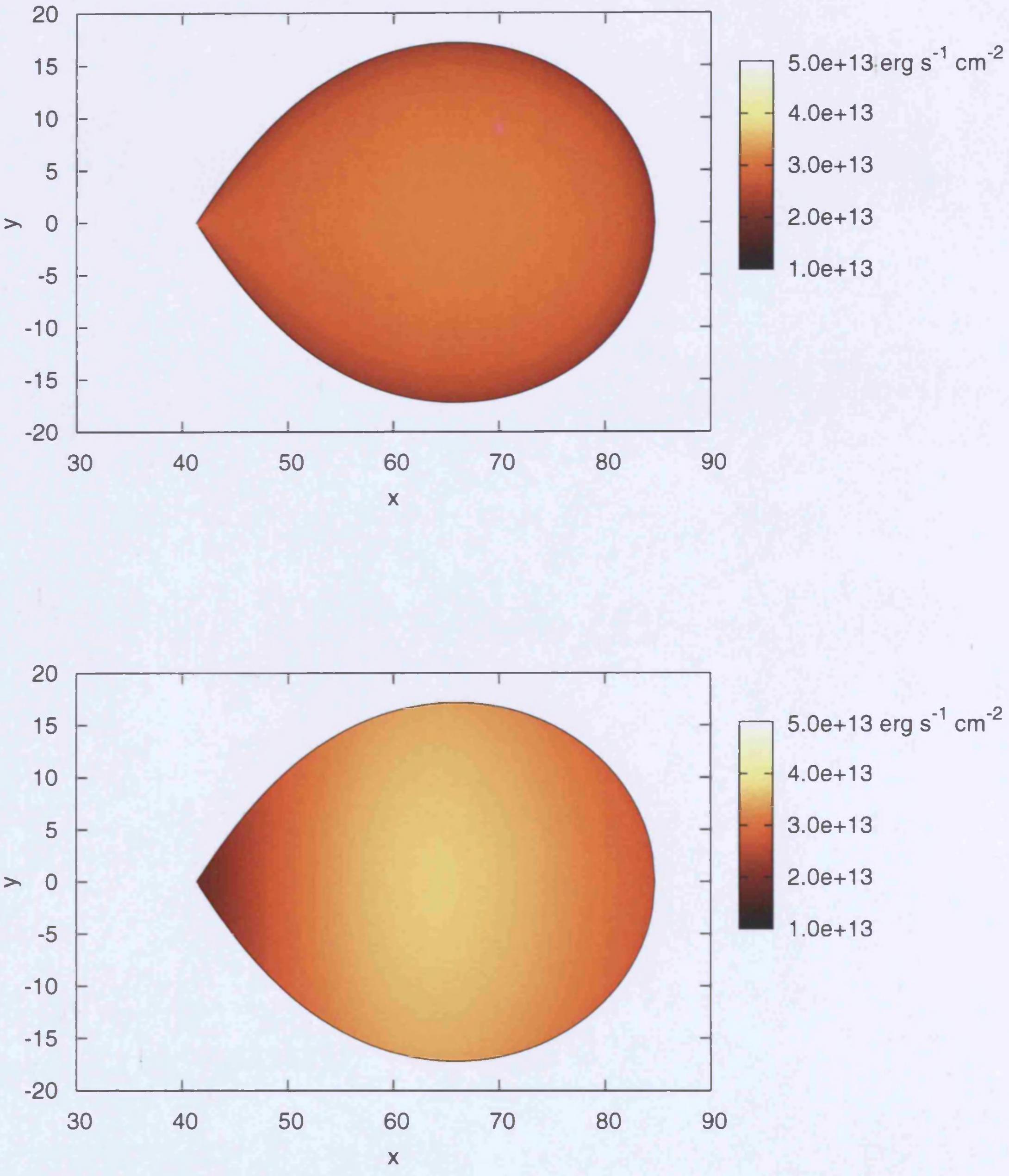

Figure 2.2: The variation in intensity $B(\tau)$ due to darkening effects, with $\tau = 2/3$. An O5V star and a BH mass of $150M_{\odot}$is used, and the effects of limb darkening (top) and gravity darkening (bottom) are shown separately. Projections in the orbital plane are plotted, with the labelled distances in units of $R_{\odot}$.

the emergent radiation over the surface of an O5 MS star, using the linear limb-darkening law.

Gravity darkening

Gravity darkening is an effect which is important for rotationally or tidally distorted stars in hydrostatic equilibrium. The surface gravity of a non-spherical star will not be constant over its entire surface. The gas in regions of lower surface gravity (such as the L1 point of a Roche lob filling star, for example) will be under less pressure, and will therefore be cooler and less dense. The von Zeipel theorem, also known as the gravity-darkening law, states that the emergent flux F from any point on the surface of the star varies proportionally to the local gravity acceleration g as $F \sim g^{\alpha}$, where α is the gravity-darkening coefficient (Von Zeipel, 1924). It follows that the effective temperature of any point on the star is expressed as $T_{eff} \sim g^{\beta}$, where $\beta = \alpha/4$ and is known as the gravity-darkening exponent.

Gravity-darkening has been studied by many authors, and the value of the gravity-darkening exponent has been examined both theoretically and observationally. The exponent varies with the internal composition of the star. It has been shown theoretically that if the energy transfer in the sub-surface layers of the star is purely radiative, then β is equal to 0.25 (Von Zeipel, 1924). Conversely, if a star has a convective envelope, then β has the theoretical value of 0.08 (Lucy, 1967). These theoretical values have generally been found to fit well with observation (see e.g. Djurašević 2003, 2006).

In this thesis I set the gravity darkening parameter β to be 0.25, representing a star with a purely radiative outer envelope. This is appropriate for the early type and evolved stars which are thought to be the donors in ULX systems. In the second plot of Figure 2.2 I illustrate this effect by plotting the emergent radiation over the surface of an O5 MS star. It can clearly be seen that the intensity of the star decreases with the local gravitational potential.

2.4.4 X-ray irradiation

I now consider the effect of the X-ray radiation on the star. I assume that the system is in a quasi-steady state, and the irradiated surfaces are in thermal, radiative, and hydrostatic equilibrium. This requires that the irradiated layers necessarily re-emit all of the radiation falling on them.

This problem could be approached very simply. I consider first the situation where we have a spherical donor star, the observer and star are in superior conjunction with respect to the BH, and the orbital plane of the binary is perpendicular to the observer's sky. The observer is therefore viewing the X-ray irradiated hemisphere of the star. If all the infalling radiation is re-emitted, the luminosity of the star will be the combination of the unperturbed luminosity of the star as a result of nuclear burning (L_2), and the luminosity as a result of X-ray irradiation. The X-ray flux at the surface of the star will be $L_1/4\pi a^2$, where L_1 is the X-ray luminosity and a is the binary separation. This will be incident on an area πR_2^2, where R_2 is the radius of the donor star. It is therefore apparent that the total observed luminosity L_{tot} of the star will be

$$L_{tot} = L_2 + \frac{1}{4}\Big(\frac{R_2}{a}\Big)^2 L_1. \tag{2.11}$$

There are a number of problems with this approach. Firstly, it does not account for the distorted, Roche lobe shape of the star as discussed in Section 2.4.1. Secondly, it does not account for the X-ray nature of incident radiation, and it does not contain any information about the nature of the re-radiated light. The majority of the X-ray emission may be effectively reflected and/or re-radiated at similarly short wavelengths for example, which would mean the spectrum of the star is a significant departure from a blackbody and the optical spectrum of the star is relatively unmodified. Finally, it does not account for the distribution of the absorbed and re-emitted radiation. All of the incident X-ray radiation is emitted towards the observer; there is no 'law of darkening' for this component.

The problem of the distribution of reprocessed radiation was approached by

Milne (1926), in the context of optical radiation incident on the surface of a star in a binary system. He used a plane-parallel model and a radiative transport formulation to describe this emission, and showed that reprocessed radiation shows greater darkening at the limb compared with unreprocessed light.

The plane-parallel model and radiative transport formulation of Milne (1926) was modified by Wu et al. (2001) to account for incident radiation at X-ray wavelengths. The modification is important because the hardness of the X-ray spectrum determines the depth at which the incident radiation deposits most of the energy. Soft X-rays are easily absorbed at the surface of the star by neutral and weakly ionized matter via bound-free transitions, while hard X-rays will only be attenuated at great depths when the matter density is significantly higher. The soft and hard X-ray components will subsequently have higher and lower opacities respectively than for the optical radiation. This means that a significant fraction of the energy in soft X-rays is deposited in the outer layers of the star, where the gas is optically thin to optical radiation. This energy is re-radiated at wavelengths shortward of the optical bands. In comparison, most of the energy from the hard X-rays is deposited deep in the star, at depths optically thick to optical radiation. This difference is most important in regions of the stellar surface where the X-rays have a grazing incidence. In these cases, the majority of the soft X-ray energy is deposited in the optically thin regions of the star, and a hot surface skin layer is formed. In general therefore, the effect on the optical properties is strengthened when the incident X-rays have a harder spectrum.

This work uses the model of Wu et al. (2001) to describe the effect of the X-ray heating on the donor star (see also Copperwheat et al. 2005). I will now summarise the model as presented in Wu et al. (2001) and Copperwheat et al. (2005).

Figure 2.3 shows the geometry of the Wu et al. (2001) plane-parallel model. The incident radiation is taken to be parallel beams of soft and hard X-rays, with effective fluxes πS_s and πS_h per unit area normal to the beams, and making an angle α to the normal to the stellar surface. The absorption coefficients of the soft

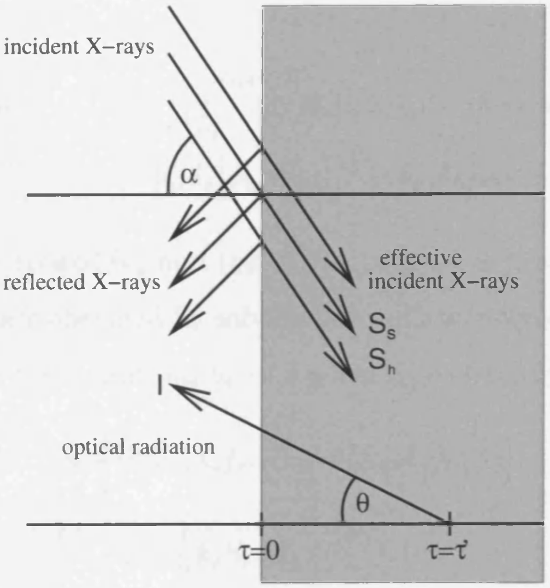

Figure 2.3: The geometry of the plane-parallel model (Wu et al., 2001)

and hard X-rays are $k_s\kappa$ and $k_h\kappa$ respectively, where κ is the absorption coefficient of the optical radiation. The soft/hard X-ray convention is defined in terms of these coefficients, with $k_s > 1$ and $k_h < 1$. The band boundary is a parameter to be determined.

The total blackbody radiation flux is a combination of a component $B_x(\tau)$ as a result of irradiative heating by the incident X-rays and the component of the radiation from the star in the absence of irradiative heating $B_s(\tau)$, where τ is the optical depth. The irradiative heating component $B_x(\tau)$ was solved in the limit of a semi infinite plane by the method of successive approximations and was found to be

$$B_x(\tau) = a - b_s \exp(-k_s\tau \sec\alpha) - b_h \exp(-k_h\tau \sec\alpha) \tag{2.12}$$

in the second approximation (Wu et al., 2001), where a, b_s and b_h are constants to be determined by the boundary conditions. For a semi-infinite slab opaque at optical wavelengths, the emergent optical/IR radiation in the direction θ is the Laplace transform of $B_x(\tau)$

$$\begin{aligned} I(0,\mu) &= \lim_{\tau_{tot}\to\infty}\Big[\int_0^{\tau tot} d\tau B_x(\tau)\exp(-\tau/\cos\theta)\Big] \\ &= a - b_s\mathcal{A}_s\big[\mathcal{A}_s+\mu\big]^{-1} - b_h\mathcal{A}_h\big[\mathcal{A}_h+\mu\big]^{-1} \quad\cdot \end{aligned} \tag{2.13}$$

where $\mathcal{A}_s$ and $\mathcal{A}_h$ are $(\cos\alpha)/k_s$ and $(\cos\alpha)/k_h$ respectively, and $\mu = \cos\theta$.

Here a, b_s and b_h are obtained by solving the radiative-equilibrium and radiative transfer equations for the conditions $b_s \to 0$ when $S_s \to 0$ and $b_h \to 0$ when $S_h \to 0$:

$$a = \frac{1}{2}\Big[k_sS_s\mathcal{A}_sf_s(\alpha) + k_hS_h\mathcal{A}_hf_h(\alpha)\Big] \tag{2.14}$$

$$b_s = \frac{1}{2}k_sS_s\Big[\mathcal{A}_s - \frac{1}{2}\Big]f_s(\alpha) \tag{2.15}$$

$$b_h = \frac{1}{2}k_hS_h\Big[\mathcal{A}_h - \frac{1}{2}\Big]f_h(\alpha) \tag{2.16}$$

where the functions $f_s(\alpha)$ and $f_h(\alpha)$ are given by

$$f_s(\alpha) = \Big[1 - \mathcal{A}_s + \mathcal{A}_s\Big(\mathcal{A}_s - \frac{1}{2}\Big)\ln(1 + k_s\sec\alpha)\Big]^{-1} \tag{2.17}$$

$$f_h(\alpha) = \Big[1 - \mathcal{A}_h + \mathcal{A}_h\Big(\mathcal{A}_h - \frac{1}{2}\Big)\ln(1 + k_h\sec\alpha)\Big]^{-1} \tag{2.18}$$

The hardness of the X-ray source is defined in terms of a hardness parameter $\xi = S_h/S_s$, with the total X-ray flux $S_x = S_s + S_h$. By expressing $B_x(\tau)$ in terms of this parameter the equation

$$\begin{aligned} B_x(\tau) = \frac{1}{2}S_x\Big\{&k_sf_s(\alpha)\Big(\frac{\xi}{1+\xi}\Big)\Big[\mathcal{A}_s - \Big(\mathcal{A}_s - \frac{1}{2}\Big)e^{-\tau/\mathcal{A}_s}\Big] \\ &+k_hf_h(\alpha)\Big(\frac{1}{1+\xi}\Big)\Big[\mathcal{A}_h - \Big(\mathcal{A}_h - \frac{1}{2}\Big)e^{-\tau/\mathcal{A}_h}\Big]\Big\} \end{aligned} \tag{2.19}$$

is obtained.

The formulation is linear and therefore the principle of superposition is applicable. The total emission can be derived using the irradiated and non-irradiated components. The local temperature stratification is therefore given by

$$T(\tau) = \Big\{\frac{\pi}{\sigma}[B_x(\tau) + B_s(\tau)]\Big\}^{1/4} \equiv \Big(\frac{\pi}{\sigma}B(\tau)\Big)^{1/4}. \tag{2.20}$$

The surface temperature of a star is effectively the temperature at an optical depth of $\tau = 2/3$. Hence, when it is viewed at a given inclination angle α, the effective temperature of the surface under irradiation is

$$T_{eff} = \left\{\frac{\pi}{\sigma}B_x(2/3) + T_{unirr}^4\right\}^{1/4} \tag{2.21}$$

where T_{unirr} is the effective temperature in the absence of any irradiation.

2.5 Modelling the accretion disc

2.5.1 Geometry

In this thesis I assume the disc follows a thin-disc geometry. This is a simple approximation, and how applicable it is to discs in ULX binaries is unclear at this time. In reality, the disc geometry may be more complicated in these systems. This is particularly relevant if the BH mass is low: if super-Eddington accretion is occuring in ULX systems, the inner disc temperatures will be very high which may prompt a deviation from the thin-disc case. For example, the central region may be dominated by a photon scattering sphere, as envisaged by King et al. (2001). However, the thin-disc approximation describes the simplest case, and a more complicated model can easily be incorporated for later work. These issues are discussed in more detail in Section 5.8.1.

A thin disc is described by its flare angle, in that the disc scale height varies in proportion to the radius. In this work I assume the local flare angle is given by $h(r) \propto r^{9/7}$ (Dubus et al., 1999), where h is the disc scale height. The constant of proportionality is determined by fixing the disc scale height at the outer disc radius r_{out}. Following de Jong et al. (1996), the disc height at the outer disc radius is taken to be $0.2\ r_{out}$.

The inner and outer radii of the disc must also be defined. I assume the inner radius of the accretion disc is at the last stable circular orbit around the BH. For a

Schwarzschild BH, this is $3R_s$, where

$$R_s = \frac{2GM_1}{c^2}. \tag{2.22}$$

I assume the outer radius of the disc is the 'tidal truncation radius', beyond which Keplerian orbits intersect. This is weakly dependent on the mass ratio (Paczyński, 1977) but is generally taken to be between 0.6 and 0.7 of the Roche lobe radius. I consider it sufficient in this work to fix the outer disc radius to be 0.6 of the Roche lobe radius.

2.5.2 Optical/IR emission (1)

The disc will emit radiation at optical/IR wavelengths as a result of viscous heating in the disc. Additionally, the disc will be heated due to X-ray irradiation. As in the case of the star, the fact that the radiation-transfer equations are linear means the principle of superposition can be used to calculate the disc temperature from the combination of both these components.

In order to determine the optical/IR emission from the disc, I calculate the temperature of the irradiated disc using Equation 2.21. For the radial temperature profile in absence of irradiation, the Shakura & Sunyaev (1973) prescription is used. The overall disc flux is then calculated by summing the flux from the series of blackbody annuli with the temperatures calculated as above from the inner to the outer radius of the disc.

2.5.3 Optical/IR emission (2)

I have also considered alternative formulations to describe the emission from an irradiated disc.In the formulation of Dubus et al. (1999), the irradiation temperature T_{irr} varies as

$$T_{irr}^4 = C\frac{\dot{M}c^2}{4\pi\sigma R^2} \tag{2.23}$$

where $\dot{M}$ is the accretion rate and R is the distance from the accreting source. The determination of C is given in Dubus et al. (1999), but if an X-ray albedo of 0.9, an efficiency η of 0.1 and a thin disc geometry (de Jong et al., 1996) is assumed, then this value is found to be $\approx 2.57 \times 10^{-3}$.

I find the results of this disc model to be very similar to the Wu et al. (2001) when a very low X-ray hardness ($\xi \sim 0.01$) is used (Copperwheat et al., 2005). Since the Wu et al. (2001) formulation allows this parameter to be varied, I prefer to use it to describe the disc. I will examine cases where $\xi = 0.01$, and in this case the Dubus et al. (1999) prescription could be substituted.

2.6 Stellar evolutionary tracks

In order to make accurate determinations of the age, mass and radius of the donor stars in ULX systems, it is important to use an up-to-date stellar evolutionary model for the input parameters into the model. Throughout this thesis, the evolutionary tracks produced by the Geneva models of Lejeune & Schaerer (2001) are used. I input the set of stellar parameters at each point along the evolutionary tracks into the model, and hence produce colours and magnitudes appropriate for the irradiated star and disc. This process is repeated as the other important parameters are varied, such as the X-ray luminosity, the inclination and orientation of the binary system, and the BH mass. The result is a multi-dimensional array of model results. By comparing this array to actual optical/IR observations of ULX counterparts, the binary parameters can be determined to a given confidence level.

The Geneva tracks cover a wide array of stellar parameters including mass, age etc. One important parameter is the stellar metallicity. A sub-solar (Z= $0.2Z_{\odot}$) metallicity is used throughout this work. This is appropriate given that many ULXs are in low-metal environments such as dwarf galaxies. Low-metal stars also lose less mass in stellar winds (Eldridge & Vink, 2006). Therefore, they may end their lives with bigger cores, which can more easily collapse directly into BHs (Heger et al., 2003). The tracks are further divided up depending on the mass-loss rate of the stars. The high mass-loss tracks are used primarily in this work, since they are recommended for use when dealing with massive stars (Maeder & Meynet, 1994). The standard tracks are used when lower mass stars are considered.

Note that these tracks are produced by a single star evolutionary code. A binary evolution code may be more appropriate but this is not necessarily the case, since the point at which the mass transfer between the two components began, and hence the extent to which the normal evolution of the star has been disrupted by the mass transfer, is unknown.

2.7 The mass accretion rate: an additional constraint

The available optical/IR observational data for ULXs is limited and may not be sufficient to determine system parameters with a good accuracy. For each source in this work two or three optical colours are known, and it is apparent from the previous sections of this chapter that the parameter space is large with many unknowns. In this section I therefore introduce an additional condition by which the parameter space can be constrained. I consider a method that makes use of the additional information provided by the X-ray data and model stellar evolutionary calculations, which is essentially independent of the optical/IR photometric observations.

2.7.1 Driving forces of mass transfer

In semi-detached binary systems, mass transfer occurs when the secondary overfills its Roche lobe. The driver for this is one of three processes. Firstly, there is orbital evolution of the binary. This is caused by the orbital angular momentum loss from the binary (by, for example, gravitational radiation), by the mass redistribution between the secondary and the primary, or by mass loss from the system (by a stellar wind from the secondary). The second driver for mass transfer is the nuclear evolution of the star. As a star evolves away from its ZAMS phase it will expand in volume and overfill its Roche lobe. Finally, the irradiative heating of the star can drive further expansion of the star.

2.7.2 Timescales of mass transfer

The timescale of mass transfer will vary depending on the driving mechanism. Processes such as gravitational radiation or magnetic braking will occur on the timescale of orbital angular momentum loss. Expansion due to irradiative heating will drive evolution on the thermal timescale and of course nuclear evolution occurs on the nuclear timescale of the star in question.

The timescale of orbital evolution as a result of mass loss or mass transfer depends on the mass distribution in the system (Frank et al., 2002). When the primary is more massive than the secondary ($q < 1$) then mass transfer onto the primary will put more matter near the centre of mass of the binary, so the secondary must move to a wider orbit in order to conserve angular momentum. This will result in an increase in the size of the Roche lobe, so there will be a tendency for the binary to become detached, halting the mass transfer. The binary will revert to a semi-detached state after expansion of the star or angular momentum loss. It is apparent therefore that the size of the Roche lobe will increase in step with the size of the star, at a rate determined by one of the three timescales already discussed.

If the primary is less massive than the secondary ($q > 1$) then mass transfer will cause the binary, and hence the stellar Roche lobe, to shrink. Unless the star contracts at a similarly rapid rate, the overfilling of the Roche lobe will become very rapid and violent, and the mass transfer rate will be very large. This will proceed on a dynamical or thermal timescale, depending on whether the stellar envelope is convective or radiative (Frank et al., 2002). In this thesis I am interested in massive stars with radiative envelopes, so the thermal timescale is applicable.

There is therefore a critical mass ratio q_{crit}, above which mass transfer is very violent and rapid. This value is $\sim$ 1; but varies slightly from this value due to the fact that the shape of the Roche lobe varies with mass transfer as well as the separation, as well as the fact that most stars will have a mass-radius relation such that they will shrink with mass loss and avoid this phase of violent transfer. The value of q will of course decrease over this phase, and will return to a normal phase of mass transfer when q falls below q_{crit}.

Qualitatively, for a quasi-steady state, the rate of mass loss from the donor star $\dot{M}_2$ can be expressed by

$$\dot{M}_2 = \frac{M_2}{\zeta_{2s} - \zeta_{2r}} \left[\frac{2}{\tau_J} - \frac{1}{\tau_{th}} - \frac{1}{\tau_{nuc}} \right] , \tag{2.24}$$

where M_2 is the mass of the donor star, ζ_{2s} and ζ_{2r} are the adiabatic indices of the mass donor star and its Roche lobe respectively, τ_J is the timescale of orbital angular momentum loss, τ_{th} is the thermal timescale of the donor star and τ_{nuc} is the nuclear evolutionary timescale of the donor star (Ritter, 1988; D'Antona et al., 1989).

The question is, which of these timescales is the dominant timescale of mass transfer in ULXs? In order to answer this, I will estimate the timescale in each case and make a subsequent estimate of the average mass transfer rate in each case. I noted in Section 2.4.1 that a ULX X-ray luminosity of $L_x = 10^{40}$ergs s^{-1} implies a mass loss rate of $\dot{M} \simeq 1.8 \times 10^{-6} M_{\odot}$/yr for the donor star, if it is assumed all mass outflow from the star is accreted onto the BH, and the accretion efficiency $\eta = 0.1$.

The timescales for angular momentum losses are very long. Wu (1997) estimates a mass transfer rate of $\sim 3 \times 10^{-11} M_{\odot}$/yr as a result of gravitational radiation losses in a typical short period binary, and a rate of $\sim 4 \times 10^{-9} M_{\odot}$/yr as a result of magnetic braking in a typical system. These rates will be even smaller when parameters appropriate for a ULX binary are used, so τ_J can be precluded as the timescale of mass transfer.

The thermal and nuclear timescales can be estimated as

$$\tau_{th} \simeq \frac{GM_2^2}{R_2 L_2} \sim 3 \times 10^7 \left(\frac{M_2}{M_\odot}\right)^2 \frac{R_\odot}{R_2}\frac{L_\odot}{L_2}\mathrm{yr} \tag{2.25}$$

and

$$\tau_{nuc} \sim 7 \times 10^9 \left(\frac{M_2}{M_\odot}\right) \frac{L_\odot}{L_2}\mathrm{yr}, \tag{2.26}$$

(Carroll & Ostlie, 2007), where M_2, R_2 and L_2 are the mass, radius and luminosity of the donor star, respectively. The average mass transfer rate for each timescale can be estimated by τ_{th}/M_2 and τ_{nuc}/M_2. When typical parameters for massive stars are used (see Table 2.1) then the mass transfer rate on the thermal timescale is found to be $\sim 10^{-5}$ - $10^{-3} M_\odot/\mathrm{yr}$, and the rate on the nuclear evolution timescale is found to be 10^{-7} - $10^{-6} M_\odot/\mathrm{yr}$.

Based on these rough estimates, mass transfer on the nuclear evolution timescale seems most appropriate for the observed X-ray luminosities: mass transfer on the thermal timescale is generally too rapid and violent. However, thermal-timescale mass transfer cannot be ruled out: one could for example assume a much lower accretion efficiency. Some of the models constructed to support stellar mass BHs in ULXs do propose they are intermediate- or high-mass X-ray binaries undergoing a phase of mass transfer on thermal time-scales (King et al., 2001; King, 2002). This implies relatively massive donors, in order to achieve $q > q_{crit}$.

In this work I will take the mass transfer to be proceeding on the nuclear evolutionary time-scale. This mechanism is most appropriate to the mass transfer rate as implied by the X-ray luminosity, and is applicable for any mass ratio q. The thermal-timescale runaway scenario is only possible in the small fraction of the parameter space where $q > q_{crit}$. However, it could be that all ULXs do exist in this small fraction of the parameter space. It can be seen from Equation 2.24 that the formalism presented in this work is versatile enough to consider thermal time-scale mass transfer in the future: the irradiation model is generally applicable irrespective of the mechanism of mass transfer. The model will only break down when the thermal timescale is comparable to the nuclear evolutionary timescale of the donor.

In this case the star cannot adjust to the mass loss fast enough to prevent runaway, unstable mass transfer. Then the outer layers of the star cannot remain in radiative equilibrium and the assumptions of the model are violated. However, the estimates in this section show that this is not the case for the massive stars expected to be typical in ULX binaries: they have a thermal timescale which is much shorter than their nuclear evolution timescale.

2.7.3 Quantifying mass transfer on the nuclear timescale

The orbital separation a and orbital angular momentum J for the two components in a binary system are related by $a = J^2(M_1 + M_2)/GM_1^2M_2^2$. Wu (1997) showed that the change in separation caused by mass loss, mass redistribution or orbital angular momentum loss is given by

$$\frac{\dot{a}}{a} = 2\frac{\dot{J}}{J} - 2\frac{\dot{M}_2}{M_2}\left[1 - \beta q - \frac{q}{2}\left(\frac{1-\beta}{1+q}\right) - \alpha(1-\beta)(1+q)\right] , \tag{2.27}$$

where β is the fraction of mass loss from the donor star accreted onto the BH and α is the specific angular momentum carried away by mass loss from the system. In this work I will assume conservative mass transfer, which is a reasonable approximation to the physical case. This means that $\dot{J} = \alpha = 0$, and $\beta = 1$. It follows that

$$\frac{\dot{M}_2}{M_2} = -\frac{1}{2}\frac{\dot{a}}{a}\left(\frac{1}{1-q}\right) . \tag{2.28}$$

The Roche-lobe radius R_L of the donor star and the orbital separation a are well aproximated by Equation 2.3. The Roche-lobe filling condition requires $R_L = R$, where R is the radius of the donor star. I assume that the mass transfer is quasi-steady, *i.e.* $\dot{R}_L = \dot{R}$. By combining these conditions with Equations 2.28 and 2.3, then

$$\frac{\dot{M}_2}{M_2} = \frac{\dot{R}}{R}\left[\frac{1}{2(q-1) + (1+q)\left[2/3 - g(q)\right]}\right] , \tag{2.29}$$

where the function $g(q)$ is given by

$$g(q) = \frac{(2/5)q^{2/3} + q^{1/3}\left[3(1+q^{1/3})\right]^{-1}}{(3/5)q^{2/3} + \ln(1+q^{1/3})} . \tag{2.30}$$

The rate of expansion of the stellar radius $\dot{R}$ can be derived from stellar evolutionary tracks. Hence with q defined the mass accretion rate $\dot{M}$ at a particular evolutionary stage of the donor star can be derived.

For mass transfer driven by nuclear evolution, Equation 2.24 can be reduced to

$$\dot{M}_2 \approx -\gamma \frac{M_2}{\tau_{nuc}} , \qquad (2.31)$$

where γ is a positive, slowly varying parameter depending on the spectral type and mass of the donor star and the orbital parameters. The faster the donor star evolves, the higher the mass transfer rate will be, and how rapidly mass transfer occurs is dictated by the evolutionary timescale. The rate of expansion of the stellar radius $\dot{R}$ and hence the mass accretion rate $\dot{M}$ at particular evolutionary stage of the donor star can be derived from stellar evolutionary tracks.

In this work, the mass accretion rate is calculated using Equation 2.29 for each star/BH combination in the parameter space. A good constraint on the parameter space is generally found by considering star/BH combinations to be consistent with observation when the calculated mass accretion rate is within an order of magnitude of that implied by the X-ray luminosity (Equation 1.4). Specifically, unless stated otherwise, the mass accretion rate for sources with X-ray luminosities $L_x \sim 10^{40}$ergs s^{-1} is assumed to be $\sim 10^{-6} M_\odot$/yr and for sources with $L_x \sim 10^{39}$ergs s^{-1} it is assumed to be $\sim 10^{-7} M_\odot$/yr.

2.8 Putting it all together

Given that the donor star is in contact with its Roche lobe, the equations of Section 2.4.1 can be used to describe completely the geometry of the system, for any given BH mass, stellar mass and undistorted stellar radius. The equations of Section 2.4.2 can be used if that formulation of radiation pressure is to be included.

The temperature of any point on the surface is given by Equation 2.21, which is the combination of the temperature of the star in the absence of any irradiation,

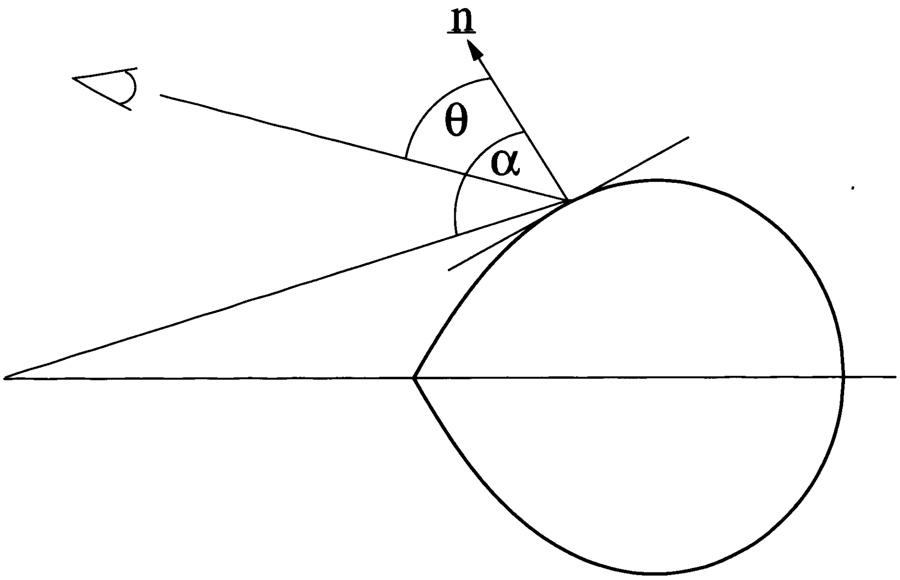

Figure 2.4: The geometry of the binary system

and the component that results from the X-ray heating. The X-ray heating is described by equations of Section 2.4.4. The unirradiated temperature of any point on the surface of the star is calculated by taking the effective temperature of the unperturbed star and applying the darkening effects described in Section 2.4.3. In addition, the additional darkening effect of an accretion disc which is opaque to optical light can be included. Using the disc geometry equations of 2.5.1, the area of the star that will be shadowed by the disc can easily be calculated.

The total heating is calculated by dividing the surface of the star into discrete cells. Each cell has a flat surface, the size of which is dependent on the distance between the central point of the cell and the central points of the neighbouring cells. The position of each point is determined through application of the Roche equation. First, the solution to the equation $\partial\Phi(x,0,0)/\partial x = 0$ is found between 0 and a; this gives the position of the L1 point. The potential at this point Φ_{L1} is determined using Equation 2.1, and all the other points on the three-dimensional equipotential surface are determined through solving $\Phi(x,y,z) - \Phi_{L1} = 0$ at regular intervals of x, y and z.

If radiation pressure is to be taken into account, the modified Roche potential of Equation 2.5 is used. This requires the calculation of a δ value for each cell, as described in Section 2.4.2, and the subsequent modification of each point on the equipotential surface. Note that the magnitude of δ at each point is dependent on the direction of the surface normal at that point. Since this will change with the calculation, this process needs to be repeated for a number of iterations in order to converge on the new equipotential solution.

Once the surface is determined the angles α and θ (required components of the heating equations, as defined in Figure 2.4) for each point can be calculated through appeal to the angle between the normal vector to the surface at the point in question, and the vector incident on the point originating at the BH (α) or the observer (θ). The intrinsic and irradiated temperatures can therefore be calculated for each cell, then combined using Equation 2.21. The resultant temperature is taken to be the temperature over the entire surface of the cell. Since the angle θ is known the cross-sectional area of each cell as seen by the observer can be calculated, and hence the total apparent stellar temperature and luminosity can be derived. This is a numerical method which increases in accuracy as the size of the cells is decreased.

In order to calculate the angle α, the source of the X-rays must be defined. The X-rays are assumed to be emitted from a point source at the centre of the BH mass. The X-ray luminosity and hardness ratio are free parameters. The hardness convention is defined by choosing appropriate values for the two parameters k_s and k_h. Using a test input spectrum consisting of a blackbody and a power law component, I sought values for k_s and k_h which give a band boundary that is physically consistent with the soft and hard X-ray absorption processes (as described in Section 2.4.4). I found for a k_s and k_h of 2.5 and 0.01 respectively, the boundary of the soft and hard band is 1.5keV. I adopt these values throughout this work.

The luminosity of the disc is calculated in a manner identical to that of the star. The disc surface is divided into cells and the heating effect on each is calculated, as determined by the incident flux and the angle of incidence α. The calculation of the disc luminosity is detailed in Section 2.5, and as noted there I will tend to use the same Wu et al. (2001) formulation which I used for the star. The heating is calculated using the equations of Section 2.4.4, which is combined with the unirradiated disc temperature using Equation 2.21. Again the emergent radiation from each cell in the direction of the observer is summed in order to calculate the disc luminosity, by modelling the disc as a series of blackbody annuli. This disc luminosity is then combined with the stellar luminosity to give the total optical/IR luminosity of the system.

Additionally, if the unperturbed donor mass, radius and effective temperature are taken from stellar evolution models as described in Section 2.6, the rate of expansion of the stellar radius $\dot{R}$ is also known. From this, the formulation of Section 2.7 can be used to calculate the mass transfer rate, and if this is inconsistent with $\dot{M}$ as derived from the X-ray luminosity, the particular parameter values chosen from the optical/IR emission can be eliminated as being inconsistent with observation.

The free parameters in this model are as follows. First, the inclination and the phase of the binary. From these, the angle to the observer θ of each cell on the stellar and disc surface is calculated, as well as the cross-sectional area of each cell. Second, the luminosity and hardness of the irradiating X-rays. These can be taken from X-ray observations. Finally, there is the mass of the BH, and the mass, radius and effective temperature of the unperturbed donor star. The BH mass, stellar mass and radius are used to determine the geometry of the system. The unperturbed temperature is one component used in determining the total temperature of the irradiated star. It is this parameter space that will be explored in the next section, and it is these parameters that will be fit to observational data in Chapters 3 and 4.

Class	$log(M/M_{\odot})$	$log(R/R_{\odot})$	$log(L/L_{\odot})$
O5 V	1.6	1.25	5.7
G0 I	1.0	2.0	3.8

Table 2.1: The two sets of stellar parameters used in sections 2.9. Values are taken from Allen (1973)

2.9 Model results

In this section the dependence of the model on various parameters is examined. Rather than use the detailed stellar evolution models in this section, the stellar parameters given in Table 2.1 will be used. These masses, radii and luminosities are taken from Allen (1973) and are indicative of the types of star that one would expect to be the donor in ULX systems, namely early-type main sequence (MS) stars and later-type supergiants. Since in this section model results are not compared to observational data, the constraint from determining the mass accretion rate is not relevant and is not applied.

2.9.1 Comparison of irradiation models

Before I investigate the model in detail, I first compare the simple model of Equation 2.11 with the full radiative transfer formulation of Section 2.4.4. The predicted change in stellar luminosity with BH mass for both models is shown in Figure 2.5. The system modelled here does not contain a disc, and radiation pressure is not accounted for. The effect of these model components will be examined later.

If the simple model is taken first, it can be seen that the stellar luminosity decreases with BH mass. This is quite simple to understand: it can be seen in Equation 2.11 that the X-ray component varies with $\frac{1}{4}\left(R_2/a\right)^2$. It can be seen from Equation 2.3 that R_2/a decreases with mass ratio $q = M_2/M_1$. Since both R_2 and M_2 are fixed in this example, as the BH mass M_1 increases the separation a also increases, and the amount of X-ray flux incident on the stellar surface decreases.

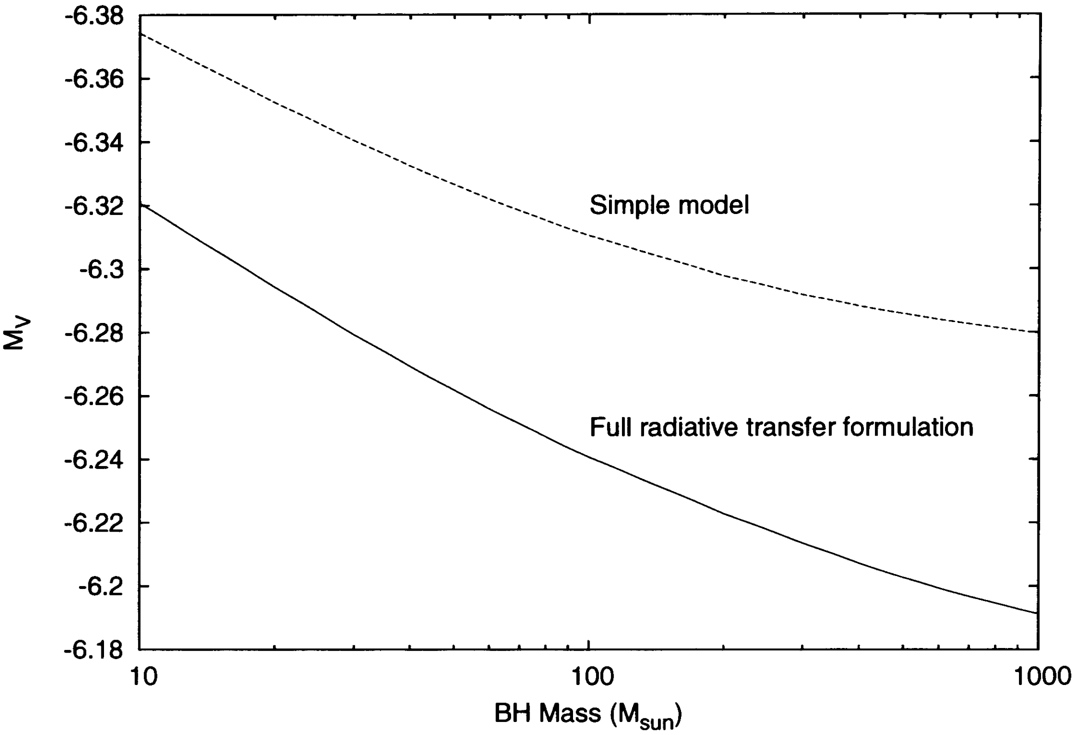

Figure 2.5: The luminosity change with BH mass for an O5V star (see Table 2.1 for parameters), under an irradiating X-ray luminosity of 10^{40}ergs s^{-1}, with χ = 0.1. The simple model of Equation 2.11 is compared with the full radiative transfer formulation of Section 2.4.4. For the radiative transfer formulation calculations, an inclination of $\cos(i)$ = 0.0 and superior conjunction are assumed, to replicate the orientation of the system that is implicit in Equation 2.11.

If the line for the full radiative transfer formulation is examined, a similar decrease in stellar luminosity with increasing BH mass is observed. Note that the stellar luminosity for this formulation is always less than that given by the simple model. This must be the case, since it is assumed in the simple model that the X-ray flux incident on the star is reprocessed and re-emitted towards the observer in its entirety. The stellar luminosity can therefore never be greater than is implied by the simple model. However, radiative equilibrium is assumed even in the radiative transfer formulation, so all of the X-ray flux incident on the star is re-emitted. Why therefore, are the two lines different?

The answer is twofold. Firstly, the plane-parallel formulation accounts for the re-distribution of the incident light, it gives (in effect) a law of darkening for the re-radiated light, which is different from the darkening laws applied to the optical light from the unirradiated star. The star used in the full formulation is a distorted, Roche lobe filling star, which will exacerbate this effect. Note also that the simple model assumes an entire hemisphere of the star is illuminated. While this is a good approximation for a large separation, as the BH mass is decreased the fraction of the star under illumination is also decreased.

Secondly, the Wu et al. (2001) formulation accounts for the X-ray nature of the incident light. It will be seen in this section that this distinction is much more important for the disc than for the star, but in general the model implies that softer X-rays tend to be absorbed at depths where the star is not optically thick, and hence have less influence on the stellar luminosity than their harder counterparts. The simple model assumes the entire incident X-ray flux is re-radiated at visible wavelengths.

2.9.2 Intensity of the stellar and disc surface

In Figure 2.6 the intensity variation over the surface of an O5V star and disc when the BH mass is taken to be $10M_{\odot}$ is shown. In Figure 2.7 a G0I star and the same

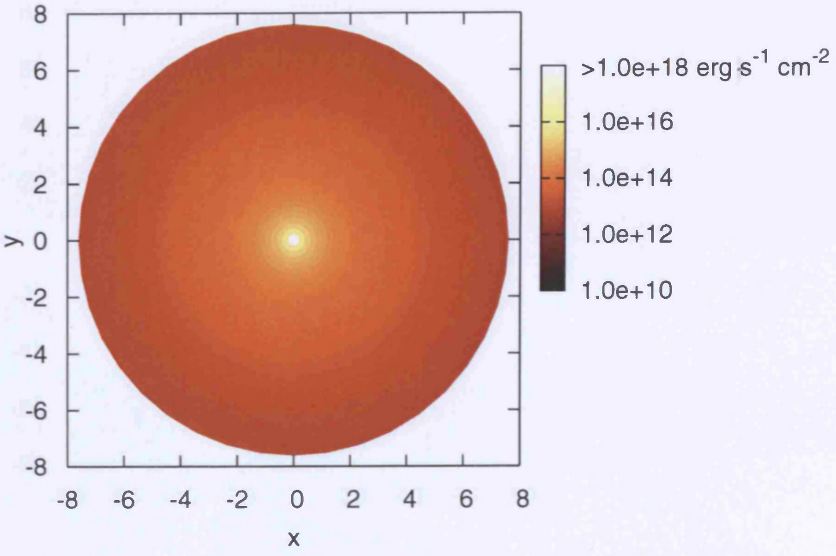

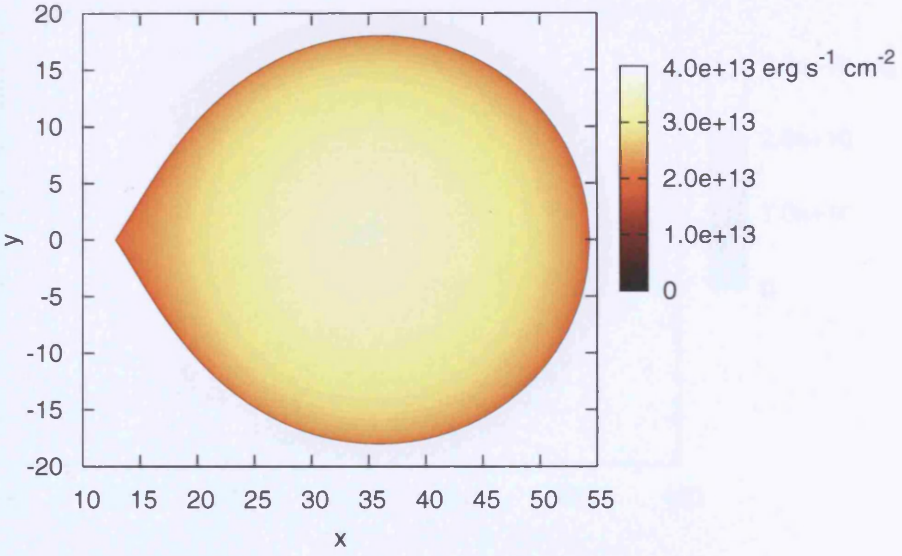

Figure 2.6: The variation in intensity $B(\tau)$ with $\tau = 2/3$ for (bottom) an irradiated O5V star and (top) a disc using $\xi = 0.01$ and a BH mass of $10M_{\odot}$. The system is viewed looking down onto the orbital plane, with the labelled distances in units of $R_{\odot}$.

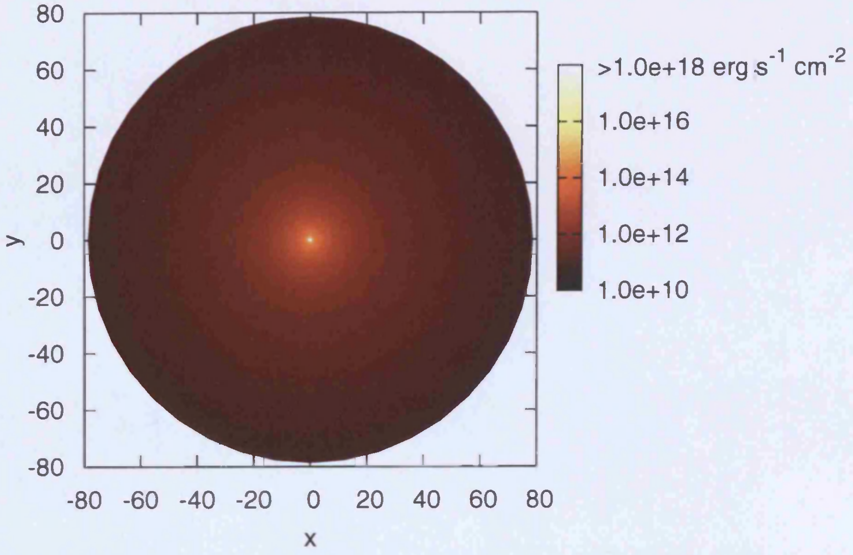

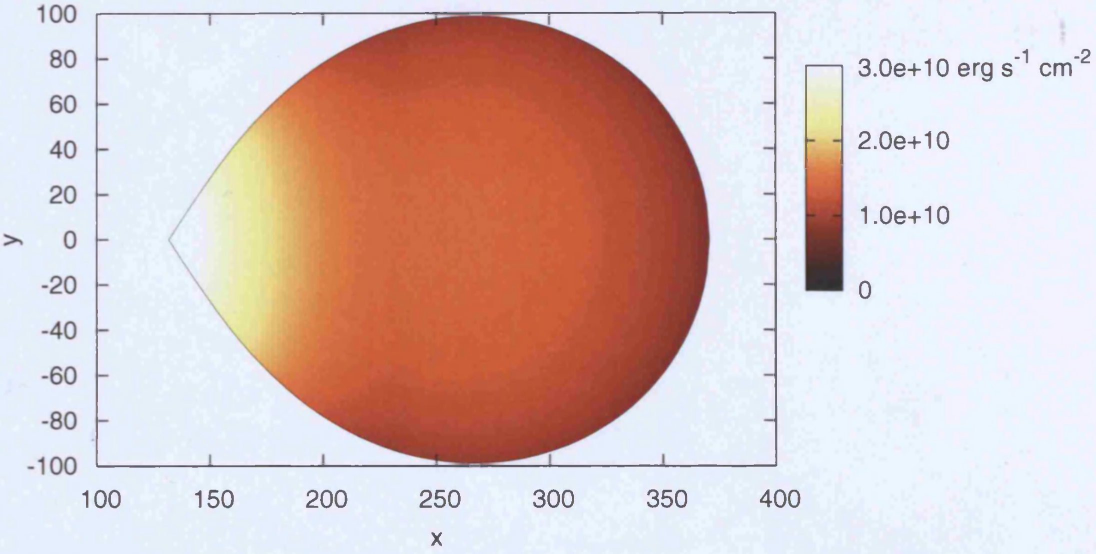

Figure 2.7: The variation in intensity $B(\tau)$ with $\tau = 2/3$ for (bottom) an irradiated G0I star and (top) a disc using $\xi = 0.01$ and a BH mass of $10M_{\odot}$. The system is viewed looking down onto the orbital plane, with the labelled distances in units of $R_{\odot}$.

BH mass is used. The quantity $B(\tau)$ is used as the measure of intensity (Equation 2.20), with τ set to 2/3, and views of the star and disc looking down on the orbital plane are shown. The stellar maps show both the irradiative and darkening effects. A low hardness ratio of $\xi = 0.01$ is used. The intention in these plots is to illustrate the effect of irradiation on the stellar surface, and so radiation pressure and disc shadowing have been neglected.

The combined surface intensity is significantly higher than would be expected for an unirradiated star. There is however a noticeable difference between the two figures. The stellar intensity of the G0I star increases in the direction of the L1 point, reaching a peak there. On the other hand, in the O5V figure the darkening effects dominate at the L1 point, so that the intensity at that point is less than the surrounding surface. Because a low hardness ratio is used, little flux penetrates to an optical depth of $\tau = 2/3$. If the hardness ratio is increased the intensity distribution becomes similar to that of the G0I star. As the BH mass increases, the separation increases, the irradiating flux decreases and the intensity distribution over the surface of both stars tends towards that shown in Figure 2.6. Any shadowing of the accretion disc on the stellar surface should magnify the darkening at the L1 point.

Figure 2.8 can be compared to Figure 2.6. The same O5V star is used, but with a higher ($150M_{\odot}$) BH mass, and hence a larger binary separation. The X-ray flux incident on the stellar surface is therefore reduced, and so the degree of X-ray heating is similarly reduced. In this figure the disc is taken to be opaque to the X-ray light, so the region of the star around the L1 point appears dark compared to the rest of the star. This figure also includes the effects of radiation pressure, and it can be seen that the shape of the star is distorted away from the Roche-lobe filling shape of the stars in Figures 2.6 and 2.7. It can be seen, particularly in the plot parallel to the orbital plane, that the effect of the radiation pressure is to 'flatten' the surface of the star in the direction of the BH. The average incidence angle of X-rays onto the stellar surface is therefore closer to $\cos\alpha = 1$ than in the figures where radiation

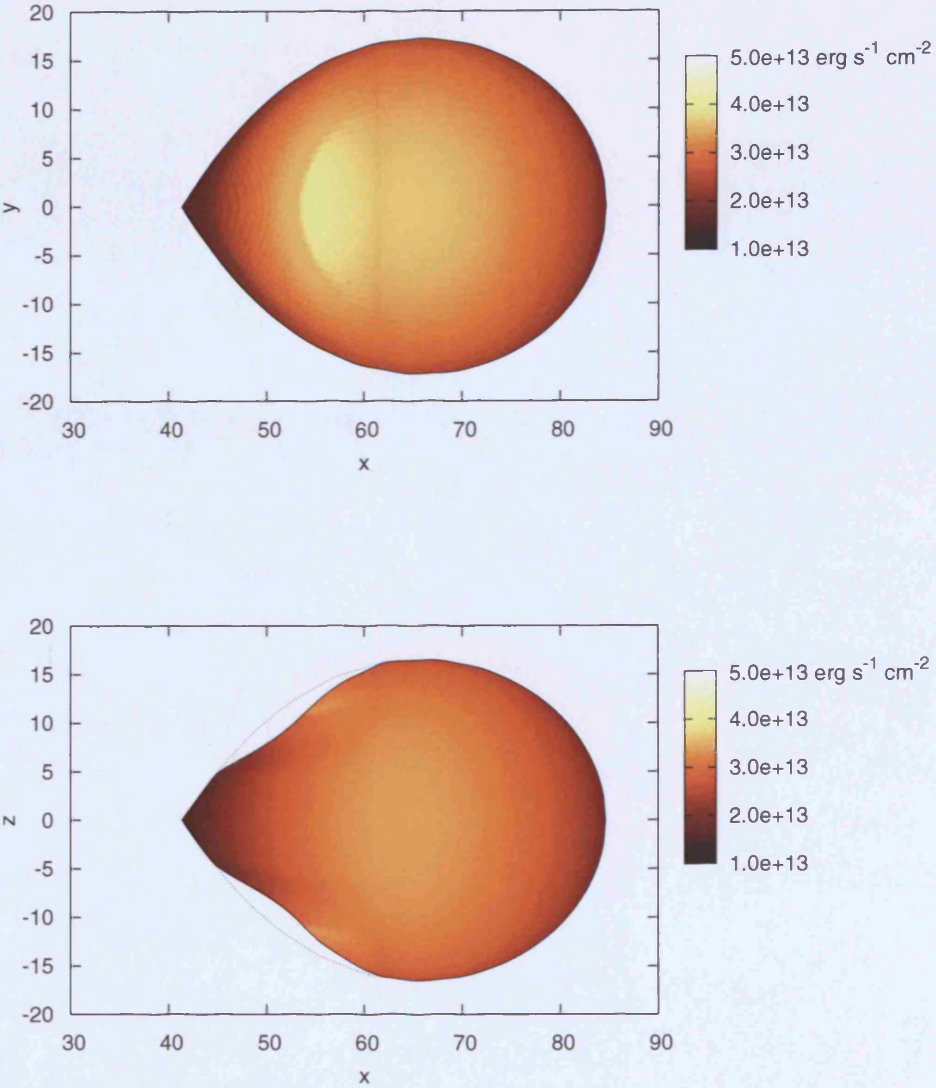

Figure 2.8: The variation in intensity $B(\tau)$ with $\tau = 2/3$ for an irradiated O5V star with a BH mass of $150 M_{\odot}$ and with disc shadowing. The formulation of Phillips & Podsiadlowski (2002) is included for the effect of irradiation pressure on the star. The disc is taken to be opaque to X-ray radiation, and so the disc is shadowed on the stellar surface. Views are shown both looking down onto (top) and in (bottom) the orbital plane, with the labelled distances in units of $R_{\odot}$.

pressure is not taken into account. In the context of Equation 2.19 therefore, it can be appreciated that including radiation pressure in the model results in an greater stellar optical luminosity due to X-ray heating than if this effect was not included. A competing effect is that the 'flattened' surface is further away from the X-ray source, but in practice this has a much smaller influence on the optical luminosity.

2.9.3 Stellar luminosity against BH mass

In Figure 2.9 I show the change in effective luminosity of an O5V star with BH mass. The V band absolute magnitude is shown against the BH mass for an unirradiated star and three different sets of irradiated star calculations. The phase angle is set to zero (so the star is in superior conjunction) and the inclination of the system is such that $\cos i = 0.5$.

Three sets of stellar calculations are shown: one for a star without disc shadowing or radiation pressure taken into account, one with shadowing taken into account, and one with shadowing and radiation pressure both taken into account. This illustrates the effect of these different components. The stellar luminosity is obviously reduced when the star is shielding by an opaque accretion disc. The effect of the radiation pressure is an increased stellar luminosity in this zero phase case, since the geometric distortion means the average X-ray incidence angle α is lowered, as discussed in Section 2.9.2. Note that in this third case I plot values only for BH masses of 100 - $1000 M_{\odot}$. This is because I find that for a BH mass of less than $100 M_{\odot}$ the flux incident on the surface is extremely high and the Phillips & Podsiadlowski (2002) formulation becomes inappropriate to describe the stellar shape.

Figure 2.9 shows that the heating effect on the star decreases with increasing BH mass, which may be counter-intuitive. This relationship was discussed in Section 2.9.1, and is a consequence of constraining the volume radius of the secondary Roche lobe to the radius of the undistorted star. As the mass ratio decreases, the Roche lobe geometry requires the binary separation a to increase. The result is a decrease

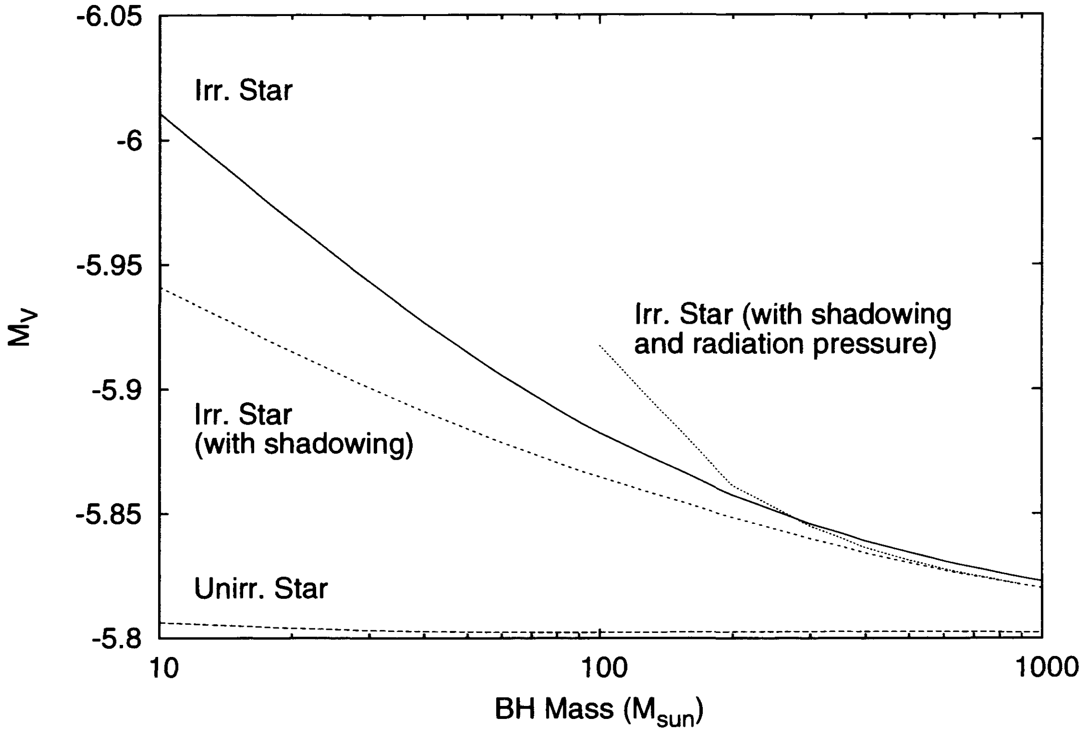

Figure 2.9: The effect of irradiation on an O5V star as a function of BH mass. The X-ray luminosity is taken to be 10^{40}ergs s^{-1} emitted isotropically, with $\cos i = 0.5$ and the star at superior conjunction. The hardness ratio ξ is set to 0.01. Lines are plotted for an unirradiated star, and three different sets of irradiated star calculations; one for a star without disc shadowing or radiation pressure taken into account, one with shadowing, and one with shadowing and radiation pressure both taken into account.

in the amount of flux incident on the stellar surface.

2.9.4 Including the accretion disc

I now investigate the effect on the overall optical luminosity of including the accretion disc. An increased BH mass leads to a larger binary separation and thus to a corresponding increase in the size of the accretion disc, since the outer disc radius is constrained by the Roche lobe size through tidal effects. The result is a large increase in disc surface area, particularly in the outer regions of the disc, and since it is these regions which respond to irradiation, the net result is that the disc total luminosity increases with BH mass, and hence compensates for the decreasing stellar total luminosity.

The luminosity class of the irradiated star is the most important factor in determining which component dominates. I illustrate this in Figures 2.10 and 2.11 where I plot the absolute magnitude dependence on BH mass for a O5V and a G0I star, along with the corresponding disc magnitudes. Hardness ratios of $\xi = 0.01$ and $\xi = 0.1$ are used. By comparing systems with identical donors but different hardness ratio, it can be seen that changing the hardness ratio has little effect on the overall stellar luminosity. The disc, however, is significantly affected by a change in this parameter.

If the stellar luminosity change as a function of BH mass is examined (in the figures), it can be seen that while the BH + MS star changes by a few tenths of a magnitude over the BH mass range, the BH + supergiant decreases by two magnitudes over that same range. The supergiant has a much larger radius, and so for a low binary separation the flux incident on the stellar surface will be high. However, when the mass ratio is decreased, this larger radius leads to a correspondingly larger binary separation than we see in the MS systems.

If the disc intensity dependence on BH mass is now examined, it can be seen that the reverse is true. If the MS star is used with $\xi = 0.01$ (Figure 2.10), the disc

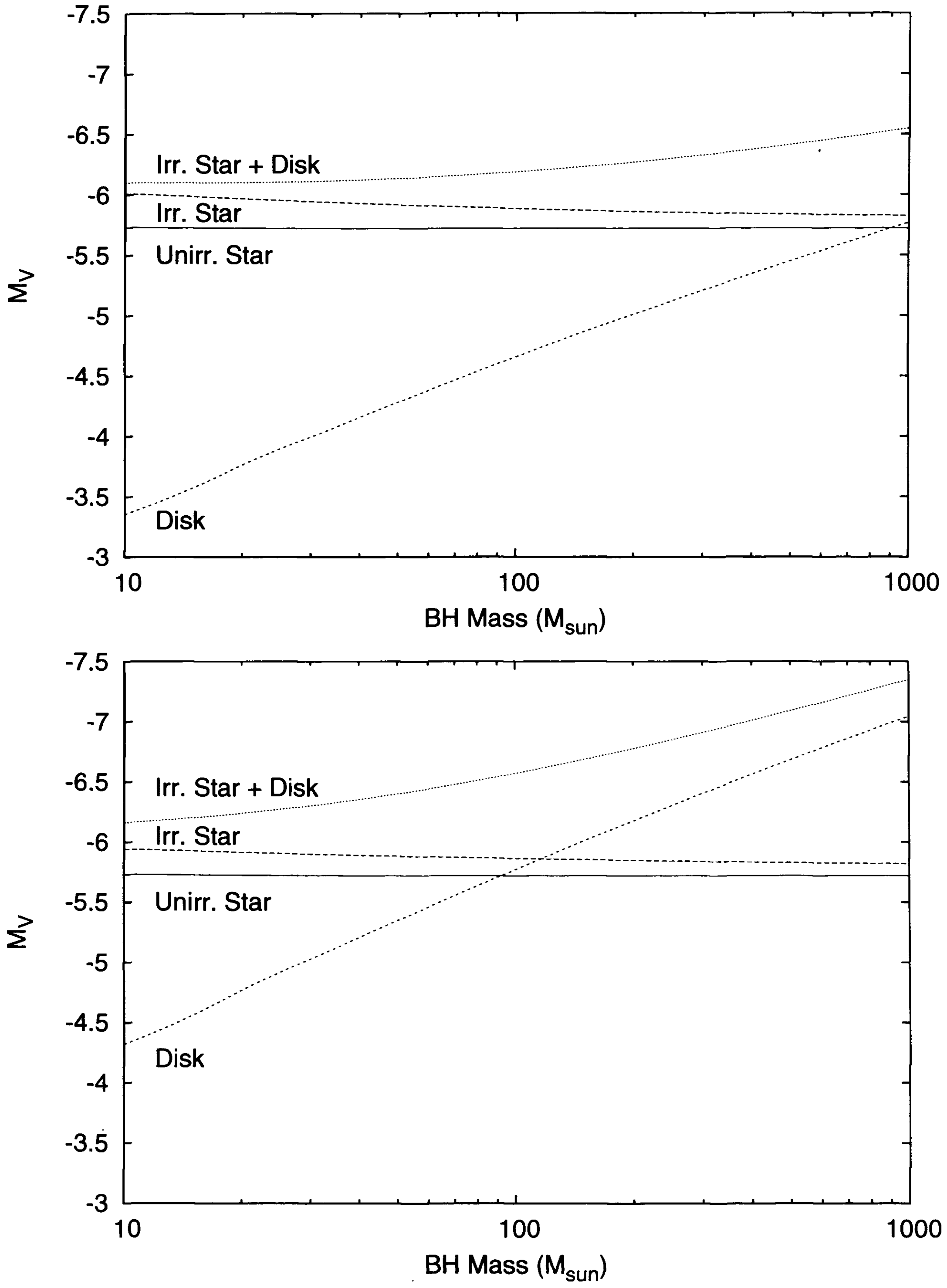

Figure 2.10: *V* band absolute magnitudes for irradiated stars and accretion discs, plotted against BH mass. The X-ray luminosity is set to $L_x = 10^{40}$ergs s^{-1}, with $\cos(i) = 0.5$ and the star at superior conjunction. Hardness ratios of $\xi = 0.01$ (top) and $\xi = 0.1$ (bottom) are used. The donor is an O5 MS star.

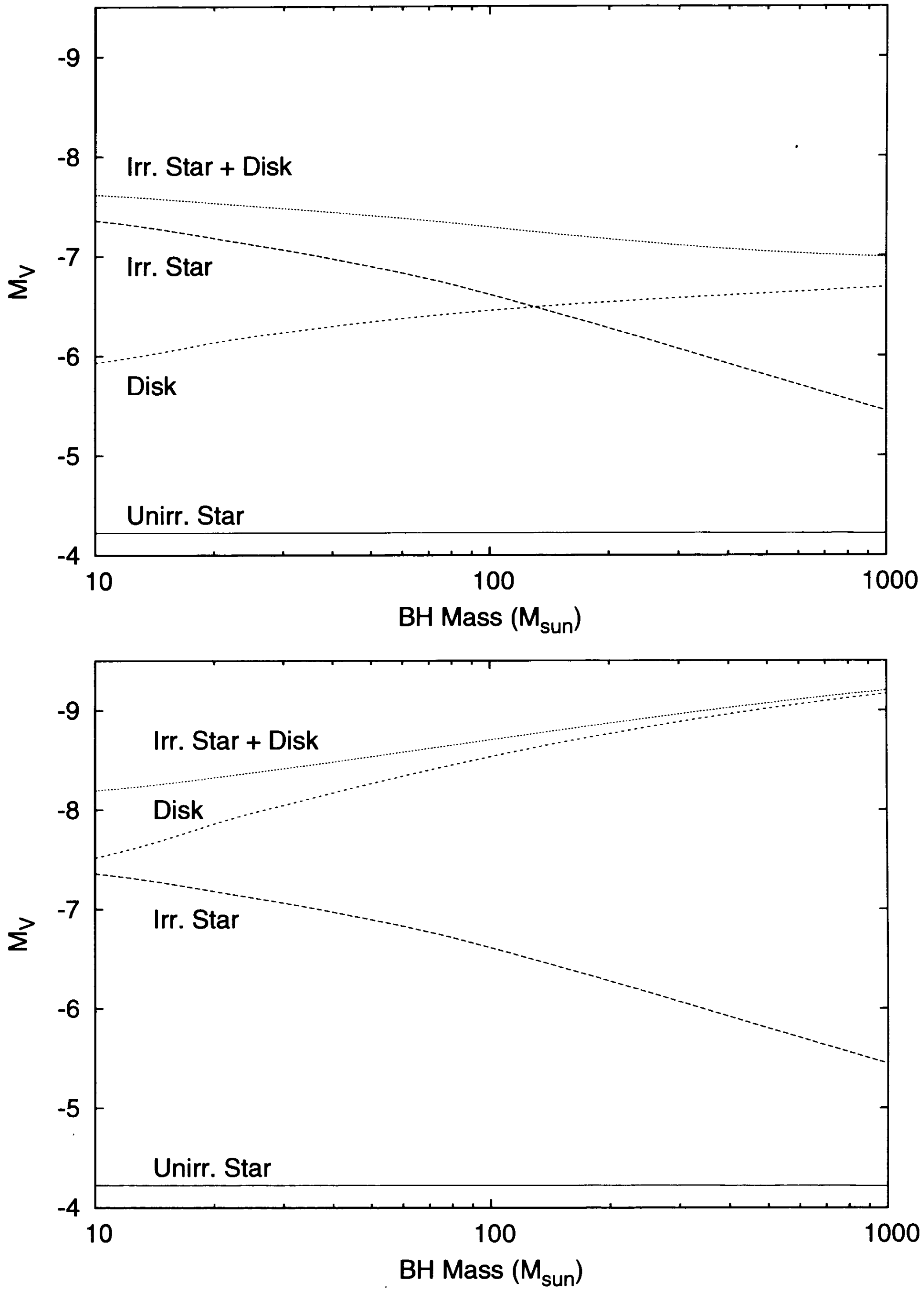

Figure 2.11: V band absolute magnitudes for irradiated stars and accretion discs, plotted against BH mass. The X-ray luminosity is set to $L_x = 10^{40}$ergs s^{-1}, with $\cos(i) = 0.5$ and the star at superior conjunction. Hardness ratios of $\xi = 0.01$ (top) and $\xi = 0.1$ (bottom) are used. The donor is a G0I star.

increases in V magnitude by more than 2.5 magnitudes over the mass range. When $\xi = 0.1$ the result is a more luminous disc, with approximately the same increase in magnitude over the mass range. In contrast, the $\xi = 0.01$ disc accompanying the supergiant (Figure 2.11) increases in V magnitude by less than a magnitude over the mass range. The disc irradiated by the harder X-rays increases by about 1.5 magnitudes. These can be explained by the fact that the supergiant leads to a large Roche lobe for all BH masses. Hence even a low BH mass results in a very bright disc, and since the temperature of the disc decreases with increasing disc radius, the effect of making a large disc larger still has a smaller effect in terms of total disc luminosity. In constrast, when the companion star is on the main sequence, the smaller size of the system at low BH masses results in a small and faint disc. When the BH mass is increased and the disc grows, the effect on its magnitude is much more significant.

These figures also show the V magnitude dependence on BH mass of the disc and star combined. It is interesting to note that were an actual O5V system to be observed, it would be much easier to constrain the BH mass with the disc component included. The same cannot be said for the system with the G0 supergiant. The gradient of the luminosity change with increasing BH mass is still dictated by the decreasing stellar luminosity, but the curve is rendered shallower by the disc component.

2.9.5 Changing the X-ray hardness ratio

In Figures 2.10 and 2.11, it was observed that the disc luminosity was very dependent on ξ, whereas the stellar luminosity was relatively unaffected. This ξ dependence will now be examined in more detail.

I begin by examining the disc. Figure 2.12 shows the disc magnitude for a hardness ratio over the range of $\xi = 10^{-4}$ - 10^{4}. The magnitude for a combination of a 10, 100 and $1000 M_{\odot}$ BH with an O5V and a G0I star is shown.

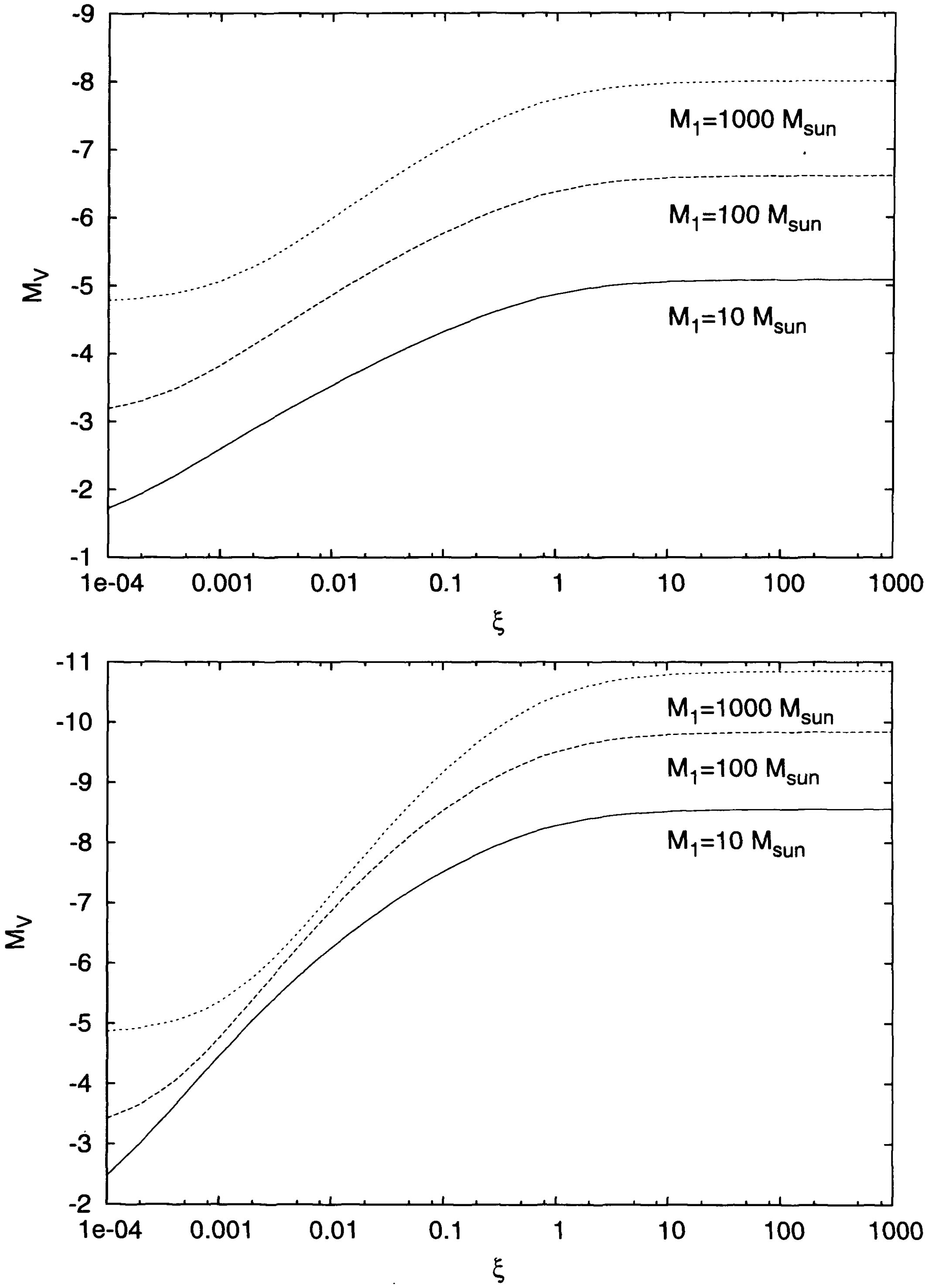

Figure 2.12: The V band absolute magnitude of an irradiated accretion disc for different values of the hardness ratio ξ. Values for BH masses of 10, 100 and $1000 M_\odot$ are plotted, for an O5 MS donor (top) and a G0 supergiant (bottom). The X-ray luminosity is set to $L_x = 10^{40}$ergs s^{-1}and $\cos(i) = 0.5$.

Firstly, it can be observed that the change in disc luminosity with ξ is very large, demonstrating the importance of this factor. A lower hardness gives a less luminous disc. This follows from the previous discussion in this chapter. Note that in Figure 2.12 the irradiating flux is kept constant. When the hardness ratio is low the majority of the X-ray energy is in soft X-ray photons. These are absorbed at the disc surface, where it is optically thin. The emission from this optically thin layer is at wavelengths shortward of the optical, and therefore does not contribute to the optical emission. The harder X-ray photons on the other hand are attenuated at a greater depth and heat the disc. A harder incident X-ray spectrum therefore leads to a greater modification of the optical properties of the disc. As the disc temperature increases the disc luminosity also increases. It can be seen in Figure 2.12 that as the X-ray hardness increases a greater fraction of the X-ray energy is in hard photons, and the disc luminosity increases. The curve reaches a plateau and flattens when the hardness is such that almost all of the energy is deposited into the deep layers of the disc, and the fraction deposited in the optically thin layer is small.

Wu et al. (2001) observed that a larger fraction of soft X-ray energy is deposited in the outer layers when the incidence angle of the X-rays is small. They found that as the angle approaches grazing incidence, a temperature inversion layer is set up; the optically thin 'skin' of the disc becomes hotter than the visible layers of the disc below it. This effect decreases as the incident angle decreases, and more of the energy is deposited into the disc. In the case of the star, the majority of the X-rays are incident on the stellar surface at an angle that is significantly less than grazing incidence. the X-ray light therefore tends to be deposited into the optically thick part of the star and the stellar luminosity is much less responsive to changes in ξ: for an O5V star a change in stellar luminosity of a few tenths of a magnitude is observed over the $0.01 < \xi < 1$ range, for example. This is appreciable, but significantly less than the disc response over the same range. It is apparent therefore that as the X-ray spectrum hardens, the disc component will tend to dominate the optical light.

2.9.6 Optical Variability

Figure 2.13 is a sample lightcurve for the O5V star. Here a BH mass of $100M_\odot$ and an inclination such that $\cos(i) = 0.5$ is used. This figure shows both the ellipsoidal variation of an unirradiated star, as well as the combination of both ellipsoidal and irradiative effects. A third line shows the magnitude when the irradiated accretion disc is included.

The peak of the optical luminosity for all three curves in Figure 2.13 is at phases 0.25 and 0.75, since the ellipsoidal variation is the dominant effect. The contribution from the X-ray heating is at a maximum at a phase of 0.5. If the binary parameters were modified so that the effect of this reprocessed emission is dominant then the lightcurve would peak at this phase. For example, if a G0I star is used with a BH mass of $10M_\odot$, then the lightcurve peaks at a phase of 0.5 with an amplitude of $\simeq 1.5$ Mag. As the BH mass is increased the heating effect decreases: when the BH mass is $1000M_\odot$ the ellipsoidal variation is dominant and lightcurve peaks at phases 0.25 and 0.75 with an amplitude of $\simeq 0.2$ Mag.

A further effect is the disc. In the thin disc approximation the contribution of the disc will be constant for any phase, so the shape of the lightcurve will not be affected, except when the inclination is such that the disc is partially or fully eclipsed by the star. For any inclination $\cos(i) \neq 0.0$ the relative amplitude of the lightcurve will be affected by the disc, decreasing by an amount which depends on the disc luminosity.

The optical variability of ULX counterparts has particular relevance when observations of a single source are available at multiple epochs. In Chapter 4 I examine sources for which such data is available. The extent to which parameters can be determined depends on the quality and quantity of such data. In Chapter 4 these issues are discussed in more detail.

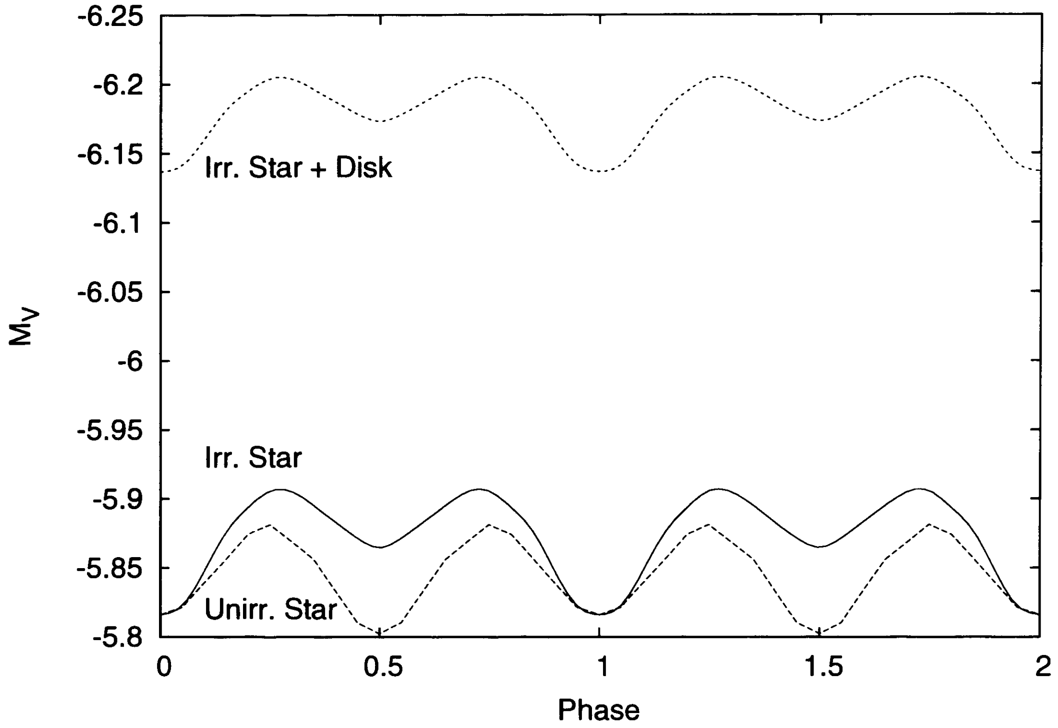

Figure 2.13: The V band absolute magnitude of the O5V star versus binary orbital phase. The BH mass is set to $100M_{\odot}$ and $\cos i = 0.5$. The magnitude variation is shown for both an unirradiated star and for a star irradiated by a source of $L_x = 10^{40}$ergs s^{-1} emitted isotropically with $\xi = 0.01$. The variation when an irradiated accretion disc is included is also shown. Phase 0 is at inferior conjunction.

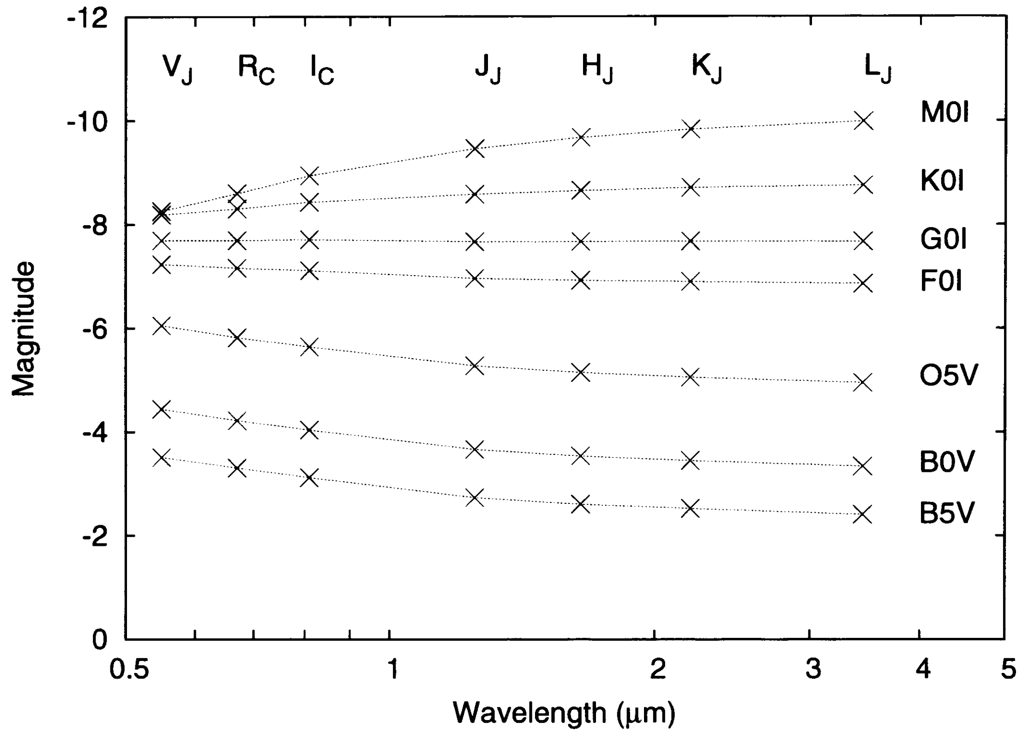

Figure 2.14: The absolute magnitude of various irradiated stars and discs at wavelengths of 0.5 – 4.0μm. The X-ray luminosity is set to 10^{40}ergs s^{-1} with $\xi = 0.01$, $\cos i = 0.5$ and the star is taken to be at superior conjunction. The BH mass is set to $10 M_{\odot}$.

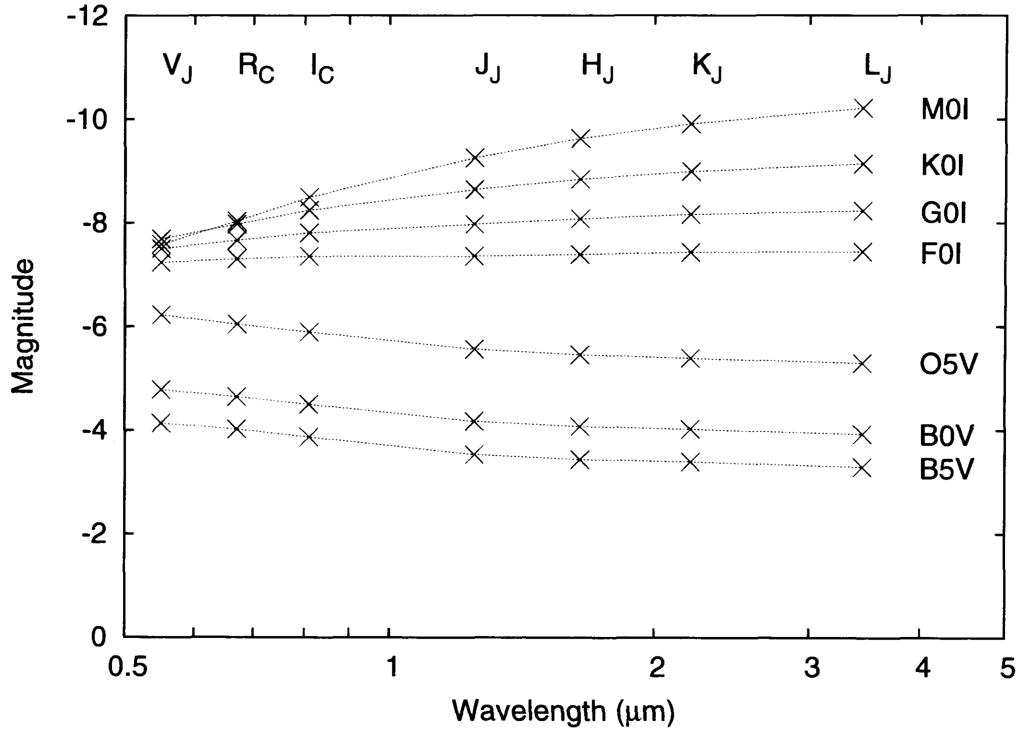

Figure 2.15: As for Figure 2.14, but with a BH mass of $100M_{\odot}$.

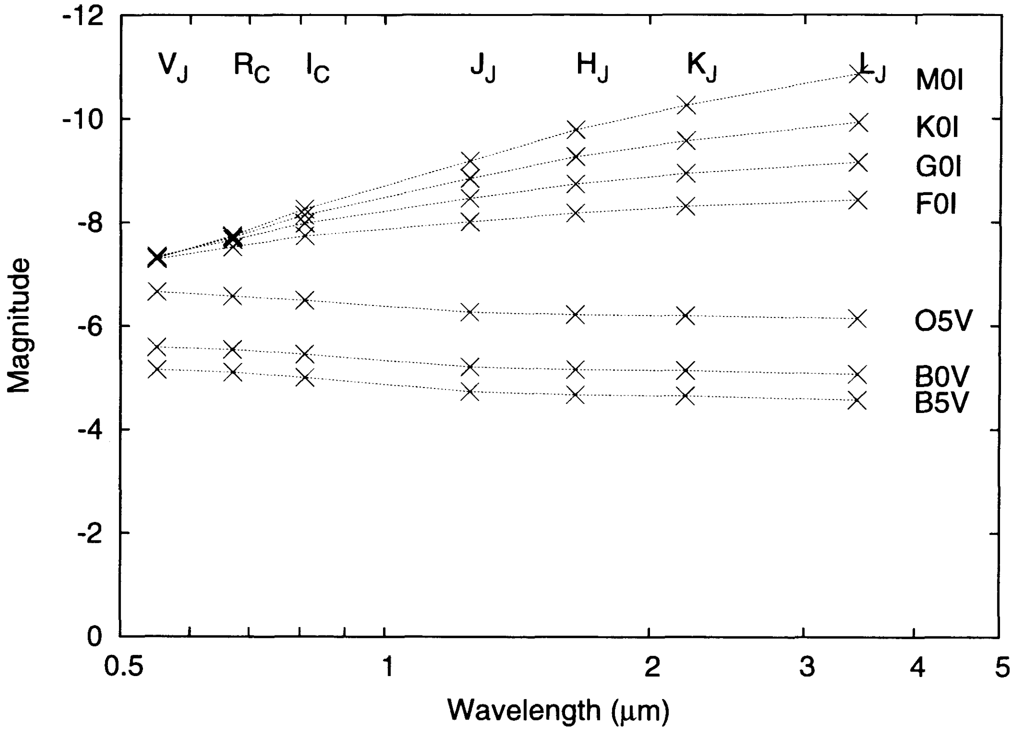

Figure 2.16: As for Figure 2.14, but with a BH mass of $1000M_\odot$.

2.9.7 Irradiation effects at infrared wavelengths

In this section I examine the magnitude change as a function of wavelength for a star and disc over a wavelength range of $0.5-4.0\mu$m, encompassing the V, R, I, J, H, K and L wavebands. I have used the Johnson filter convention, with the Kron/Cousins convention for the R and I bands. Figures 2.14 – 2.16 show calculations for the stars in Table 2.1, using three different BH masses and a hardness ratio of $\xi = 0.01$. A $10M_\odot$ BH is used in Figure 2.14, a $100M_\odot$ BH in Figure 2.15 and a $1000M_\odot$ BH in Figure 2.16. Shadowing of the star by the disc is incorporated into the stellar irradiation model.

Firstly, it can be seen that there is a very large range in magnitude between these different systems. Secondly, it can be seen that as the mass of the BH increases, it becomes progressively harder to distinguish between different star/disc combinations with a V band observation alone. Thirdly, it can be seen that there is a much more clear distinction when observations are extended to longer wavelengths. Note that there is a clear separation between the MS stars and the supergiants which becomes more apparent as BH mass is increased. This suggests that infrared observations will have more diagnostic power in determining the characteristics of the ULX than observations at optical wavelengths.

2.9.8 Summary

To summarise this section, I have shown that the stellar luminosity component is at its greatest for low BH masses and the disc component is at its greatest for high BH masses. If a MS star, a supergiant star, a disc in a BH/MS system and a disc in a BH/supergiant system are considered separately, the biggest changes in magnitude over the BH mass range occur for a supergiant star or a BH/MS disc. In general then, while the emission will always consist of a disc and a star component, the stellar component will dominate for a MS star / low mass BH combination, and the disc component will dominate in the case of a supergiant / high mass

BH. This assumes the X-ray radiation is soft: when the hardness of the X-rays is increased, the contribution of the disc component will increase for all BH masses, and in the supergiant systems in particular the disc component begins to dominate over the entire mass range. The optical counterpart will be variable when the stellar component dominates. IR observations may have more diagnostic power than optical observations (the combination of the two would be particularly powerful) and a very luminous counterpart at IR wavelengths would indicate an evolved donor.

Chapter 3

Application to individual sources

3.1 Introduction

In this chapter I apply the model of Chapter 2 to the optical counterparts of a number of ULXs, in order to make determinations of the physical parameters of these systems.

The fraction of the ULX population for which there are optical counterparts is small. In this work I examine all sources for which there are data available, and which have so far been seen to be persistently ultraluminous ($L_x > 10^{39}$ergs s^{-1}). I have divided these sources into two groups. The sources in this chapter have been observed in the optical at a single epoch. The phase of the system at the time of observation is therefore unknown. The sources in Chapter 4 have multiple sets of data available, so variability can be studied in these systems.

3.2 Input parameters

3.2.1 X-ray data

Each of the six sources in this section have been identified as having an X-ray luminosity that is persistently greater than 10^{39}ergs s^{-1}. For each source I quote in the following sections the average X-ray luminosity as reported in the literature, and I use this luminosity as the input parameter into the model. However at the time of the optical observation the X-ray luminosity may be different from the average. Since none of the sources detailed in this chapter have been observed simultaneously at X-ray and optical wavelengths, this will add some uncertainty.

As was discussed in Chapter 2, the absorption coefficients for the soft and hard X-rays are set to $k_s = 2.5$ and $k_h = 0.01$ respectively. The band boundary is a free parameter to be determined. When an input spectrum consisting of a blackbody and power-law component, a soft/hard band boundary of 1.5keV was found to be appropriate for these absorbtion coefficients.

The final X-ray parameter is the hardness ratio $\xi = S_h/S_s$, where S_h and S_s are the hard and soft components of the flux respectively. It was shown in Section 2.9.5 that the results of the irradiative calculations could depend sensitively on this parameter, but determining the hardness ratio for any given ULX is not straightforward and is complicated by the presence of absorption. Absorption tends to harden the X-rays. If the absorbing region which produces the hardened spectrum is intrinsic to the X-ray emitting region itself, then the disc and star will be irradiated by X-rays with the same hard spectrum as is observed. If the absorbing region is located between the binary system and the observer, then the irradiating X-rays will be much softer than is observed. This is illustrated in Figure 3.1.

By examining X-ray observations from ULX X-7 in NGC 4559 (Cropper et al., 2004) it was seen that for this source, reasonable physical values for the hardness ratio range from $\xi \sim 0.1$ to ~ 1. In this chapter, the hardness ratio is set to 0.1, since a locally soft irradiating spectrum is expected. In Section 5.8.3 the effect of changing this parameter is discussed in detail.

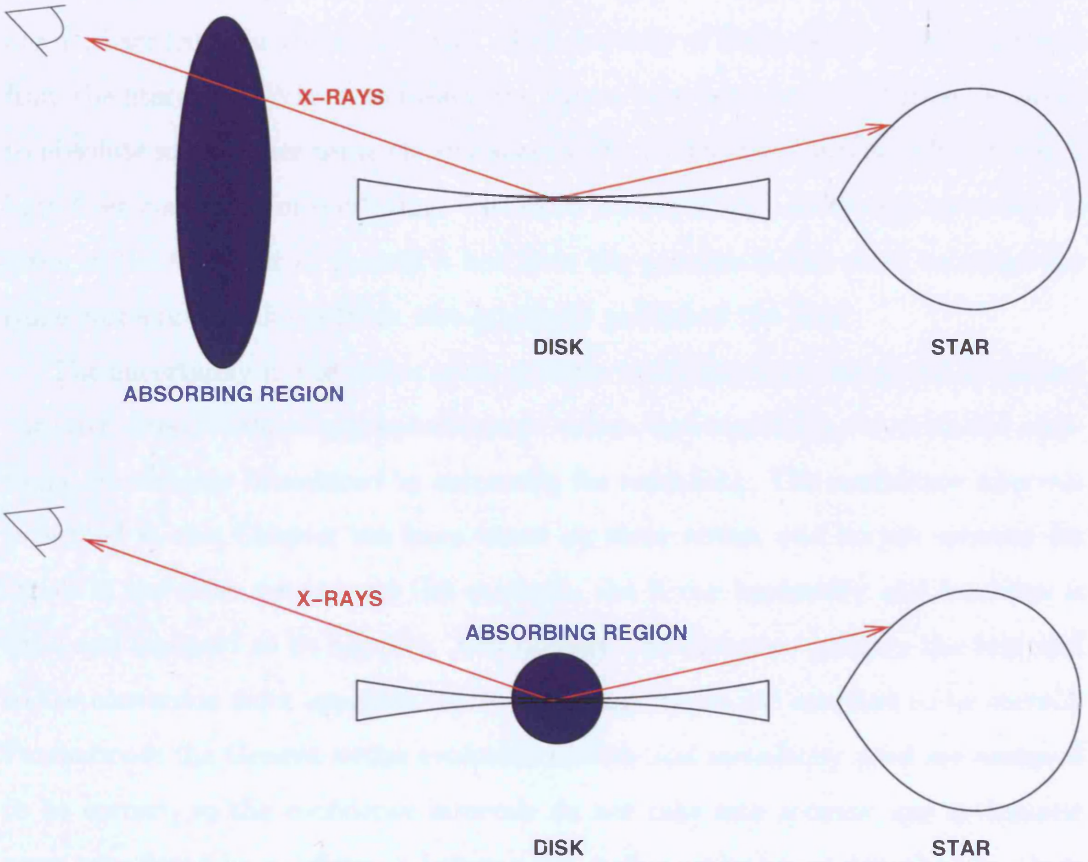

Figure 3.1: Cartoon illustrating how absorption complicates the determination of the hardness ratio. Absorption tends to harden the X-rays. In the top diagram, the absorption region (blue) is located between the observer and the ULX system. In this case, the X-rays (red) as seen by the observer will have a harder spectrum than those incident on the surfaces of the star and disc. In the bottom diagram, the absorbing region is intrinsic to the X-ray emitting region. In this case, the disc and star will be irradiated by X-rays with the same hard spectrum as is observed.

3.2.2 Optical data

The six ULXs studied in this chapter have all been observed with *HST*, and one or more candidates proposed for the optical counterpart. The photometric values which are used are listed in Tables 3.3 to 3.7. The majority of these values have been taken from the literature. Where necessary, the values have been converted from apparent to absolute magnitudes using the distances given in the text. Additionally, the data have been corrected for reddening. The exact nature of each reddening correction is given in the text, but in general it has been the practise in this work to adopt the same correction as the authors who originally published the data.

The uncertainty in the values given in these tables has been calculated by taking the error given for the original photometric values, and combining this with the additional uncertainty introduced by correcting for reddening. The confidence intervals presented in this Chapter has been based on these errors, and do not account for errors in the other parameters (for example, the X-ray luminosity and hardness is fixed and assumed to be correct). Additionally, the distances given in the text and so the conversion from apparent to absolute magnitudes are assumed to be correct. Furthermore the Geneva stellar evolution models and metallicity used are assumed to be correct, so the confidence intervals do not take into account any systematic error introduced by a difference between the stellar evolution as described by those models, and the evolution of a donor in the ULX.

3.2.3 Inclination and orientation

For all ULXs the inclination with respect to the observer is unknown. At one extreme, the orbital plane of a binary is perpendicular to the plane of the sky ($\cos(i) = 0.0$). In this case with a thin disc, all of the optical flux that is observed will be from the star. For any other inclination the optical flux will also contain a disc component, the relative contribution of which will increase as $\cos(i)$ is increased to 1.0. It should be noted that if beaming is important, then face-on ($\cos(i) = 1.0$)

systems would be expected.

The phase of the companion star at the time when the observations were made is also unknown. If the star is in superior conjunction with respect to the observer, the observation will be of the irradiated hemisphere of the star. If the star and the observer are in inferior conjunction, the observation will be of the hemisphere facing away from the BH and therefore the flux from the star will contain little or no irradiated component.

It was noted in Section 2.9 that the geometric constraints of the binary system determined whether reprocessed light from the disc or the star dominated the optical/IR emission. The disc is truncated by tidal forces, and so when the separation between the star and the BH is large, the disc is also large and hence more likely to be the dominant optical component. A large separation is a consequence of assuming a high BH mass, so a high BH mass implies disc dominated optical/IR emission. It would therefore be expected that inclination would dominate the geometrical effects in high BH mass systems. A low BH mass generally implies the emission is dominated by the donor star. It would therefore be expected that the phase of the star has a significant effect on the results only in the cases where a low BH mass is assumed.

In this chapter, the analysis is concentrated on the general case where there is an irradiated component from both the star and the disc. In this case, the inclination is therefore assumed to be $\cos(i) = 0.5$. This orientation already results in a strong contribution to the optical flux from the disc, and increasing the inclination to $\cos(i) = 1.0$ has little additional effect on the total luminosity. For this inclination, I consider the cases where the star is in superior and inferior conjunction. These are the phases where the stellar contribution to the observed optical emission is strongest and weakest for this inclination. Additionally, the case where the star is in superior conjunction and $\cos(i) = 0.0$ is considered. This describes the situation when all of the optical flux is from the irradiated hemisphere of the star. When inferior conjunction and $\cos(i) = 0.0$ is assumed, only the unirradiated hemisphere of the star is observed. In this case it would be appropriate to use a standard unirradiated star. By examined these extreme states, the inclination and phase orientation parameter space can be explored relatively completely.

3.2.4 Radiation pressure

As was discussed in Section 2.4.2, the radiation pressure formulation incorporated into the model contains some restrictive approximations, which means it describes an extreme state of maximal stellar distortion which is not correct. It also breaks down for particularly low BH masses. Therefore, in this chapter this component of the model will be neglected. In Section 5.8.2 this will be examined in more detail, and the effect on these results of adding radiation pressure to the model will be discussed.

3.2.5 Black hole mass

The compact object in the binary system is assumed to be a BH, but it is not assumed to be an IMBH. For all sources, BH masses of 10 – $1000M_{\odot}$ are used in the model, a range that encompasses both a stellar mass and an intermediate mass nature for the BH. At $1000M_{\odot}$ the optical emission is dominated by the large disc, and increasing the BH mass beyond this is found to have a diminishing effect on the model results.

3.3 Method

The method of analysis in this chapter is as follows. The evolutionary tracks produced by the Geneva models of Lejeune & Schaerer (2001) are used as inputs into the model, and the other model parameters are varied so as to generate a large, multidimensional array, giving the optical emission from a star and disc for many combinations of input parameters. For each source the X-ray luminosity is fixed from the value given in the literature, and an appropriate hardness parameter is selected (see Section 3.2.1). An inclination, phase and BH mass are assumed, and the relevant elements from the array are selected. From this dataset, the calculated optical colours of each point are compared with the available photometric observations, and the χ-squared statistics for the points are calculated. Points where the implied mass transfer rate is inconsistent with the observed X-ray luminosity are automatically rejected. The array of χ-squared values is then used to determine the range of the important parameters to the 68%, 90%, 95% and 99% confidence levels. The important parameters are the stellar mass, radius and age. This process is then repeated, but a different set of points are selected which apply to a different BH mass. The range of the BH mass parameter can therefore also be determined to any given confidence level.

This process is then repeated, but for a different assumed phase or orientation. The phases and orientation used in this study are detailed in Section 3.2.3.

The results are given in the remaining sections of this chapter. Note that all four confidence levels are shown in the figures, but the values quoted in the text are taken at the 90% confidence level.

3.4 ULX X-10 in NGC 4559

3.4.1 Observations

X-10 in NGC 4559 is a ULX with a luminosity of $\sim 10^{40}$ergs s^{-1} (Cropper et al., 2004). We have observed this source with the *HST* ACS instrument, and identified candidates for the counterpart in the X-ray error circle. The luminosity of each candidate was calculated using aperture photometry, and I converted these values to standard BVI magnitudes following Sirianni et al. (2005). I list the absolute magnitudes in Table 3.1, assuming a distance to NGC 4559 of 10Mpc (Cropper et al., 2004). These data have been corrected for Galactic reddening by using the

Table 3.1: Photometric data for ULX X-10 in NGC 4559. Data are given for all seven candidates which lie in the *Chandra*error circle.

	M_B	M_V	M_{I_c}
C1	-6.54 ± 0.11	-6.65 ± 0.10	-6.95 ± 0.29
C2	-6.26 ± 0.14	-6.48 ± 0.12	-6.84 ± 0.12
C3	-5.29 ± 0.23	-5.38 ± 0.23	-5.58 ± 0.16
C4	-5.12 ± 0.24	-5.37 ± 0.18	-5.63 ± 0.24
C5	-4.99 ± 0.39	-5.60 ± 0.24	-6.56 ± 0.15
C6	-4.54 ± 0.29	-4.58 ± 0.15	-5.65 ± 0.25
C7	-3.73 ± 0.75	-5.05 ± 0.14	-7.84 ± 0.25

Galactic $E(B-V)$ values towards NGC 4559 given in Soria et al. (2005), and $A_V/E(B-V) = 3.1$. These candidates have been labelled C1 – C7 in descending order of their M_B luminosity.

3.4.2 Determining the counterpart

Since this ULX has not been previously studied at optical wavelengths, the counterpart has not been established. I first aim therefore to establish if any of the sources are inconsistent with the irradiation model.

In Figure 3.2 I show M_V against $(B-V)$ and $(V-I)$. I plot the colours and magnitudes for the seven sources overlaid on to the standard, unmodified Geneva tracks for stars in the mass range $1 - 60M_\odot$. It can be seen that the stars in the error circle have masses $\simeq 7 - 12M_\odot$. They lie on these tracks at points corresponding to ages of $\sim$ 20Myr. No candidate stands out as being significantly more luminous than the others, although C7 does have an extremely large $(V-I)$ colour. This may be due to local reddening, but the very high luminosity in the I band suggests this is more likely due to a coincidence with a bad pixel in the relevant *HST* image file.

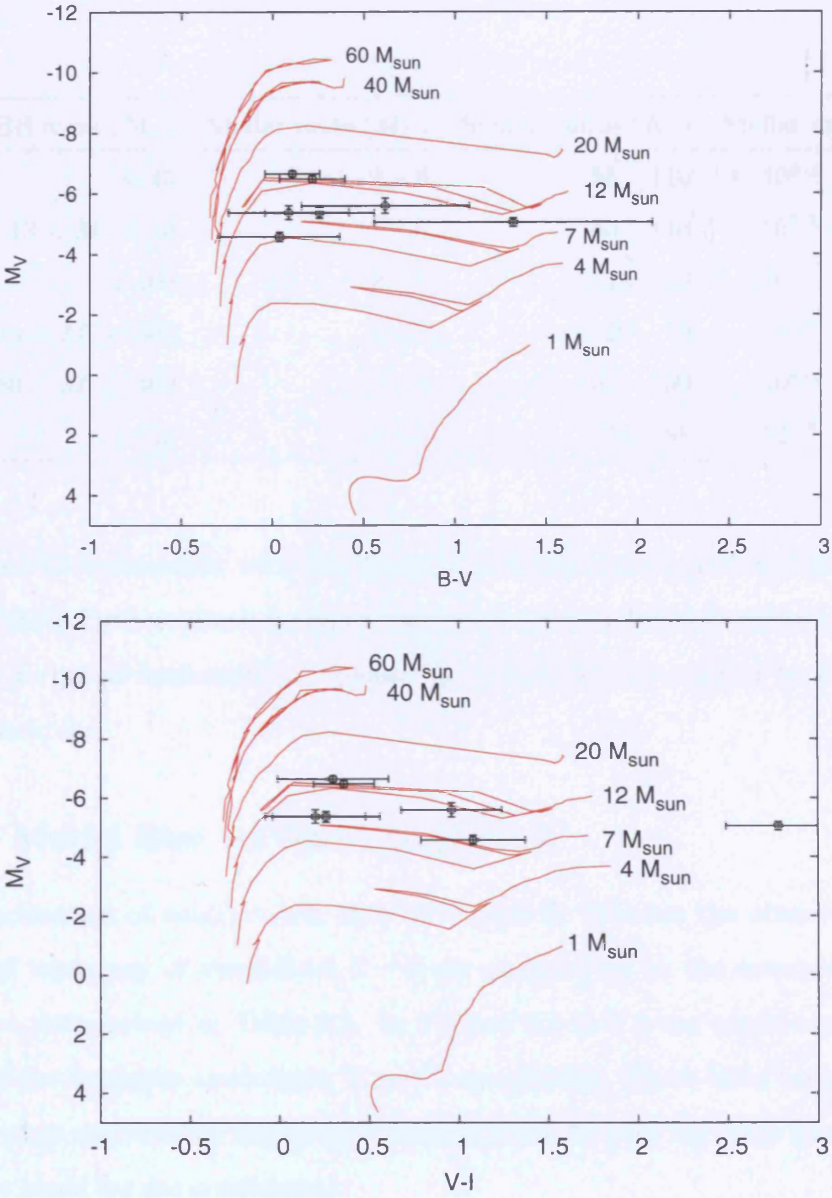

Figure 3.2: Colour magnitude diagrams in $(B-V)/M_V$ and $(V-I)/M_V$ space for X-10 in NGC 4559. The candidates for the optical counterpart are plotted along with the unmodified Geneva stellar evolution tracks. Each track is labelled with its ZAMS mass.

Table 3.2: Stellar and BH parameters for ULX X-10 in NGC 4559, for an assumed inclination of cos(i) = 0.0. Parameters are determined separately for each counterpart candidate.

	BH mass ($M_\odot$)	Stellar mass ($M_\odot$)	Stellar radius ($R_\odot$)	Stellar age (yr)
C1	< 45	2 - 6	55 - 110	$10^{8.0}$ - $10^{8.7}$
C2	$13 < M_1 < 60$	2 - 5	60 - 110	$10^{7.9}$ - $10^{8.7}$
C3	< 400	2 - 5	18 - 63	$10^{8.0}$ - $10^{8.7}$
C4	$14 < M_1 < 500$	2 - 5	20 - 70	$10^{8.0}$ - $10^{8.7}$
C5	$80 < M_1 < 400$	2 - 6	105 - 200	$10^{8.0}$ - $10^{8.7}$
C6	> 250	2 - 5	36 - 88	$10^{7.9}$ - $10^{8.7}$

This colour is inconsistent with the X-ray irradiation model, so I will not consider this candidate further. Since no one of the other six is noticeably different from the others in terms of luminosity or colour, the model will be applied to each one of them separately.

3.4.3 Model fits: no disc component

For an inclination of $cos(i) = 0.0$, there is a good fit between the observations and the model when any of candidates 1 – 6 are assumed to be the counterpart. The results are summarised in Table 3.2. In Figures 3.4 to 3.5 the confidence contours for two of the brightest candidates, 1 and 3, are plotted. These have been chosen as example plots due to their luminosity, although the fit with all six is good and any candidate could be the counterpart.

If the stellar parameters are examined first, it can be seen in Table 3.2 that the stellar mass and the stellar age is determined to be approximately the same irrespective of which candidate is used as the counterpart. Conversely, the fitted radius varies significantly from candidate to candidate.

It might be seen as quite suprising that the mass range is consistent for each candidate, but note that when the unirradiated tracks were used in Figure 3.2, the mass range was also consistent for all candidates. When an irradiative heating component is added the fitted masses are decreased but remain similar to each other. The candidates were inconsistent with very high mass stars when the unirradiated tracks were used due to fact that they were fainter and of a redder colour than the high mass tracks. Since the effect of irradiation is to make the tracks bluer and more luminous, the high mass tracks remain inconsistent with observation.

It was noted in Section 2.9.4 that changing the stellar radius has a much greater effect than changing the stellar mass on the luminosity of an X-ray irradiated star. This explains the large difference in the fitted stellar radius for different candidates. While the similar fitted masses means the candidates all lie on the same stellar tracks, the different fitted radii reveal they fall at different positions on those tracks. However, these positions are not that different, as revealed by the consistent stellar ages. They all exist on regions of the stellar tracks where the star is approaching the end of its life and evolving extremely rapidly in radius.

This is to be expected, since the radius evolution is necessarily large in order to be consistent with the observed X-ray luminosity, because the mass transfer rate in the model is linked to it. If a very massive star is found to be consistent with the observation, then this rapid radius evolution can occur early on in its life. However, when stars of mass $\sim 5M_{\odot}$ or less are fitted with the observation, as is the case here, the star must be have evolved off the main sequence in order to exhibit the radius evolution the X-ray luminosity requires.

The calculations for all six of the candidates produce a constraint on the BH mass. In two cases this is an upper limit, in one case it is a lower limit, and in the other three cases an upper and lower limit is obtained. If the candidate with the lower limit is ignored (candidate 6, the faintest of the six) then the BH mass is found to be $500M_{\odot}$ or less. The two most luminous candidates are fitted with lower mass BHs, of $60M_{\odot}$ or less.

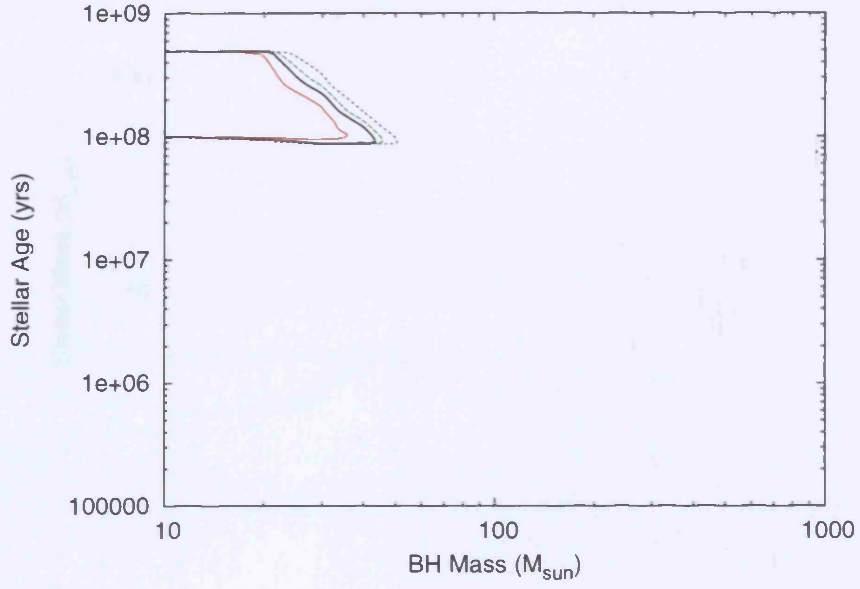

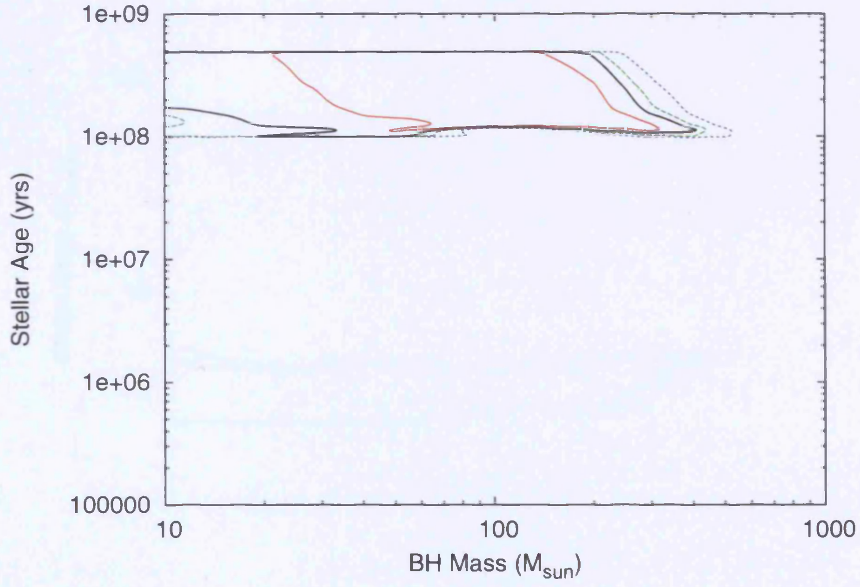

Figure 3.3: Confidence contours for the binary parameters for the source X-10 in NGC 4559. These plots show the stellar age against the BH mass, and assume a binary inclination of $\cos(i) = 0.0$, superior conjunction, a stellar metallicity of Z= $0.2Z_{\odot}$ and an X-ray hardness ratio of $\xi = 0.1$. The red, black (solid), green and blue lines denote the 68%, 90%, 95% and 99% confidence intervals respectively. In the top plot the counterpart is assumed to be candidate C1, while in the bottom plot candidate C3 is assumed.

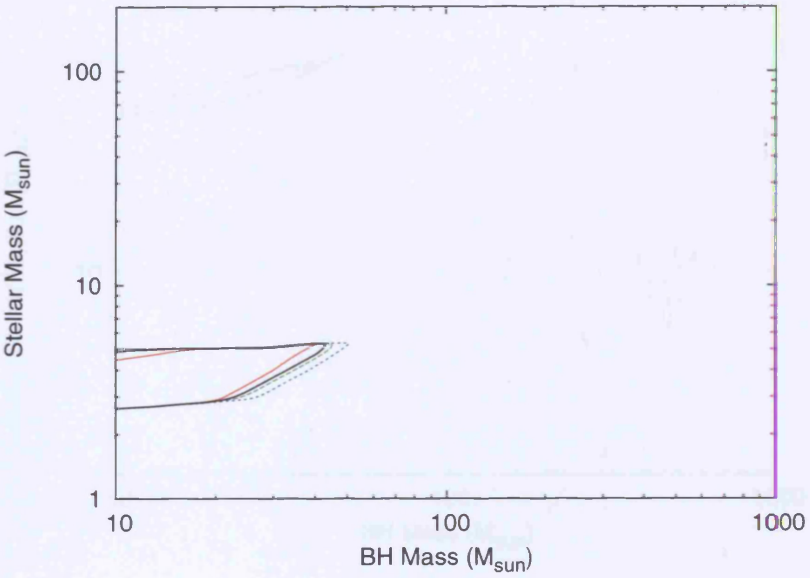

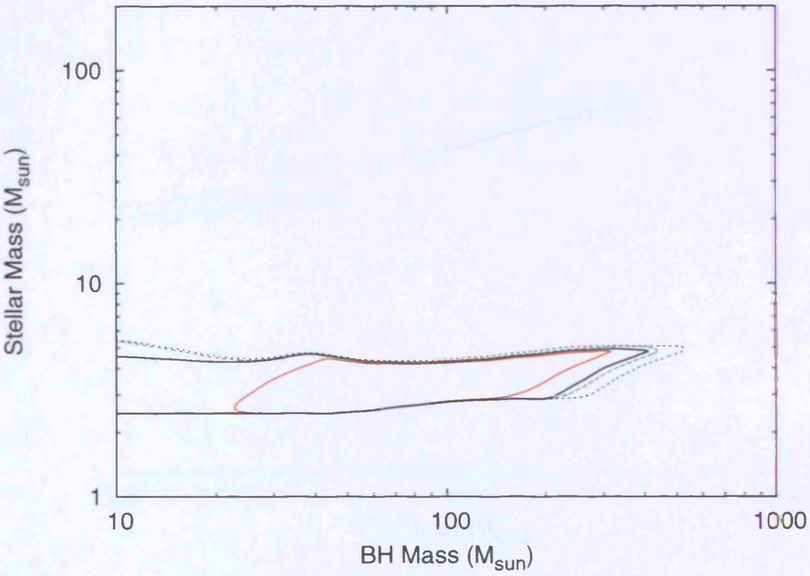

Figure 3.4: Confidence contours for the binary parameters for the source X-10 in NGC 4559. These plots show the stellar mass against the BH mass, and assume a binary inclination of $\cos(i) = 0.0$, superior conjunction, a stellar metallicity of $Z = 0.2Z_{\odot}$ and an X-ray hardness ratio of $\xi = 0.1$. The red, black (solid), green and blue lines denote the 68%, 90%, 95% and 99% confidence intervals respectively. In the top plot the counterpart is assumed to be candidate C1, while in the bottom plot candidate C3 is assumed.

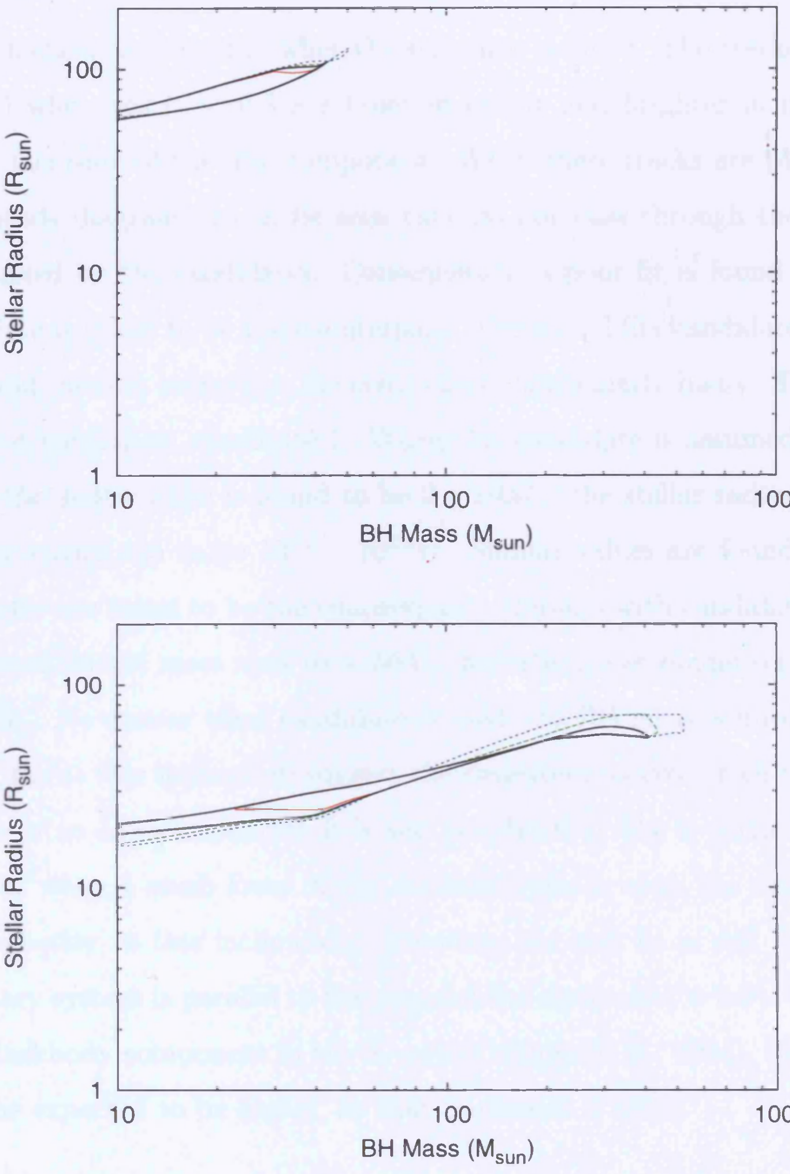

Figure 3.5: Confidence contours for the binary parameters for the source X-10 in NGC 4559. These plots show the stellar radius against the BH mass, and assume a binary inclination of $\cos(i) = 0.0$, superior conjunction, a stellar metallicity of Z= $0.2Z_{\odot}$ and an X-ray hardness ratio of $\xi = 0.1$. The red, black (solid), green and blue lines denote the 68%, 90%, 95% and 99% confidence intervals respectively. In the top plot the counterpart is assumed to be candidate C1, while in the bottom plot candidate C3 is assumed.

3.4.4 Model fits: with disc component

The picture changes considerably when the system is inclined. The tracks produced by the model when $\cos(i) = 0.5$ are bluer in colour and brighter in magnitude, owing to the inclusion of the disc component. When these tracks are plotted on a colour-magnitude diagram, it can be seen they do not pass through the region of the plot occupied by the candidates. Consequently, a poor fit is found no matter which candidate is taken to be the counterpart. The model fits candidates 5 and 6, the reddest and faintest sources in the error circle, particularly badly. The best fit is the brightest candidate, candidate 1. When this candidate is assumed to be the counterpart, the stellar mass is found to be $2 - 10M_{\odot}$, the stellar radius to be $4 - 20R_{\odot}$ and the stellar age to be $10^{7.5} - 10^{8.7}$yr. Similar values are found when the other candidates are taken to be the counterpart, although with candidates 3 and 4 the upper bound on the mass rises to $\sim 50M_{\odot}$ and the upper bound on the radius falls to $\sim 10R_{\odot}$. No matter what candidate is used, the BH mass is unconstrained.

The poor fits at this inclination suggest the emission observed from this system contains little or no disc component. It is also possible that disc is particularly faint in this system: when a much lower X-ray hardness ratio is used, the disc is fainter and the fit is better at this inclination. However, the best fit is still for the case when the binary system is parallel to the plane of the sky ($\cos(i) = 0.0$). Given that there is no blackbody component in the X-rays (Cropper et al., 2004), the hardness ratio would be expected to be higher, so that constrains it more.

3.5 ULX X-6 in M81

3.5.1 Observations

This source has an average X-ray luminosity of 2×10^{39} ergs s^{-1} (Roberts & Warwick, 2000). Liu et al. (2002) found an optical counterpart they considered unique to this ULX (designated NGC 3031 X-11 in that paper), and reported M_B, M_V and

Table 3.3: Photometric data for ULX X-6 in M81. From Liu et al. (2002).

M_B	-4.28 ± 0.04
M_V	-4.18 ± 0.03
M_{I_c}	-4.20 ± 0.07

M_I magnitudes derived from HST ACS observations. These values are listed in Table 3.3. Liu et al. (2002) assumed a distance to M81 of 3.63Mpc, and included a correction in these values for Galactic reddening.

3.5.2 Model fits: with disc component

I examine the case where this source is at superior conjunction and $\cos(i) = 0.5$ first. The model is found to be a poor fit to the observation at the 90% confidence level for this inclination: the irradiated disc/star are together too luminous to match the observation for any combination of star and BH. I have therefore lowered the hardness ratio of the irradiating X-ray spectrum in this case in order to fit the model to the observation. When ξ is lowered to 0.01, a good fit to the data can be found. The confidence contours are shown in Figures 3.6 to 3.8. It can be seen that the stellar age ranges from 10^6 – $10^{8.7}$yr, with a lower stellar age implying a higher BH mass. The stellar mass ranges from 1.5 – $14M_\odot$, and the stellar radius ranges from 2.5 – $8R_\odot$.

When the star is assumed to be in inferior conjunction, a reduced hardness ratio of $\xi = 0.01$ is again required in order to obtain a good fit. Most of the parameter space that was found to fit with the model for the superior conjunction case is contained within that here. In addition, for low BH masses, larger stars of radius 10 – $17R_\odot$ can be fitted with the observation. These parameters represent cases where the majority of the optical emission is from the unirradiated hemisphere of the star. The small, but not insignificant disc contribution, as well as the Roche lobe shape of the star, accounts for the difference between the fitted stellar parameters and those of Liu et al. (2002) in this inferior conjunction case. At higher BH masses the emission is disc dominated and the results are not strongly dependent on the phase of the star.

3.5.3 Model fits: no disc component

I now examine the case when $\cos(i) = 0.0$ (Figures 3.6 to 3.8). In this orientation, the model can be fit with the observation for a hardness ratio of $\xi = 0.1$. It should be noted first of all that there is an upper bound on the BH mass of $33M_\odot$. The stellar age that fits with the observation ranges from $10^{7.9}$ – $10^{8.7}$yr, and the mass and radius range from 3 – $5.5M_\odot$ and 10 – $15R_\odot$ respectively. These values fit equally well, when $\xi = 0.01$, since the stellar luminosity is much less sensitive to changes in the X-ray hardness than the disc, and for this inclination there is no disc component to the emission.

3.5.4 An additional constraint on the stellar age

Liu et al. (2002) found the field stars in the vicinity of this ULX range in age from 1.0×10^6 – 1.0×10^8yr. If the donor in the ULX binary is assumed to be of a similar age, it can be seen from Figures 3.6 to 3.8 that the stellar parameters are very tightly constrained in the $\cos(i) = 0.0$ case. In the $\cos(i) = 0.5$ case, it can be seen that there is a lower limit on the BH mass of $20M_\odot$ if the stellar age is constrained in this way.

3.6 ULX in NGC 5204

3.6.1 Observations

HST WFPC2 and ACS observations of the optical counterpart to a ULX in NGC 5204 were described in Liu et al. (2004). This source has an X-ray luminosity of

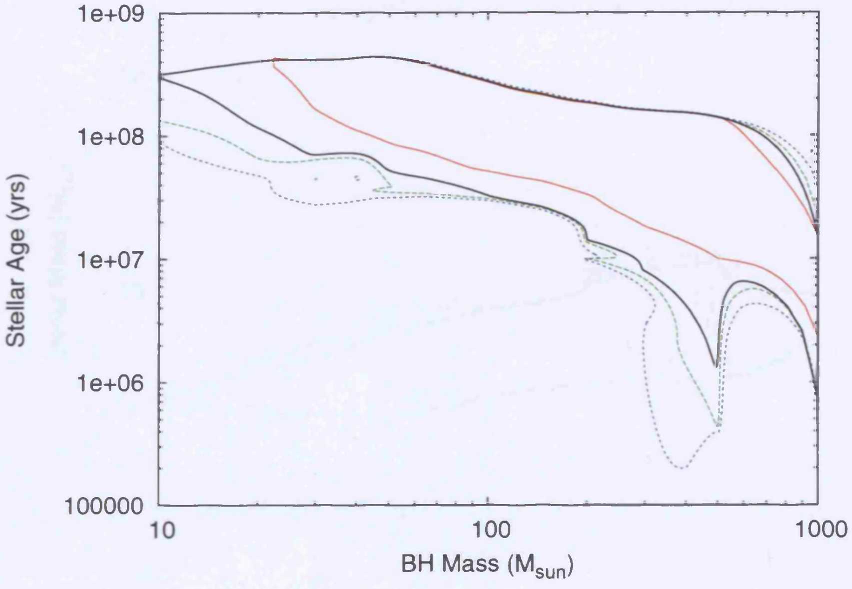

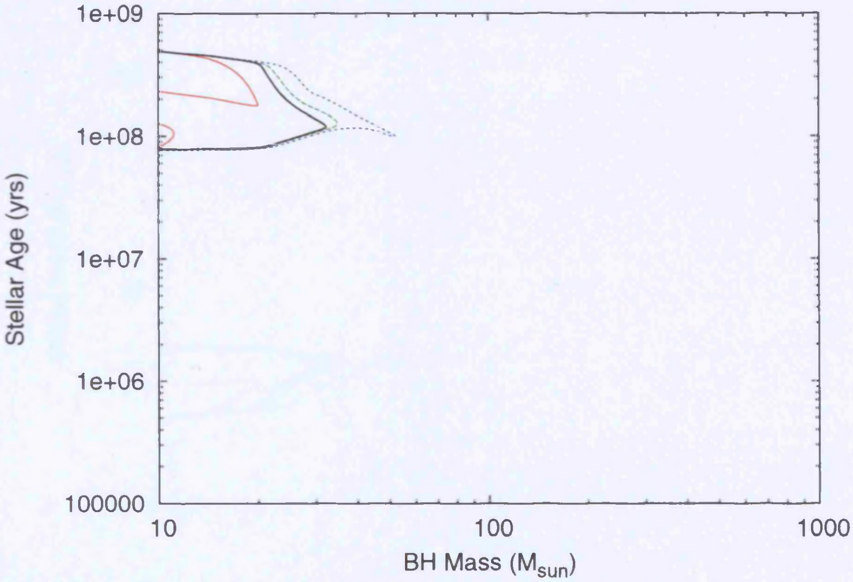

Figure 3.6: Confidence contours for the binary parameters for the source X-6 in M81. These plots show the stellar age against the BH mass, and assume superior conjunction, a stellar metallicity of Z= $0.2Z_{\odot}$ and an X-ray hardness ratio of $\xi = 0.1$. The red, black (solid), green and blue lines denote the 68%, 90%, 95% and 99% confidence intervals respectively. In the top plot a binary inclination of $\cos(i) = 0.5$ is used, while $\cos(i) = 0.0$ is used in the bottom plot.

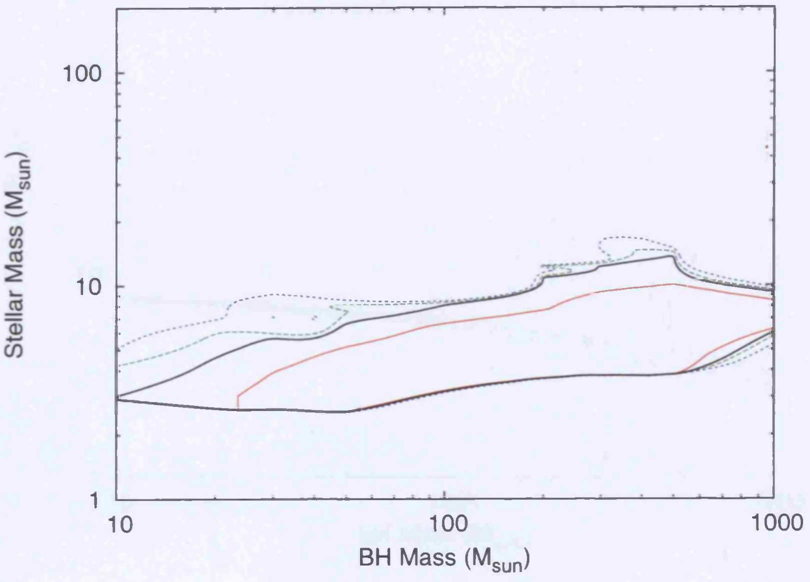

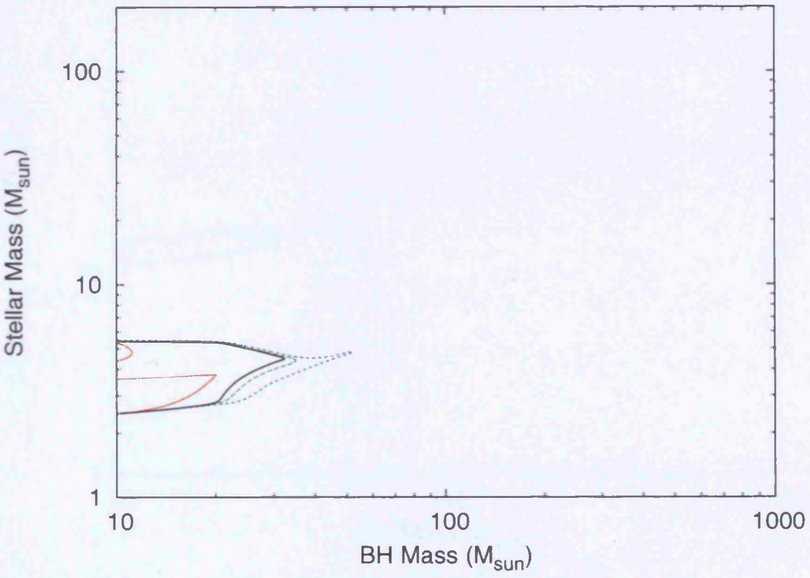

Figure 3.7: Confidence contours for the binary parameters for the source X-6 in M81. These plots show the stellar mass against the BH mass, and assume superior conjunction, a stellar metallicity of Z= $0.2Z_{\odot}$ and an X-ray hardness ratio of $\xi = 0.1$. The red, black (solid), green and blue lines denote the 68%, 90%, 95% and 99% confidence intervals respectively. In the top plot a binary inclination of $\cos(i) = 0.5$ is used, while $\cos(i) = 0.0$ is used in the bottom plot.

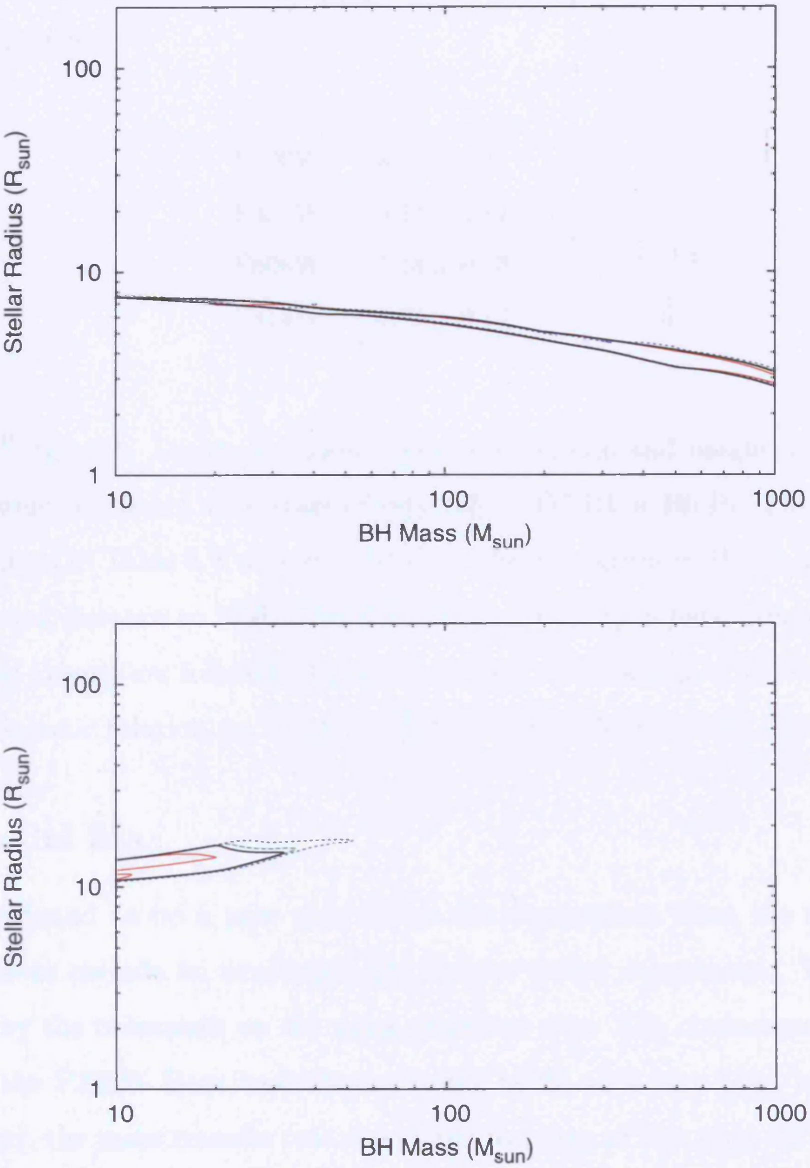

Figure 3.8: Confidence contours for the binary parameters for the source X-6 in M81. These plots show the stellar radius against the BH mass, and assume superior conjunction, a stellar metallicity of Z= $0.2Z_\odot$ and an X-ray hardness ratio of $\xi = 0.1$. The red, black (solid), green and blue lines denote the 68%, 90%, 95% and 99% confidence intervals respectively. In the top plot a binary inclination of $\cos(i) = 0.5$ is used, while $\cos(i) = 0.0$ is used in the bottom plot.

Table 3.4: Photometric data for the ULX in NGC 5204, using the HSTMAG system. From Liu et al. (2004).

F220W	-8.51 ± 0.11
F435W	-6.49 ± 0.11
F606W	-5.44 ± 0.13
F814W	-4.38 ± 0.13

$L_x \simeq 3 \times 10^{39}$ergs s^{-1}. Liu et al. (2004) found the colours and magnitudes of the counterpart were consistent with stars of type O5 V, O7 III or B0 Ib. The absolute magnitudes given in Table 3.4 were derived from the data given in Liu et al. (2004), with an assumed distance to NGC 5204 of 4.3Mpc. These data have been corrected for interstellar absorption following Liu et al. (2004), who use $n_H = 10^{21}$ cm^{-2} and assume the Galactic relation $n_H = 5.8 \times 10^{21} E(B-V)$ (Bohlin et al., 1978).

3.6.2 Model fits

The model is found to be a very poor fit to the observation when the system is oriented so as to include an irradiated disc and/or stellar component. This poor fit is caused by the constraint on the mass accretion rate. The counterpart is very luminous in the F220W filter, and thus can only be fit with very blue, early type stars. However, the mass transfer rate calculated for stars of this type are in excess of that which is implied by the X-ray luminosity by an order of magnitude or more. The best solution is for a BH mass of $1000 M_\odot$ and a stellar age, mass and radius of $10^{5.3}$yr, $52 M_\odot$ and $9 R_\odot$ respectively, but this is a poor fit to the model. The mass transfer rate constraint is therefore removed. In this case, the results imply a companion star with a mass of 60 to $110 M_\odot$, a radius of 13 – $15 R_\odot$ and an age of $10^{6.3}$yr or less, for an inclination of $\cos(i) = 0.5$ and superior conjunction. Similar results are found when the star is placed in inferior conjunction, and also when

Table 3.5: Photometric data for ULX-1 in M101. From Kuntz et al. (2005).

M_B	-6.19 ± 0.15
M_V	-5.92 ± 0.12
M_{I_c}	-5.81 ± 0.16

$\cos(i) = 0.0$.

There is an upper bound on the BH mass of $240M_\odot$ when an inclination of $\cos(i) = 0.5$ is assumed but this upper bound does not exist for $\cos(i) = 0.0$.

3.7 M101 ULX-1

3.7.1 Observations

The source designated ULX-1 in M101 has a peak X-ray luminosity of $\simeq 1.2 \times 10^{39}$ergs s^{-1}, making it the least X-ray luminous object studied in this work. Kuntz et al. (2005) reported a unique optical counterpart observed with the *HST* ACS instrument. Kuntz et al. (2005) give M_B, M_V and M_I values which assume a distance to M101 of 7.2Mpc and include a correction for Galactic reddening and reddening from the disc of M101. These data are given in Table 3.5.

3.7.2 Model fits

A good fit is found between the model and the observation only when a disc component is included in the emission ($\cos(i) \neq 0.0$). As in the case of the ULX in NGC 5204, this poor fit for $\cos(i) = 0.0$ results from the upper bound on the mass accretion rate – when this constraint is not used, a star of age $10^{7.0}$yr to $10^{7.3}$yr, mass 11 – $100M_\odot$ and radius 12 – $33R_\odot$ is found to fit with the observation. There is no constraint on the BH mass.

When an inclination of $\cos(i) = 0.5$ is used, the optical data is found to be consistent with the mass accretion rate as determined from the X-ray luminosity. The donor age is determined to have an age of 10^8 – $10^{8.7}$yr, a mass of 2 – $7M_\odot$ and a radius of 6 – $30R_\odot$. Again, there is no constraint on the BH mass, but the fitted stellar radius is found to depend strongly on the BH mass, with the lower radius values implying a more massive BH.

The constraints on the stellar parameters determined here are much looser than those reported by Kuntz et al. (2005). This is to be expected: by allowing emission from both an irradiated star and disc component, the observation fits with a much wider range of binary systems.

3.8 ULX in NGC 5408

3.8.1 Observations

NGC 5408 contains a ULX with an X-ray luminosity of 10^{40}ergs s^{-1}. This source was initially thought to be consistent with a beamed microquasar (Kaaret et al., 2003). More recent studies have shown a soft component in the disc emission and QPOs, which could be interpreted as evidence for an IMBH of mass $1000M_\odot$ or greater (Soria et al., 2004; Strohmayer et al., 2007). However, these may also be explained by alternative scenarios that are consistent with masses $\sim 100M_\odot$ (Stobbart et al., 2006; Goncalves & Soria, 2006). Therefore, we examine whether optical observations can be used to constrain these system parameters.

The archival HST/WFPC2 and Subaru observations are used to determine M_B, M_V and M_I photometric magnitudes for the optical counterpart.There are in fact a number of candidates for the optical counterpart within the *Chandra* error circle: it is assumed here the counterpart is the source which appears most luminous in the V-band *HST* observation. A distance to NGC 5408 of 4.8Mpc is assumed. These data are listed in Table 3.6.

Table 3.6: Photometric data for the ULX in NGC5408. From *Subaru* and *HST* archival data.

M_B	-6.4 ± 0.2
M_V	-6.4 ± 0.2
M_{I_c}	-6.1 ± 0.1

3.8.2 Model fits

Examining the cos(i) = 0.5 case first (Figures 3.9 to 3.11), it can be seen that a donor star of mass 6 – $24M_\odot$ can be fitted to the observational data over the entire BH mass range. These stars have ages $\sim 10^7$yr and radii of 23 – $44R_\odot$. It can be seen also that when a BH mass of greater than $100M_\odot$ is assumed, more massive ($< 107M_\odot$), younger and more compact stars can also be fitted to the observation. A very massive ($> 67M_\odot$) donor is also possible when a BH mass of less than $30M_\odot$ is used.

In the cos(i) = 0.0 case, it can be seen that an upper bound on the BH mass of $110M_\odot$ exists. The donor star has an age of 10^7 – $10^{7.8}$yr, a mass of 6 – $15M_\odot$ and a radius of 23 – $43R_\odot$. A very massive ($> 80M_\odot$) donor is also possible when a very low BH mass is used.

3.9 ULX in Holmberg II

3.9.1 Observations

This ULX has an X-ray luminosity measured at up to 10^{40}ergs s^{-1} (Kaaret et al., 2004), although it is highly variable. It is associated with a diffuse, photoionised nebula, whose energetics suggests that the X-ray emission from the accreting source is truly luminous and not strongly beamed. Kaaret et al. (2004) gives both the M_V

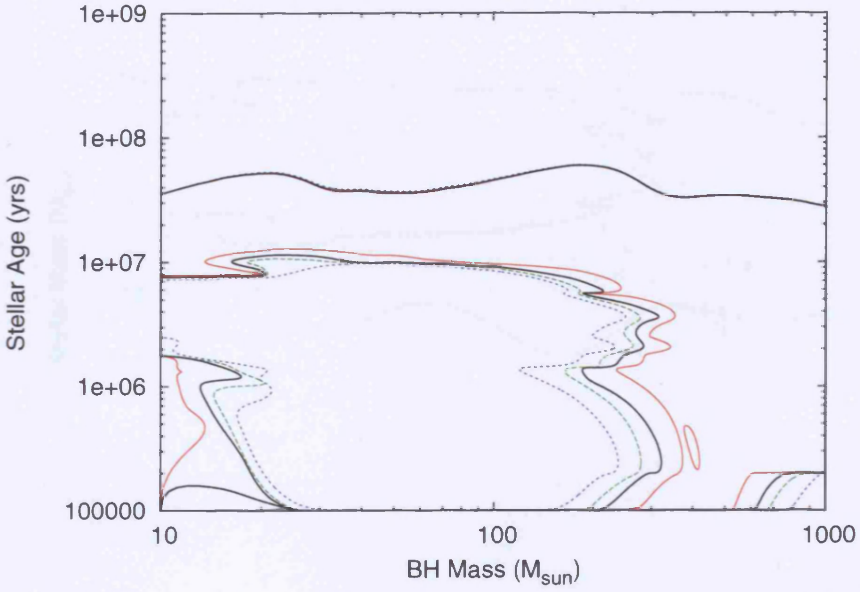

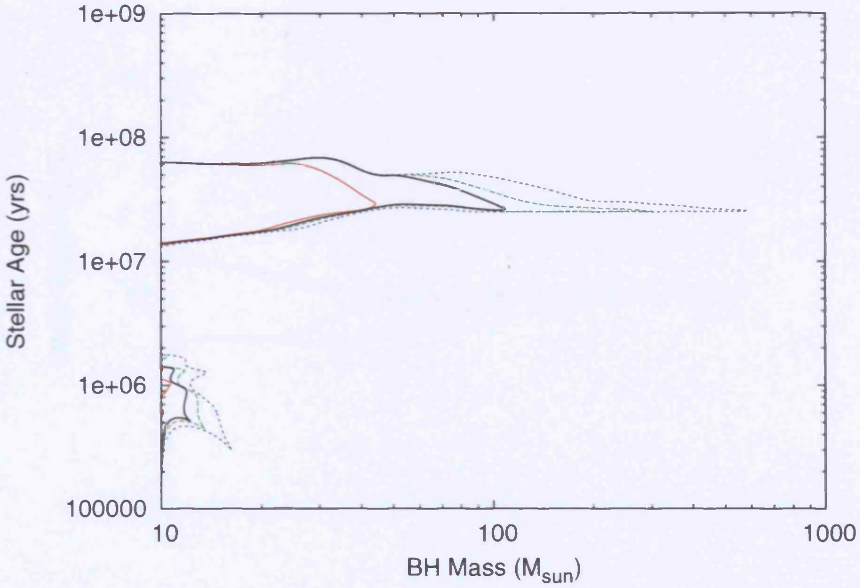

Figure 3.9: Confidence contours for the binary parameters for the ULX in NGC 5408. These plots show the stellar age against the BH mass, and assume superior conjunction, a stellar metallicity of Z= $0.2Z_{\odot}$ and an X-ray hardness ratio of $\xi = 0.1$. The red, black (solid), green and blue lines denote the 68%, 90%, 95% and 99% confidence intervals respectively. In the top plot a binary inclination of $\cos(i) = 0.5$ is used, while $\cos(i) = 0.0$ is used in the bottom plot.

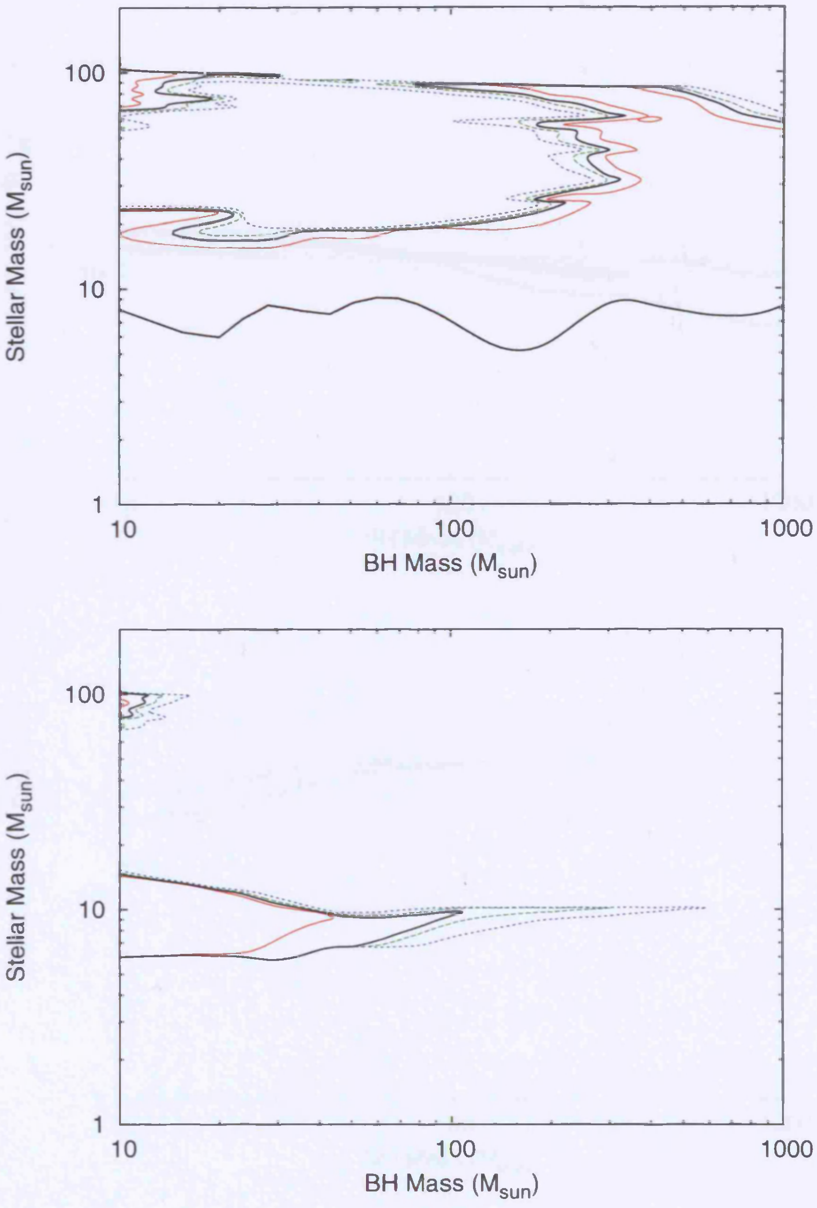

Figure 3.10: Confidence contours for the binary parameters for the ULX in NGC 5408. These plots show the stellar mass against the BH mass, and assume superior conjunction, a stellar metallicity of Z= $0.2Z_{\odot}$ and an X-ray hardness ratio of $\xi = 0.1$. The red, black (solid), green and blue lines denote the 68%, 90%, 95% and 99% confidence intervals respectively. In the top plot a binary inclination of $\cos(i) = 0.5$ is used, while $\cos(i) = 0.0$ is used in the bottom plot.

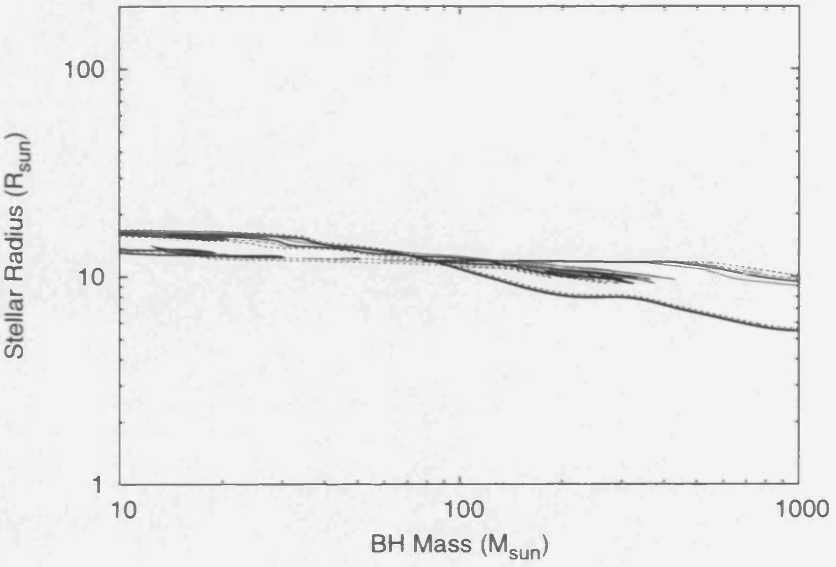

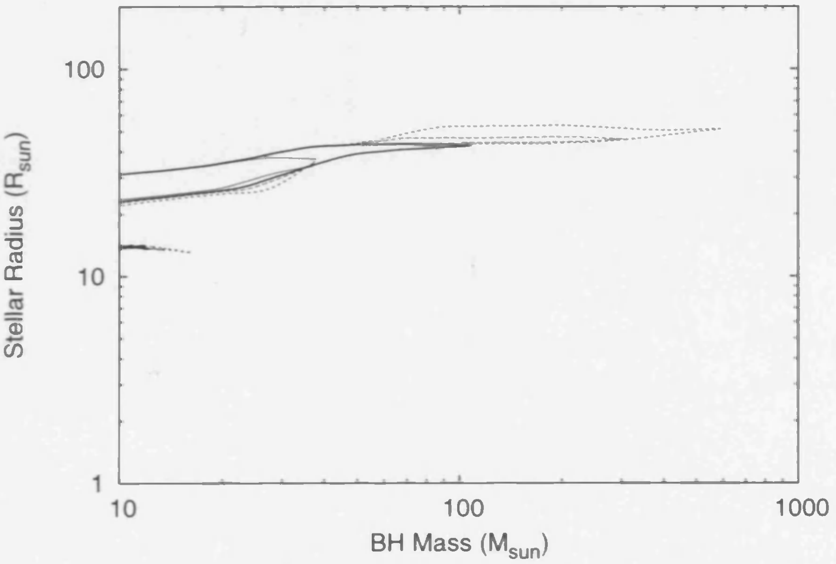

Figure 3.11: Confidence contours for the binary parameters for the ULX in NGC 5408. These plots show the stellar radius against the BH mass, and assume superior conjunction, a stellar metallicity of Z= $0.2Z_{\odot}$ and an X-ray hardness ratio of $\xi = 0.1$. The red, black (solid), green and blue lines denote the 68%, 90%, 95% and 99% confidence intervals respectively. In the top plot a binary inclination of $\cos(i) = 0.5$ is used, while $\cos(i) = 0.0$ is used in the bottom plot.

Table 3.7: Photometric data for the ULX in Holmberg II. From Kaaret et al. (2004).

M_B	-6.03 ± 0.19
M_V	-5.78 ± 0.11

magnitude of the counterpart and its (B-V) colour, assuming a distance to Holmberg II of 3.05Mpc. They apply a reddening correction to this, accounting for extinction within our Galaxy. From those they deduce the companion to be an O4V or B3Ib star (their M_B and M_V magnitudes are given in Table 3.7).

3.9.2 Model fits

The constraints on the parameters for this source are poor, owing to the fact that the optical emission is measured in only two filters. The BH mass cannot be constrained for any orientation. As regards the parameters of the donor star, it can be seen in Figures 3.12 to 3.14 that if $\cos(i) = 0.5$ the stellar age and mass are poorly constrained, with the mass ranging from 6 to $82M_\odot$ and the age ranging from 10^5 to $10^{7.85}$yr. The stellar radius is better defined, and lies between 4 and $12R_\odot$.

For the $\cos(i) = 0.0$ case the picture is more complicated. The results suggest two discrete possibilities for the donor star parameters. It can either be a star of mass $37 - 92M_\odot$ and radius $10 - 12R_\odot$, or a much older object with mass $5 - 34M_\odot$ and radius $12 - 55R_\odot$. These two possibilities are more tightly constrained as the BH mass increases.

3.10 Summary

In this chapter I have applied the model of the previous chapter to observations of the optical counterparts of six ULXs. In five of these sources, previous authors have inferred a single candidate for the counterpart, and I have used this candidate. For

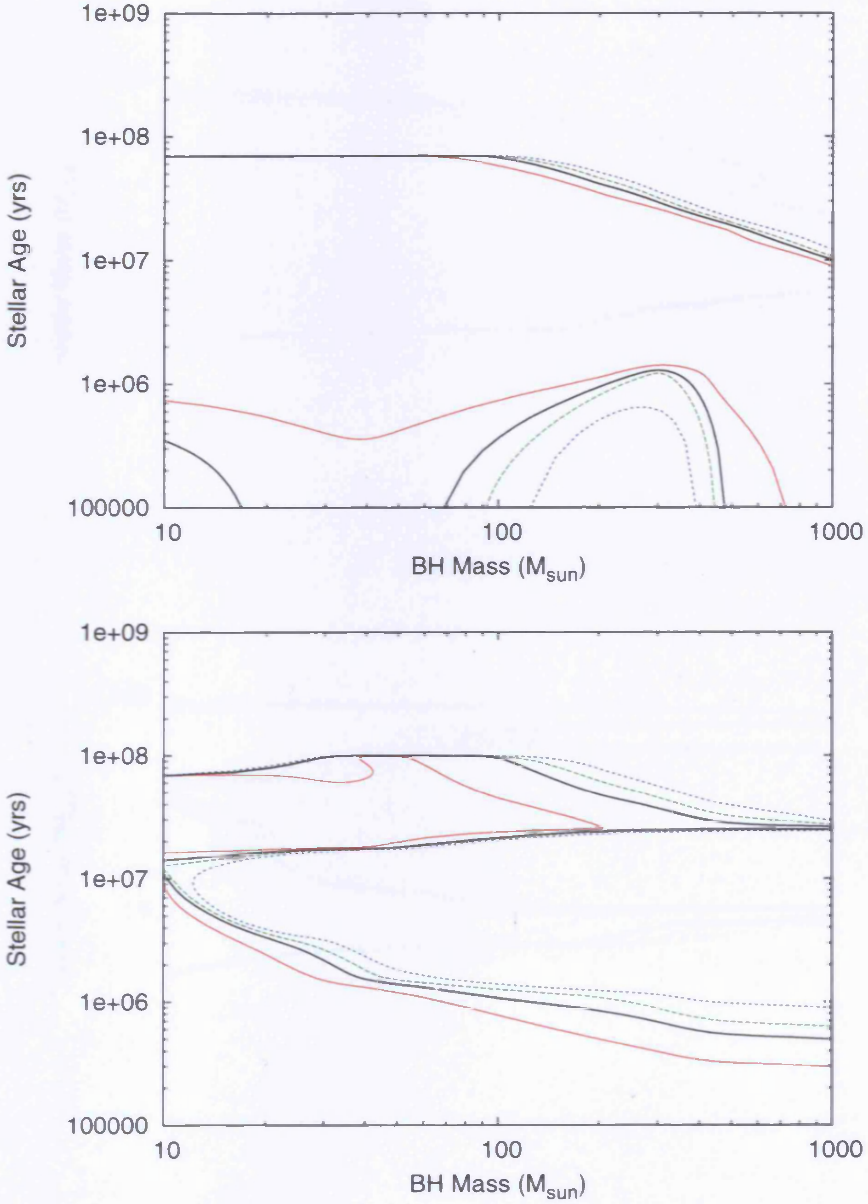

Figure 3.12: Confidence contours for the binary parameters for the ULX in Holmberg II. These plots show the stellar age against the BH mass, and assume superior conjunction, a stellar metallicity of Z= $0.2Z_{\odot}$ and an X-ray hardness ratio of $\xi = 0.1$. The red, black (solid), green and blue lines denote the 68%, 90%, 95% and 99% confidence intervals respectively. In the top plot a binary inclination of $\cos(i) = 0.5$ is used, while $\cos(i) = 0.0$ is used in the bottom plot.

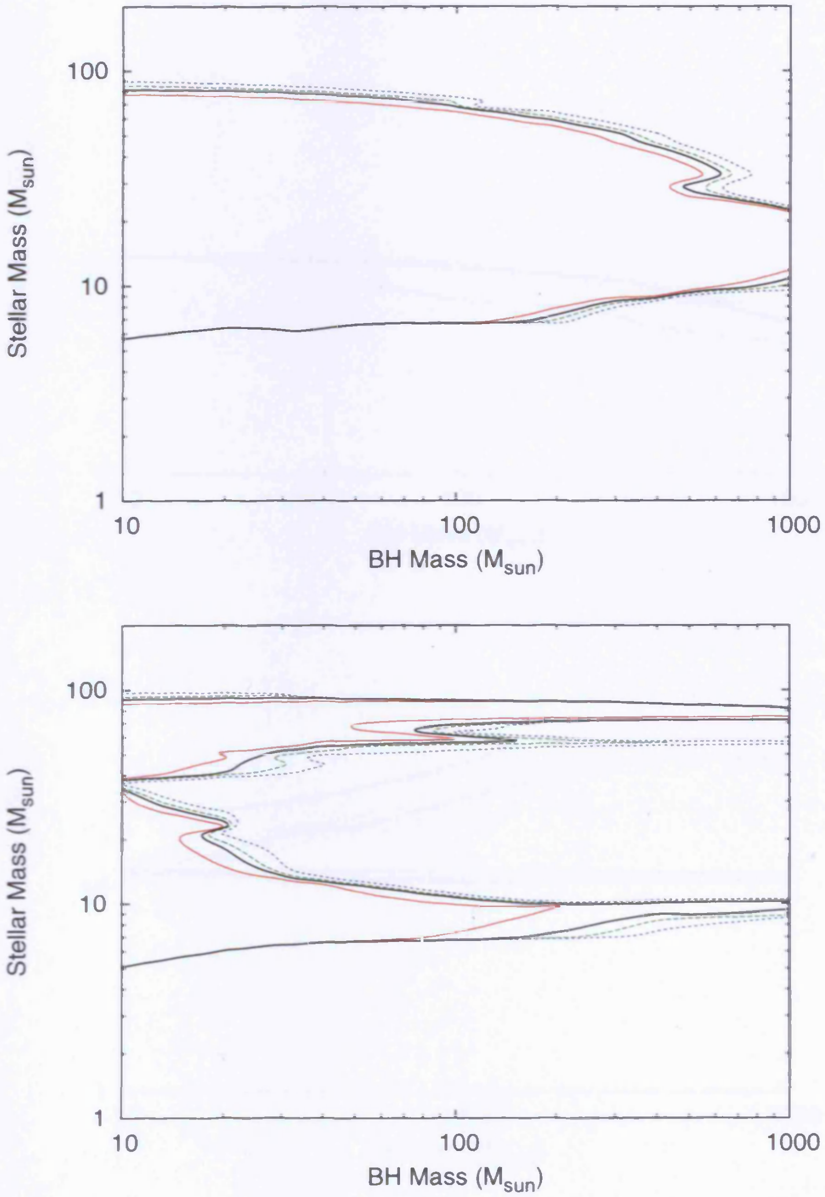

Figure 3.13: Confidence contours for the binary parameters for the ULX in Holmberg II. These plots show the stellar mass against the BH mass, and assume superior conjunction, a stellar metallicity of Z= $0.2Z_\odot$ and an X-ray hardness ratio of $\xi = 0.1$. The red, black (solid), green and blue lines denote the 68%, 90%, 95% and 99% confidence intervals respectively. In the top plot a binary inclination of $\cos(i) = 0.5$ is used, while $\cos(i) = 0.0$ is used in the bottom plot.

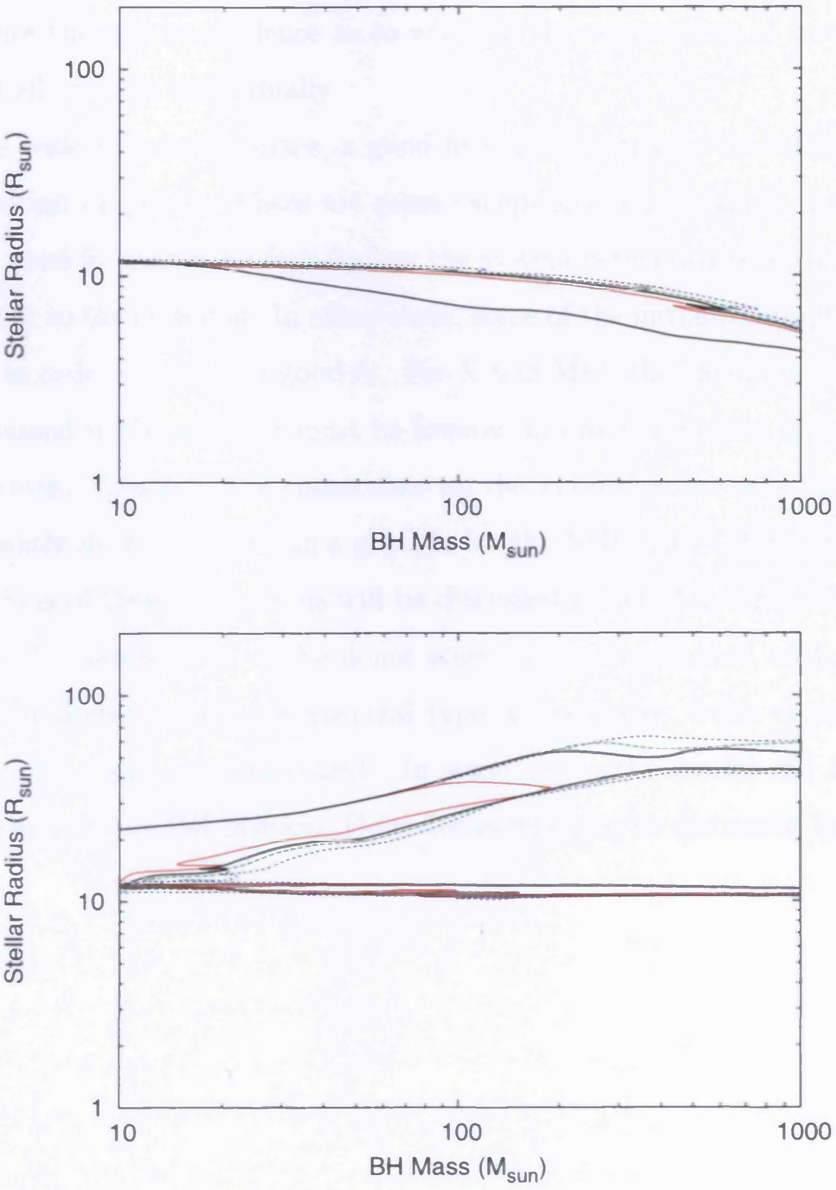

Figure 3.14: Confidence contours for the binary parameters for the ULX in Holmberg II. These plots show the stellar radius against the BH mass, and assume superior conjunction, a stellar metallicity of Z= $0.2Z_{\odot}$ and an X-ray hardness ratio of $\xi = 0.1$. The red, black (solid), green and blue lines denote the 68%, 90%, 95% and 99% confidence intervals respectively. In the top plot a binary inclination of $\cos(i) = 0.5$ is used, while $\cos(i) = 0.0$ is used in the bottom plot.

X-10 in NGC 4559, I find a number of candidates within the X-ray observation error circle and since there is no evidence as to which is the counterpart, I have applied the model to all of them individually.

Given the wide parameter space, a good fit can generally be found for any assumed inclination or phase. There are some exceptions: for example, for X-10 in NGC 4559 a good fit cannot be found when the system is inclined so that there is a disc component to the emission. In other cases, some of the initial assumptions have been altered in order to obtain a good fit. For X-6 in M81, the hardness ratio of 0.1 generally assumed in this chapter must be lowered in order to obtain a good fit for some inclinations. Similarly, the constraints on the mass transfer rate needs to altered significantly in order to obtain a good fit for the NGC 5204 ULX counterpart. The implications of these alterations will be discussed in detail in Chapter 5.

In general, the parameters of the donor stars can be determined with some accuracy. The luminosity class and spectral type of the donor, both currently and at ZAMS can therefore be determined. In some cases, the model fits have provided constraints on the BH masses. These issues will also be discussed in detail in Chapter 5.

Chapter 4

Variability in optical counterparts

4.1 Introduction

Some optical counterparts of ULXs have been observed on more than one occasion. In this chapter. I investigate sources for which there is more than one set of photometric data available.

4.2 A discussion on variability

In Section 2.9.6 I briefly discussed how. by varying the orbital phase parameter. a model optical lightcurve could be generated. In Figure 2.13 I gave example lightcurves. demonstrating how the optical luminosity varies with phase.

The variability is due mainly to two effects. Firstly. a Roche lobe filling star will display ellipsoidal variation. owing to the fact that it is not spherical and so its cross-sectional area. and therefore the observed optical luminosity. will vary with phase. The maximum observed luminosity will be when the binary components are at their greatest elongation (phase 0.25 and 0.75). The minimum luminosity will be when the binary components are in conjunction with the observer (phase 0 and 0.5). The second effect is the X-ray heating. The hemisphere facing the BH will be heated and the hemisphere facing away from it will not. The apparent stellar luminosity will therefore be highest from the heating effect when the star and observer are in superior conjunction with respect to the BH (a phase of 0.5) and lowest when they are at inferior conjunction (a phase of 0).

The phase at which the optical luminosity peaks will depend on whether the ellipsoidal variation or the irradiative heating is the dominant effect. In the theoretical lightcurve in Figure 2.13 it can be seen that the ellipsoidal variation is dominant when an O5V donor is used, although the results of the previous chapter suggest that more evolved donors are more typical in these sources. In that case, the irradiative heating is more likely to be the dominant effect. I now consider how varying the model parameters affects the amplitude of this variation: the difference in apparent stellar luminosity between a phase of 0 and the peak of the optical lightcurve (at a phase of 0.25 or 0.5, depending on the dominant effect). This quantity will be referred to as Δm_{max}. ΔV_{max} will be used to refer to the amplitude in the V band, ΔI_{max} for the I band amplitude, and so on.

It is obvious that Δm_{max} at optical wavelengths will increase as the irradiating luminosity is increased, since the temperature difference between the stellar hemisphere facing the BH and the hemisphere facing away will be increased. The parameters determining the Roche lobe geometry (BH mass, stellar mass, stellar radius) will also be important here, since they determine the binary separation, and hence the amount of flux incident on the stellar surface. It can be seen in Figure 2.11 that increasing the binary separation by decreasing the mass ratio M_2/M_1, reduces the luminosity of the irradiated hemisphere and hence will reduce the amplitude of the lightcurve. Increasing the stellar radius also increases the separation, but by comparing Figure 2.11 with Figure 2.10 it can be seen that when a supergiant donor is used instead of a MS star, the luminosity is enhanced owing to the larger surface area on which the X-rays are incident. This compensates for the increase in separation. The binary geometry also affects the extent of the ellipsoidal effect, but it is quite a small difference. To summarise then, Δm_{max} will tend to be greatest when the BH mass is low and the star is evolved and larger in radius. An additional important parameter is the inclination. Δm_{max} will be greatest when the binary plane is perpendicular to the plane of the sky ($\cos(i) = 0.0$), decreasing to zero as $\cos(i)$ is increased to 1.0.

The contribution of the disc has not yet been considered in this discussion. The luminosity of the disc is constant, and so the addition of the disc component will mean the optical luminosity of the ULX will increase by the same amount over the entire phase range. The absolute variation in Δm_{max} will therefore not be affected, but the relative Δm_{max} will. If the optical light is dominated by a very luminous disc, the lightcurve will be flat, irrespective of the other parameters. It has been shown in previous chapters that the disc will be more luminous if the X-ray luminosity of the source is increased, if the hardness of the X-rays is increased or if the binary separation is increased. In addition, the apparent disc luminosity will change with inclination. When the binary is perpendicular to the sky there is no disc contribution, but as $\cos(i)$ is increased the disc component will increase, until $\cos(i) = 1.0$, where the disc is observed 'face-on'. The disc contribution therefore reinforces the point that a higher BH mass and/or inclination will lead to a flatter lightcurve.

4.3 Application to photometric data

In order to generate an optical lightcurve for a ULX counterpart, the binary period of the source must be sampled sufficiently. This has not yet been done. What is available for the sources discussed in this chapter are sets of observations taken at two or three separate epochs. This gives us two or three different points that will lie somewhere on the lightcurve of the source, but since the binary phase at the time of the observation is unknown, the position of these points on the lightcurve is also unknown. This is quite a limitation; if, coincidentally, the two sets of observations were both taken at the same phase, there will be no difference between the amount of optical flux we measure, irrespective of the binary parameters. If, just as coincidentally, one set of observations was taken at a binary phase of 0 and the other at the binary phase corresponding to the peak luminosity, then the difference between the two will be the lightcurve amplitude, Δm_{max}. Most likely, the binary was at different and arbitrary phases for each observation. The luminosity difference between the two will therefore be between 0 and Δm_{max}.

It is apparent therefore that there is a high degree of uncertainty in drawing any kind of conclusions about the variability of the optical counterpart from only two observations. As in the previous chapter, a multi-dimensional array of results can be generated by using the stellar evolution code as an input into the model, and varying the other model parameters such as BH mass, X-ray luminosity, inclination etc. This time however, I additionally determine the lightcurve amplitudes ΔB_{max}, ΔV_{max} and ΔI_{max} for each set of model parameters.

As before, I fit the observations to the theoretical photometric calculations. The Δm_{max} provides an additional constraint. If the luminosity difference between two observations of the source is large, then solutions where Δm_{max} is less than this can be excluded. When the luminosity difference is not statistically significant, then no solutions can be excluded. It may be that the lightcurve is flat, or it may be that the two observations were taken when the source was at a similar binary phase. However, it can be presumed that a solution with a flat lightcurve is more likely, since it does not require a coincidental similarity of binary phase between the two observations. Solutions with progressively larger Δm_{max} values require progressively more improbable coincidences in order to display no variation between the two observations.

Table 4.1: Photometric data for the counterpart to ULX X-9 in M51. The WFPC2 data are taken from Terashima et al. (2006) and the ACS data are taken from Liu et al. (2005). Both have been converted to absolute magnitudes as described in the text. In addition, the variation between the two observations is given, where $\Delta m = m^{WFPC2} - m^{ACS}$.

	HST WFPC2	*HST* ACS	$\|\Delta m\|$
M_B	-3.644 ± 0.229	-4.26 ± 0.56	0.62 ± 0.79
M_V	-3.870 ± 0.093	-3.94 ± 0.64	0.07 ± 0.73
M_{I_c}	-4.353 ± 0.192	-3.39 ± 0.51	0.96 ± 0.70

4.4 ULX X-9 in M51

4.4.1 Observations, and determination of the counterpart

This ULX was found by Terashima & Wilson (2004) to have an X-ray luminosity of $L_x = 3 \times 10^{39}$ergs s^{-1}. There exist two epochs of optical observations of this source taken with *HST*: Liu et al. (2005) report WFPC/2 observations and Terashima et al. (2006) report ACS observations. Note that this source is refered to as X-5 in Liu et al. (2005). Liu et al. (2005) reported several possible candidates to this ULX, but the astrometry of Terashima et al. (2006) find candidate 1 in Liu et al. (2005) to be the counterpart. The two sets of photometric data for this candidates are listed in Table 4.1. Terashima et al. (2006) find the amount of Galactic extinction to be negligible, and so no correction for absorption has been made. The apparent magnitudes given by the authors have been converted to absolute magnitudes, assuming a distance to M51 of 7.7Mpc.

4.4.2 Determining the binary parameters

With disc component

The fitted model parameters for an inclination of $\cos(i) = 0.5$ are shown in Figures 4.1 to 4.3. Fits to both sets of data are shown on separate plots, although the binary parameters are better determined when the WFPC2 data are used owing to the smaller photometric errors.

It can be seen that there is an upper limit on the BH mass of $300M_\odot$ when the fit is made to the WFPC2 data. The stellar age is found to be $< 10^{8.19}$yr, and the stellar mass and radius are found to be $3 - 20M_\odot$ and $1.5 - 5R_\odot$ respectively. The constraints are looser when the ACS data is used, and the constraint on the BH mass disappears.

No disc component

When $\cos(i) = 0.0$, the stellar parameters are very poorly constrained when the model is fit to the ACS observations. Figures 4.4 and 4.5 display the fitted parameters when the WFPC2 data is used.

It can be seen that in this superior conjunction case, there is a lower bound on the BH mass of $70M_\odot$. The stellar age, mass and radius are found to be $10^8 - 10^{8.70}$yr, $2 - 5M_\odot$ and $15 - 50R_\odot$ respectively.

In the inferior conjunction case, the fit is very poor, owing to the constraint on the mass transfer rate. When this constraint is removed the donor is found to be of age $\sim 10^{7.7}$, mass $7M_\odot$ and radius $15 - 35R_\odot$.

4.4.3 Counterpart variability

In Table 4.1 the luminosity variation Δm between the two observations is shown for each passband. There is very little evidence for variation in the optical luminosity of the source between the two observations. In the B and V bands, there is no measurable variation in luminosity at the 1σ level determined by the errors on the

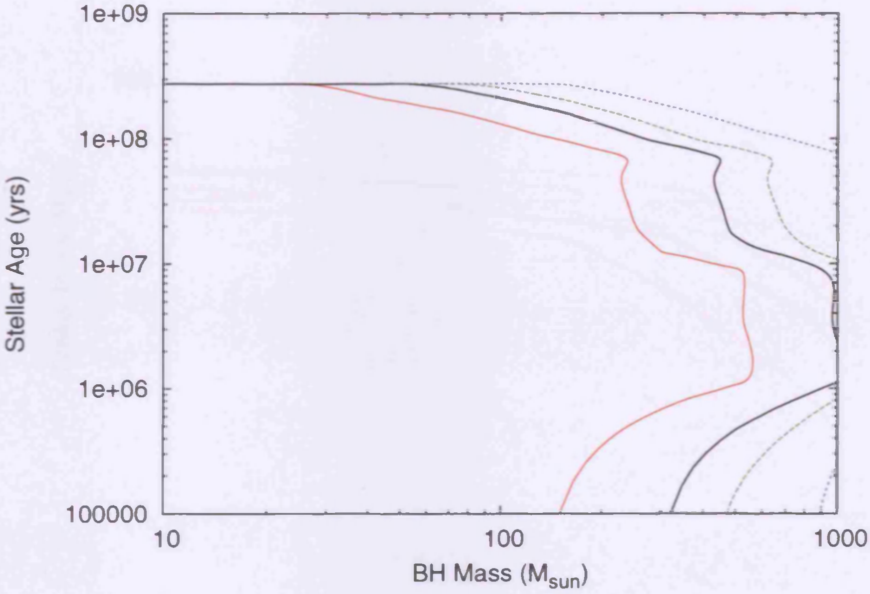

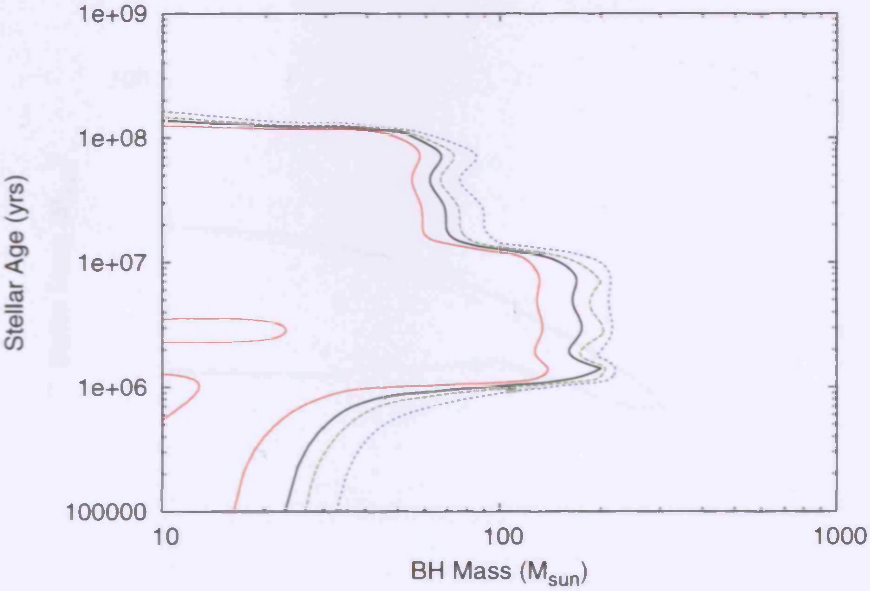

Figure 4.1: Confidence contours for the binary parameters for ULX X-9 in M51. These plots show the stellar age against the BH mass, assuming a binary inclination of $\cos(i) = 0.5$, superior conjunction with respect to the observer and the star, a stellar metallicity of Z= $0.2Z_{\odot}$, and an X-ray hardness ratio of $\xi = 0.1$. The red, black (solid), green and blue lines denote the 68%, 90%, 95% and 99% confidence intervals respectively. The top plot uses the *HST* ACS photometric data, while the bottom plot uses the *HST* WFPC2 data.

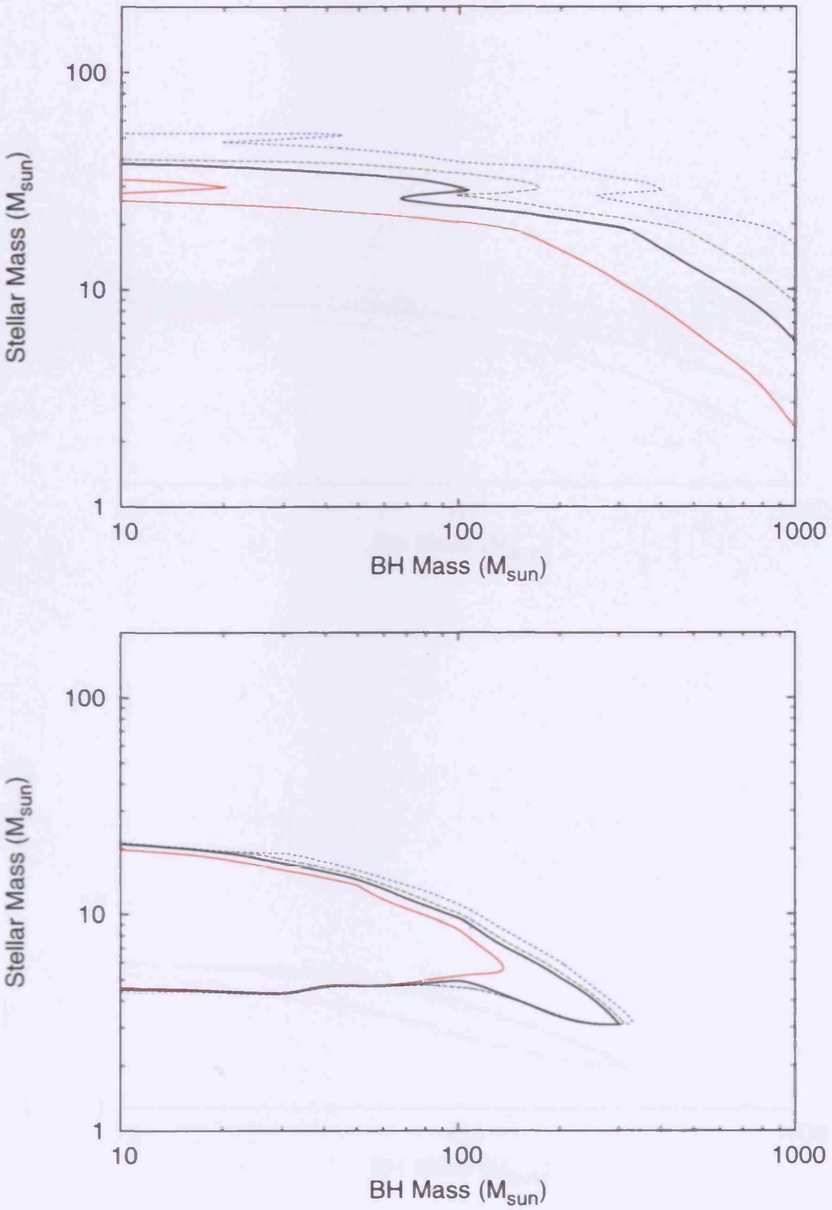

Figure 4.2: Confidence contours for the binary parameters for ULX X-9 in M51. These plots show the stellar mass against the BH mass, assuming a binary inclination of $\cos(i) = 0.5$, superior conjunction with respect to the observer and the star, a stellar metallicity of Z= $0.2Z_{\odot}$, and an X-ray hardness ratio of $\xi = 0.1$. The red, black (solid), green and blue lines denote the 68%, 90%, 95% and 99% confidence intervals respectively. The top plot uses the *HST* ACS photometric data, while the bottom plot uses the *HST* WFPC2 data.

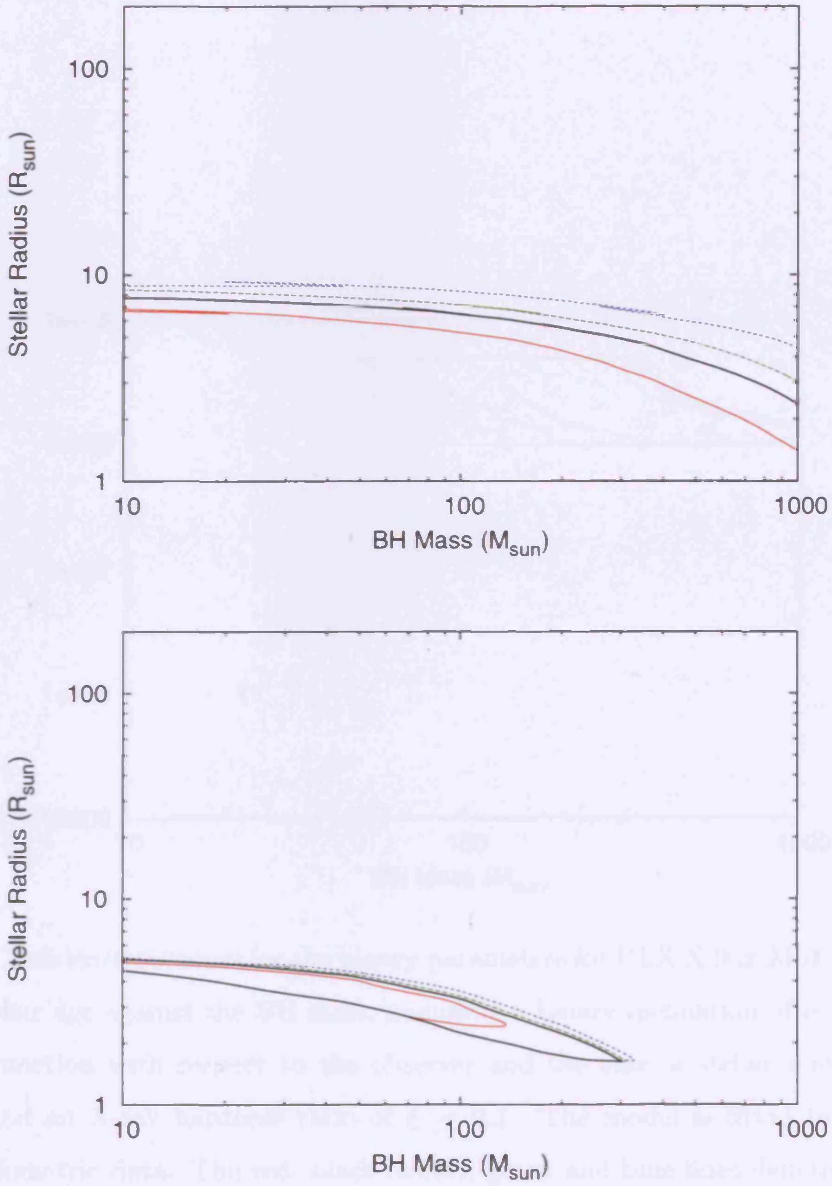

Figure 4.3: Confidence contours for the binary parameters for ULX X-9 in M51. These plots show the stellar radius against the BH mass, assuming a binary inclination of $\cos(i) = 0.5$, superior conjunction with respect to the observer and the star, a stellar metallicity of Z= $0.2Z_{\odot}$, and an X-ray hardness ratio of $\xi = 0.1$. The red, black (solid), green and blue lines denote the 68%, 90%, 95% and 99% confidence intervals respectively. The top plot uses the *HST* ACS photometric data, while the bottom plot uses the *HST* WFPC2 data.

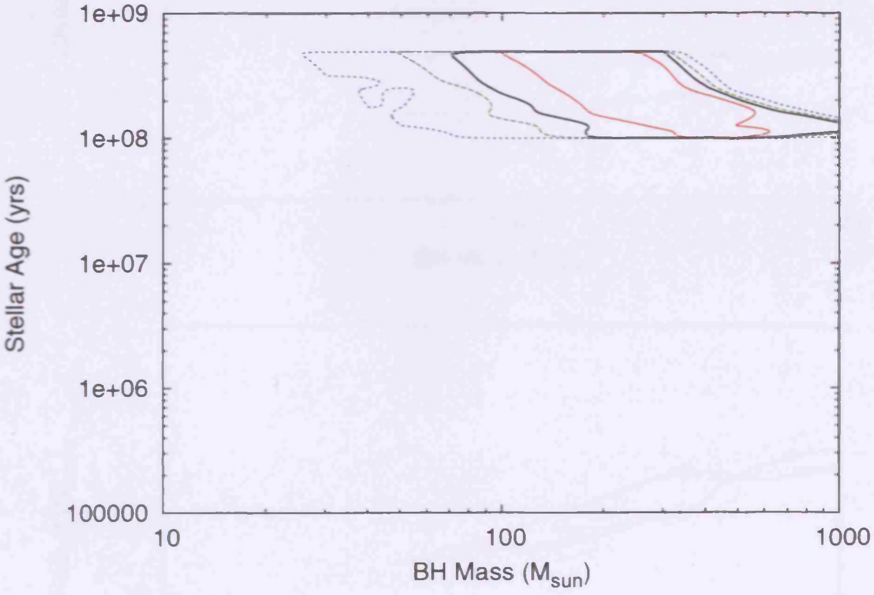

Figure 4.4: Confidence contours for the binary parameters for ULX X-9 in M51. This plot shows the stellar age against the BH mass, assuming a binary inclination of $\cos(i) = 0.0$, superior conjunction with respect to the observer and the star, a stellar metallicity of Z= $0.2Z_{\odot}$, and an X-ray hardness ratio of $\xi = 0.1$. The model is fitted to the *HST* WFPC2 photometric data. The red, black (solid), green and blue lines denote the 68%, 90%, 95% and 99% confidence intervals respectively.

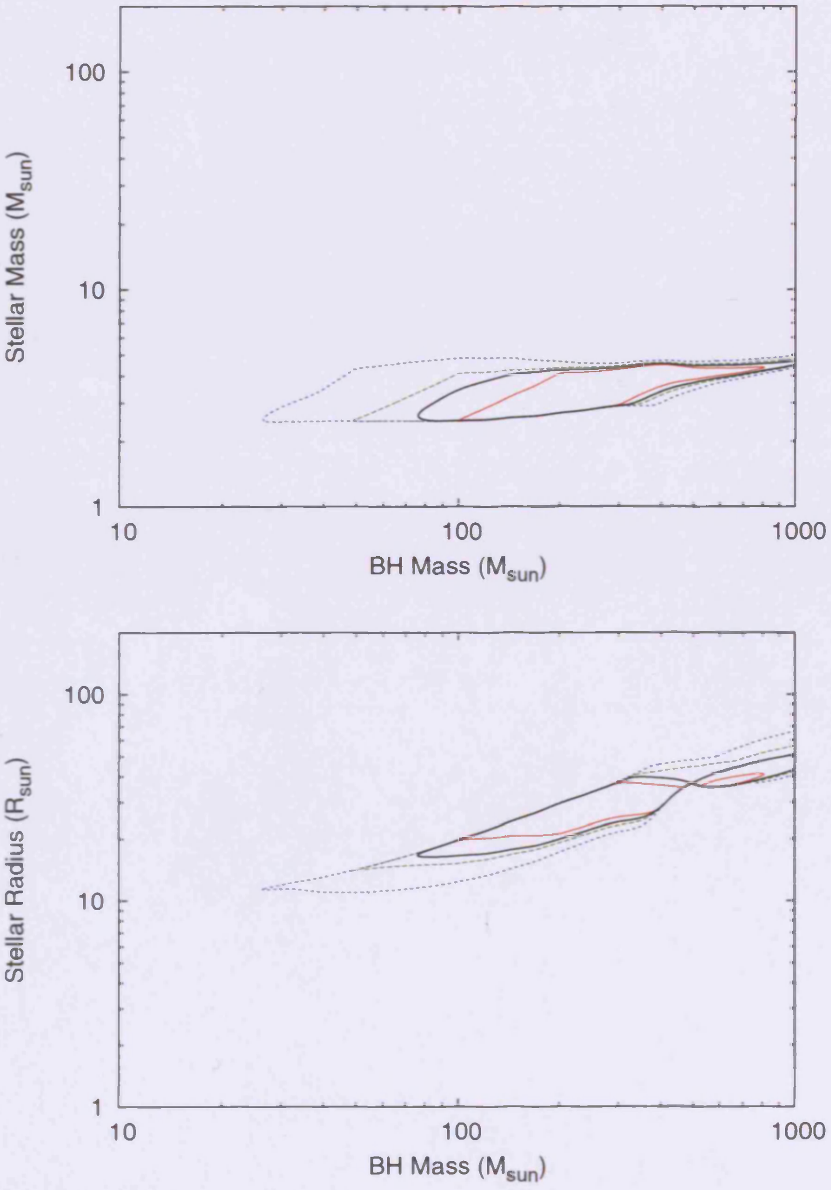

Figure 4.5: Confidence contours for the binary parameters for ULX X-9 in M51. These plots show the stellar mass and radius against the BH mass, assuming a binary inclination of $\cos(i) = 0.0$, superior conjunction with respect to the observer and the star, a stellar metallicity of Z= $0.2Z_{\odot}$, and an X-ray hardness ratio of $\xi = 0.1$. The model is fitted to the *HST* WFPC2 photometric data. The red, black (solid), green and blue lines denote the 68%, 90%, 95% and 99% confidence intervals respectively.

datapoints. Taking the error on Δm into account, there is an apparent variation in the I_c band of between 0.26 and 1.66 magnitudes. Of course, since the errors given on these measurements are only at the 1σ level, this is at best a marginal detection of variability in this source. In this section, the fitted binary parameters will be compared with the maximum I-band variation ΔI_{max}. I will determine if the binary parameters are further constrained if this variation in I of > 0.26 is assumed to be real.

With disc component

Figures 4.6 and 4.7 show the confidence contours for $\Delta \mathrm{I}_{max}$ plotted against BH mass, stellar mass and stellar radius. A plot for stellar age is not included since this parameter is not further constrained by the variability information.

If Figure 4.6 is examined first, it can be seen that if the minimum possible $\Delta \mathrm{I}_{max}$ is assumed to be 0.26, the upper bound on the BH mass is reduced from $300M_{\odot}$ to $\sim 30M_{\odot}$. This is to be expected: since the disc is assumed to be constant in optical luminosity; optical variability implies the stellar component is at the very least an important component in the emission, which in turn implies a low BH mass (See Section 2.9.4).

In Figure 4.7, it can be observed that the assuming $\Delta \mathrm{I} > 0.26$ has the effect of excluding some low mass, low radius stars. The minimum stellar mass is increased from 3 to $4M_{\odot}$, and the minimum stellar radius is increased from 1.5 to $3.5R_{\odot}$.

No disc component

When the inclination is set to $\cos(i) = 0.0$ such that all of the optical emission is coming from the donor, the optical variation with phase tends to be greater. This is because the fitted star for this inclination tends to be more luminous and larger. It was shown in Section 2.9.4 that the change in stellar luminosity as a result of X-ray heating is greater for larger stars, and so the optical variation is larger. In addition the fully irradiated and unirradiated hemispheres are viewed face-on at superior and

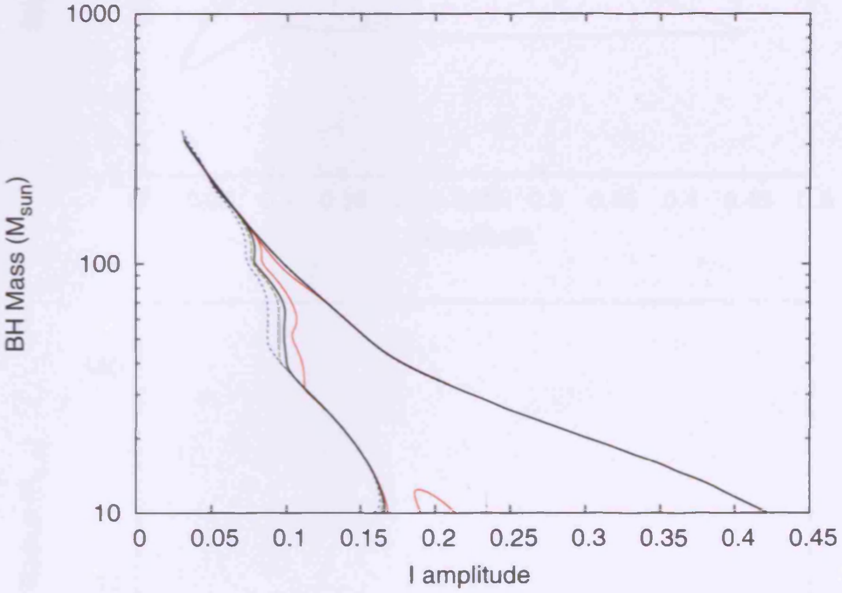

Figure 4.6: Confidence contours for the source X-9 in M51. ΔI_{max} is plotted against BH mass. This plot assumes a binary inclination of $\cos(i) = 0.5$, a stellar metallicity of Z= $0.2Z_{\odot}$ and an X-ray hardness ratio of $\xi = 0.1$. The red, black (solid), green and blue lines denote the 68%, 90%, 95% and 99% confidence intervals respectively. These contours use the *HST* WFPC2 photometric data.

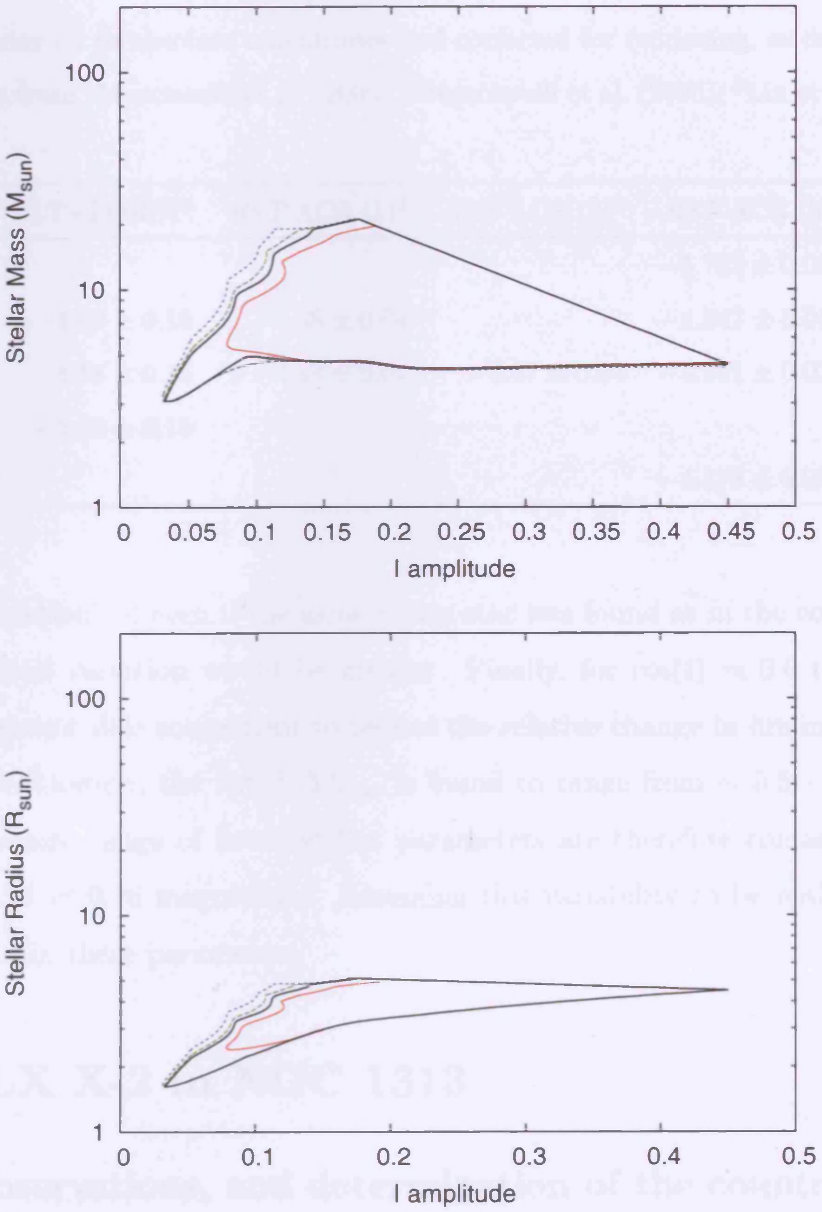

Figure 4.7: Confidence contours for the source X-9 in M51. ΔI_{max} is plotted against stellar mass (top plot) and stellar radius (bottom plot). These plots assume a binary inclination of $\cos(i) = 0.5$, a stellar metallicity of Z= $0.2Z_{\odot}$ and an X-ray hardness ratio of $\xi = 0.1$. The red, black (solid), green and blue lines denote the 68%, 90%, 95% and 99% confidence intervals respectively. These contours use the *HST* WFPC2 photometric data.

Table 4.2: Photometric data for the optical counterpart to ULX X-2 in NGC 1313. Values have been converted to absolute magnitudes and corrected for reddening, as described in the text. Data from [1]Mucciarelli et al. (2005), [2]Mucciarelli et al. (2006), [3]Liu et al. (2007).

	VLT+FORS1[1]	*HST* ACS (1)[2]	*HST* ACS (2)[2]	*HST* ACS (3)[3]
M_U				-5.783 ± 0.067
M_B	-4.80 ± 0.15	-4.58 ± 0.04		-4.847 ± 0.018
M_V	-4.58 ± 0.15	-4.43 ± 0.04	-4.57 ± 0.04	-4.551 ± 0.027
M_{R_c}	-4.40 ± 0.15			
M_{I_c}				-4.378 ± 0.053

inferior conjunction, so even if the same donor star was found as in the $\cos(i) = 0.5$ case, the optical variation would be greater. Finally, for $\cos(i) = 0.0$ there is of course no constant disc component to reduce the relative change in luminosity.

For this inclination, the fitted ΔI_{max} is found to range from $\sim 0.5 - 3$ magnitudes. The entire range of fitted stellar parameters are therefore consistent with a minimum ΔI of 0.26 magnitudes. Assuming this variability to be real does not further constrain these parameters.

4.5 ULX X-2 in NGC 1313

4.5.1 Observations, and determination of the counterpart

NGC 1313 contains a number of ULXs, one of which has an average X-ray luminosity of $L_x = 10^{40}$ergs s^{-1} and has been designated source X-2. There are three epochs of optical photometric data available for this source. Mucciarelli et al. (2005) analysed archive ESO VLT+FORS1 photometric data. They found two possible candidates for the optical counterpart of this ULX within the *Chandra* error circle. They gave B, V and R magnitudes for the candidate designated C1 in that paper, and V

and R magnitudes for the candidate C2. This second candidate was not detected in the B-band. Mucciarelli et al. (2006) reported further observations taken with the *HST* ACS instrument, split into two epochs. The first epoch of *HST* data were taken before the VLT observations, and gave B and V observations of both candidates. The second *HST* observation took place after the VLT observation, and gave V magnitudes for both candidates. The two epochs of *HST* observations were also studied by Liu et al. (2007), who listed measurements in four different *HST* filters for the first epoch. In addition, the more precise astrometry of Liu et al. (2007) finds the position of C2 to be inconsistent with the error circle of the X-ray source. Candidate C1 is therefore taken to be the optical counterpart to this ULX. In addition to these data, (Pakull et al., 2006) studied optical emission from the environoments of this source. They report the parent stellar cluster of the ULX to have an age of $\sim$ 60Myr, and from this they deduce an upper limit on the mass of the donor star of $8M_{\odot}$.

The photometric data for C1 are listed in Table 4.2. The first column of this table contains the VLT data given in Mucciarelli et al. (2005). The second and third columns contain the two epochs of *HST* data given in Mucciarelli et al. (2006). These data have been converted to absolute magnitudes using a distance to NGC 1313 of 3.7Mpc, and have been corrected for Galactic reddening, using the Galactic $E(B-V)$ value of 0.11 given in Mucciarelli et al. (2005) and $A_V/E(B-V) = 3.1$. The final column of Table 4.2 contains the *HST* ACS data as derived from Liu et al. (2007). Liu et al. (2007) give optical magnitudes in four *HST* filters; I have converted these to standard U,B,V,I magnitudes following Sirianni et al. (2005). These data have then been converted to absolute magnitudes and corrected for Galactic reddening in the same way as the other observations of this source.

Mucciarelli et al. (2006) and Liu et al. (2007) use the same set of *HST* observations; the M_B and M_V magnitudes given in the *ACS (1)* and *ACS (3)* columns of Table 4.2 should therefore be the same. In fact, there is a discrepancy, particularly in the M_V case. This discrepancy has presumably been introduced owing to differing methods of photometry.

In the determinations of the binary parameters given here the data given by Liu et al. (2007) are favoured, since those data have the most precisely defined errors and measurements are provided in four different filters. Calculations using the Mucciarelli et al. (2006) data were also made, and differences noted. The discrepancy between the Mucciarelli et al. (2006) and Liu et al. (2007) results does not have a larger effect on the determined binary parameters, but care has to be taken when optical variability is examined.

4.5.2 Determining the binary parameters

With disc component

The BH mass against stellar age, mass and radius for an inclination of $\cos(i) = 0.5$ is plotted in Figures 4.8 to 4.10. Separate plots show the determined parameters when either the *ACS (1)* or the *ACS (3)* data of Table 4.2 is used. It can be seen that there is little difference between the two. The results of using the *VLT* data are also consistent with these figures, albeit with looser constraints on the parameters.

There is an upper bound on the BH mass in both sets of plots. When the *ACS (1)* data are used this upper bound is $\sim 50 M_\odot$; this increases to $\sim 100 M_\odot$ when the model is fit to the *ACS (3)* data. This makes sense: the counterpart is measured to be more luminous in the *ACS (3)* data, which implies a bigger accretion disc, which in turn implies a more massive BH. The stellar parameters are consistent over the two sets of plots; the stellar age is found to be $< 10^{7.1}$yr, the stellar mass lies between 9 and $22 M_\odot$ and the radius is $3 - 6 R_\odot$.

Without disc component

The BH mass against stellar age, mass and radius for an inclination of $\cos(i) = 0.0$ are plotted in Figures 4.11 to 4.13. The results of fitting the model to the *ACS (1)* and the *ACS (3)* data of Table 4.2 are shown separately. Again, the two sets

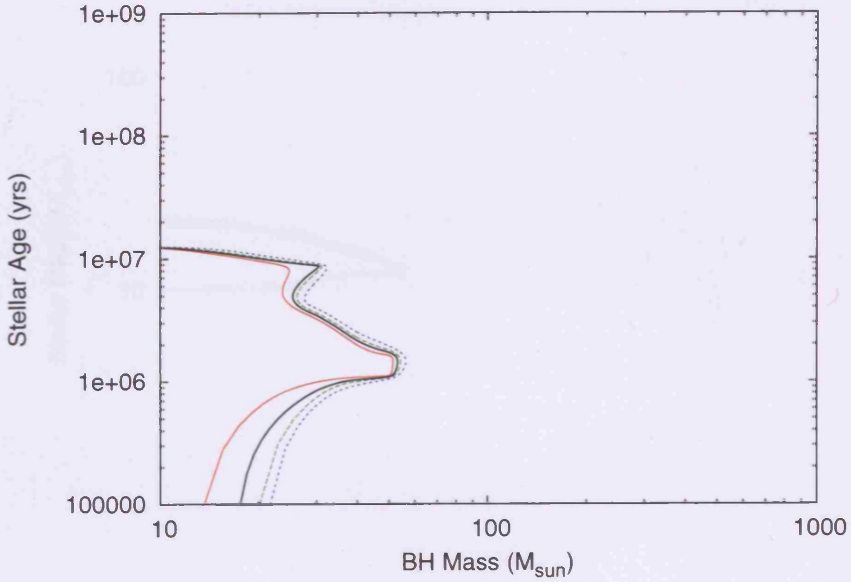

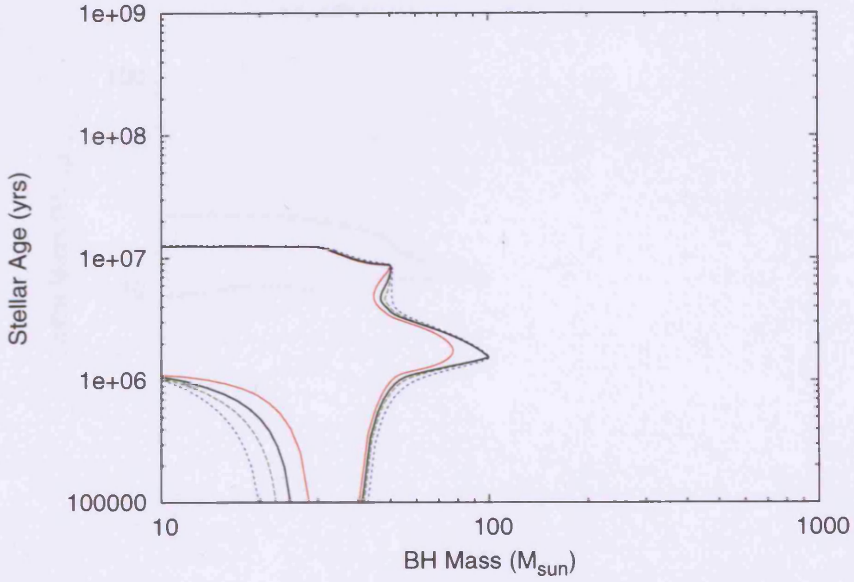

Figure 4.8: Confidence contours for the binary parameters for ULX X-2 in NGC 1313. These plots show the stellar age against the BH mass, assuming a binary inclination of $\cos(i) = 0.5$, superior conjunction with respect to the observer and the star, a stellar metallicity of Z= $0.2Z_{\odot}$, and an X-ray hardness ratio of $\xi = 0.1$. The red, black (solid), green and blue lines denote the 68%, 90%, 95% and 99% confidence intervals respectively. The top plot uses the *ACS (1)* data, while the bottom plot uses the *ACS (3)* data, both from Table 4.2.

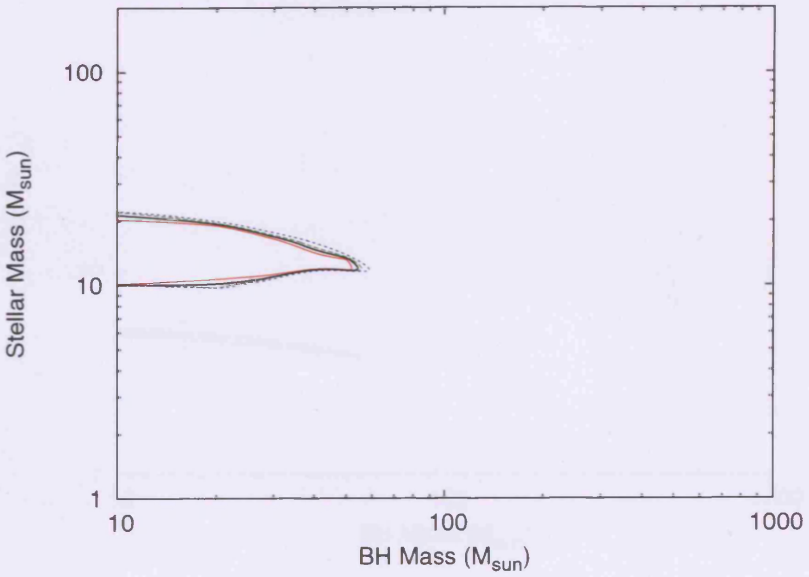

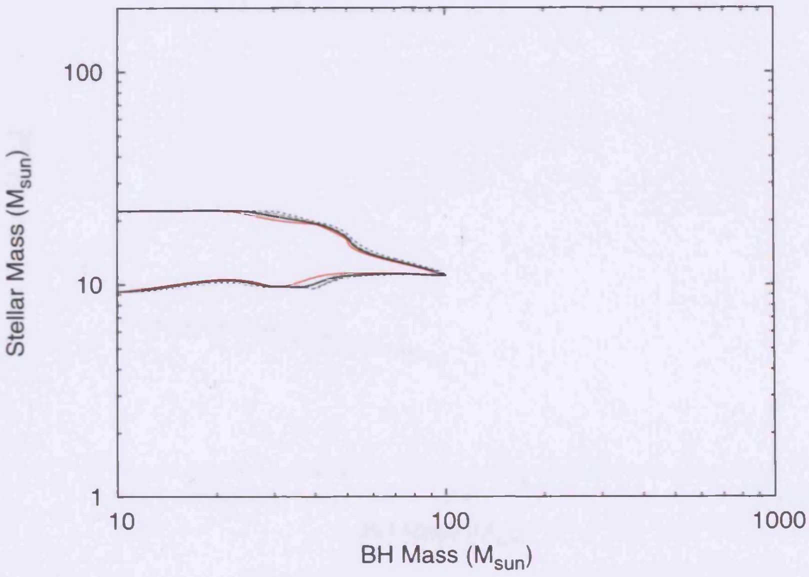

Figure 4.9: Confidence contours for the binary parameters for ULX X-2 in NGC 1313. These plots show the stellar mass against the BH mass, assuming a binary inclination of $\cos(i) = 0.5$, superior conjunction with respect to the observer and the star, a stellar metallicity of Z= $0.2Z_{\odot}$, and an X-ray hardness ratio of $\xi = 0.1$. The red, black (solid), green and blue lines denote the 68%, 90%, 95% and 99% confidence intervals respectively. The top plot uses the *ACS (1)* data, while the bottom plot uses the *ACS (3)* data, both from Table 4.2.

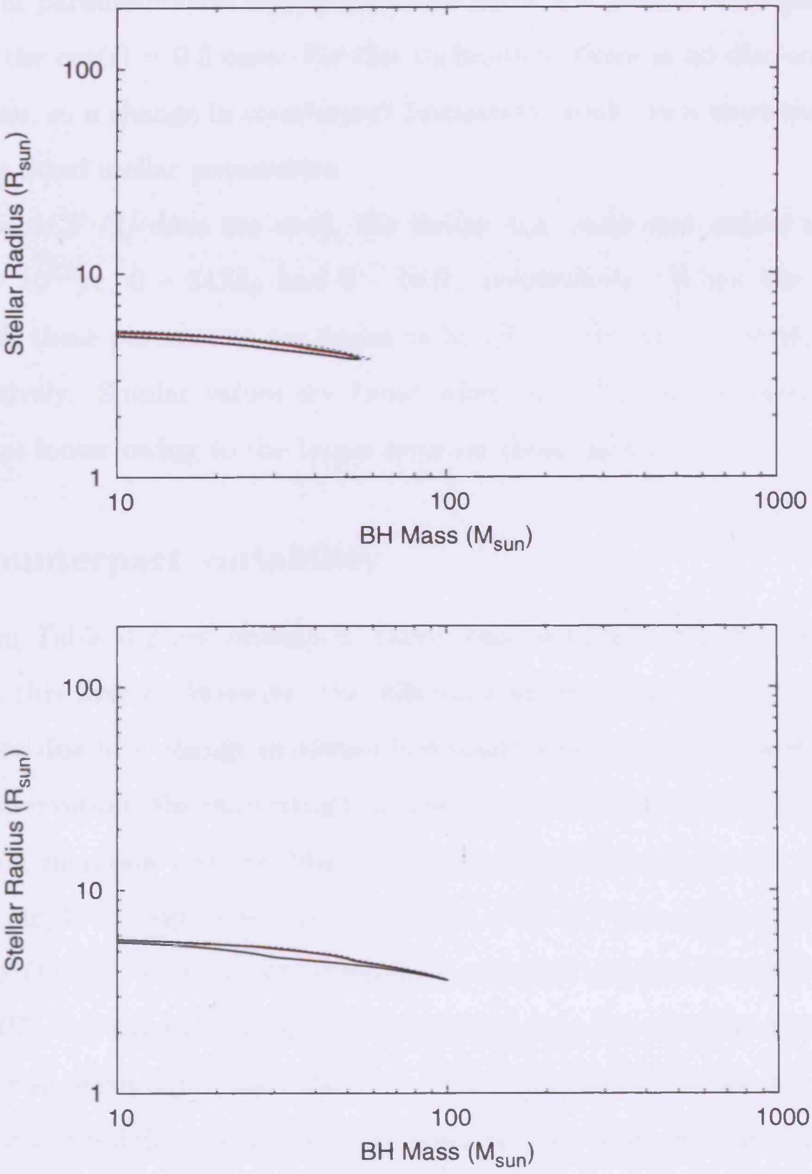

Figure 4.10: Confidence contours for the binary parameters for ULX X-2 in NGC 1313. These plots show the stellar radius against the BH mass, assuming a binary inclination of $\cos(i) = 0.5$, superior conjunction with respect to the observer and the star, a stellar metallicity of Z= $0.2Z_{\odot}$, and an X-ray hardness ratio of $\xi = 0.1$. The red, black (solid), green and blue lines denote the 68%, 90%, 95% and 99% confidence intervals respectively. The top plot uses the *ACS (1)* data, while the bottom plot uses the *ACS (3)* data, both from Table 4.2.

of fitted stellar parameters are very similar, but there is a greater discrepancy than there was in the $\cos(i) = 0.5$ case. For this inclination, there is no disc component to the emission, so a change in counterpart luminosity results in a more measurable change in the fitted stellar parameters.

When the *ACS (1)* data are used, the stellar age, mass and radius are found to be $10^{6.7}$ - $10^{8.0}$yr, 6 - $34M_\odot$ and 6 - $16R_\odot$ respectively. When the *ACS (3)* data are used, these parameters are found to be $10^{6.5}$ - $10^{7.9}$yr, 6 - $38M_\odot$ and 6 - $11R_\odot$ respectively. Similar values are found when the *VLT* data is used, but the constraints are looser owing to the larger error on those data.

4.5.3 Counterpart variability

If the data in Table 4.2 are examined, there some marginal evidence for optical variability in this source. However, the difference between the *ACS (1)* and *ACS (3)* data is not due to a change in source luminosity since they are taken from the same *HST* observation; the discrepancy is down to a difference in the photometric data reduction methods used by Mucciarelli et al. (2006) and Liu et al. (2007). However the single V-band observation labelled *ACS (2)* was taken at a different epoch to *ACS (1)/(3)*. This cannot be reliably compared with the *ACS (3)* results of Liu et al. (2007), but can be compared with *ACS (1)* since the method of Mucciarelli et al. (2006) was presumably self-consistent. The *VLT* data in Table 4.2 are of no use for studying variability owing to their comparatively large photometric error.

The difference in V-band luminosity between the two Mucciarelli et al. (2006) datapoints is 0.14 ± 0.08. Note also that Liu et al. (2007) also noted the variation between these two epochs of *HST* observation, and reported a change of 0.153 ± 0.047 in the $F555W$ band (approximately V-band) of the ACS Wide Field Camera.

As in the case of M51 X-9 (Section 4.4), if this variation is real then it implies a lower limit on ΔV_{max} and can be used to further constrain the parameter space. Model fits where the maximum variation in V luminosity is less than this can be

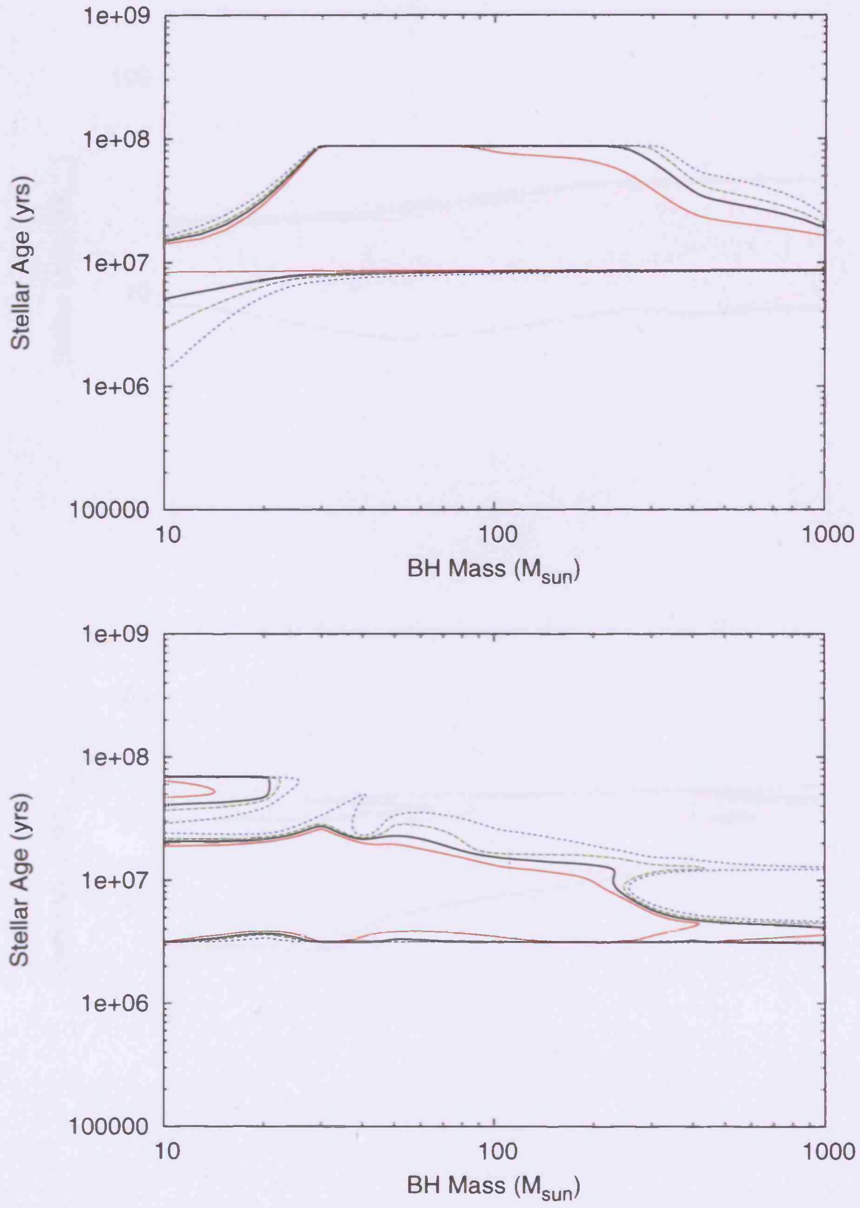

Figure 4.11: Confidence contours for the binary parameters for ULX X-2 in NGC 1313. These plots show the stellar age against the BH mass, assuming a binary inclination of $\cos(i) = 0.0$, superior conjunction with respect to the observer and the star, a stellar metallicity of Z= $0.2Z_{\odot}$, and an X-ray hardness ratio of $\xi = 0.1$. The red, black (solid), green and blue lines denote the 68%, 90%, 95% and 99% confidence intervals respectively. The top plot uses the *ACS (1)* data, while the bottom plot uses the *ACS (3)* data, both from Table 4.2.

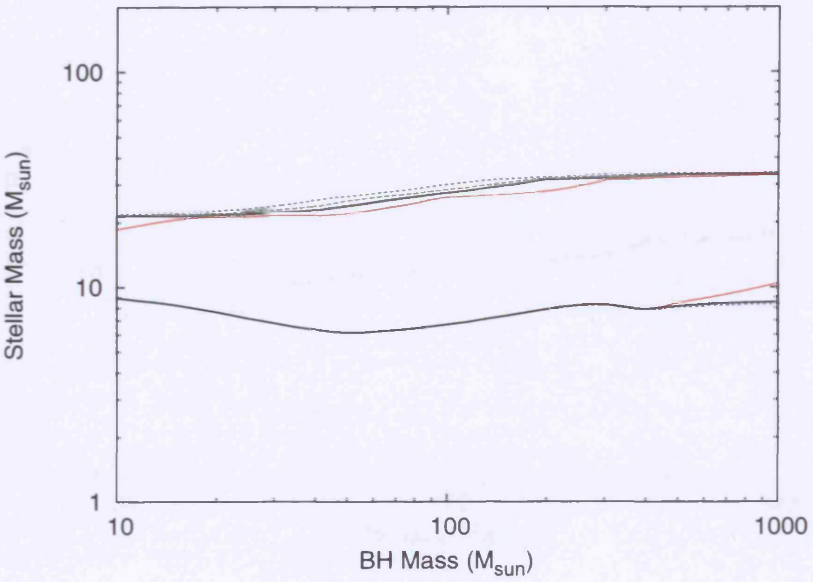

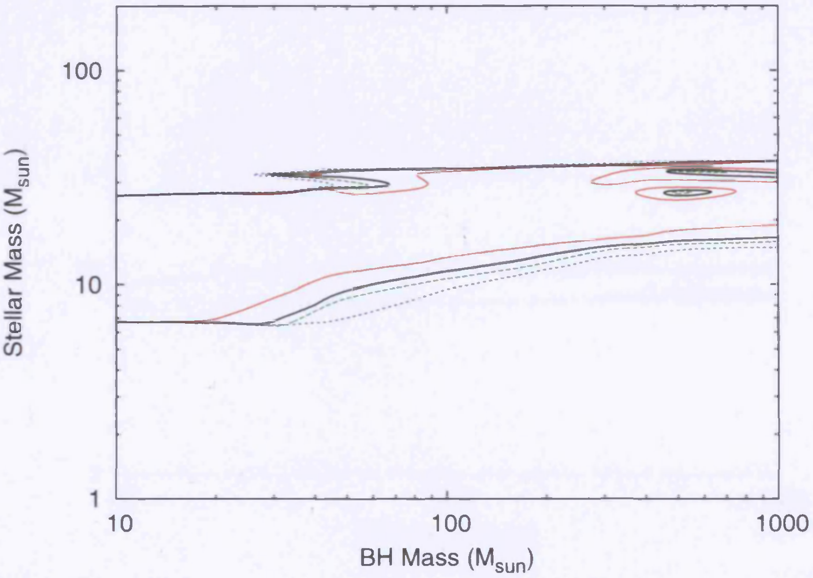

Figure 4.12: Confidence contours for the binary parameters for ULX X-2 in NGC 1313. These plots show the stellar mass against the BH mass, assuming a binary inclination of $\cos(i) = 0.0$, superior conjunction with respect to the observer and the star, a stellar metallicity of Z= $0.2Z_{\odot}$, and an X-ray hardness ratio of $\xi = 0.1$. The red, black (solid), green and blue lines denote the 68%, 90%, 95% and 99% confidence intervals respectively. The top plot uses the *ACS (1)* data, while the bottom plot uses the *ACS (3)* data, both from Table 4.2.

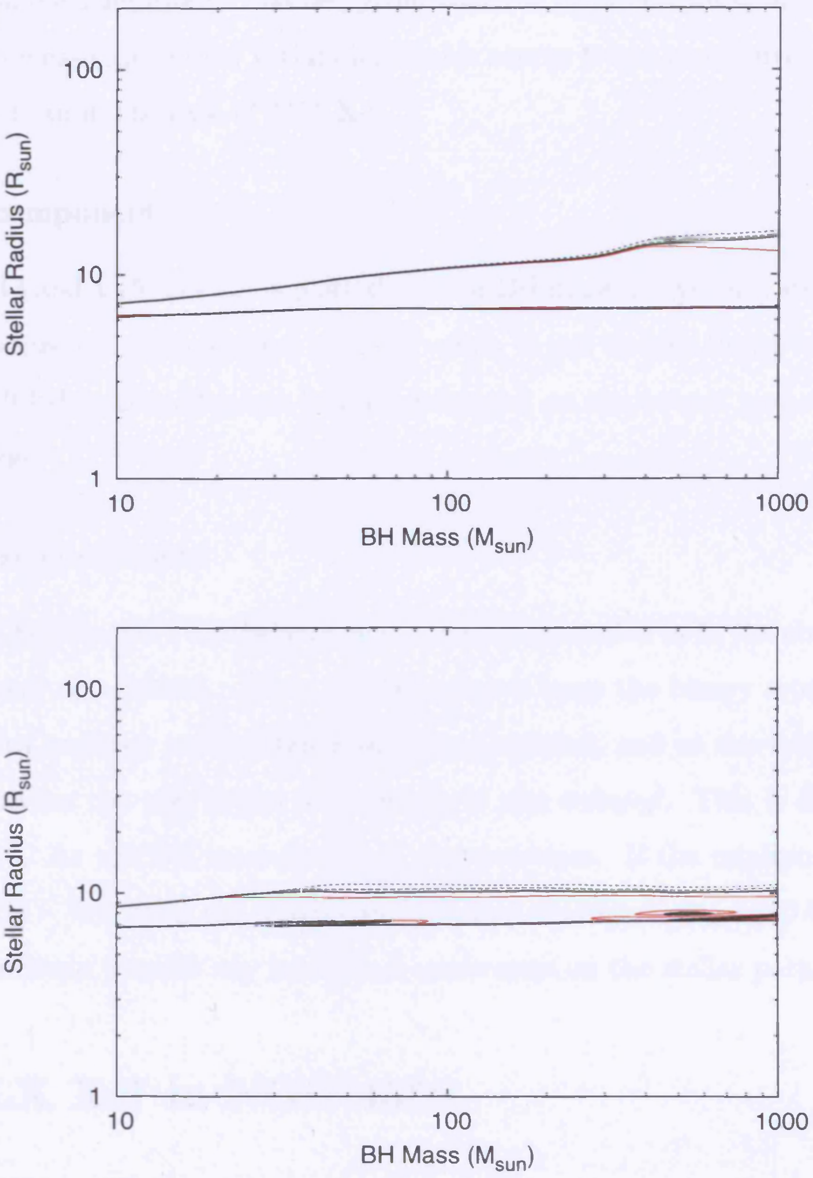

Figure 4.13: Confidence contours for the binary parameters for ULX X-2 in NGC 1313. These plots show the stellar radius against the BH mass, assuming a binary inclination of $\cos(i) = 0.0$, superior conjunction with respect to the observer and the star, a stellar metallicity of Z= $0.2Z_{\odot}$, and an X-ray hardness ratio of $\xi = 0.1$. The red, black (solid), green and blue lines denote the 68%, 90%, 95% and 99% confidence intervals respectively. The top plot uses the *ACS (1)* data, while the bottom plot uses the *ACS (3)* data, both from Table 4.2.

excluded from consideration. However, given that the errors on these datapoints is 1σ level, so the case for optical variability in this source is not conclusive, although it is stronger than in the case of M51 X-9.

With disc component

In Figures 4.14 and 4.15, ΔV_{max} is plotted against BH mass, stellar age, stellar mass and stellar radius, for an inclination of $\cos(i) = 0.5$. It can be seen that a lower limit on ΔV of ~ 0.1 does not offer any further constraint on the output parameters for this inclination.

Without disc component

It was seen in Section 4.5.2 that when $\cos(i) = 0.0$, it is possible to fit the observation with BH masses of $> 100 M_{\odot}$. When the BH mass is large the binary separation is large. The flux incident on the stellar surface is reduced, and so the temperature difference between the two stellar hemispheres is also reduced. This is illustrated in Figure 4.16. As the BH mass increases, the decreases. If the minimum ΔV is assumed to be ~ 0.1, then the maximum BH mass is reduced to $\sim 600 M_{\odot}$. This lower limit does not provide any additional constraints on the stellar parameters.

4.6 ULX X-7 in NGC 4559

4.6.1 Observations

Soria et al. (2005) used *HST* WFPC2 observations to study the optical environment of ULX X-7 in NGC 4559, a source with an average X-ray luminosity of 10^{40}ergs s^{-1} (Cropper et al., 2004). They found eight possible candidates for the ULX optical counterpart, listing the B, V and I_C standard magnitudes for each in table 2 of that paper. We have made a further observation of this source at a subsequent epoch with the *HST* ACS instrument. The apparent magnitudes of the candidates were

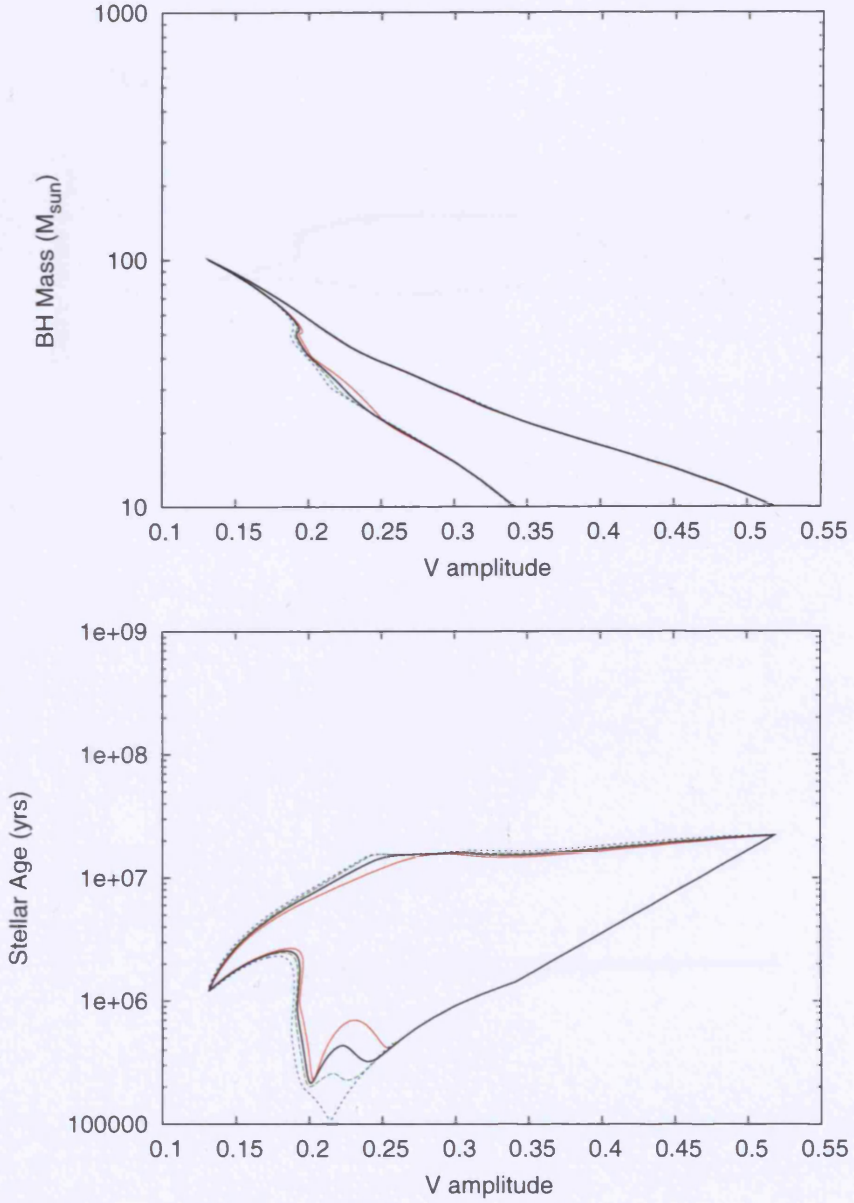

Figure 4.14: Confidence contours for the source X-2 in NGC 1313. ΔV_{max} is plotted against BH mass (top plot) and stellar age (bottom plot). These plots assume a binary inclination of $\cos(i) = 0.5$, a stellar metallicity of Z= $0.2Z_{\odot}$ and an X-ray hardness ratio of $\xi = 0.1$. The red, black (solid), green and blue lines denote the 68%, 90%, 95% and 99% confidence intervals respectively. These contours use the *ACS (3)* data from Table 4.2.

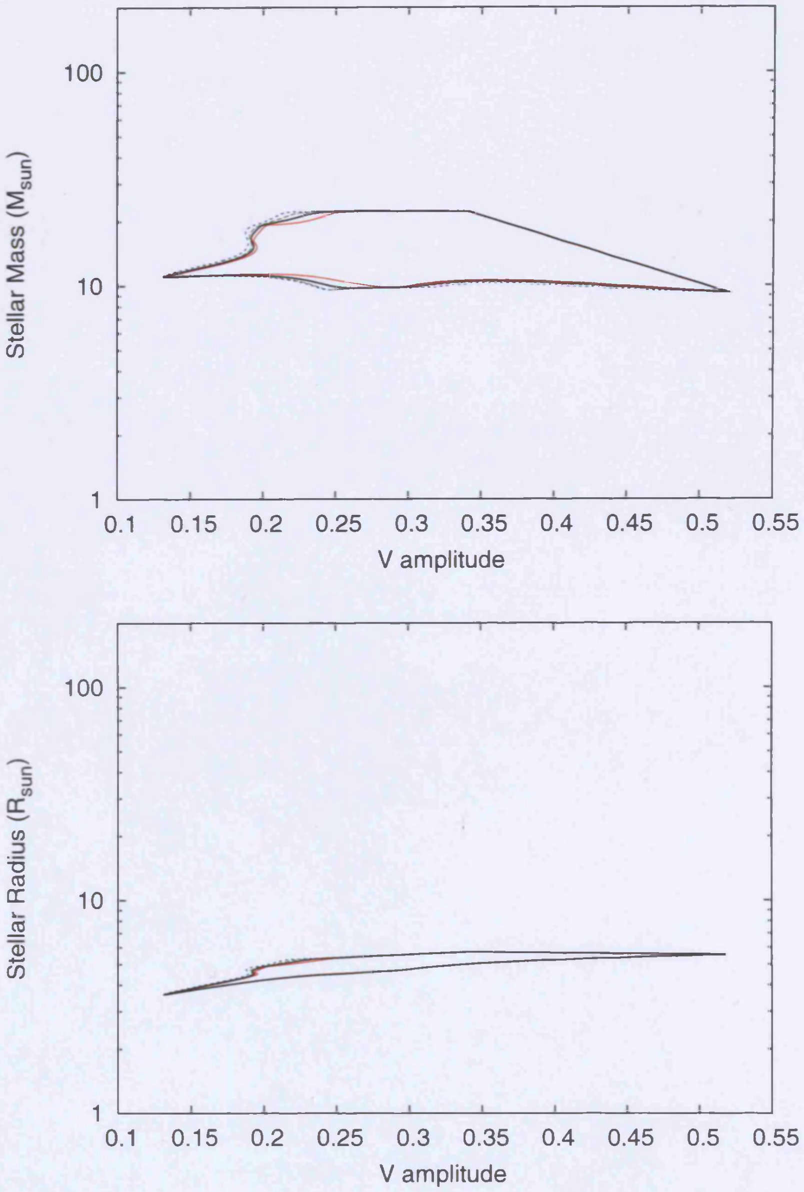

Figure 4.15: Confidence contours for the source X-2 in NGC 1313. ΔV_{max} is plotted against stellar mass (top plot) and stellar radius (bottom plot). These plots assume a binary inclination of $\cos(i) = 0.5$, a stellar metallicity of Z$= 0.2Z_{\odot}$ and an X-ray hardness ratio of $\xi = 0.1$. The red, black (solid), green and blue lines denote the 68%, 90%, 95% and 99% confidence intervals respectively. These contours use the *ACS (3)* data from Table 4.2.

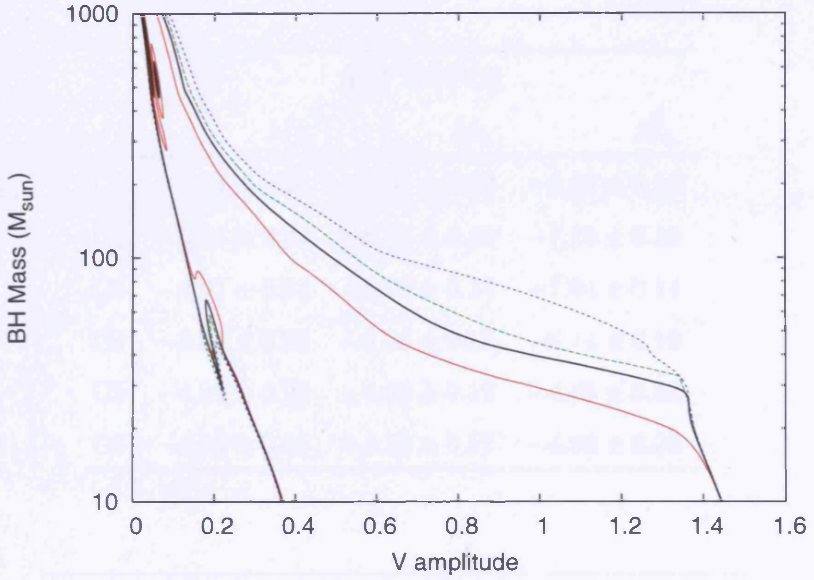

Figure 4.16: Confidence contours for the source X-2 in NGC 1313. ΔV_{max} is plotted against BH mass. This plot assumes a binary inclination of $\cos(i) = 0.0$, a stellar metallicity of Z= $0.2Z_{\odot}$ and an X-ray hardness ratio of $\xi = 0.1$. The red, black (solid), green and blue lines denote the 68%, 90%, 95% and 99% confidence intervals respectively. These contours use the *ACS (3)* data from Table 4.2.

Table 4.3: Photometric data for ULX X-7 in NGC 4559. The WFPC2 data are taken from Soria et al. (2005) and have been converted to absolute magnitudes and corrected for reddening, as described in the text. Data are given for all candidates which lie in the *Chandra* error circle.

	HST WFPC2		
	M_B	M_V	M_{I_c}
C1	-7.24 ± 0.16	-7.03 ± 0.12	-6.98 ± 0.12
C2	-5.84 ± 0.24	-6.33 ± 0.16	-7.16 ± 0.16
C3	-4.91 ± 0.24	-5.79 ± 0.14	-7.04 ± 0.14
C4	-5.00 ± 0.25	-5.56 ± 0.13	-6.14 ± 0.16
C5	-4.92 ± 0.22	-4.63 ± 0.19	-4.65 ± 0.48
C6	-4.64 ± 0.25	-4.73 ± 0.17	-4.98 ± 0.33

	HST ACS		
	M_B	M_V	M_{I_c}
C1	-7.280 ± 0.086	-7.023 ± 0.091	-6.869 ± 0.123
C2a	-5.477 ± 0.205	-5.652 ± 0.185	-6.016 ± 0.208
C2b	-4.160 ± 0.833	-5.479 ± 0.220	-6.717 ± 0.194
C3	-4.517 ± 0.602	-5.652 ± 0.203	-6.850 ± 0.160
C4	-3.803 ± 0.535	-4.522 ± 0.302	-5.469 ± 0.251
C5	-4.457 ± 0.298	-4.152 ± 0.348	-4.133 ± 0.431
C6	-4.598 ± 0.286	-4.210 ± 0.320	-4.346 ± 0.401

determined using aperture photometry, and converted to standard BVI magnitudes by following Sirianni et al. (2005). In Table 4.3 I list the photometric data obtained in both observational campaigns. Both sets of data have been corrected for Galactic reddening by using the reddening correction of Cardelli et al. (1989), with the Galactic $E(B-V)$ values given in Soria et al. (2005) and $A_V/E(B-V) = 3.1$. The conversion to absolute magnitudes was made by assuming a distance to NGC 4559 of 10Mpc.

Soria et al. (2005) found eight candidates within the *Chandra* error circle. With the improved astrometry of the ACS observations, I determine candidates 7 and 8 to be too distant from the X-ray source and so have been omitted from the list in Table 4.3. Note also that the improved resolution of the ACS instrument has meant that the source originally identified as candidate 2 in the WFPC2 data is determined in the ACS observation to be two separate point sources. In the ACS data in Table 4.3, these point sources are labelled as C2a and C2b.

4.6.2 Determining the counterpart

It is necessary to select one object from the list of candidates as the optical counterpart, to which the model can be applied. I do this in three ways; I investigate which candidate has been selected as the counterpart by previous authors, I look for variability in the candidates, and I see if the model contained in this work can be used to exclude any sources, by virtue of a poor statistical fit.

Determinations of previous authors

By fitting the WFPC2 observations to the unmodified Geneva tracks, Soria et al. (2005) deduced parameters for the candidate stars. Those values will be accurate for all of the candidates except the counterpart, the optical characteristics of which will have been modified by irradiation. They found that, with one exception, all the candidates were consistent with blue or red supergiants with masses $10-15M_{\odot}$ and ages $\approx$ 20Myr. The exception was candidate 1, which was consistent with a blue supergiant of mass $\approx 20M_{\odot}$ and age of only $\approx$ 10Myr. Soria et al. (2005) suggested this candidate was the most likely counterpart.

Variability

If the ACS data is compared with the WFPC2 data, it can be seen first that the two sets observations are broadly consistent. In both sets of data, Candidate 1 is significantly more luminous than the other observed sources. There is no noticeable variation in the luminosity of the source between the two observations. The other candidates are less luminous than Candidate 1, and by comparing the two datasets some variability is apparent.

The fact that a candidate is variable between the two observations might be an indication that it is the counterpart, since while it is unknown as to whether the candidate will vary or not, the field stars would not be expected to vary. I have pointed out that Candidate 1 does not vary between the two observations. Candidate 2 cannot be considered since it is known to be a confused source in the WFPC2 data. The other four sources all appear fainter in the ACS observation, with differing degrees of significance.

This variability is unlikely to be related to the ULX, since all four candidates cannot be the counterpart. The variability can be attributed to the fact that the resolution of the WFPC2 image is lower and the sources are more confused, which has affected the result of the photometry calculation. The sources therefore appear artificially luminous in the WFPC2 data. Since Candidate 1 is significantly more luminous than its neighbours, it suffers less from this problem.

Application of the model

By applying my model to each counterpart in turn, I aimed to eliminate some candidates from contention by finding poor model fits. Of the seven point sources, Candidates 1, 5 and 6 were found to fit well with the model for a range of inclinations, orientations and BH masses. Candidates 2, 3 and 4 could be fit with the model, but only when an inclination of $\cos(i) = 0.0$ and a BH mass of $\simeq 1000M_{\odot}$ or greater was used. In other words, these candidates could only be fit when there is no disc component and the binary separation is large such that the effect of irradiative heating is small; these candidates have the appearance of unirradiated single stars.

Determining the counterpart - conclusion

I will assume that Candidate 1 is the optical counterpart to this ULX. This candidate is one of only three which can be fitted with a irradiated star and disc over a large fraction of the parameter space. It is significantly brighter than its neighbours, and it has been found to be consistent with a much larger and younger stars than its stellar neighbours, by fitting it with unmodified stellar tracks. By fitting this candidate with a model irradiated donor and disc, a new set of stellar parameters will be determined. If these parameters are consistent with those of the stellar neighbourhood, this would provide further justification to the selection of this candidate as the counterpart.

4.6.3 Determining the binary parameters

In Figures 4.17 to 4.19 the confidence contours are plotted for the stellar age, mass and radius against the BH mass, for inclinations of $\cos(i) = 0.5$ and $\cos(i) = 0.0$. The star is assumed to be in superior conjunction in both cases. In these figures, the *HST* ACS data are used.

If the $\cos(i) = 0.5$ case is examined first it can be seen that the age ranges from 10^7 - 10^8yr, the mass ranges from 5 - $20M_{\odot}$ and the radius is between 8 and $30R_{\odot}$, with the lower radii implying a higher BH mass. A similar stellar mass and age is found when the star is assumed to be in inferior conjunction, but the upper bound on the stellar radius increases to $50R_{\odot}$ at the lower end of the BH mass range. These figures are the result of a model fit to the ACS data: for both conjunctions, similar results are found when the WFPC2 data are used.

For the $\cos(i) = 0.0$ case, a very tight constraint exists on the binary parameters. The stellar mass is found to be $10 - 13M_\odot$, the radius to be $51 - 57R_\odot$ and the stellar age is $10^{7.23}$ - $10^{7.40}$yr. In addition, it can be seen that the BH mass is $\sim 10M_\odot$. When the WFPC2 data are used the constraints are less tight: the lower bound on the stellar mass drops to $6M_\odot$ and the upper bound on the stellar radius increases to $72R_\odot$. In addition, the upper bound on the BH mass increases to $\sim 35M_\odot$.

When the phase and inclination is such that an irradiated disc and/or stellar component is included, the values for both inclinations are therefore consistent with candidate 1 being of a similar mass and age to the other candidates within the error circle, with its increased luminosity owing to the effects of irradiative heating.

It is also interesting to note that when no X-ray heated component to the emission is assumed (the $\cos(i) = 0.0$ and inferior conjunction case), the fit is very poor. This results from the constraint on the mass transfer rate. When this constraint is removed stellar parameters similar to those reported in Soria et al. (2005) are found, as would be expected.

4.6.4 Counterpart variability

Candidate 1 exhibits no significant optical variability between the two *HST* observations. Interpreting this result is a different challenge from that which was faced with the other two sources where there was some evidence for variability, albeit marginal. While the lack of variability implies a flat lightcurve, the possibility that the two observations were made at coincidentally identical binary phases cannot be ruled out. In this section, attempts will be made to estimate the likelyhood of such a coincidence.

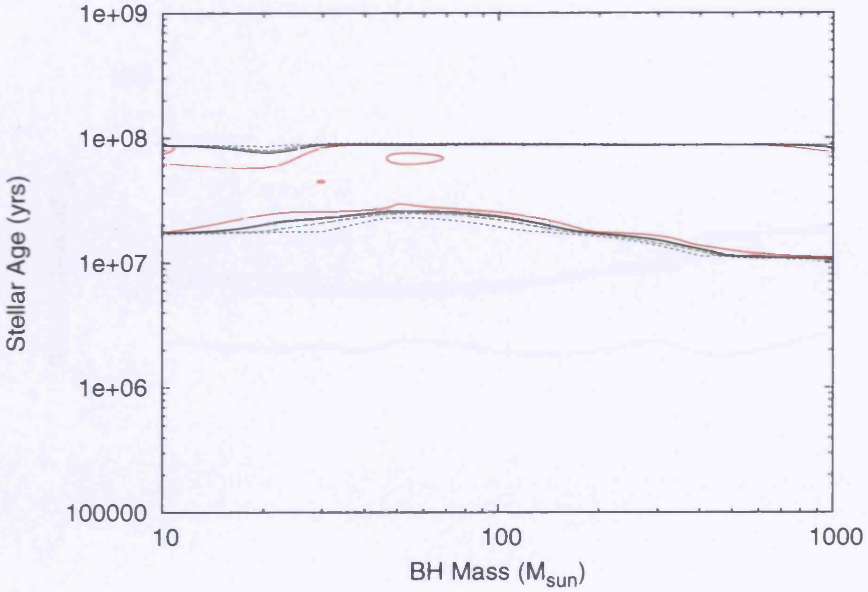

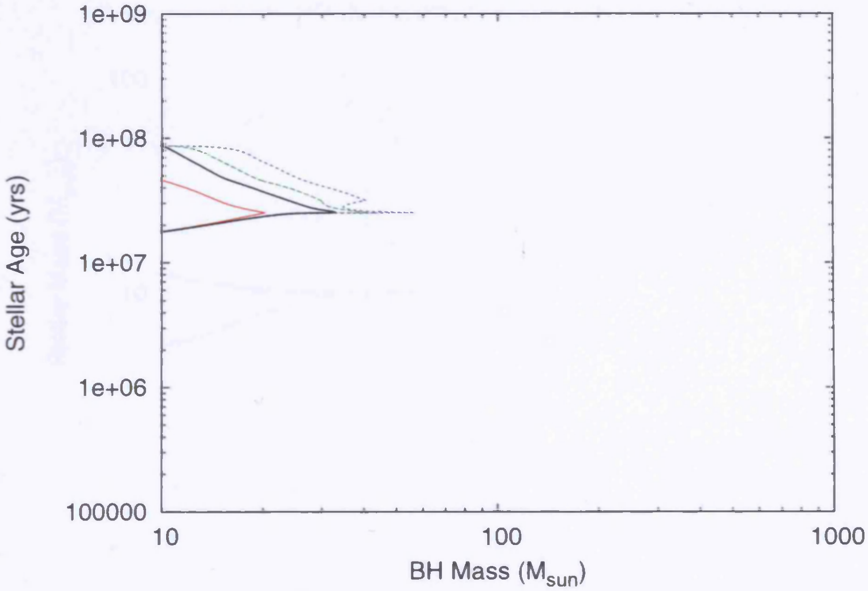

Figure 4.17: Confidence contours for the binary parameters for the source X-7 in NGC 4559, assuming candidate 1 is the optical counterpart. These plots show the stellar age against the BH mass, and assume superior conjunction, a stellar metallicity of Z= $0.2Z_{\odot}$ and an X-ray hardness ratio of $\xi = 0.1$. The red, black (solid), green and blue lines denote the 68%, 90%, 95% and 99% confidence intervals respectively. In the top plot a binary inclination of $\cos(i) = 0.5$ is used, while $\cos(i) = 0.0$ is used in the bottom plot.

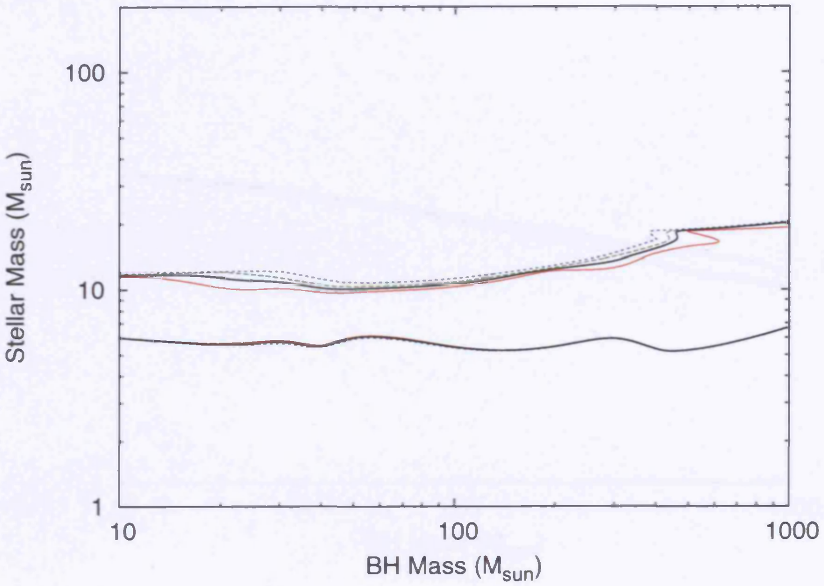

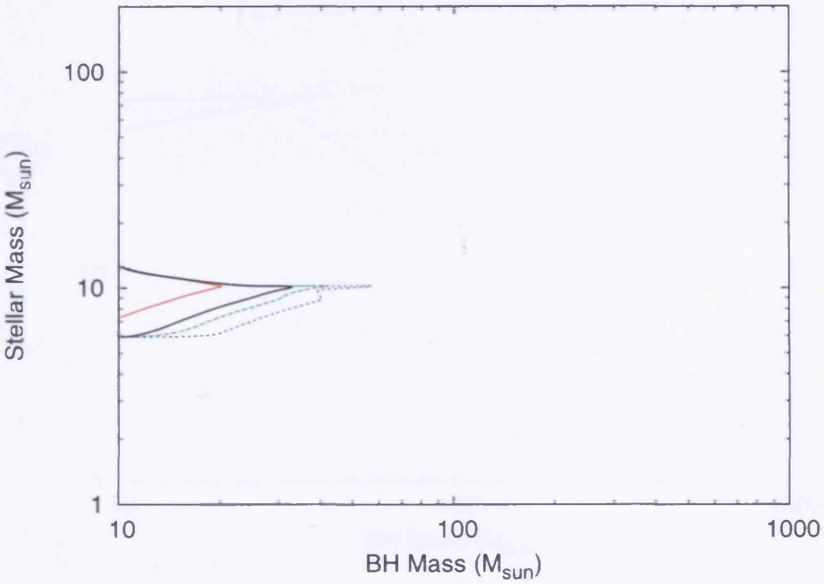

Figure 4.18: Confidence contours for the binary parameters for the source X-7 in NGC 4559, assuming candidate 1 is the optical counterpart. These plots show the stellar mass against the BH mass, and assume superior conjunction, a stellar metallicity of Z= $0.2Z_{\odot}$ and an X-ray hardness ratio of $\xi = 0.1$. The red, black (solid), green and blue lines denote the 68%, 90%, 95% and 99% confidence intervals respectively. In the top plot a binary inclination of $\cos(i) = 0.5$ is used, while $\cos(i) = 0.0$ is used in the bottom plot.

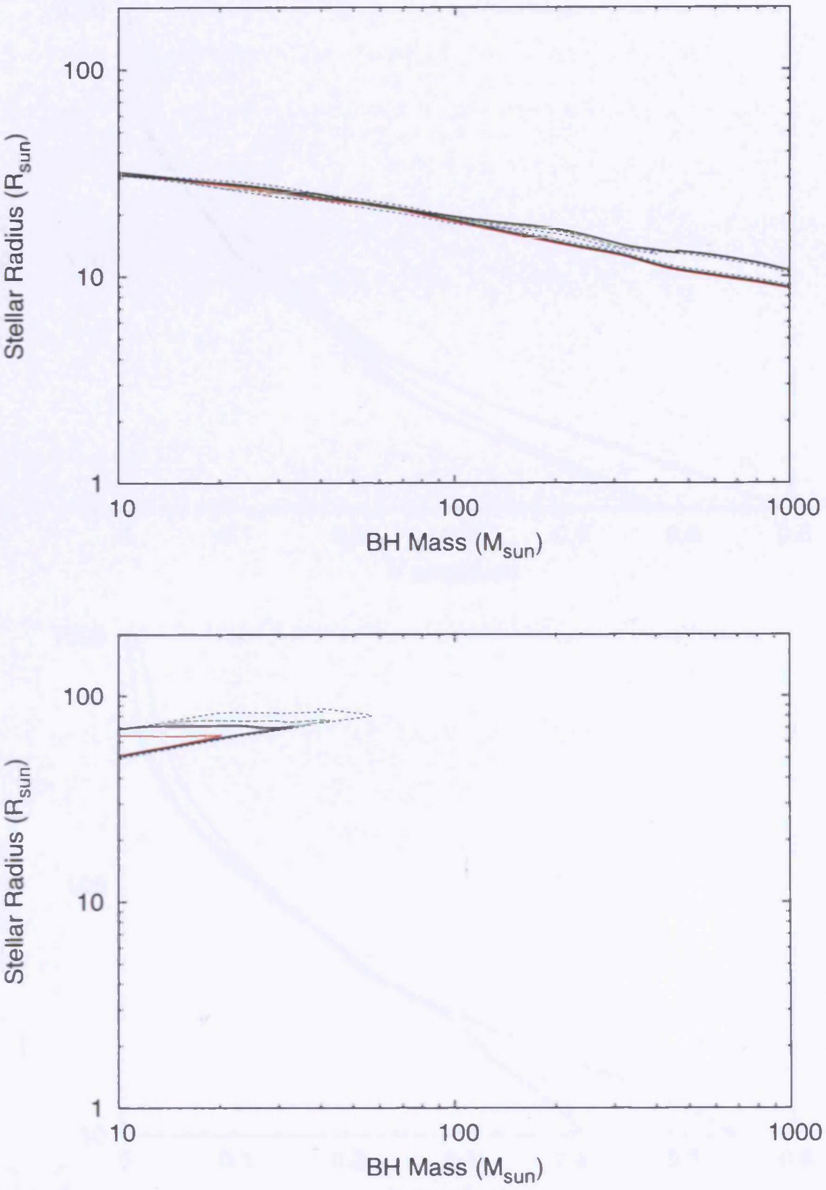

Figure 4.19: Confidence contours for the binary parameters for the source X-7 in NGC 4559, assuming candidate 1 is the optical counterpart. These plots show the stellar radius against the BH mass, and assume superior conjunction, a stellar metallicity of Z= $0.2Z_{\odot}$ and an X-ray hardness ratio of $\xi = 0.1$. The red, black (solid), green and blue lines denote the 68%, 90%, 95% and 99% confidence intervals respectively. In the top plot a binary inclination of $\cos(i) = 0.5$ is used, while $\cos(i) = 0.0$ is used in the bottom plot.

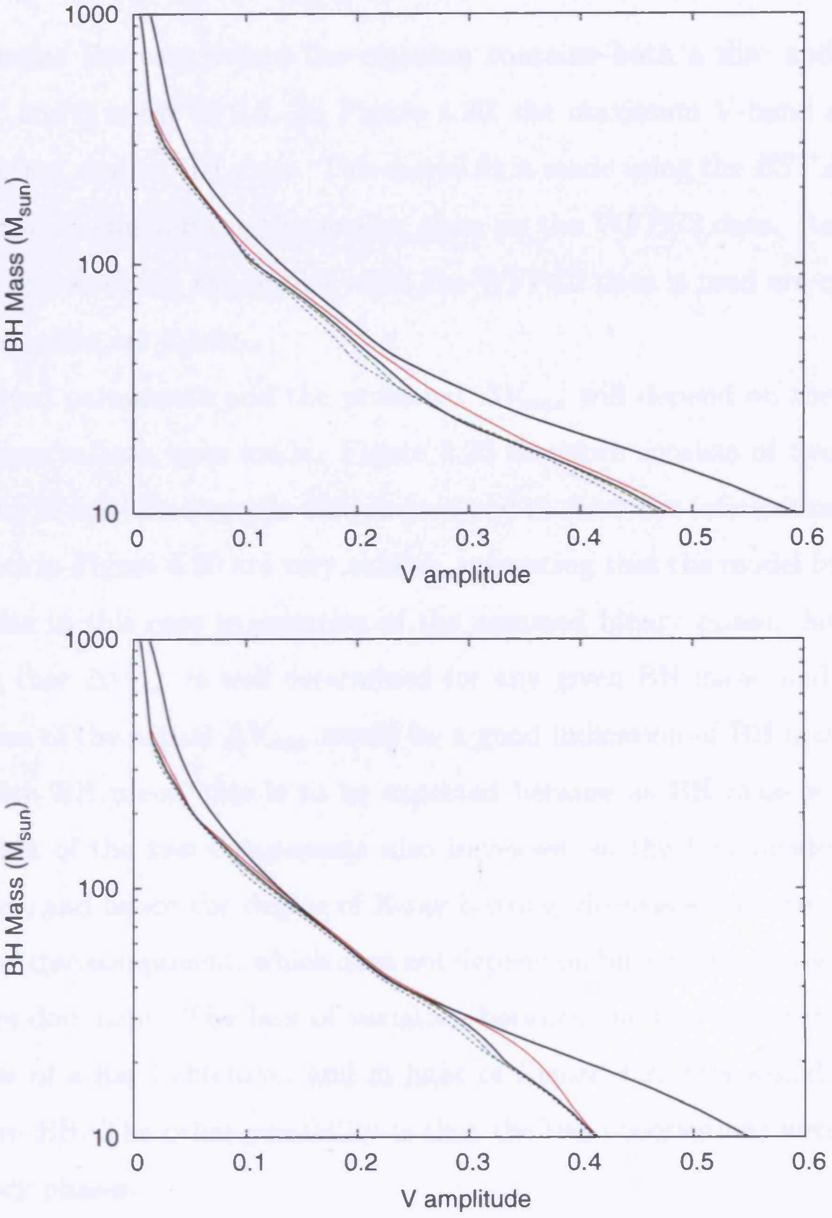

Figure 4.20: Confidence contours for the source X-7 in NGC 4559, assuming candidate 1 is the optical counterpart. ΔV_{max} is plotted against BH mass. These plots assume an inclination of $\cos(i) = 0.5$, a stellar metallicity of $Z= 0.2Z_{\odot}$ and an X-ray hardness ratio of $\xi = 0.1$. The red, black (solid), green and blue lines denote the 68%, 90%, 95% and 99% confidence intervals respectively. The top plot assumes this observation was made at superior conjunction, while the bottom plot assumes inferior conjunction.

$\cos(i) = 0.5$: **Star and disc component to the emission**

First, I examine the case where the emission contains both a disc and a stellar component. $\cos(i)$ is set to 0.5. In Figure 4.20, the maximum V-band amplitude ΔV_{max} is plotted against BH mass. This model fit is made using the *HST* ACS data, since the error on this data is the smaller than on the WFPC2 data. As with the other output parameters, the results when the WFPC2 data is used are consistent, but the constraints are looser.

The derived parameters and the predicted ΔV_{max} will depend on the phase at which the observations were made. Figure 4.20 therefore consists of two separate fits, assuming in one case superior conjunction and in the other inferior conjunction. The two plots in Figure 4.20 are very similar, suggesting that the model fit provides similar results in this case irrespective of the assumed binary phase. Secondly, it can be seen that ΔV_{max} is well determined for any given BH mass, and therefore determination of the actual ΔV_{max} would be a good indication of BH mass. ΔV_{max} decreases with BH mass: this is to be expected because as BH mass is increased the separation of the two components also increases, so the flux incident on the donor surface, and hence the degree of X-ray heating, decreases. As the separation increases, the disc component, which does not depend on binary phase, also increases and becomes dominant. The lack of variation between the two observations could be indicative of a flat lightcurve, and in light of Figure 4.20 this would suggest a more massive BH. The other possibility is that the two observations were made at similar binary phases.

Given the large number of degenerate model solutions to the optical data, there are many possible lightcurves which fit the observations. In order to explore the parameter space I assume BH masses of 10, 100 and $1000M_{\odot}$, and determine the best fit stellar parameters for each. This is done for an assumed binary phase at the time of observation of 0 (inferior conjunction) and 0.5 (superior conjunction). These results are listed in Table 4.4. These results used the *HST* ACS data; but

Table 4.4: Best fit model parameters for the optical counterpart of NGC 4559 X-7, based on the *HST* ACS data. An inclination of $\cos(i) = 0.5$, a stellar metallicity of $Z = 0.2Z_\odot$ and an X-ray hardness ratio of $\xi = 0.1$ is assumed.

BH mass	$10M_\odot$	$100M_\odot$	$1000M_\odot$
Superior conjunction			
Stellar Mass ($M_\odot$)	11.3	9.8	17.9
Stellar Radius ($R_\odot$)	33.2	20.3	11.2
Stellar Age (Myr)	20	25	10
Inferior conjunction			
Stellar Mass ($M_\odot$)	5.1	5.7	17.9
Stellar Radius ($R_\odot$)	49.5	18.9	11.2
Stellar Age (Myr)	87	69	10

similar results are found when the WFPC2 data are used.

It was noted in Section 2.9.4 that the stellar radius is the most important stellar parameter in determining the optical luminosity of the system. Not only does increasing the stellar radius increase the amount of stellar surface area which is X-ray heated, but it also determines the size of the accretion disc, since in the model the scale of the Roche lobe geometry is set by the volume radius of the donor. It can be seen in Table 4.4 that the best-fit stellar radius is more or less unaffected by stellar phase when a BH mass of 100 or $1000M_\odot$ is used, owing to the disc being dominant for these BH masses. In the $10M_\odot$ case, it can be seen that the fitted stellar radius changes significantly between the two phases. This implies a stellar dominated emission; in the inferior conjunction case the heated hemisphere of the star is barely observed, so a larger, more luminous donor is required in order to match the observational data.

In Figure 4.21, model lightcurves are plotted using the parameters of Table 4.4. As in Figure 4.20, separate plots show the cases where the observation is assumed

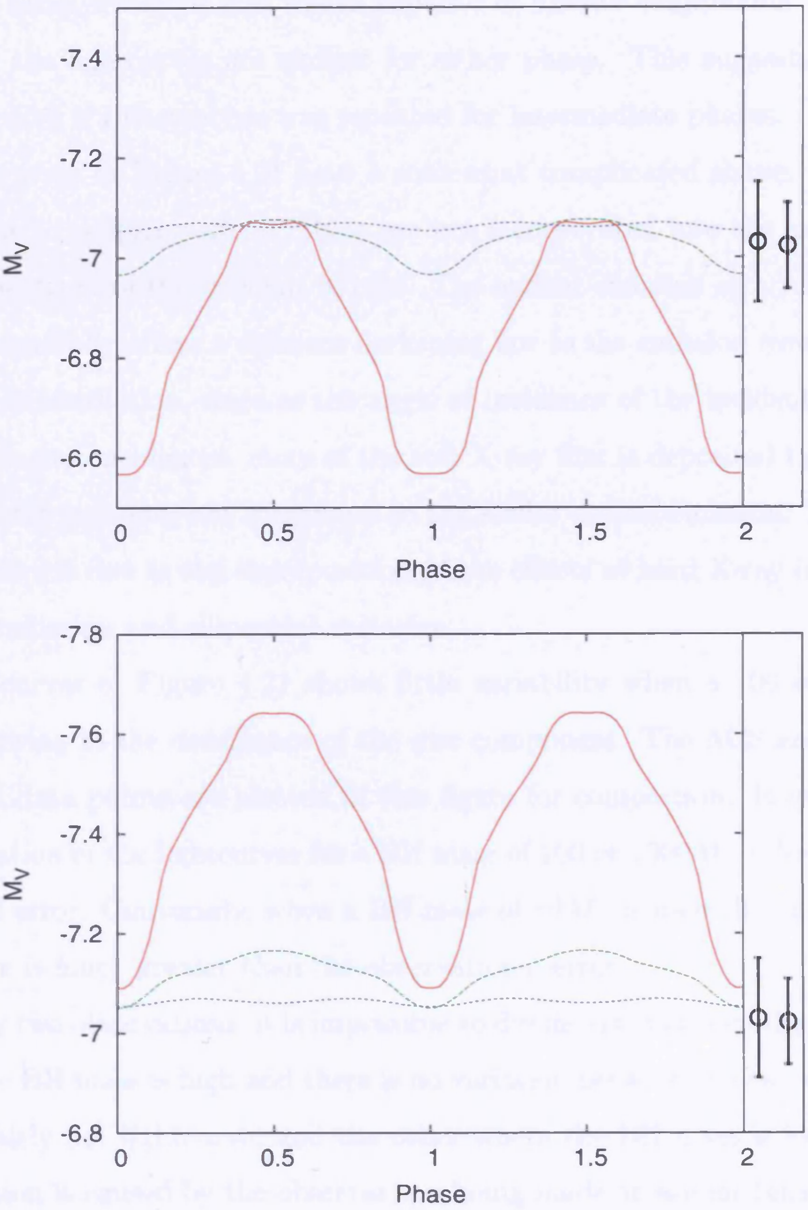

Figure 4.21: Model V-band lightcurves for the source X-7 in NGC 4559, produced by using the best fit parameters to the *HST* ACS data, as given in Table 4.4. The top plot assumes the observation was made at superior conjunction. The bottom plot assumes the observation was made at inferior conjunction. These plots assume a stellar metallicity of Z= $0.2Z_{\odot}$ and an X-ray hardness ratio of $\xi = 0.1$. The red, green and blue lines denote the cases where a BH mass of 10, 100 and $1000M_{\odot}$ is used respectively. To the right of the plots, the ACS and WFPC2 observations are shown with their error bars for comparison.

to have been taken when the star was in superior or inferior conjunction. Note that the shape of the lightcurves are similar for either phase. This suggests a similar shaped lightcurve if this analysis was repeated for intermediate phases.

The lightcurves in Figure 4.21 have a somewhat complicated shape. Note that this is not due to eclipsing effects; these are not incorporated into the model. It is due to the spectrum of the incident X-rays. The optical emission as a result of the soft X-rays essentially obeys a different darkening law to the emission resulting from the hard X-ray irradiation, since as the angle of incidence of the incident radiation approaches grazing incidences, more of the soft X-ray flux is deposited in the outer layers of the star and does not contribute to the stellar optical emission. The shape of the lightcurve is due to the superposition of the effects of hard X-ray irradiation, soft X-ray irradiation and ellipsoidal variation.

The lightcurves of Figure 4.21 shows little variability when a 100 or $1000M_\odot$ BH is used, owing to the dominance of the disc component. The ACS and WFPC2 observational data points are plotted in this figure for comparison. It can be seen that the variation in the lightcurves for a BH mass of 100 or $1000M_\odot$ is less than the observational error. Conversely, when a BH mass of $10M_\odot$ is used the amplitude of the lightcurve is much greater than the observational error.

With only two observations, it is impossible to distinguish between the two cases: one where the BH mass is high and there is no variation between the two datapoints owing to a fairly flat lightcurve, and the other where the BH mass is low and the lack of variation is caused by the observations being made at similar binary phases. However, given that the amplitude of the $10M_\odot$ BH lightcurve is much greater than the error on the observations (~ 0.5 compared to ~ 0.1), a BH mass of $>\sim 100M_\odot$ seems more likely.

Stellar component only

It was seen in Section 4.6.3 that the fitted BH mass is $\sim 10M_\odot$ for this source when the star is in superior conjunction and $\cos(i) = 0.0$. The model fit is poor in the

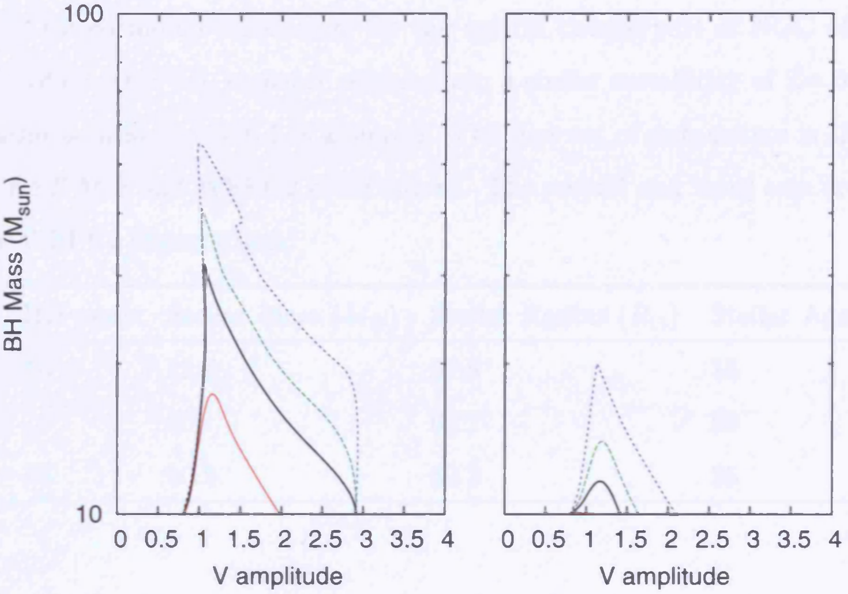

Figure 4.22: Confidence contours for the source X-7 in NGC 4559. ΔV_{max} is plotted against BH mass. These plots assume an inclination of $\cos(i) = 0.0$. The left plot uses the *HST* WFPC2 data and the right plot uses the ACS data. The red, black (solid), green and blue lines denote the 68%, 90%, 95% and 99% confidence intervals respectively.

inferior conjunction case. It is therefore reasonable to assume that both observations must have been made close to superior conjunction, when there is a strong heated stellar component to the emission.

I plot in Figure 4.22 ΔV_{max} against BH mass for this inclination. It can be seen that when the ACS data is used ΔV_{max} is tightly constrained. When the WFPC2 data is used, the range of values which ΔV_{max} can take is large. In both cases, the fitted ΔV_{max} values are larger than those found in the $\cos(i) = 0.5$ case (Figure 4.20). This results from the fully irradiated and unirradiated hemispheres being viewed face-on at superior and inferior conjunction respectively for this inclination. In addition, there is no constant disc component to reduce the relative change in luminosity.

I list in Table 4.5 three sets of BH and donor parameters. These have been chosen as example parameters which fit with the observations, and lightcurves using

Table 4.5: Fitted model parameters for the optical counterpart of NGC 4559 X-7. An inclination of $\cos(i) = 0.0$, superior conjunction, a stellar metallicity of $Z = 0.2Z_\odot$ and an X-ray hardness ratio of $\xi = 0.1$ is assumed. The first set of parameters is the best fit to both the *HST* ACS and WFPC2 observations. The second and third sets are alternative fits to the WFPC2 observations.

	BH mass	Stellar Mass ($M_\odot$)	Stellar Radius ($R_\odot$)	Stellar Age (Myr)
(1)	10	12.6	51.8	18
(2)	10	5.9	69.1	69
(3)	30	10.2	69.3	25

these parameters are plotted in Figure 4.23. The first set of parameters is the best-fit solution to the ACS data. The quality of the ACS data gives a very tight constraint on the stellar parameters, and so other sets of parameters which fit the ACS observation are very similar. The first set of parameters in Table 4.5 is also the best-fit solution for the WFPC2 data, but these data can be fitted well with a wider range of parameters. The second and third set of parameters in Table 4.5 have been selected for comparitive purposes. The second set have been selected because they imply a large (~ 3 magnitudes) amplitude, and the third set use a larger BH mass.

If Figure 4.23 is examined it can be seen that the lightcurve amplitude is indeed large for all three fitted solutions. The amplitude is larger when the second and third sets of parameters are used: if Table 4.5 is referred to this can be understood, since the donors in these cases are older, more evolved stars with larger radii, and hence have a larger surface area which is heated by the incident X-rays.

The amplitudes of these solutions are higher than those for the $\cos(i) = 0.5$: in Figure 4.23 it can be seen that the amplitudes are much larger than the observational errors. This makes them less likely to be correct, since the likelyhood of two observations showing no variation is much lower than in the $\cos(i) = 0.5$ case.

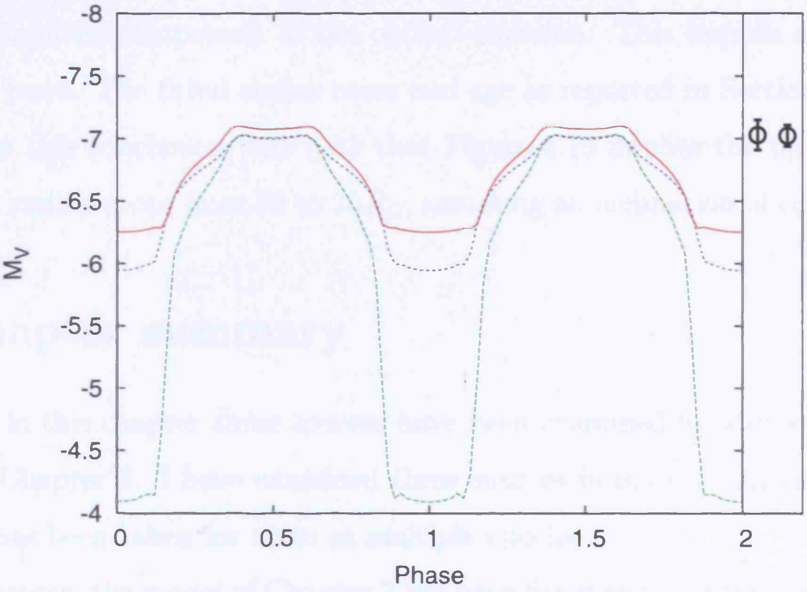

Figure 4.23: Model V-band lightcurves for the source X-7 in NGC 4559, using the stellar and BH parameters listed in table 4.5.The red, green and blue lines denote the first, second and third sets of parameters respectively. To the right of the plots, the two observations are shown with their error bars for comparison.

Variability conclusions

While a variation in optical luminosity between two discrete datapoints can be used as an additional constraint on the parameters of the source, a lack of variation between those two points does not allow one to make any definite conclusions. The possibility that the two observations were made at a coincidentally identical phase cannot be ruled out. However, it can be concluded that in this source it is more likely that the system is inclined so as to include a disc component, and that this disc is the dominant component of the optical emission. This implies a BH mass of $100M_\odot$ or more. The fitted stellar mass and age as reported in Section 4.6.3 are unchanged by this conclusion, but note that Figure 4.19 implies the upper bound on the stellar radius drops from 30 to $20R_\odot$, assuming an inclination of $\cos(i) = 0.5$.

4.7 Chapter summary

In summary, in this chapter three sources have been examined in addition to those discussed in Chapter 3. I have examined these sources in more detail since photometric data has been taken for them at multiple epochs.

For each source, the model of Chapter 2 has been fitted to the optical counterpart in the same way as in Chapter 3. As with the sources in that chapter, a good fit can generally be found for any assumed inclination or orientation, due to the wide parameter space. Nevertheless, the parameters of the donor stars can be determined with good accuracy, and in some cases the model fits have provided constraints on the BH masses.

For the two sources where the data suggests optical variability, comparing these data with model predictions has led to some further constraints on the binary parameters, for some inclinations. In particular, since the maximum predicted optical variability will tend to decrease with increasing BH mass, the measurement of variability tends to imply an upper limit on the BH mass. For the source where the available data suggests little or no optical variability it isn't possible to make any strong conclusions, but if the lightcurve for this source is indeed flat then this would suggest a massive BH in this system.

The results of this chapter show that future temporal observational campaigns of optical counterparts will be powerful diagnostic tools in determining binary parameters, in particular the BH mass.

Chapter 5

Discussion

5.1 Introduction

In this chapter, I discuss the results presented in Chapters 3 and 4 in more detail. I classify the donor stars in the systems based on the parameters determined in Chapters 3 and 4, and I examine the constraints on the BH masses. I then discuss the consequences of these results on the current understanding of the nature of ULXs with particular reference to their formation, evolution and lifetime. I make some comments on the variability observed in the three sources in Chapter 4. Finally, I discuss some additional systematic effects which have not yet been examined in detail.

5.2 Classification of the donor stars

The current spectral type and luminosity class of the donor stars can be inferred from the stellar mass and radius determinations of Chapters 3 and 4. The most likely classifications are listed in Table 5.1. In addition, the stellar evolutionary tracks also give constraints on the Zero Age Main Sequence (ZAMS) stellar masses and temperatures. These constraints are listed in Tables 5.2 and 5.3. The stellar evolutionary tracks that have been used in this work are for single stars, and so these

Table 5.1: Spectral type of the donor stars. The classification given by previous authors is compared with the determination of the current and ZAMS spectral types made in this work. The most likely type is given in each case and this is elaborated on in the text. (* assuming the most luminous candidate is the counterpart. ** applies only when a constraint is not applied on the mass accretion rate.). References:[1](Liu et al., 2002), [2](Liu et al., 2004), [3](Kuntz et al., 2005), [4](Kaaret et al., 2004), [5](Terashima et al., 2006), [6](Soria et al., 2005), [7](Mucciarelli et al., 2005).

	Previous spectral type	Determination in this thesis: Current	ZAMS
NGC 4559 X-10	-	Late B supergiant	B4 - B0 *
M81 X-6	O8V / O9V[1]	B MS/giant	B9 - B2
NGC 5204 ULX	B0Ib[2]	O MS **	O5 or earlier **
M101 ULX-1	B supergiant[3]	A/B MS/giant	A0 - O4
NGC 5408 ULX	-	B giant/supergiant (or O MS)	B4 or earlier
Holmberg II ULX	O4V / B3Ib[4]	B giant/supergiant (or O MS)	B5 or earlier
M51 X-9	F2 - F5 supergiant[5]	B MS/giant	A0 - B0
NGC 4559 X-7	O / B supergiant[6]	Late B - A giant/supergiant	B5 - B0
NGC 1313 X-2	B0 - O9 MS[7]	B MS/giant	B6 - O6

ZAMS values do not account for any loss due to to the mass accretion, but they do include wind losses incorporate in the evolutionary tracks. The ZAMS masses therefore need to be increased by some amount depending on when the mass transfer began. The donor stars are in general found to be consistent with main sequence or evolved giant/supergiant stars of type B, except in the case of the NGC 5204 ULX. Not suprisingly, the donor stars are found to be larger, less massive and older than inferred when irradiation is not taken into account. Donors of type A or later can be ruled in most cases.

I now comment on individual sources, giving the currently observed spectral type in each case. The main aim is to compare the parameters determined in Chapters 3 and 4 to the determinations in the literature.

5.2.1 NGC 4559 X-10

There is no previous determination of the spectral type of the donor in NGC 4559 X-10 (not to be confused with X-7). Indeed, the counterpart itself has yet to be identified: there are a number of possible candidates within the X-ray error circle. Separate calculations were performed with each candidate in turn, and the fitted stellar mass was found to be within a common range no matter which candidate was used as the counterpart. The stellar radius however, varied significantly from candidate to candidate. The radius is consistently high, and combined with the mass determination, the donor is found to be a supergiant. A spectral type B is most likely, but depending on which candidate and BH mass are used, spectral types of A or F are also possible.

5.2.2 M81 X-6

Liu et al. (2002) found the photometric observations of the counterpart to M81 X-6 fitted with an MS O-star. They noted that although the photometric data can be fit by considering an O9 MS star the colour of the data is redder than would be expected. They corrected for this by assuming intrinsic extinction by the dusty environment of the ULX, which changed their determination of the spectral type to an O8 star. I argue here instead that the red excess could be explained in terms of a disc component adding to the optical emission (as in LMC X-3, van Paradijs et al. 1987). The stellar parameters calculated clearly identify the donor as an MS or giant evolved B-star.

5.2.3 ULX in NGC 5408

For the ULX in NGC 5408, the best fit model is a giant, evolved B star, but the possibility of a very massive ($> 45M_{\odot}$) O-type donor star cannot be ruled out. When the inclination is assumed to be such that the plane of the disc is perpendicular to the plane of the sky, the radius implied by the model increases, and matches that of a B-type supergiant.

5.2.4 ULX in Holmberg II

For the Holmberg II ULX, when $\cos(i) = 0.5$ a tight constraint is found on the stellar radius, but the possible mass range is large. These results are consistent with the donor being either an MS O-star or a giant B-star. There are two distinct possibilities in the $\cos(i) = 0.0$ case as well, but here the solutions corresponding to a lower stellar mass give a higher stellar radius, so the donor can be classifed as either an MS O-star or a B supergiant. Kaaret et al. (2004) suggested the donor was of type O4V or B3Ib, which is consistent with the finding presented in this work.

5.2.5 M51 X-9

Terashima et al. (2006) suggested that the donor in M51 X-9 was a F2 – F5 supergiant. There are two epochs of optical data for this source but the stellar parameters are only constrained well in one of them. The mass determination suggests the donor in this system is a B-star. When there is a disc component to the emission the fitted stellar radius is low and indicative of a MS star; when the orbital plane of the binary is assumed to be perpendicular to the plane of the sky the radius determination increases to that of a giant, evolved B-star.

5.2.6 NGC 1313 X-2

For ULX X-2 in NGC 1313, there are two epochs of observation, and consistent determinations of stellar parameters are found through calculations with either set of data. The candidate designated C1 in Mucciarelli et al. (2005) is found to be the most likely optical counterpart, which is consistent with the conclusions of previous authors. The low stellar radius found from the model fit suggest the donor is a main sequence star. The most likely spectral type is B, although a late O-type is also a possibility, especially when $\cos(i) = 0.0$. Mucciarelli et al. (2005) suggested that the donor is an MS star of type O9 – B0, and Liu et al. (2007) suggested it was an O7 MS star. Both of these conclusions are consistent with the findings presented in this work.

5.2.7 NGC 4559 X-7

For ULX X-7 in NGC 4559, the determination of the mass and radius suggest the star is a supergiant, of spectral type B (if an inclination such that there is a disc component to the emission is assumed) or spectral type A (if it is assumed that the plane of the disc is perpendicular to the sky – $\cos(i) = 0.0$). These results are consistent with the donor being of approximately the same age and mass as the stars in its immediate neighbourhood (Soria et al., 2005).

5.2.8 ULX in NGC 5204

For the ULX in NGC 5204, Liu et al. (2004) reported the multi-band photometry to be consistent with stars of type O5 V, O7 III or B0 Ib. They also reported *HST*/STIS far-ultraviolet spectral observations, and on the basis of those they suggest the star is most likely to be of type B0 Ib, although they note the spectrum does contain some peculiarities for a star of this type. The STIS data are also consistent with the presence of an X-ray illuminated accretion disc. The model presented in this work does not provide good fits when the mass accretion rate is fixed. When this constraint is relaxed the observation is found to be consistent with a very massive O-type MS star, and a mass accretion rate of an order of magnitude or more greater than would be expected from the observed X-ray luminosity.

The conclusion that the donor is an MS O-star disagrees with Liu et al. (2004), and in contrast to most of the sources presented here I find the donor to be a more massive and compact star than originally thought. Liu et al. (2004) found the photometric observations to be consistent with an MS or giant O-type donor star, but concluded that the star is a B-type supergiant based on the additional *HST*

STIS MAMA/FUV data. Specifically, the equivalent width of the Si_{III} λ1299 line is suggestive of a star cooler than 25000K. An MS O-star would be hotter than this, even on its unirradiated hemisphere. If I assume my interpretation of the optical data is correct, I must therefore suggest that this line originates somewhere other than on the surface of the star.

5.2.9 ULX in M101

For the ULX in M101, the donor is found to be a B-type star if the optical emission has an observable disc and a star component. If the disc is perpendicular to the plane of the sky, the fit is poor when the mass accretion rate is fixed, as in the NGC 5204 ULX. If the mass accretion rate constraint is relaxed, the observation is consistent with the donor being a late O or B supergiant, or possibly an MS O star.

5.3 Comments on mass accretion rate constraints

I have found found that the mass accretion rate as inferred from the nuclear evolution timescale (via the evolutionary tracks) is larger in the NGC 5204 ULX than is inferred from the X-ray luminosity. This can be explained in one of three ways. Firstly, it can be assumed that the interpretation of the optical data given in this work is correct and the donor is an MS O-star. This implies that the radiative efficiency $\eta \sim 0.01$, an order of magnitude less than for standard disc accretion; mass outflows or advective inflows are well-known possible reasons for sub-nominal radiative efficiency.

The second possibility is that the BH is mostly fed by stellar winds rather than Roche lobe overflow. This invalidates both the irradiation model and the calculation of the mass accretion rate, since both of them are dependent on Roche lobe overflow as the accretion mechanism. Given that this source is a lower-luminosity ULX (3×10^{39}ergs s^{-1}) when compared to the others in the sample, a supergiant donor feeding the ULX via a wind is a reasonable conclusion. However, this is inconsistent

Table 5.2: Calculated stellar ZAMS parameters for the donor stars in the ULXs listed in Chapter 3. These values do not account for any loss due to to the mass accretion, and so should be increased by an amount depending on when the mass transfer began (* assumes the most luminous optical candidate is the counterpart. ** applies only for a hardness ratio of $\xi = 0.01$. *** applies only when the mass accretion rate is not constrained.)

	BH Mass = $10M_\odot$		BH Mass = $100M_\odot$		BH Mass = $1000M_\odot$	
	Mass ($M_\odot$)	Log Temp (K)	Mass ($M_\odot$)	Log Temp (K)	Mass ($M_\odot$)	Log Temp (K)
NGC 4559 X-10						
$\cos(i) = 0.5$, superior conjunction *	5.37 - 14.34	4.31 - 4.51	5.67 - 12.19	4.32 - 4.48	7.38 - 65.4	4.38 - 4.70
$\cos(i) = 0.5$, inferior conjunction *	5.68 - 12.19	4.32 - 4.48	5.08 - 12.19	4.30 - 4.48	7.38 - 65.4	4.38 - 4.70
$\cos(i) = 0.0$, superior conjunction *	7.38 - 65.4	4.38 - 4.70	7.95 - 10.18	4.39 - 4.44	-	-
M81 X-6						
$\cos(i) = 0.5$, superior conjunction **	-	-	3.38 - 7.10	4.20 - 4.37	6.36 - 9.10	4.35 - 4.42
$\cos(i) = 0.5$, inferior conjunction **	-	-	2.56 - 8.03	4.12 - 4.39	6.56 - 9.10	4.35 - 4.42
$\cos(i) = 0.0$, superior conjunction	2.48 - 5.37	4.11 - 4.31	-	-	-	-
NGC 5204 ULX						
$\cos(i) = 0.5$, superior conjunction ***	68.4 - 109.3	4.71 - 4.74	72.0 - 95.3	4.71 - 4.73	-	-
$\cos(i) = 0.5$, inferior conjunction ***	69.4 - 110.3	4.71 - 4.74	72.0 - 95.3	4.71 - 4.73	-	-
$\cos(i) = 0.0$, superior conjunction ***	65.1 - 116.3	4.70 - 4.75	69.6 - 117.3	4.71 - 4.75	73.4 - 118.3	4.71 - 4.75
M101 ULX-1						
$\cos(i) = 0.5$, superior conjunction	2.46 - 4.13	4.11 - 4.24	2.48 - 4.81	4.11 - 4.28	2.93 - 6.35	4.16 - 4.35
	81.3 - 84.3	4.72				
$\cos(i) = 0.5$, inferior conjunction	3.24 - 4.03	4.18 - 4.24	2.94 - 4.58	4.16 - 4.27	2.93 - 6.35	4.16 - 4.35
	81.3 - 84.3	4.72			45.0 - 52.4	4.67 - 4.69
$\cos(i) = 0.0$, superior conjunction ***	15.7 - 101.3	4.52 - 4.74	19.0 - 100.4	4.56 - 4.74	15.7 - 104.3	4.52 - 4.74
NGC 5408 ULX						
$\cos(i) = 0.5$, superior conjunction	5.08 - 23.49	4.30 - 4.59	5.68 - 18.98	4.32 - 4.56	8.32 - 57.4	4.40 - 4.69
	68.4 - 117.3	4.71 - 4.75	84.3 - 88.3	4.72 - 4.73		
$\cos(i) = 0.5$, inferior conjunction	5.37 - 14.3	4.31 - 4.51	5.67 - 19.0	4.32 - 4.56	8.32 - 57.4	4.40 - 4.69
	70.4 - 117.3	4.71 - 4.75	86.3 - 88.3	4.72 - 4.73		
$\cos(i) = 0.0$, superior conjunction	5.08 - 14.35	4.30 - 4.51	9.80	4.44	-	-
	79.2 - 117.3	4.72 - 4.75				

Table 5.3: Calculated stellar ZAMS parameters for the donor stars in the ULXs listed in Chapter 4. These values do not account for any loss due to to the mass accretion, and so should be increased by an amount depending on when the mass transfer began.

	BH Mass = $10M_\odot$		BH Mass = $100M_\odot$		BH Mass = $1000M_\odot$	
	Mass ($M_\odot$)	Log Temp (K)	Mass ($M_\odot$)	Log Temp (K)	Mass ($M_\odot$)	Log Temp (K)
Holmberg II ULX						
$\cos(i) = 0.5$, superior conjunction	5.68 - 81.4	4.32 - 4.72	6.71 - 68.4	4.36 - 4.71	10.82 - 22.1	4.45 - 4.58
$\cos(i) = 0.5$, inferior conjunction	5.68 - 88.3	4.32 - 4.73	5.67 - 68.4	4.32 - 4.71	10.82 - 22.1	4.45 - 4.58
$\cos(i) = 0.0$, superior conjunction	5.08 - 90.3	4.30 - 4.73	4.81 - 9.11	4.28 - 4.42	10.28	4.45
			57.2 - 88.3	4.70 - 4.73	72.3 - 84.3	4.71 - 4.72
M51 X-9						
$\cos(i) = 0.5$, superior conjunction	3.85 - 21.2	4.23 - 4.58	5.56 - 8.1	4.32 - 4.40	-	-
$\cos(i) = 0.5$, inferior conjunction	3.73 - 22.2	4.22 - 4.58	5.96 - 10.1	4.33 - 4.44	-	-
$\cos(i) = 0.0$, superior conjunction	-	-	2.47 - 4.12	4.11 - 4.24	4.57	4.27
NGC 4559 X-7						
$\cos(i) = 0.5$, superior conjunction	5.08 - 12.19	4.30 - 4.48	5.08 - 9.80	4.30 - 4.44	5.67 - 20.73	4.32 - 4.57
$\cos(i) = 0.5$, inferior conjunction	5.68 - 12.68	4.32 - 4.49	5.68 - 9.11	4.32 - 4.42	5.67 - 20.73	4.32 - 4.57
$\cos(i) = 0.0$, superior conjunction	5.97 - 12.77	4.33 - 4.49	-	-	-	-
NGC 1313 X-2						
$\cos(i) = 0.5$, superior conjunction	9.29 - 23.1	4.42 - 4.59	10.3 - 12.1	4.45 - 4.48	-	-
$\cos(i) = 0.5$, inferior conjunction	6.71 - 27.11	4.36 - 4.61	11.0 - 15.3	4.46 - 4.52	-	-
$\cos(i) = 0.0$, superior conjunction	5.68 - 26.11	4.32 - 4.61	5.37 - 35.5	4.32 - 4.65	7.56 - 37.5	4.38 - 4.65

with the findings of Liu et al. (2004), as they report the FUV spectrum shows evidence of Roche lobe overflow.

A third possibility is that these objects are confused in current observations at optical wavelengths, with more than one star contributing to an unresolved counterpart.

For the ULX in M101, the same problem as for the NGC 5204 ULX is found if the inclination of the system is set to $\cos(i) = 0.0$. This can be explained by ruling out an inclination of $\cos(i) = 0.0$ in this case. Alternatively, this can be explained by either of the three possibilities detailed above. Given that this source has the weakest X-ray luminosity (1×10^{39}ergs s^{-1}) of those examined in this work, a wind-fed BH may be an appropriate description of the system.

It is interesting to note that this same problem occurs in a number of other cases when the star is in inferior conjunction and $\cos(i) = 0.0$. This represents the case where there is no disc component and only the unirradiated hemisphere of the star is visible. This arrangement has not been discussed in the same amount of depth in this thesis as other regions of the orientation/inclination parameter space, because the determined parameters are the same as those that would be found when unmodified stellar tracks are fit to the observation. Results consistent with the work of those authors are found when the model is fit to observation for this orientation and inclination, but in a number of cases the determined mass accretion rate is in excess of that which is implied by the X-ray luminosity. This illustrates the importance of a model that accounts for the presence of X-ray heating and a disc component; when these factors are not accounted for a very massive and early type donor star is found, but such a star will evolve at a very high rate and one of the three scenarios detailed in this section will be required for consistency with X-ray observations.

Table 5.4: BH mass constraints, and the inclination for which they apply (* applies only when a constraint on the mass accretion rate is not used. ** applies only for a hardness ratio of $\xi = 0.01$.)

NGC 4559 X-10	$< 45M_\odot$ for $\cos(i) = 0.0$
M81 X-6	$> 20M_\odot$ for $\cos(i) = 0.5$ **
	$< 33M_\odot$ for $\cos(i) = 0.0$
NGC 5204 ULX	$< 240M_\odot$ for $\cos(i) = 0.5$ *
NGC 5408 ULX	$< 110M_\odot$ for $\cos(i) = 0.0$
M51 X-9	$< 300M_\odot$ for $\cos(i) = 0.5$
	$> 70M_\odot$ for $\cos(i) = 0.0$
NGC 1313 X-1	$< 50M_\odot$ for $\cos(i) = 0.5$
NGC 4559 X-7	$\sim 10M_\odot$ for $\cos(i) = 0.0$

5.4 Constraining the BH mass

5.4.1 Constraints from model fits

A key to understanding the nature of ULXs is the determination of the BH mass. In seven of the systems examined in this work, I can constrain the mass of the BH based on model fits. In each case, these constraints are only applicable for certain inclinations. These seven cases are listed in Table 5.4.

An upper limit on the BH mass in NGC 4559 X-10 can be found if the binary is assumed to have an inclination of $\cos(i) = 0.0$. The actual determination depends on which of the candidates are assumed to be the optical counterpart. The determinations are listed in Table 3.2. It can be seen that an upper limit on the BH mass of $500M_\odot$ exists irrespective of which candidate is selected. If the most luminous candidate (candidate 1) is assumed to be the counterpart, then this upper bound is reduced to $45M_\odot$.

The ULX in NGC 5204 has a maximum BH mass of $\simeq 240M_{\odot}$ when an inclination of $\cos(i) = 0.5$ and a low accretion efficiency of 0.01 is assumed. The constraint disappears when $\cos(i) = 0.0$. The X-ray data supports the presence of a cool thermal disc component (Roberts et al., 2005) which may be produced by an IMBH or by a stellar-mass disc cooled by other processes. Unfortunately, the optical mass constraints are not strong enough to discriminate between the stellar-mass and IMBH scenarios.

If an inclination of $\cos(i) = 0.0$ is used for the ULX in NGC 5408, a maximum BH mass of $110M_{\odot}$ is found. When the system is inclined so as to include a disc component, the upper limit increases. In both cases this is consistent with the X-ray data, which implies a BH mass of $\sim 100M_{\odot}$, assuming accretion at the Eddington limit (Soria et al., 2004).

When an inclination of $\cos(i) = 0.5$ is assumed for the ULX in NGC 1313, an upper limit on the BH mass of $100M_{\odot}$ is found. This upper limit increases as the disc component is reduced, and vanishes when $\cos(i) = 0.0$. This BH range is consistent with a BH mass of $\sim 100M_{\odot}$ previously inferred from the X-ray data (Zampieri et al., 2004).

If the ULX X-7 in NGC 4559 is assumed to have an inclination of $\cos(i) = 0.0$, then the BH is found to have a modest mass. If the WFPC2 data is used I find an upper limit on the BH mass of $\simeq 35M_{\odot}$, whereas if the ACS data is used the mass is found to be $\sim 10M_{\odot}$. Analysis of the X-ray data has suggested a lower limit on the BH mass of $50M_{\odot}$(Cropper et al., 2004). This inconsistency can be accounted for by inclining the binary system in the model so that the optical emission includes a disc component. This results in the upper limit on the BH mass increasing. By the time an inclination of $\cos(i) = 0.5$ is reached, the upper limit has disappeared.

The M51 X-9 and M81 X-6 sources are interesting because the BH mass is constrained in both the $\cos(i) = 0.0$ and 0.5 cases, but is an upper limit for one inclination and a lower limit for the other. This may mean that it will be easier to determine the nature of these sources after further observations, since one inclination implies an lower mass BH whereas the other implies a higher mass BH. Determination of either the inclination or the BH mass will help in the determination of the other.

For M51 X-9 the BH mass is found to be less than $300M_{\odot}$ for $\cos(i) = 0.5$ and greater than $70M_{\odot}$ when $\cos(i) = 0.0$. Liu et al. (2005) suggested that the mass of the BH might be $\sim 120M_{\odot}$, based on the X-ray luminosity and accretion at 10% of the Eddington rate. This suggestion is consistent with the mass constraint given here for either inclination.

It can be seen for ULX X-6 in M81 that when $\cos(i) = 0.0$ there is an upper limit on the BH mass of $33M_{\odot}$, but if $\cos(i) = 0.5$ a lower limit on the BH mass of $20M_{\odot}$ is found. The existence of this lower limit is dependent on the irradiating X-ray spectrum being softer than has otherwise been assumed and the age of the donor being comparable to the of the field stars. This BH has been suggested to have a mass of $18M_{\odot}$ based on analysis of X-ray data, but this was model dependent (Liu et al., 2002).

5.4.2 H-ionisation instabilities in ULX accretion discs

If the effective temperature in any region of a thin disc falls below $\sim 10,000$K, it triggers an instability due to ionisation of hydrogen. This instability rapidly propogates throughout the disc and causes large variations in disc luminosity (see, *e.g.*, Done et al. 2007 for a recent review). Since transient behaviour is not observed in any of the ULXs discussed in this thesis it is reasonable to assume that this instability does not occur in these systems, and therefore no region of these discs is below $10,000$K in temperature.

The disc temperature is a function of radius, so a larger disc will have cooler outer regions than a smaller disc. The size of the accretion disc in the model is determined by the mass ratio of the two components and the radius of the donor star. Given that the stellar parameters are known from the model fits, the absence of this instability implies an upper limit on the BH mass. I now investigate if this constrains these systems more.

I calculated the outer disc temperature T_{out} for stars of different spectral class and luminosity type for a BH mass range of 10-1000$M_{\odot}$. The disc is large (and hence has a low T_{out}) when the stellar radius is large or the BH is massive. I find that when an X-ray luminosity of $\sim 10^{40}$ergs s^{-1} is used then T_{out} drops below $10,000$K only when the donor is a supergiant of type A0 or later and the BH is $> 800M_{\odot}$. Since the donors are generally found to be of type B, the discs in these systems will be unaffected by the instability irrespective of the assumed BH mass.

The four lower luminosity ULXs (M81 X-6: 2×10^{39}ergs s^{-1}, NGC 5204: 3×10^{39}ergs s^{-1}, M101: 1×10^{39}ergs s^{-1}and M51 X-9: 3×10^{39}ergs s^{-1}) are a different matter. When $L_x \sim 10^{39}$ergs s^{-1} and the BH mass is large (of order $100M_{\odot}$ or greater) then discs in systems containing evolved B-stars can be affected by this instability. The M81, M101 and M51 ULXs were all found to have a B-type donor, and since we do not observe the disc instability in these systems the implication is that some of the upper limits on the BH mass given in Section 5.4.1 for these sources may be too conservative. A BH mass of $< 100M_{\odot}$may be required in these systems. Alternatively, the donors in these systems may be type B MS stars. This implies smaller discs which do not fall below the instability temperature for any BH mass. The donor in the NGC 5204 ULX is most likely an O-type MS star, which also implies a disc which is not affected by this instability.

5.4.3 Summary

When the constraints on the BH masses on these seven systems are viewed together, a consistent picture emerges. The model fits tend to suggest either a stellar mass BH or an intermediate mass BH of up to a few hundred solar masses. Without additional constraints on the parameter space, it is not possible to distinguish between these two possibilities for any of the sources considered in this work.

It is however worth noting that when IMBH were first postulated in order to explain ULX luminosities, it was suggested that their masses could be $\sim 100 - 10^5 M_{\odot}$. With the possible exception of the two sources for which the BH mass is unconstrained, IMBH at the upper end of this theoretical mass range are ruled out. If it is assumed that the primaries in these systems are indeed IMBH, then their mass suggests they are much more closely related to stellar mass BH in XRB that SMBH in AGN. In other words, the ULX population are more appropriately described as an extension to the luminosity function of the established population of XRB rather than an evolutionary link between the two populations of XRB and AGN. If ULX represented an evolutionary link between these two populations, one would expect to find some IMBH with masses of $10^4 M_{\odot}$, $10^5 M_{\odot}$ or more. This work is however framed within an 'XRB-like' nature for ULXs, since it fundamentally assumes accretion onto the BH through Roche-lobe overflow of a single companion star. If a physical nature for ULX was assumed which is more in keeping with the standard model of accretion onto SMBH in AGN, a different set of conclusions may have been reached.

5.5 The evolution and history of ULXs

If IMBHs do indeed exist, it is of great importance to clarify how the ULX/IMBH and the star formation process in their vicinity are related. The open question to resolve is whether the donor star is coeval to the BH progenitor or captured by the BH some time after formation. If the star and the BH formed together, determining the age of the donor star also determines the age of the BH. If the star was captured by the BH, then the statistics of the spectral type and mass distribution of the donor stars can be used to set constraints on the capture rate and hence provide estimates to the IMBH populations.

In this study, it has been found that the donor stars are mainly of spectral type B, and are significantly older than previously determined. For example, (Liu et al.,

2002) inferred the donor star in M81 X-6 ULX to have an age of less than $10^{6.7}$yr. In this work the minimum stellar age is found to be an order of magnitude greater, if the BH mass is assumed to be $<\sim 100M_{\odot}$. I note that in a number of cases, the photometric data alone allows one to infer the donor is of spectral type B. In other cases, a range of (more massive) possibilities exist, but by applying constraints on the mass accretion rate a B-type star is found to be the most likely donor. In the case where the optical data points to a massive, O-type donor, the implied mass accretion rate is inconsistent with that which would be expected from the X-ray observation, given the assumed radiative efficiency of $\eta = 0.1$. I suggest therefore, that donor stars of a narrow spectral and mass range are necessary to produce a very luminous, Roche lobe fed ULX, and the finding of large fraction of B-type stars in the ULX sample may be significant.

If the compact objects in these systems are indeed IMBHs, and if the capture scenario is assumed, then the fact that a B-type donor is sufficient to fuel a ULX allows a lower spatial density for IMBHs for the observed population of ULXs than if the donors were found to be of type O, since B-type stars are more common and so the chances of forming a ULX binary are higher. However, this is not necessarily true since the capture probability is the probability that the star comes close enough to be captured but far enough not to be tidally destroyed. Various authors have modelled the tidal capture of a donor star by an IMBH (see *e.g* Hopman 2004; Blecha et al. 2006). There are various competing effects: for example an O star may more easily survive tidal squeezing. The capture rate appears to be $\sim$ stellar number density, but is only weakly dependent on stellar mass. This would imply that more B stars than O stars should be captured. I note also that tidal capture of isolated stars is only one process through which an IMBH might aquire a companion; another process is by capturing stars in binary systems, which may have a different frequency of occurence and period distribution for B or O stars.

It is also interesting to note that the two lowest luminosity ULXs in this sample, those in M81 and M101, are also those where a very old, less massive donor of age

$\sim 10^8$Myr is a possibility. This may be related to the existence of a population of low-luminosity sources ($<\sim 2 \times 10^{39}$ergs s^{-1}) also found in old elliptical galaxies, probably identified as low-mass XRBs. Conversely, the ULXs more luminous than 2×10^{39}ergs s^{-1} are almost always found in star-forming galaxies, and the donor stars are found to be of age $\sim 10^7$Myr or less.

5.6 X-ray variability

In Chapter 4 I studied the optical variability of three ULXs counterparts. There was the suggestion of variability of 0.1 – 0.2 magnitudes in two out of the three sources, but this detection was marginal at best. In part of the analysis of that chapter, it was assumed that this variation was real and due to a change in binary phase between the two observations. All other parameters were assumed to be fixed. This is not necessarily true: in particular, the assumption that the X-ray luminosity is constant may be false. ULXs are persistently luminous sources, but do vary in luminosity by some degree, and they may vary on a timescale comparable to that which separates the two epochs of optical observation (Mucciarelli et al., 2006). An increase in X-ray luminosity will result in an increased irradiative heating effect, and the optical properties of the star and disc will be affected. In this section I will assume the marginal detection of optical variability in NGC 1313 X-2 and M51 X-9 is real, and determine the degree to which the X-ray luminosities have to be varied from their mean value in order to induce this change.

5.6.1 NGC 1313 X-2

A marginal variation of ~ 0.1 magnitudes in the V-band was detected in two *HST* observations of NGC 1313 X-2 made three months apart (Mucciarelli et al., 2006). I list in Table 5.5 the best-fit stellar parameters for this source, for inclinations of $\cos(i) = 0.0$ and $\cos(i) = 0.5$, and BH masses of 10, 100 and $1000M_\odot$. These stellar parameters were used to produce Figure 5.1, which shows the effect of varying

Table 5.5: Best fit model parameters for the optical counterpart of NGC 1313 X-2. An X-ray luminosity of 10^{40}ergs s^{-1}, an X-ray hardness ratio of $\xi = 0.1$ and a stellar metallicity of Z= $0.2Z_{\odot}$ is assumed.

BH mass	$10M_{\odot}$	$100M_{\odot}$	$1000M_{\odot}$
$\cos(i) = 0.0$, superior conjunction			
Stellar Mass ($M_{\odot}$)	9.1	6.7	13.9
Stellar Radius ($R_{\odot}$)	7.1	10.8	10.0
Stellar Age (Myr)	28	49	14
$\cos(i) = 0.5$, superior conjunction			
Stellar Mass ($M_{\odot}$)	13.5		
Stellar Radius ($R_{\odot}$)	5.0		
Stellar Age (Myr)	6.9		

the X-ray luminosity on the V-band magnitude of the optical counterpart. I plot the *VLT* and *HST* observations for comparision. It can be seen in this figure that varying the X-ray luminosity by ±75% induces V-band luminosity changes of the order of a few tenths of a magnitude. In the $\cos(i) = 0.0$ case the change decreases with increasing BH mass, since for large BH masses the binary separation is large and the amount of X-ray flux incident on the stellar surface is small. When the optical emission contains a disc component, the effect of changing X-ray luminosity on optical luminosity is approximately constant for increasing BH mass.

As well as noting the variation in the optical counterpart, Mucciarelli et al. (2006) reported quasi-simultaneous X-ray observations made with XMM-*Newton*. The inferred X-ray luminosities of these observations are clustered around the average value of 10^{40}ergs s^{-1} which was used for this source, but a short duration flare was observed, during which the X-ray luminosity increased to $\sim 1.5 \times 10^{40}$ergs s^{-1}. This X-ray flare was concurrent with the *VLT* observation, labelled 1 in Figure 5.1.

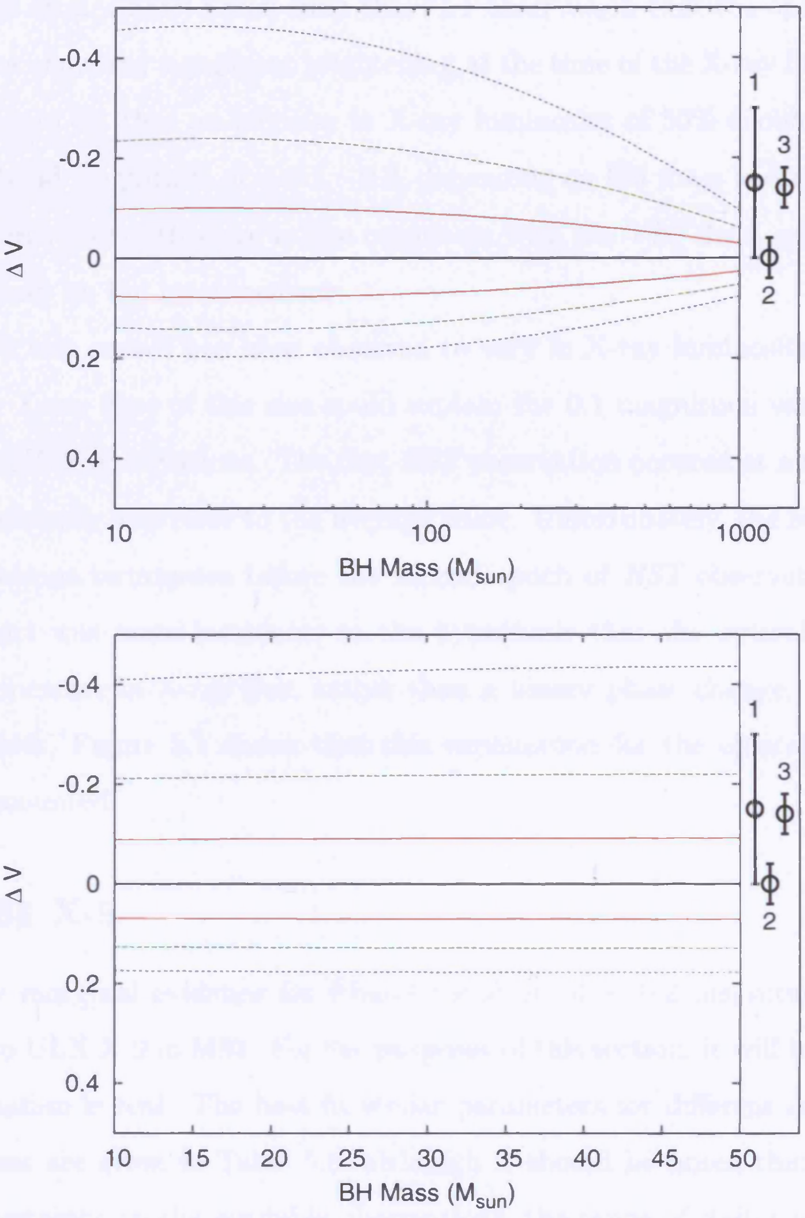

Figure 5.1: The effect of varying the X-ray luminosity on the optical luminosity of the counterpart of X-2 in NGC 1313. The change in model-determined V-band luminosity is plotted against BH mass, using the best-fit stellar parameters listed in Table 5.5. The black line is for an X-ray luminosity of 10^{40}ergs s^{-1}, and the red, green and blue lines show the effect of varying this by ±25%, ±50% and ±75% respectively. The top plot assumes an inclination of $\cos(i) = 0.0$, while the bottom plot assumes $\cos(i) = 0.5$. The observational data, taken from Table 4.2, are plotted on the right hand side of the plot, where *1* indicates the *VLT* observation, and *2* and *3* are the first and second *HST* epochs respectively.

Mucciarelli et al. (2006) noted from the *VLT* observation that the optical counterpart did not show any significant brightening at the time of the X-ray flare. It can be seen in Figure 5.1 that an increase in X-ray luminosity of 50% should induce a change in V-band magnitude of $\sim 0.1 - 0.2$, depending on BH mass and inclination. A luminosity increase of this size is also consistent with the *VLT* data, owing to the large uncertainty on the measurement.

Given that this source has been observed to vary in X-ray luminosity by up to 50%, another X-ray flare of this size could explain the 0.1 magnitude variation between the two *HST* observations. The first *HST* observation occured at a time when the X-ray luminosity was close to the average value. Unfortunately, the sequence of X-ray observations terminates before the second epoch of *HST* observation where the counterpart was more luminous, so the hypothesis that the optical variation is due to an increase in X-ray flux, rather than a binary phase change, cannot be tested. However, Figure 5.1 shows that this explanation for the optical variation cannot be discounted.

5.6.2 M51 X-9

There is very marginal evidence for I-band variation of ~ 0.2 magnitudes in the counterpart to ULX X-9 in M51. For the purposes of this section, it will be assumed that this variation is real. The best fit stellar parameters for different inclinations and BH masses are given in Table 5.6, although it should be noted that owing to the large uncertainty on the available observations, the range of stellar parameters which fit well with the data is large.

I show in Figure 5.2, the change in I-band magnitude of the counterpart induced by varying the X-ray luminosity by up to ±75%. As with NGC 1313 X-2, when the inclination is set to $\cos(i) = 0.0$ the induced change in luminosity decreases with increasing BH mass, whereas in the $\cos(i) = 0.5$ case the BH mass has little effect.

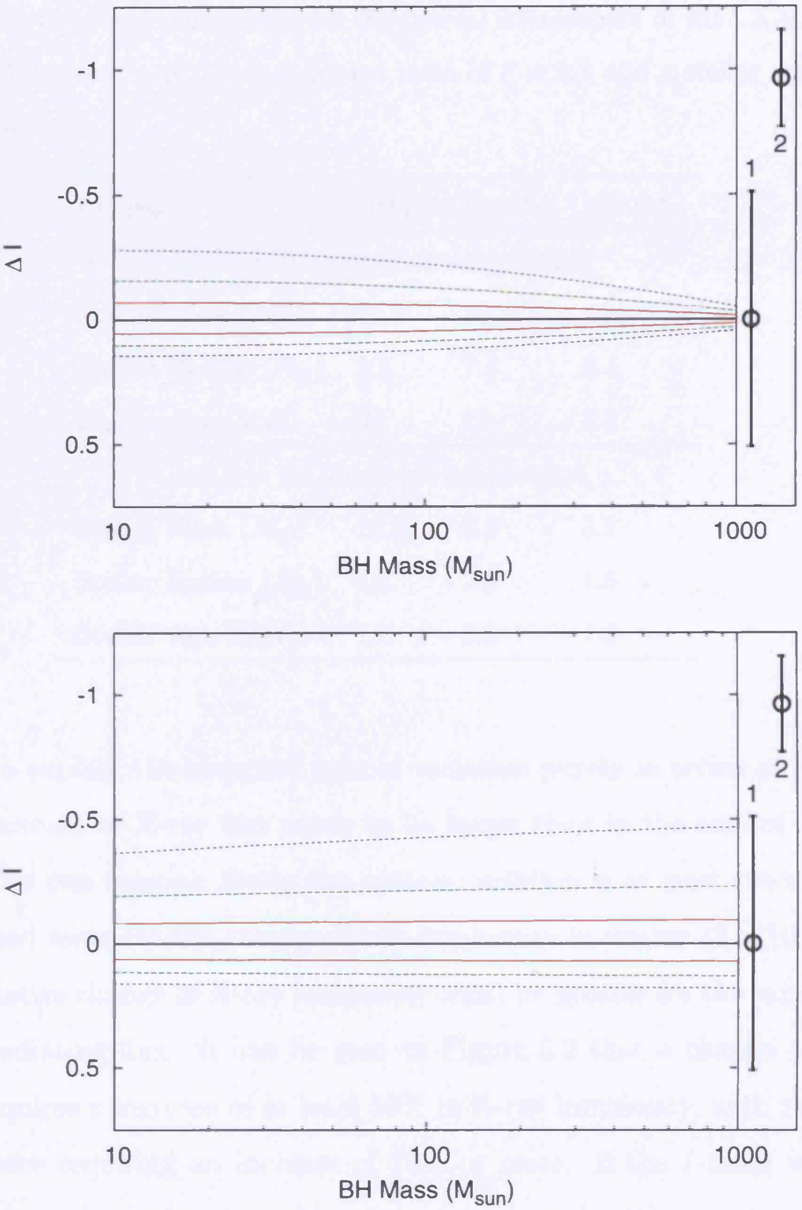

Figure 5.2: The effect of varying the X-ray luminosity on the optical luminosity of the counterpart of X-9 in M51. The change in model determined *I*-band luminosity is plotted against BH mass, using the best-fit stellar parameters listed in Table 5.6. The black line is for an X-ray luminosity of 3×10^{39}ergs s^{-1}, and the red, green and blue lines show the effect of varying this by ±25%, ±50% and ±75% respectively. The top plot assumes an inclination of $\cos(i) = 0.0$, while the bottom plot assumes $\cos(i) = 0.5$. The observational data, taken from Table 4.1, are plotted on the right hand side of the plot, where *1* and *2* indicate the ACS and WFPC2 observations respectively.

Table 5.6: Best fit model parameters for the optical counterpart of M51 X-9. An X-ray luminosity of 3^{39}ergs s^{-1}, an X-ray hardness ratio of $\xi = 0.1$ and a stellar metallicity of Z= $0.2Z_{\odot}$ is assumed.

BH mass	$10M_{\odot}$	$100M_{\odot}$	$1000M_{\odot}$
$\cos(i) = 0.0$, superior conjunction			
Stellar Mass ($M_{\odot}$)	22.2	10.5	24.0
Stellar Radius ($R_{\odot}$)	5.3	7.4	6.4
Stellar Age (Myr)	0.1	22	2.2
$\cos(i) = 0.5$, superior conjunction			
Stellar Mass ($M_{\odot}$)	16.0	6.8	3.1
Stellar Radius ($R_{\odot}$)	4.6	2.6	1.6
Stellar Age (Myr)	1.4	0.8	1.2

In order to explain the observed optical variation purely in terms of X-ray variability, the increase in X-ray flux needs to be larger than in the case of NGC 1313 X-2. This is for two reasons; firstly the optical variation is at least twice as big for this source, and secondly the average X-ray luminosity is weaker (3×10^{39}ergs s^{-1}) and so the relative change in X-ray luminosity must be greater for the same absolute change in irradiating flux. It can be seen in Figure 5.2 that a change of ~ 0.2 in the I-band requires a increase of at least 50% in X-ray luminosity, with much of the parameter space requiring an increase of 75% or more. If the I-band variation is assumed to be much greater than this minimum value, then the required change in X-ray flux becomes vary large indeed.

5.7 Optical variability and binary orientation

The data available on the optical variability of ULX counterparts is limited, so it is difficult to make any general conclusions at this time. It should however be noted that these counterparts currently appear remarkably constant in luminosity. The counterpart of NGC 4559 X-7 shows no variability at all, and there is at best marginal evidence for very modest variation in the counterparts of NGC 1313 X-2 and M51 X-9. I have shown in Section 5.6 that these modest optical variations can be explained by a changing irradiating X-ray flux, and in particular in the case of NGC 1313 X-2 the observed optical variation matches that which would be expected based on previously observed X-ray variability.

It is interesting to compare this slight or non-existent variability with the many figures of Chapter 4, where the maximum V/I-band amplitude is plotted against binary parameters for these three sources. These figures show that the region of the parameter space which fits with the observation in the main predicts an optical variation in excess of that which is observed in these sources. In particular, when the binary is perpendicular to the plane of the sky, the predicted optical variation tends to be large; a magnitude or more. Even in the $\cos(i) = 0.5$ cases, the majority of the fitted parameter space suggests a variation that is a few times bigger than has been observed to date. In general of course, the optical amplitude will decrease as $\cos(i)$ approaches 1. The low variation in these three counterparts may suggest that their orbital planes are close to being parallel to the plane of the sky. If future optical observations of ULX counterparts continue to show little or no variation, then this could be an indication of a general property for ULXs. If ULXs have a preferential orientation of $\cos(i) = 1$ then one conclusion is that their ultraluminous nature is the result of beaming. The other explanation for little optical variation is that the emission is dominated by light from the disc, which suggests a more massive BH. These possibilities could be explored by future temporal studies of counterparts of ULXs, particulary for sources where there is existing evidence to suggest a very low or very high BH mass.

5.8 Systematic effects

A number of assumptions have been in this work. Some of the effects that will have an influence on the conclusions will be re-eamined here.

5.8.1 System geometry

This work has assumed mass transfer via Roche lobe overflow. It has been shown in two sources that this may be inappropriate, as the transfer mechanism is also consistent with a stellar wind. I note that these two sources are at the low-luminosity end of the ULX class. Mass transfer via a wind is much less likely for the $\sim 10^{40}$ergs s^{-1} ULXs, which are represented by four of the remaining five objects in the sample.

A thin disc is assumed in this work, but as was noted in Chapter 1, some authors have suggested more complicated disc models, with a thin disc covered by a Comptonised corona (Socrates & Davis, 2005). These models are being used to support the possibility of super-Eddington accretion in ULX systems. The corona emits hard X-rays which are reflected by the ionized surface of the inner disc. As in the disc model used in this thesis, the bulk of the optical emission comes from the outer regions of the disc, due to these regions having a much larger surface area than the inner parts of the disc. However, the corona model will result in a harder X-ray spectrum incident on the outer disc. Given that the hardness ratio assumed in this work is an estimate based on the observed X-ray spectra rather than theoretical models, the simple thin disc approximation is sufficient for the purposes of this work. I examine the effect of changing the X-ray hardness in more detail in Section 5.8.3. Additionally, since the corona extends away from the disc surface the angles of incidence of the X-rays on the outer disc regions are changed, but the extent of the corona is probably not large enough for this to have a significant effect.

5.8.2 Radiation pressure

In the results that have been presented here, the effects of radiation pressure have not been included. The effects of radiation pressure on the shape of a Roche lobe filling star are unclear: some authors suggest that the shape will be unaffected (Howarth, 1997), whereas others predict a significant effect in very X-ray luminous binaries (Phillips & Podsiadlowski, 2002). It was shown in Figure 2.9 that under the Phillips & Podsiadlowski (2002) formulation, radiation pressure has an increasing effect on the shape and luminosity of the donor as the BH mass is decreased. This is because as the BH mass is decreased the binary separation also decreases, and the X-ray flux incident on the stellar surface increases. Model calculations show also that the effect decreases when a donor of later spectral type is used, for the same reason. For most of the fitted solutions, where the BH mass lies between 100 and $1000M_{\odot}$ and the donor is found to be a star of type B or later, the effect of including radiation pressure on the results is therefore small. An appreciable deviation from the results reported in this work are observed when a BH mass of $\sim 100M_{\odot}$ and a main sequence, O-type donor are used. Even in this case, the fitted stellar mass only changes by 1 or $2M_{\odot}$, which is a small percentage of the total stellar mass and not enough to alter the classification of the star. A more significant deviation would be expected for low ($\sim 10M_{\odot}$) BH masses, but the Phillips & Podsiadlowski (2002) formulation used in this work for radiation pressure becomes inappropriate at this point, since it does not allow for any circulatory currents in the stellar surface driven by the irradiation. This means it tends to represent an extreme case of maximum stellar distortion, and in this extreme case the radiation pressure is very large, to the point of stripping the outer layers away from the donor so that it looks quite unlike an ordinary star. A radiation pressure formulation which included circulatory currents would predict a lessened effect on the stellar shape. Shielding by the disc will mitigate this effect further.

Given that the actual effect of radiation pressure on the stellar shape in ULX systems is not fully understood, I consider the omission of this component in this work to be appropriate. I do however note this introduces an additional source of uncertainty, particularly for low BH masses.

5.8.3 X-ray hardness

The hardness of the X-ray spectrum determines the depth at which the incident radiation deposits most of the energy. Soft X-rays are easily absorbed at the disc surface, while hard X-rays attenuate only at large optical depths. For incident X-rays with a soft spectrum, a hot surface skin layer is formed at depths optically thin to optical radiation, and the emission from the skin layer is at wavelengths shortward of the optical bands. However, for incident X-rays with a hard spectrum, most of the energy is deposited at depths optically thick to optical radiation. This heats the internal regions of the disc plane and hence leads to a more luminous disc at the optical wavelengths. This was illustrated in Figure 2.12, where it can be seen that as the X-ray hardness is increased, the disc V magnitude similarly increases. It was noted also in Section 2.9.5 that the effect of varying the hardness ratio on the stellar luminosity was small.

Because the hardness of the X-ray spectrum incident on the irradiated surfaces in these systems is unknown (as discussed in Section 3.2.1) a fixed hardness ratio of $\xi = 0.1$ has generally been used. The effect of varying the hardness ratio on the results presented in this work will now be discussed.

In Figure 5.3, I plot determinations of the masses and radii of the donor stars in NGC 4559 X-7 and the NGC 5408 ULX. The inclination is fixed to $\cos(i) = 0.5$, the BH mass to $100M_\odot$ and the stellar age to 10Myr. If the results for the ULX in NGC 4559 are examined, it can be seen that varying ξ has little to no effect on the determination of the mass of the donor star. The determination of the radius however, decreases with increasing hardness ratio. A similar decrease in stellar radius with increasing ξ is seen in the case of NGC 5408. An appreciable decrease

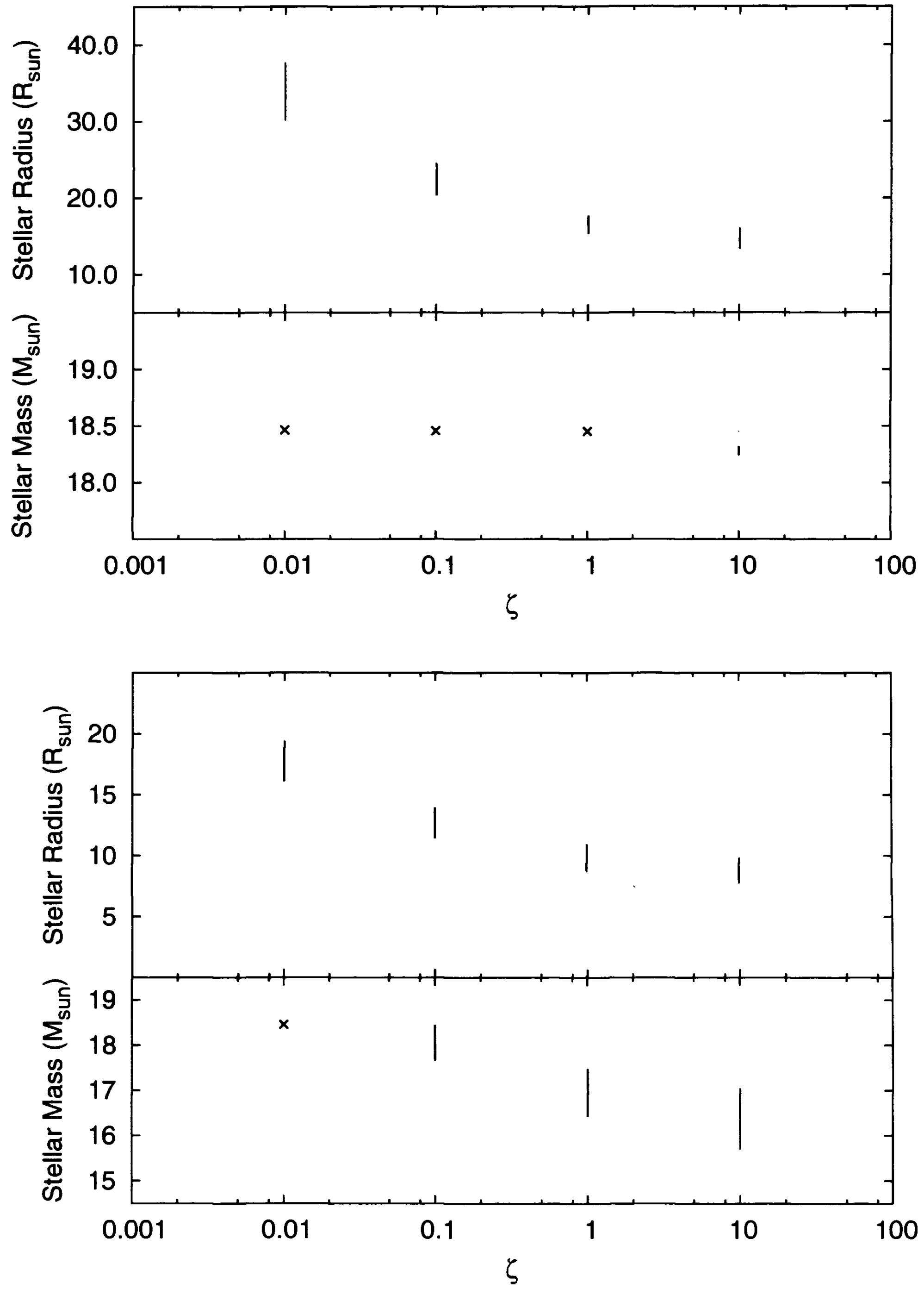

Figure 5.3: The change in stellar mass/radius with hardness ratio ξ for ULX X-7 in NGC 4559 (left) and the ULX in NGC 5408 (right). An inclination of $\cos(i) = 0.5$, a BH mass of $100M_\odot$ and a stellar age of 10Myr are used. The lines show the range of stellar parameters that fitted with the model at the 90% confidence level. For clarity, cases where the model produce a single unique solution are marked with an 'x'.

in stellar mass is seen also in this case, but this decrease is still much smaller than the decrease in stellar radius.

In a Roche lobe geometry the shapes of the lobes is determined by the mass ratio of the two components, and the scale of the system is set by their separation. In the model presented in this work the scale is determined by setting the volume radius of the secondary Roche lobe to be equal to the undistorted radius of the donor star. The results of Figure 5.3 can therefore be understood as follows. A harder incident X-ray spectrum leads to an accretion disc which is more luminous at optical wavelengths. If the disc in the model is hotter, then to keep it consistent with the observation it must be smaller, so the scale of the Roche lobes must be decreased. The model calculations therefore result in a smaller fitted stellar radius. Since the mass ratio affects only the shape of the Roche lobes and not the scale, the size of the disc is only weakly dependent on stellar mass, and so varying the hardness ratio will tend to have little effect on this parameter.

In both ULXs, the changes in stellar parameters are smaller than might be expected, given the significant variation in disc luminosity with hardness ratio shown in Figure 2.12. This is because that figure did not include the stellar component. Changing the mass ratio results in a different determination of the stellar radius, but changing this parameter results in a change in the luminosity of both the star and the disc. The radius therefore does not need to be changed by much to have a large effect on the overall luminosity.

Through examination of available X-ray data, ξ has been found to vary from ~ 0.1 to ~ 1 in NGC 4559 X-7. This has been assumed to be a physically appropriate hardness ratio range for all the ULXs in the sample, and most sources in this work have been fit to the model using $\xi = 0.1$. Figure 5.3 indicates that the general findings in this paper will not be invalidated if the X-ray spectrum in these systems is harder than we have assumed. It can be seen that increasing the X-ray hardness to $\xi = 1$ causes no change in the stellar mass in one case and a decrease of $\sim 1 M_\odot$ in the other. A decrease in the stellar radius of $2 - 5 R_\odot$ is also seen as ξ is increased from 0.1 to 1. It can be concluded therefore that, if the X-ray spectrum is harder, the determinations of the spectral type of the donors are still valid but they may be somewhat smaller and less evolved than our results suggest.

Some of the sources in this work were initially fit to the model using $\xi = 0.1$, but for certain inclinations and orientations the fit was found to be poor for this value of ξ, and indeed for all values of ξ between 0.1 and 1. These areas of the parameter space cannot be entirely eliminated from contention however; an adequate fit can be found when a very low hardness ratio of 0.01 is used. Note from Figure 5.3 that decreasing ξ from 0.1 to 0.01 has a more appreciable affect on the stellar parameters than increasing it from 0.1 to 1. A value of $\xi = 0.01$ is outside of the range determined for NGC 4559 X-7, but it may be that the X-ray spectrum is particularly soft in these few sources.

5.8.4 Perturbation of the donor as a result of mass transfer

A key distinguishing feature between the IMBH evolutionary scenarios is the epoch at which the steady mass transfer began. For any given ULX there are two possibilities: (a) the system is currently at the stage in its life where mass transfer has not yet significantly affected the state of the star, and so the single star models are a fair description of the donor; (b) The mass transfer has already significantly altered the state of the star and a binary evolution code is required for proper modelling.

Note that even in cases when a binary evolution code is necessary the results presented here are not invalidated. The method of this work is to determine the star which, in the presence of the intense X-ray radiation field produced by the ULX, will have the appearance of the observed donor, as it exists at the current epoch. Therefore, assuming the model assumptions (such as the assumption that the star is in thermal equilibrium) are correct, the masses and radii will be reasonably accurate, since these parameters depend on the current physical state of the star, not its history. Conversely, the determinations of parameters which do depend on the stellar history, such as the stellar age and ZAMS mass, will be less accurate if the star has lost a significant amount of its mass through Roche lobe overflow.

A binary stellar evolutionary code is neccessary when studying a ULX in which the mass transfer has endured long enough for the appearance of the donor to be significantly modified. It is unclear as to how long it takes for a star to deviate in characteristics from the single star evolutionary tracks when it is undergoing mass loss at the rates we have inferred. The mass loss can be assumed to have little affect on very massive stars ($\sim 40M_\odot$ and above) since over the course of their short lives they will transfer only a small percentage of their mass onto the BH through Roche lobe overflow. On the other hand, it has been shown that low mass stars ($\simeq 1M_\odot$) deviate from single star models very rapidly when undergoing phases of high mass transfer (Schenker et al., 2002).

It is reasonable to expect that a star that has transferred, say, 50% of its mass onto the BH through Roche lobe overflow will be significantly perturbed. When the calculations of the accumulated mass loss for star with ZAMS mass $10 - 20M_\odot$ are examined, it can be estimated that to lose 50% takes $\sim 2 - 3$Myr when an X-ray luminosity of 10^{40}ergs s^{-1} is assumed, although this varies depending on the point in the stellar evolution at which the mass transfer begins. This is a short length of time, but the model predicts the length of time in which any star can sustain mass transfer at ULX rates is also short, even when the effect of the mass loss on the star is not considered. Massive stars can transfer mass at ULX rates from ZAMS, but have intrinsically short (< 10Myr) lifespans. Lower mass donors only begin to transfer mass at the required rate towards the end of their time on the MS. The maximum duration of the binary as a ULX, assuming a 10^{40}ergs s^{-1} X-ray luminosity and a donor ZAMS mass of $10 - 20M_\odot$, is around $6 - 8$Myr. Note that assuming a lower mass transfer rate, as would be expected in ULXs with X-ray luminosities of $\sim 10^{39}$ergs s^{-1}, means that the donor takes significantly longer to be perturbed by the mass transfer. In addition it should be noted again that these conclusions are dependent on the assumed accretion efficiency being correct for these systems.

Note that in these estimations it has been assumed that the donor is unperturbed at the beginning of the ultraluminous X-ray emitting phase of the binary. The model calculations suggests that low mass stars can transfer mass at sub-ULX rates in the early part of their lives, assuming they evolve to a semi-detached state shortly after ZAMS. This would mean that the star would already be appreciably perturbed before it began its ULX phase. Similarly, if the star has at some point in its past undergone a phase of extreme mass transfer (such as thermal-timescale mass transfer, as discussed in Section 2.7.2), then a binary evolution code would almost certainly be necessary. Note also that very high rates of mass transfer are possible even when the driver is nuclear evolution: very massive stars can transfer mass to the BH at a rate of $\sim 10^{-5} M_{\odot}/\mathrm{yr}$ or more, particularly towards the end of their MS life and beyond. This would result in rapid and significant deviation from the single star tracks that have been used. Mass transfer at this rate is in excess of what would be expected for the ULXs in this sample, but some very X-ray luminous systems such as the $L_x = \sim 10^{41}$ergs s^{-1} ULX in M82 could have very early type donors in states of extreme mass loss.

I conclude therefore that a binary evolution code may be necessary in some of the sources discussed here, but given that the timescales of the ULX active phase and the timescale for the star to be perturbed by the mass loss are similar, the use of single star tracks is reasonable to start with, and should be reasonably accurate for some of the sources considered. Application of a full binary evolutionary code to this and future photometric data is an important avenue for future investigation of the nature of ULXs, but is beyond the scope of this work.

Chapter 6

Conclusions

6.1 Motivation

X-ray observations of ULXs have not yet been able to determine their nature, owing to the fact that accretion at the implied high rates is poorly understood and model dependent. While many authors have studied the X-ray properties of these sources, in this work I have sought to complement this work with an investigation of the optical characteristics. Their optical properties will also be heavily influenced by the intense X-ray radiation field, this is a useful avenue of investigation. This approach has not been pursued to any extent in the literature, despite the discovery in recent years of unique optical counterparts for several ULXs.

6.2 Summary of this work

This thesis assumes a binary nature for ULX, and details a model which has been constructed to describe the heating effect of the X-rays on the accretion disc and the companion star. The model uses a radiative transfer formulation to account for the incident X-rays and the distribution of the re-radiated thermal emission. I incorporate the distorted Roche lobe filling geometry of the star, and account for the limb- and gravity-darkening effects. The effect of radiation pressure on the shape of the star is also examined.

The accretion disc is assumed to have a thin disc geometry. I used the stellar evolution tracks of Lejeune & Schaerer (2001) as an input into this model, and by comparing the model results with the optical colours of the ULX counterparts, the parameters of the donor stars can be determined for any inclination, orientation and BH mass. Additionally, I use the mass transfer rate as implied by the observed X-ray luminosity as an additional constraint on the donor star parameters. This assumes that the nuclear evolution of the star is the driver for the mass transfer, and so the model mass transfer rate is determined from the rate of increase in radius of the model star from the stellar evolution tracks.

I examined the predictions from the model as a function of the various model parameters. The effects of changing the hardness of the X-ray spectrum, binary phase, black hole mass and donor spectral type and luminosity class were discussed. One key result is that for a given donor type, the effects of irradiation on the star decreases as the mass of the BH in the system (and hence binary separation) is increased. The stellar luminosity therefore decreases as BH mass increases. In contrast, the accretion disc luminosity increases as the BH mass increases, since the disc has a larger surface area when the binary separation is larger. The optical light therefore tends to be dominated by emission from the star when the BH mass is small, and by emission from the disc when the BH mass is large.

I also demonstrated the value of temporal observations and showed that observations at infrared wavelengths make it easier to distinguish between different systems.

The first set of results presented were for six sources for which there exists a single epoch of optical observations. In most cases, there is a single known candidate for the optical counterpart, or a most-likely candidate can be inferred with reasonable confidence. I determined the parameters of the donor stars, by fitting the multi-band photometric observations to the optical emission predicted by the model for different sets of stellar parameters. I examined and discussed the dependence of the determined donor type on parameters such as binary inclination, position of the star with respect to the observer when the observation was made, BH mass and stellar metallicity. For many of these systems, previous authors have concluded the donors to be MS O-stars or early-type supergiants. The calculations presented in this work suggest the donors are older and less massive than this, and are generally consistent with MS stars or evolved giants/supergiants of spectral type B. This is a reasonably tight spectral and mass range, which may be significant. The fact that a B-type donor is sufficient to fuel a ULX allows a lower spatial density for IMBHs for the observed population of ULXs than if the donors were found to be of type O, since B-type stars are more common and so the chances of forming a ULX binary are higher. However there are potentially competing effects: a more massive star may be able to more easily resist tidal disruption by the BH in a capture scenario. Additionally, the B-star donors implied by this work tend to have ages of order 10 – 100Myr. However, the accretion rate necessary to fuel an X-ray luminosity of 10^{40}ergs s^{-1} will result in a B-star being completely consumed in 5 – 10Myr. This suggests that if the donor star and the BH formed in the same epoch, then the star has only begun to overflow its Roche lobe and transfer mass relatively recently.

Some sources do not conform exactly to these findings, particularly the ULX in NGC 5204. The model cannot provide a good fit with the observation in this case, owing to the constraint applied on the mass transfer rate. When this constraint is removed the best solution is for a MS O-star in NGC 5204: a more massive donor than has been suggested for this system by other authors. However, these fits require a much higher mass transfer rate than would be expected from the X-ray luminosity. This source could have a low radiative efficiency due to an advective flow, or alternatively this ULX may be wind fed, instead of via Roche lobe overflow as we have assumed. In some other sources, the fit is poor unless the X-ray hardness ratio is varied from the value that is generally assumed in this work. There is a difficulty in determining the correct value of this parameter for any individual source as it is unknown whether the X-ray spectrum incident on the irradiated surface of the star and disc is the same as that which is observed. I investigated and discussed this potential source of uncertainty.

The second set of results included in this work are for three sources for which there exist optical observations at two or more separate epochs. This affords the opportunity to study optical variability in these systems, which may provide additional constraints on the system parameters. These sources were examined in the same way as the first six sources, and I reached similar conclusions about the nature of the donor stars. In all three systems, little or no optical variability was observed. This may be significant, sugessting either disc-dominated optical emission (and hence a more massive BH) or perhaps that the orbital plane of these binaries is close to parallel to the plane of the sky. No firm conclusions can be reached until a well sampled optical lightcurve is taken of these and other sources. Nevertheless, these possibilities are interesting avenues for future pursuit.

In more than half of the systems discussed in this work, the mass of the BH can be constrained based on the optical observations. However, the constraints are dependent on the inclination that is assumed for any individual system. Where constraints exist they tend to be upper bounds on the BH mass of a few hundred $M_\odot$ or less, supporting the idea that the accretors in ULX systems are stellar mass BHs or IMBHs of realtively modest mass. However for most sources an inclination can be found for which a very massive IMBH primary is a possibility. It is not very surprising that the inclination affects the model fits at high BH masses more so than it does at low BH masses, since it changes the ratio of disc emission to stellar emission significantly for high BH masses, whereas for low BH masses (and hence smaller discs) the star will tend to dominate irrespective of inclination.

6.3 Future Work

Optical counterparts of ULXs are faint and in densely populated environments. Observations are therefore difficult, and this work has been limited by the available optical data, in particular the limited spectral and temporal coverage. With few input constraints the extent to which the model parameters can be determined is limited, though large parts of the parameter space can be excluded. I have therefore resisted complicating the model used in this work any more than is necessary.

However, future observations will be increasingly powerful. There are definite avenues for increasing the fidelity of the model. One key advance will be the use of binary stellar evolution codes as an input into the model. This introduces other parameters, but allows for a donor star which has been significantly perturbed by mass loss to the BH. Given the timescales of mass transfer it is very possible that a number of the objects discussed here contain donor stars which are quite different from single stars. While the determinations of the stellar masses and radii presented here should be reasonably accurate, a binary stellar code is necessary to properly understand the history of the binary system, which will give further insight into the nature of ULXs. A second obvious direction for future work is improving the disc model. The thin disc used in this work is an acceptable first approximation, but the high accretion rates in these systems are more appropriately described by a more detailed model. I suggest that the effect on the optical emission which arises in the outer parts of the disc may not be that great, but concede that a more exotic disc model should not be too difficult to include.

I have attempted to show that temporal observations of ULX optical counterparts will be key in understanding their nature. The available data suggests that there is little to no optical variability in some counterparts. If this could be confirmed, this would be an interesting result. If variability was observed in a source, then the binary period could be determined. This would be a key step towards understanding its nature. While the parameters of the fitted donor star do not vary greatly with BH mass (the finding that the donors are generally B-stars is true irrespective of whether a $10M_{\odot}$ or $1000M_{\odot}$ BH is used), the binary period is an extremely useful probe of the BH mass. This can be seen to be true in Table 6.1, where I list predictions for the binary periods for the sources covered in this work, based on the parameters determined from the model fits. Because of the different limitations on the parameter space, note also the markedly different predictions when the binary inclination is changed. Some sources are particularly good targets for this kind of study; for example it can be seen that X-6 in M81 has a period of > 100 hours if the BH mass is assumed to be $10M_{\odot}$, but this decreases to only ~ 15 hours when a $1000M_{\odot}$ BH is assumed. In this system a low BH mass also implies an inclination of $\cos(i) \simeq 0.0$, with a more inclined system implying a higher BH mass and a larger discs. The donor in the $10M_{\odot}$ case is also a much larger, more evolved object and so the predicted lightcurve amplitude is large. If little variability was to be observed in this system then it would be a strong candidate for a $> 100M_{\odot}$ BH.

I have also noted in this work that observations at infrared wavelengths may be an important diagnostic in determining the nature of ULXs. This is an avenue which has hardly been explored observationally to date, but I illustrate the point in Figure 6.1. This shows colour-magnitude diagrams for B against $(B - V)$ and H against $(H - K)$ for the optical counterpart of the ULX in NGC 5408. In both cases, I plot the sections of the evolutionary tracks which fit the optical data to the 90% confidence level, for inclinations of $\cos(i) = 0.5$ and $\cos(i) = 0.0$ with the star in superior conjunction. In the B versus $(B - V)$ plot, the sets of tracks for the two inclinations are similar in colour and magnitude. However, it can be seen that at infrared wavelengths there is a clear distinction between the $\cos(i) = 0.5$ tracks and the $\cos(i) = 0.0$ tracks in both colour and magnitude. It is clear therefore that the combination of IR and optical observations will allow the parameters in ULX systems to be constrained with much higher precision.

6.4 Closing Remarks

In conclusion, the aim of this work was to better understand the nature of ULXs by determining the parameters of the BHs and donor stars in these systems, through

Table 6.1: Predictions of the orbital periods of these systems, in hours, based on the determinations of the donor star parameters in Chapters 3 and 4 (* applies only when a constraint on the mass accretion rate is not used. ** applies only for a hardness ratio of $\xi = 0.01$.)

BH mass	$10M_\odot$	$100M_\odot$	$1000M_\odot$
$\cos(i) = 0.5$, superior conjunction			
NGC 4559 X-10			
M81 X-6 **	–	47.9 - 59.5	15.9 - 16.2
NGC 5204 ULX *	27.4 - 42.0	37.8 - 44.5	–
M101 ULX-1	767 - 873	271 - 295	77.6 - 82.9
	26.6 - 26.9		
NGC 5408 ULX	114 - 277	94.9 - 112	33.4 - 36.6
	27.5 - 39.3	37.1 - 37.4	
Holmberg II ULX	27.2 - 152	35.4 - 61.5	21.1 - 22.1
M51 X-9			
NGC 4559 X-7	418 - 732	260 - 276	67.0 - 78.8
NGC 1313 X-2 C1	22.6 - 36.4	21.8 - 27.4	–
$\cos(i) = 0.0$, superior conjunction			
NGC 4559 X-10			
M81 X-6	136 - 287	–	–
NGC 5204 ULX *	27.5 - 46.7	38.8 - 56.4	41.8 - 57.7
M101 ULX-1 *	27.2 - 387	38.2 - 394	40.6 - 376
NGC 5408 ULX	247 - 732	760	–
	27.5 - 41.0		
Holmberg II ULX	27.0 - 417	542 - 1500	783
		35.3 - 37.3	36.2 - 38.5
M51 X-9			
NGC 4559 X-7	864 - 2060	–	–
NGC 1313 X-2 C1	26.0 - 96.2	28.4 - 157.5	28.3 - 190.4

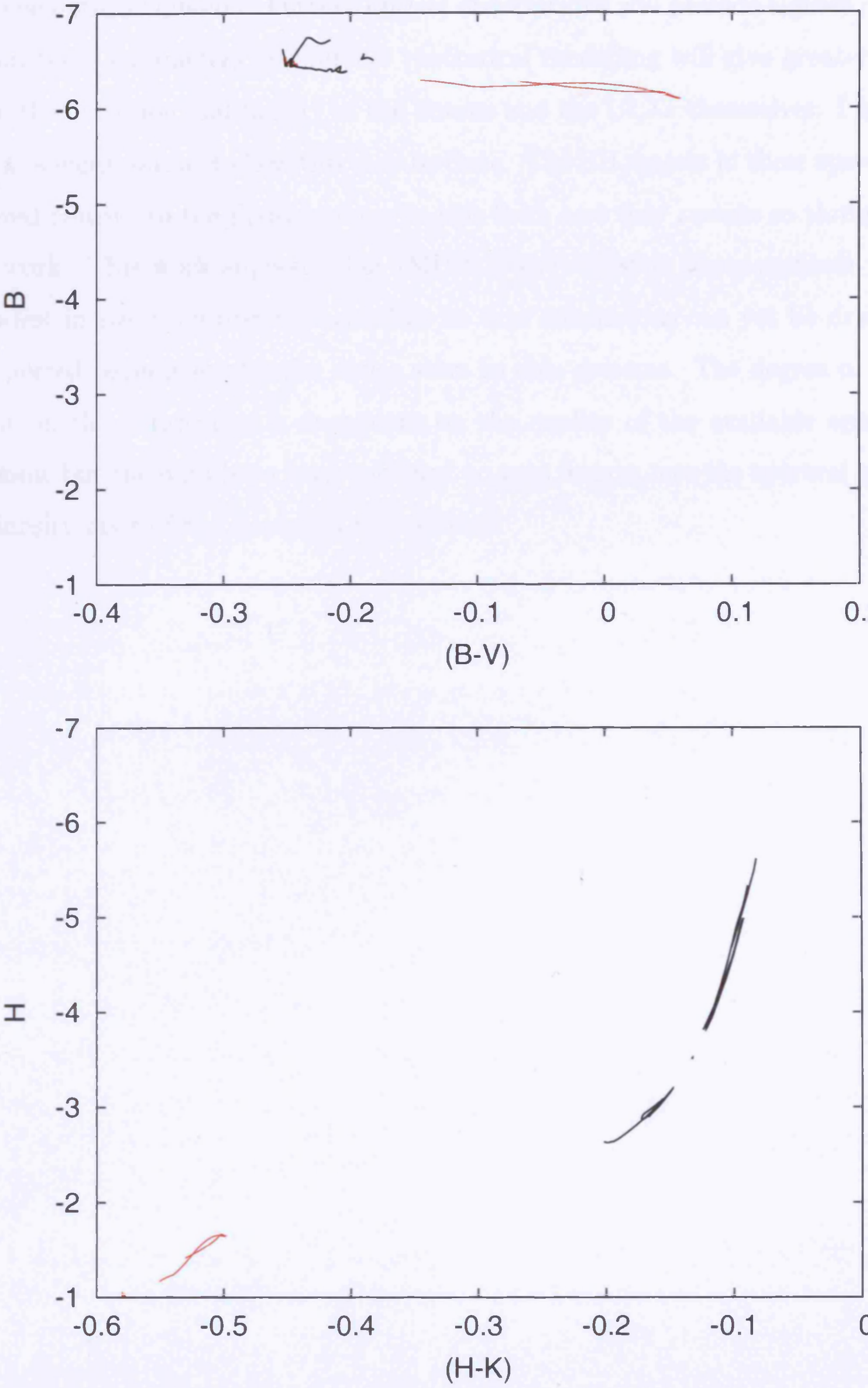

Figure 6.1: Colour-magnitude diagrams showing the 90% confidence contours for the optical counterpart of the ULX in NGC 5408, for inclinations of $\cos(i) = 0.5$ (black) and $\cos(i) = 0.0$ (red) with the star in superior conjunction.

study of the optical emission. Further optical observations will provide tighter constraints on these parameters and further theoretical modelling will give greater insight into the evolution and history of the donors and the ULXs themselves: I have made some suggestions as to how this may be done. The BH masses in these systems have proved ellusive to the many authors in this field, and they remain so throughout this work. This work suggests that IMBH, if they exist in these systems, are more modest in size than first thought, but no firm conclusions can yet be drawn. I have reported parameters for the donor stars in nine systems. The degree of the constraint on the parameters is dependent on the quality of the available optical observations, but the data have been sufficient to gain insight into the spectral type and luminosity class of the donors in the systems.

Acknowledgements

First and foremost, I would like to thank my supervisor Mark Cropper, for his constant support over the course of my PhD, and for always prioritising me over his many other responsibilities. I would also like to thank the many other members of the MSSL Astrophysics group (too numerous to list) who guided me over the years. I am particularly indepted to my co-supervisor Kinwah Wu and to Roberto Soria, both of whom gave up much of their time to support my studies. Thanks also to my examiners, Ian Howarth and Chris Done, for a relatively painless viva!

I would like to thank all of my friends at MSSL and elsewhere for their encouragement and friendship. Again, this page is too small to contain all of their names. but I would like to at least mention my various MSSL flatmates. Thanks therefore go to Steve, Pat, Rob, Tom, Sushan, Yasir, Jo, Gemma, Paul, Hillary, Sam, Glyn, Andy and Alex for a fun few years and some great games of Scrabble.

I would like to thank my Mum, Dad for their encouragement throughout all of my student career. I couldn't have managed without the support of my parents, be it emotional, or (at times) financial! Thanks also to Susan and Heather for their support.

Finally, I would like to acknowledge the funding I received for the three years of my PhD from the Particle Physics and Astronomy Research Council (PPARC).

Bibliography

Allen C.W., 1973, *Astrophysical Quantities*, (London, UK: Athlone Press)

Bahcall J.N. & Bahcall N.A., 1972, ApJ, 178, L1

Bauer, F.E., Brandt W. N., Sambruna R. M., Chartas G., Garmire G. P., Kaspi S., Netzer H. 2001, AJ, 122, 182

Beer M.E. & Podsiadlowski P., 2002, MNRAS, 335, 358

Begelman M.C., 2002, ApJ, 568, L97

Belczynski K., Sadowski A., Rasio F. A., 2004, ApJ, 611, 1068

Blecha L., Ivanova N., Kalogera V., Belczynski K., Fregeau J., Rasio F., 2006, ApJ, 642, 427

Bohlin R., Savage B.D., Drake J.F., 1978, ApJ, 224, 132

Bolton C.T., 1972, Nature, 235, 271

Bombaci I., 1996, A&A, 305, 871

Cardelli J.A., Clayton G.C., Mathis J.S., 1989, ApJ, 345 ,245

Carroll B.W. & Ostlie D.A., 2007, *An Introduction To Modern Astrophysics: 2nd ed* (San Francisco, USA: Addison-Wesley)

Casares J., 2006, in *IAU Symposium 238: Black Holes: From Stars to Galaxies – Across the Range of Masses* (astrop-ph/0612312)

Claret A. & Giménez A., 1990, A&A, 230, 412

Colbert E.J.M. & Mushotzky R.F., 1999, ApJ, 519, 89

Colbert E.J.M. & Ptak A.F., 2002, ApJS, 143, 25

Copperwheat C.M., Cropper M., Soria R., Wu K., 2005, MNRAS, 362, 79

Copperwheat C.M., Cropper M., Soria R., Wu K., 2007, MNRAS, 376, 1407

Cropper M., Soria R., Mushotzky R.F., Wu K., Markwardt C.B., Pakull M., 2004, MNRAS, 349, 39

D'Antona F., Mazzitelli I., Ritter H., 1989, A&A, 225, 391

de Jong J.A., van Paradijs J., Augusteijn T., 1996, A&A, 314, 484

Dewangan G.C., Griffiths R.E., Rao A.R., 2006, ApJ, 641, 2

Done C. & Kubota A., 2006, MNRAS, 371, 1216

Done C., Gierliński M., Kubota A., 2007, A&AR (astro-ph/0708.0148)

Dubus G., Lasota J-P., Hameury J-M., Charles P., MNRAS, 303, 139

Djurašević G., Rovithis-Livaniou H., Rovithis P., Georgiades N., Erkapić S., Pavlović R., 2003, A&A, 402, 667

Djurašević G., Rovithis-Livaniou H., Rovithis P., Georgiades N., Erkapić S., Pavlović R., 2006, A&A, 445, 291

Ebisawa K., Życki P., Kubota A., 2001, in *X-ray Emission from Accretion onto Black Holes*, eds. T. Yaqoob, J.H. Krolik

Ebisawa K., Życki P., Kubota A., Mizuno T., Watari K., 2003, ApJ, 597, 780

Eggleton P.P., 1983, ApJ, 268, 368

Eldridge J.J. & Vink J.S., 2006, A&A, 452, 295

Fabbiano G., 1989 ARA&A, 27, 87

Fabbiano G., White N.E., 2003 in *Compact Stellar X-ray Sources*, eds., W. Lewin, W., van der Klis, M., (Cambridge, UK: Cambridge Univ. Press) (astro-ph/0307077)

Fabbiano G., 2004, RevMexAA (Serie de Conferencias), 20, 46

Fabrika S. N., 2004, Astrophys. Space Phys. Rev., 12, 1

Fath E., 1909, Lick Observatory Bulletin, 5, 71

Ferrarese L., Ford H., 2004, Space Science Reviews, 116, 523 (astro-ph/0411247)

Frank J., King A., Raine D.J., 2002, *Accretion Power in Astrophysics: 3rd ed* (Cambridge, UK: Cambridge University Press)

Fryer C.L., Kalogera V., 2001, 554, 548

Genzel R., Eckart A., Ott T., Eisenhauer R., 1997, MNRAS, 291, 219

Gerend D. & Boynton P.E., 1976, ApJ, 209, 562

Giacconi R., Gursky H., Paolini F.P., Rossi B.B., 1962, Phys. Rev. Lett., 9, 439

Gierliński, M., Done, C., 2004, MNRAS, 349, L7

Gilfanov M., Grimm, H.-J., Sunyaev, R., 2004, NuPhS, 132, 369

Goad M.R., Roberts T.P., Reeves J.N., Uttley P., 2006, MNRAS, 365, 191

Goncalves A.C., Soria R., 2006, MNRAS, 371, 673

Grimm H.-J., Gilfanov M., Sunyaev R., 2006, in *Populations of High Energy Sources in Galaxies*, eds. Meurs E.J.A., Fabbiano G.

Heger A., Fryer C.L., Woosley S.E., Langer N., Hartmann D.H., 2003, ApJ, 591, 288

Hopman C., Portegies Zwart S.F., Alexander T., 2004, ApJL, 604, L101

Howarth I.D. & Wilson B., 1983, MNRAS, 202, 347

Howarth I.D., 1997, Observatory, 117, 335

Humphrey P.J., Fabbiano G., Elvis M., Church M.J., Bałucińska-Church M., 2003, MNRAS, 344, 134

Kaaret P. et al., 2001, MNRAS, 321, L29

Kaaret P., Corbel S., Prestwich A.H., Zezas A., 2003, Science, 299, 365

Kaaret P., Ward M.J., Zezas A., 2004, MNRAS, 351, 83

Körding E., Falcke H., Markoff S., 2002, A&A, 382, L13

King A.R., Davies M.B., Ward M.J., Fabbiano G., Elvis M., 2001, ApJ, 552, L109

King A. R., 2002, MNRAS, 335, L13

Klinglesmith D.A. & Sobieski S., 1970, AJ, 75, 175

Kuntz K.D., Gruendl R.A., Chu Y.-H., Rosie Chen C.-H., Still, M., Muka K., Mushotzky R.F., 2005, ApJ, 620, L31

Lejeune T. & Schaerer D., 2001, A&A, 366, 538

Liu J.-F., Bregman J.N., Seitzer P., 2002, ApJ, 580, L31

Liu J.-F., Bregman J.N., Seitzer P., 2004, ApJ, 602, 249

Liu J.-F., Bregman J.N., Seitzer P., Irwin J., 2005, AJ submitted astro-ph/0501310

Liu J.-F., Bregman J.N., Miller J., Kaaret P., 2007, A&A submitted

Lucy L.B., 1967, Zs. f. Ap., 65, 89

Madau P., Rees M.J., 2001, ApJ, 551, 27

Maeder A. & Meynet G., 1994, A&A, 287, 803

Makishima K. et al., 2000, ApJ, 551, L27

Manduca A., Bell R.A., Gustafsson N., 1977, A&A, 61, 809

Markowitz A., Edelson R., Vaughan S., Uttley P., George I. M., Griffiths R. E., Kaspi S., Lawrence A., McHardy I., Nandra K., Pounds K., Reeves J., Schurch N., Warwick R., 2003, ApJ, 593, 96

Matsumoto H. et al., 2001, ApJ, 547, L25

Matsushita S., Kawabe R., Matsumoto H., Tsuru T.G., Kohno K., Morita K.-I., Okumura S.K., Vila-Vilar B., 2000, ApJ, 545, L107

McHardy I. M., Koerding E., Knigge C., Uttley P., Fender, R. P., 2006, Nature, 444, 730

Michell J., 1784, Phil. Trans. Roy. Soc., 74, 35

Miller J.M., Fabbiano G., Miller M.C., Fabian A.C., 2003, ApJ (letters), 585, 37

Miller J.M., Fabian A.C., Miller M.C., 2004, ApJ, 607, 931

Miller J.M., Zezas A., Fabbiano G., Schweizer F., 2004, ApJ, 609, 2

Miller M.C., Hamilton D.P., 2002, MNRAS, 330, 232

Miller M.C. Colbert E.J.M., 2004, IJMPD, 13, 1 (astro-ph/0308402)

Miller N.A., Mushotzky R.F., Neff S.G., 2005, ApJ, 623, L109

Milne E.A., 1926, MNRAS, 87, 43

Mirabel F., 2006, in *IAU Symposium 238: Black Holes: From Stars to Galaxies – Across the Range of Masses* (astrop-ph/0612188)

Mucciarelli P., Zampieri L., Falomo R., Turolla R., Treves A., 2005, ApJ, 633, L101

Mucciarelli P., Zampieri L., Treves A., Turolla R., Falomo R., 2006, ApJ, 658, 999

Mueller A., 2007, PoS, 017 (astro-ph/0701228)

Paczyński B., 1977, ApJ, 216, 826

Pakull. M.W. & Mirioni L., 2002. (astro-ph/0202488)

Pakull M.W., Grisé F.,Motch C., 2006, in *Populations of High Energy Sources in Galaxies*, eds. Meurs E.J.A., Fabbiano G. (astro-ph/0603771)

van Paradijs J., van der Klis M., Augusteijn T., Charles P., Corbet R.H.D., Ilovaisky S., Maraschi L., Motch C., Pakull M., Smale A.P., Treves A., van Amerongen S., 1987. A&A. 184. 201

van Paradijs J., McClintock J.E., 1994. A&A. 290. 133

Phillips S.N. & Podsiadlowski P., 2002, MNRAS. 337. 431

Podsiadlowski P., 1991. Nat. 350. 136

Porquet D., Reeves J.N., O'Brien P., Brinkmann W., 2004. A&A, 422, 85

Portegies Zwart S.F., McMillam S.L.W., 2002, ApJ, 576, 899

Rappaport S.A., Podsiadlowski P., Pfahl E., 2005, MNRAS, 356, 401

Rees M.J., 1984. ARA&A, 22, 471

Ritter H., 1988. A&A. 202, 93

Roberts T.P. & Warwick R.S., 2000, MNRAS, 315, 98

Roberts T.P., Warwick R.S., Ward M.J., Goad M.R., Jenkins L.P., 2005, MNRAS, 357, 1363

Ruderman M., Shamam J., Tavani M., 1989, ApJ, 336, 507

Schenker K., King A. R., Kolb U., Wynn G. A., Zhang Z.,2002, MNRAS, 337, 1105

Seyfert C.K., 1943, ApJ, 97, 28

Shakura N.I. & Sunyaev R.A., 1973, A&A, 24, 337

Sirianni M., Jee M.J., Benítez, N., Blakeslee J.P., Martel A.R., Meurer G., Clampin M., De Marchi G., Ford H.C., Gilliland R., Hartig G.F., Illingworth G.D., Mack J., McCann W.J., 2005, PASP, 117, 1049

Socrates A. & Davis S.W., 2005, (astro-ph/0511549)

Soria R., Motch C., Read A., Stevens I., 2004, A&A, 423, 955

Soria R., Cropper M., Pakull M., Mushotzky R., Wu K., 2005, MNRAS, 356, 12

Soria R., Fender R.P., Hannikainen D.C., Read A.M., Stevens I.R., 2006, MNRAS, 368, 1527

Stobbart A.-M., Roberts T.P., Wilms J., 2006, MNRAS, 368, 397

Strohmayer T.E. & Mushotzky R.F., 2003, ApJ, 586, L61

Strohmayer T.E., Mushotzky R.F., Winter L., Soria R., Uttley P., Cropper M., 2007, ApJ accepted, (astro-ph/0701390)

Sugiho M., Kotoku J., Makishima K., Kubota A., Mizuno T., Fukazawa Y., Tashiro M. 2001, ApJ, 561, L73

Swartz D.A., Ghosh K.K., Tennant A.F., Wu K., 2004, ApJS, 154, 519

Terashima Y. & Wilson A.S., 2003, ApJ, 583, 145

Terashima Y. & Wilson A.S., 2004, ApJ, 601, 735

Terashima Y., Inoue H., Wilson A.S., 2006, ApJ, 645, 264

van Hamme W., 1993, AJ, 106, 2096

von Zeipel H., 1924, MNRAS, 84, 702

Vrtilek S.D., Quantrell H., Boroson B., Still M., Fiedler H., O'Brien K., McCray R., 2001, ApJ, 549, 522

Wade R.A., & Rucinski S.M., 1985, A&AS, 60, 471

Warner B., 1995, *Catalclysmic Variable Stars*, (Cambridge, UK: Cambridge University Press)

Wellstein S., Langer N., Braun H., 2001, A&A, 369, 939

Wu K., 1997, ASP Conference Series, 121, 283

Wu K., Soria R., Hunstead R.W., Johnston H.M., 2001, MNRAS, 320, 177

Zampieri L., Mucciarelli P., Falomo R., Kaaret P., Di Stefano R., Turolla R., Chieregato M., Treves A., 2004, ApJ, 603, 523

Zezas A., Fabbiano G., Rots A.H., Murray S.S., 2002, ApJ, 577, 710

Zezas A., Fabbiano G., Baldi A., Schweizer F., King A.R., Ponman T.J., Rots A.H, 2006, ApJS, 166, 211